MOLECULAR WEIGHT DISTRIBUTION AS A MEANS TO CONTROL POLYMER PROPERTIES

A Dissertation

Presented to the Faculty of the Graduate School

of Cornell University

In Partial Fulfillment of the Requirements for the Degree of

Doctor of Philosophy

by

Dillon Gentekos

August 2019

MOLECULAR WEIGHT DISTRIBUTION AS A MEANS TO CONTROL POLYMER PROPERTIES

Dillon Gentekos, Ph. D.

Cornell University 2019

A process for the precise control of polymer molecular weight distribution (MWD) shape is developed. Temporal control of polymer chain initiation was achieved through the metered addition of discrete initiating species to controlled radical polymerizations and anionic polymerizations. Series of polymers can be prepared with the same molar mass and breadth but with vastly different MWD shapes. Using anionic polymerization, living polymers with skewed distribution functions can be chain extended to afford well-defined block copolymers with systematically deviating compositions of molecular weights. Rheological measurements reveal that the MWD shape has an important influence on the viscoelastic behavior of homopolymer melts such as viscosity and storage modulus. Dynamic mechanical analysis showed that the Young's modulus of block copolymers can be tuned over a broad range by modifying the shape of the MWD in one block. Investigation of the phase behavior of block copolymers by transmission small-angle X-ray scattering and grazing-incidence small-angle X-ray scattering demonstrates that the distribution symmetry enables tuning of the thin film domain spacing and the boundaries of the bulk morphological phase diagram. Additionally, the development of a kinetic model for the predictive design of MWDs is explored.

ACKNOWLEDGMENTS

I want to start by thanking my advisor, Brett P. Fors. After our serendipitous introduction at the University of California Santa Barbara's graduate school visitation weekend, I was extremely lucky to have the chance to be one of the first students to join the Fors Group. I would not have been able to complete my PhD without his continued trust and guidance (read: patience). Brett's optimism is truly admirable and has taught me a great deal about how to approach my professional and personal life goals. I am eternally thankful for Brett's mentorship and support, and I hope that in my future career I can represent a favorable image of him and his group.

Other faculty to whom I owe my gratitude are David B. Collum and Geoffrey W. Coates. I had a truly fantastic thesis committee. Our discussions throughout my graduate career have been extremely insightful. I sincerely appreciate their approachability and guidance over these past several years. I would also like to thank Robert A. DiStasio Jr. Our discussions have been interesting to say the least, and I will continue to reflect on his advice in the future.

I also need to thank the post-docs with whom I worked during my early PhD career. Dongbing Zhao and Quentin Michaudel, who served as mentors during my first few years of graduate school, taught me a substantial amount about organic chemistry and how to approach scientific problem solving. I am forever grateful for their patience with my early (and numerous) lab mistakes and answering my questions. The graduate students I had the opportunity to

work with in the Fors group were truly fantastic. Jacob Trotta, who was part of the first class of graduate students with me, became a roommate of 4 years and a great friend. Brian Peterson and Parker Singleton, who were part of the second wave of graduate students, will also be lifelong friends. I owe them a great deal of thanks for many reasons; for example, without them, I would have barely left the lab in my second year. I want to also thank Veronika Kottisch. We've had many good discussions, and she is a good friend and collaborator. I am thankful for all the relationships I developed along the way. I hope that I was able to have a similar impact on them as they've had on me, and I wish them the best in their future careers.

I would be remiss not to mention the childhood friends on Chock St. who have indirectly impacted my career trajectory. They have always helped me keep perspective and provided innumerable funny moments that I will never forget. I can always count on them to keep things interesting.

Most importantly, I need to thank my family for all they have done for me throughout my life. My Mom and Dad are amazing parents who gave me the freedom to choose my own path and learn from my mistakes. They taught me the value of discipline and perseverance, two values which will help guide me through the rest of my life. I would not have been able to get where I am without their love and support. Thank you both for everything.

TABLE OF CONTENTS

LIST OF FIGURES

LIST OF TABLES

LIST OF ABBREVIATIONS

MWD	Molecular weight distribution
NMP	Nitroxide-mediated polymerization
SEC	Size-exclusion chromatography
GPC	Gel permeation chromatography
NMR	Nuclear magnetic resonance spectroscopy
PS	Polystyrene
EBiB	Ethyl-2-bromoisobutyrate
PMDETA	Pentamethyldiethylenetriamine
TIPNO	2,2,5-Trimethyl-4-phenyl-3-azahexane-3-nitroxide
s-BuLi	*secondary*-butyllithium
PI	Polyisoprene
PS-*b*-PI	Polystyrene-*block*-polyisoprene
CaH_2	Calcium hydride
$CDCl_3$	Deuterated chloroform
DMA	Dynamic mechanical analysis
DSC	Differential scanning calorimetry
BHT	Butylated hydroxyltoluene
DCM	Dichloromethane
HME	Hot melt extrusion
3DP	3D printing
TGA	Thermogravimetric analysis

PMMA — Poly(methyl methacrylate)

PS-*b*-PMMA — Polystyrene-*block*-poly(methyl methacrylate)

DPE — Diphenylethylene

GISAXS — Grazing-incidence small-angle X-ray scattering

AFM — Atomic force microscopy

FFT — Fast Fourier transform

MSE — Mean signed error

MAE — Mean absolute error

RMSE — Root mean squared error

MAXE — Maximum error

LOO — Leave-one-out cross validation

LiCl — Lithium chloride

CHESS — Cornell high energy synchrotron source

THF — Tetrahydrofuran

2VP — 2-vinylpyridine

P2VP — Poly(2-vinylpyridine)

PS-*b*-P2VP — Polystyrene-*block*-poly(2-vinylpyridine)

L — Lamellae

P — Perforated lamellae

G — Gyroid

C — Hexagonally packed cylinders

S — Spheres

SAXS — Small-angle X-ray scattering

TEM	Transmission electron microscopy
n-BuLi	n-Butyllithium
Oct_3Al	Trioctylaluminum
DMF	Dimethylformamide
LiBr	Lithium bromide

LIST OF SYMBOLS

M_n — Number-average molar mass

M_w — Weight-average molar mass

M_z — z-average molar mass

M_{z+1} — z+1-average molar mass

$Đ$ — Dispersity

M_p — Peak maximum

σ — Standard deviation

A_s — Asymmetry factor

α_3 — Skewness

α_4 — Kurtosis

f_v — Volume fraction

E — Young's modulus

T_g — Glass transition temperature

η^* — Apparent viscosity

G' — Storage modulus

T_d — Decomposition temperature

d^* — Domain spacing

M_1 — First statistical descriptor of molecular weight distribution

M_2 — Second statistical descriptor of molecular weight distribution

M_3 — Third statistical descriptor of molecular weight distribution

μ_1 — First central moment

μ_2 — Second central moment

μ_3 — Third central moment

Λ_1 — Normalized deviation of the first statistical descriptor

Λ_2 — Normalized deviation of the second statistical descriptor

Λ_3 — Normalized deviation of the third statistical descriptor

c_{ijk} — Power series expansion coefficient

α_c — Critical angle

α_I — Incident angle

q^* — Principle scattering vector

χ — Flory-Huggins interaction parameter

N — Degree of polymerization

PREFACE

This thesis was largely adapted from the following published articles co-written by the author:

Gentekos, D. T.; Dupuis, L. N.; Fors, B. P.; "Beyond Dispersity: Deterministic Control of Polymer Molecular Weight Distributions," *J. Am. Chem. Soc*. 2016, 138, 1848. (*C&EN Science and Technology Concentrates, Featured February 2016)*

Kottisch, V.; Gentekos, D. T.; Fors, B. P.; "Shaping the Future of Molecular Weight Distributions in Anionic Polymerization," *ACS Macro Lett*. 2016, 5, 796. (*ACS Macro Letters Cover Article, Featured July 2016*)

Nadgorny, M.; Gentekos, D. T., Xiao, Z.; Singleton, S. P.; Fors, B. P.; Connal, L. A. "Manipulation of Molecular Weight Distribution Shape as a New Strategy to Control Processing Parameters," *Macromol. Rapid Commun*. 2017, 38, 1700352.

Gentekos, D. T.; Jia, J.; Tarado, E. S.; Barteau, K. P.; DiStasio, R. A. Jr.; Fors, B. P.; "Exploiting Molecular Weight Distribution Shape to Tune Domain Spacing in Block Copolymer Thin Films," *J. Am. Chem. Soc*. 2018, 140, 4639.

Gentekos, D. T.; Fors, B. P.; "Molecular Weight Distribution Shape as a Versatile Strategy for Tailoring Block Copolymer Phase Behavior," *ACS Macro Lett.* 2018, 7, 677.

Chapter 7 of this thesis was adapted from a manuscript in preparation in collaboration with Sergii Domanskyi at Clarkson University:

Domanskyi, S.; Gentekos, D. T.; Privman, V.; Fors, B. P.; *submitted.*

CHAPTER 1

LITERATURE REVIEW

1.1 Abstract

The manipulation of polymer properties without altering their chemical composition has emerged as a grand challenge in the fields of polymer chemistry, materials science, and engineering. To confront this endeavor, recent advances have enabled the direct investigation of the influence of molecular weight distribution (MWD) breadth and shape on polymer properties. While variables such as chemical structure, branching, molecular weight, and dispersity have been thoroughly investigated as a means to control polymer architecture and physical properties, only recently has there been a drive to understand the profound impact the shape of a MWD can have over material function. Modern synthetic strategies now make it possible to explore the importance of skew and the higher moments of the molecular weight distribution function. In this review, we discuss early accounts of the effect of MWD shape on properties, a number of synthetic strategies for controlling MWD shape; current endeavors into understanding the influence of MWD shape on rheological properties, mechanical properties, and phase behavior; and brief insight into the future of MWDs and their importance in the utility of polymeric materials.

1.2 Introduction

The molecular weight distributions (MWDs) of polymers have a striking impact over their properties, from processability and mechanical strength to nearly all aspects of morphological phase behavior.[1-23] The most common molecular parameter used to describe polymer MWDs is dispersity (*Đ*), the normalized standard deviation of chain sizes in a polymer sample, defined as the ratio of weight-average molar mass (M_w) to number-average molar mass (M_n). In this regard, *Đ* has been utilized as an important molecular characteristic to manipulate the vast array of properties in polymeric materials.[23-31] However, *Đ* is an incomplete representation of a polymer's true distribution since it describes only the relative breadth of a MWD and contains no information regarding the precise shape and composition of polymer chain lengths.[25,26] In fact, this observation has sparked interest in using the entire distribution of masses of a polymer sample in order to dictate its function rather than altering its chemical composition. In theory this prospect would allow for limitless variation of the distribution function, which renders this strategy for governing polymer properties highly general. Until recently however, this avenue of controlling polymer structure and function remained largely unexplored owing to the lack of versatile methods for command of the absolute composition of chain lengths in a polymer sample. In this review, we explore the recent advances in synthetic control of polymer MWD shape by various means: from temporally controlled polymer initiation and termination to reactant feeds in continuous flow setups which produce homopolymers and block copolymers with precisely

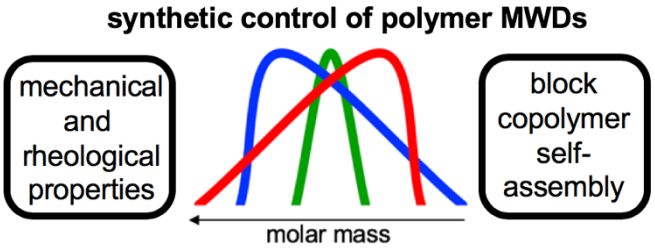

Figure 1.1 Schematic illustration of different polymer MWD shapes. Gaining synthetic control of polymer MWDs allows for the direct exploration of MWD shape on mechanical and rheological properties to many facets of block copolymer self-assembly.

defined MWD shapes and compositional gradients. We also highlight the marked impact of the distribution function on polymer properties from rheological properties like viscosity to a variety of morphological characteristics such as domain spacing and the position of morphological phase boundaries (Figure 1.1).

1.3 MWDs and the Limits of Dispersity

Polymer MWDs are defined most typically using a combination of the molar mass averages M_n and M_w found through size-exclusion chromatography (SEC) and are defined below in eqn (1.1) and (1.2).

$$M_n = \frac{\sum M_i N_i}{\sum N_i} \tag{1.1}$$

$$M_w = \frac{\sum M_i^2 N_i}{\sum M_i N_i} \tag{1.2}$$

Using these two molar mass averages, $Đ$ is defined by eqn (1.3),

$$Đ = \frac{M_{\mathrm{w}}}{M_n} \tag{1.3}$$

which is related to the standard deviation (σ) of the distribution function by the relationship in eqn (1.4).

$$Đ = \frac{\sigma^2}{M_n^2} + 1 \tag{1.4}$$

Eqns (1.1) – (1.4) reveal that *Đ* is the relative breadth of the molecular weight distribution function, or, more specifically, it describes the standard deviation of chain lengths normalized to the number-average molar mass. It becomes clear that *Đ* provides relevant information regarding MWD breadth only when the average molar mass of the polymers being compared is constant, namely, polymers can have the same *Đ* but contain vastly different breadths of their respective MWDs.[25,32-34]

In addition to being a limited description of the relative span of molecular weights in a polymer sample, *Đ* offers no information over the shape of a distribution function. Fundamentally, a polymer's MWD shape can be varied infinitely while maintaining the same M_{n} and *Đ*. In fact, several reports have suggested that the absolute composition of polymer chain lengths should have a significant influence over polymer properties.[22,35] In recent years, using the MWD shape as a strategy for controlling or fine-tuning polymer function without

altering the chemical composition of the final material has become a promising path forward. In this regard, looking toward the higher moments or precise

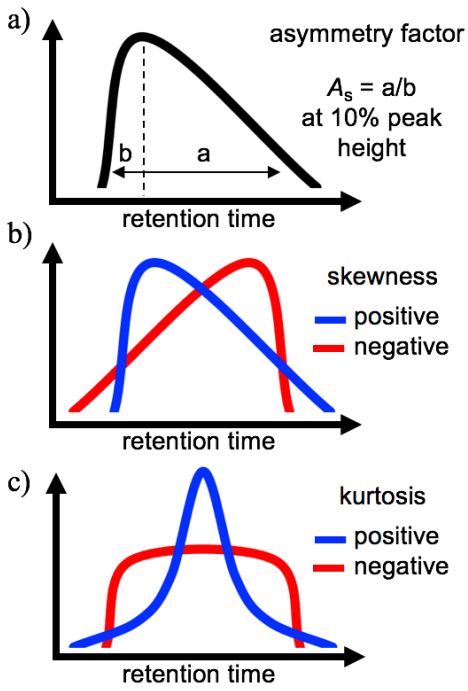

Figure 1.2. The higher moments of a distribution function to describe shape. (a) asymmetry factor (A_s), (b) skewness, and (c) kurtosis of a polymer's size-exclusion chromatogram can be used to better represent overall polymer composition by quantifying the asymmetry and tailing of a MWD.

shape of the distribution function becomes a necessity (Figure 1.2). One convenient parameter to measure the asymmetry of a MWD is the asymmetry factor (A_s) which gives a qualitative measure of the skew of a distribution (Figure 1.2a). This factor is found by taking the ratio of the distance from the peak maximum to the front of the peak over the distance from the peak maximum to the back of the peak at 10% of the peak height. Additionally, the skewness (third moment, Figure 1.2b) and kurtosis (fourth moment, Figure 1.2c) of the MWD

are of immediate interest. They describe the relative degree of asymmetry and the population of the tails in a distribution function, respectively.[36-39]

Box 1.1 | Molecular Weight Distributions and Moments in Probability Statistics

The vast majority of synthetic polymers contain a distribution of chain lengths. The corresponding molecular weight distribution functions are dependent on the kinetics of the polymerization reaction in question, and the MWDs resulting from different polymerization processes have been described using a variety of probability functions. For example, the Flory-Schulz distribution is a single parameter function that is typically used to describe the MWDs of polycondensation reactions.[40] This probability distribution is useful for modeling step-growth polymerization because small chains are favored which affords MWDs tailing towards high molar mass. For anionic polymerization processes, where initiation is much faster than propagation and termination reactions are nonexistent, the resulting distribution of chain lengths is often very narrow and is accurately portrayed by the Poisson distribution.[41] Additionally, the shapes of distributions afforded through controlled radical polymerizations (such as atom-transfer radical polymerization) can be typically defined by the Schulz-Zimm distribution, a two-parameter function, due to the presence of some termination events leading to a buildup of low molar mass polymer chains.[30,35] Furthermore, the Gaussian or logarithmic normal distributions have been used to describe functions which are symmetric about the number-

average molar mass.[42] However, to avoid the difficulty of using a diverse array of functional forms to represent experimental MWDs, the concept of moments in probability statistics can be applied. The n^{th} moment (μ_n) provides a specific quantitative measure of the shape of a distribution function and is described by $\mu_n = \int_{-\infty}^{\infty}(x-c)^n f(x)\,dx$.[36] These are typically referred to as moments "about" some arbitrary value "c". When c = 0 the moment is defined as raw or crude. The first raw moment is the expected value of x and therefore represents the mean or number average (μ) of the distribution. The second moment is often written as a central moment about the mean (where c = μ) and corresponds to the variance of the distribution. Moreover, higher moments are most useful when reported in standardized form which is found by normalizing the higher central moment (μ_n) to the previous moment (μ_{n-1}) so that comparison can be made between differently shaped distributions.[38] The third standardized moment is the skewness of the distribution while the fourth standardized moment describes its kurtosis.

1.4 Synthetic Control of Polymer MWD Shape

On the basis that polymer properties depend significantly on the breadth as well as the shape of the MWDs in the final polymeric material,[5,22] a number of approaches have been developed to control polymer *Đ*. Due to the early synthetic difficulty in controlling both the molar mass averages as well as MWD breadth in a one-pot setup, initial studies employed post-polymerization blending strategies to tailor MWD composition.[43-48] However, this process

requires the synthesis of multiple polymers under highly controlled conditions and results in multimodal MWDs. Although these studies have provided novel insight into the influence of MWD on polymer properties, such highly heterogeneous molar mass compositions are unsuitable for some applications due to the potential for undesirable macrophase separation.[43,44] Therefore, systems which produce polymers with continuous monomodal MWDs in one reactor setup would be much more desirable. Uncontrolled polymerizations is one such synthetic strategy for producing monomodal MWDs with large breadths.[49-51] While this approach has proven useful in generating polymers with $Đ \sim 2$, it grants little control over M_n or the shape of the resultant MWD. This issue has been circumvented by leveraging polymer chain growth kinetics in radical, ring-opening, and anionic polymerizations to prepare polymers with controllable *Đ*s.[52-55] Interestingly, more recent work has made significant strides in using deep reinforcement learning to simulate the production of a vast repertoire of MWDs in ATRP.[56] These numerical simulations have yielded reactor control policies that should afford targeted MWD shapes, from monomodal distributions with deviating *Đ*'s to multimodal MWDs. Alternatively, to tune polymer *Đ*, researchers have developed an organocatalyzed process which takes advantage of monomer mixtures to manipulate the dispersity of any block of a block copolymer.[57] While the aforementioned approaches do not offer a means of governing the precise composition or shape of the polymer MWD, they can be used to modify *Đ* with high fidelity.

While most strategies for modifying polymer MWD have been limited to the relative span of molar masses in a sample, there exists a few examples which have taken steps at customizing the absolute shape of MWDs. Early efforts by Meira and Johnson have demonstrated that some control over the MWD shape can be imparted in anionic polymerization of styrene through oscillating monomer and alkyllithium initiator feed rates in continuous flow reactors.[58,59] The aim of this method was to monitor the MWD in real time and use computer modeling to alter the flow rates of the reacting species to provide automatic control of the target polymer MWD. In the initial experimental study of this continuous flow process the final polymers had the same *general* MWD shape as the desired material, but significant differences between the anticipated and measured MWDs were observed. It was proposed that these deviations were the result of two idealized reactor conditions not being met; the setup did not result in 100% monomer conversion and termination of the living polymer chain ends could not be eliminated due to the experimental unfeasibility of excluding all impurities from the monomer solution. In a subsequent series of studies, an attempt to account for the issue of monomer purity was explored in a semibatch process.[60] The authors employ a rederivation of the automatic control process to account for the concentration of impurities in the reactor feeds. Using this new mathematical model, it was found that there was better agreement between the predicted and measured MWDs but still substantial deviations between these MWDs and the *a priori* desired distribution function

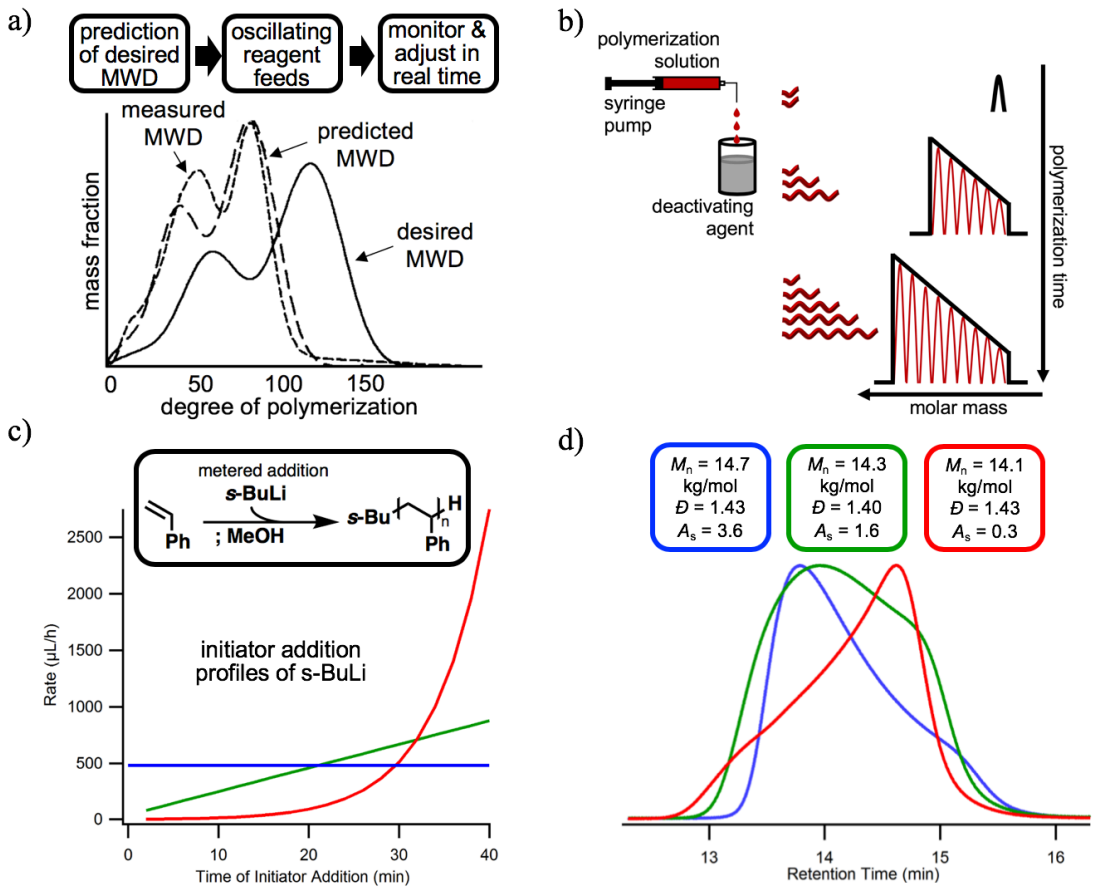

Figure 1.3. Reagent and polymer feed strategies for temporal control of polymer MWD shape (a) The desired, predicted, and measured molecular weight distributions from manipulating the monomer and initiator feed rates to a semibatch anionic polymerization. Adapted from ref. 59 with permission from the Journal of Applied Polymer Science. (b) Strategy for the manipulation of polymer MWDs through the metered deactivation of active chains in cationic polymerization. Revised from ref. 62 with permission from the Journal of Polymer Science Part A: Polymer Chemistry. (c) Synthetic control of polystyrene MWD breadth and shape by metered addition of alkyllithium initiating species in anionic polymerization, showing (d) three polymers with the same M_n and $Đ$ but with very different MWD asymmetries. Adapted from ref. 65 with permission ACS Macro Letters.

(Figure 1.3a). Even though the authors consider the presence of impurities in the control model, termination of the active polymer chains can only be

approximated. The discrepancies between the desired, predicted, and measured MWDs are likely the result of the polymerization kinetics being highly sensitive to the impurity concentration as well as the initial concentration of alkyllithium initiating species. More recently, additional efforts have been made in developing such a fully automated control system for continuous stirred-tank reactors using an inverse process model to gain better control of MWD shape in homopolymers has been explored.[61]

While the above processes offered some degree of control over polymer MWDs, they also exemplify the importance of gaining absolute control of the molar mass distribution function in order to manipulate material properties from an engineering perspective. In addition, several studies have explored this phenomenon in a small scale chemical laboratory setting. Aoshima has developed a strategy for tuning the MWD function in diblock copolymers prepared through cationic polymerization (Figure 1.3b), in which a solution of growing polymer chains was steadily added to a solution of a deactivating agent (aqueous ammonia) using a syringe pump to precisely control the addition rate.[62] This polymerization approach was suitable for tuning the MWD in a variety of vinyl ethers from isobutyl vinyl ether (IBVE) to 2-ethoxyethyl vinyl ether (EOVE) and 2-methoxyethyl vinyl ether (MOVE) and was amenable to the growth of block copolymers. One particular drawback of this process is that to tune the MWD, the polymerization must be carried out in a syringe, which may not be suitable for polymerization reactions that require vigorous stirring.[63] Aside from the limited mechanistic scope of this method, the synthesis of block

copolymers through controlled termination also necessitates the block to be tuned is prepared as the last step of the synthesis. This results in the loss of valuable information about the precise distribution function of the final polymer since the MWD of each block cannot be decoupled from the overall measured MWD.[26]

In addition to these controlled reactant feeds and termination methods for dictating polymer MWD shape, Fors and coworkers have developed a process for temporally controlled initiation in polymerization reactions that utilize a discrete initiating species.[64,65] By taking advantage of the kinetics of controlled polymerization processes, where initiation is fast and all chains propagate at about the same rate, metered addition of a discrete initiating species dictates the molar quantities of each chain length. Initial proof of concept focused on nitroxide-mediated polymerization (NMP), whereby metering in a solution of alkoxyamine initiator at predetermined rates of addition, the breadth and shape of polymer MWDs could be predictably controlled. More specifically, polymers that are initiated early in the reaction afford chains with higher molar mass than those initiated later in the polymerization, i.e. the addition time of each initiating species dictates the length of that chain. Initially, constant rates of addition were utilized and longer addition times lead to increased $Đ$, and the MWD breadth was linearly related to the overall addition time. Furthermore, when the addition rate profiles were altered from constant to linearly increasing rates the polymers produced had distributions tilted into the low molecular weight region ($A_s < 1$) corresponding to more polymers being generated later in the polymerization

reaction. This study also revealed that using different initiator addition rate profiles was sufficient to yield polymers with the same M_n and $Đ$ but with different MWD shapes. In all addition rate profiles examined in this study the $Đ$ as well as σ were linearly related to the initiator addition time, providing a convenient calibration curve for tuning the M_n, breadth, and shape of the MWD. Moreover, this process also offered the ability to prepare multimodal distributions as well as the synthesis of relatively low molar mass block copolymers. While this approach provided command over the MWD shape, there were a few issues inherent to NMP which render this process impractical for fundamental studies of the influence of MWD shape on polymer properties. For example, radical polymerizations have limited chain end fidelity and cannot be run to full monomer conversion which significantly limits the practicality of this approach.[33] To address these challenges, the process of temporally controlled polymer initiation was extended to anionic polymerization processes due to their truly living nature, broad monomer scope, and model ability to prepare functional block copolymers.[32] These studies explored the anionic polymerization of styrene in hydrocarbon solvents (Figure 1.3c). First, by adding alkyllithium initiating species at constant rates of addition, polymer MWDs were prepared with significant tailing into the low molecular weight region (A_s > 1). Conversely, exponentially increasing rate profiles were used to prepare polymers skewed substantially in the opposite direction (A_s < 1). The initiator addition profiles in anionic polymerization were significantly different than in radical polymerization to achieve the same general shape of the polymer MWD

likely due to the different polymerization kinetics of the system. Moreover, anionic polymerization could also be used to prepare sets of polymers with vastly different MWD shapes but with the same M_n and $Đ$ (Figure 1.3d). Lastly, this strategy could be used to prepare a variety of well-defined block copolymers and was extended to ATRP to show the utility of this process in manipulating MWDs in any controlled polymerization reaction that uses a discrete initiator.[64,65]

In addition to using conventional thermally induced polymerization, there has been substantial recent effort towards photo-mediated strategies to synthesize polymers with well-defined structures, and architectures due to the broad utility of light as a versatile stimulus.[66] With this in mind, the use of photoinduced electron transfer-reversible addition fragmentation (PET-RAFT) polymerization in a flow reactor has been introduced by Boyer and coworkers as a novel approach for governing polymer MWD composition.[67] Hypothetically, modification of the reaction rate or chemical concentrations during continuous flow would yield materials with different molecular weights which are then merged in the flow reactor to yield tailored MWDs. In this approach the flow rates dictate the instantaneous concentration of reactive species while the visible light stimulus commands the overall reaction rate. Interestingly, by adjusting the irradiation intensity or wavelength at fixed flow rates the monomer conversion could be controlled at each step of the process, dictating the precise mixtures of molar masses that are combined in the collection reservoir. Additionally, altering the flow rate or chemical concentration of the reagents

under constant irradiation conditions afforded the same results. Although the level of control over MWD shape in this study was modest, likely due to unfavorable fluid mixing behavior, it highlights and exciting opportunity for the use of photochemistry to fine-tune polymer MWDs. One particular advantage of the photoinduced continuous flow process is the ability to prepare block copolymers with controlled block compositional gradients in their MWDs, a feature which is not yet achievable in conventional batch polymerization chain extension processes. By altering the flow reactors setup (Figure 1.4a) to fully separate each polymer fraction with a distinct molar mass in a plug flow process, subsequent treatment of these fractions a second monomer allows the growth of a second block before mixing of each polymer fraction. This semi-continuous flow process allows each polymer fraction to be extended with a different quantity of the second monomer, thereby producing block copolymers with gradient compositions of molar masses in both blocks in a single pass.

In contrast to the previously mentioned processes which utilize reagent feeds or alterations of the polymerization reaction kinetics, Cölfen and coworkers have developed an alternative process for the manipulation of polymer MWDs uses analytical ultracentrifugation.[68] The well-established sedimentation equilibrium of chemical compounds in centrifugal fields has been exploited to produce a desired concentration gradient of a macroinitiating species while the monomer remains homogeneously distributed followed by photoinduced polymerization directly in the centrifuge tube (Figure 1.4b). The top of the reactor will have a lower concentration of initiator relative to monomer

while the bottom of the reactor consists of a higher relative ratio of initiator to monomer. By adjusting the centrifugal field, the precise concentration distribution can be fine-tuned leading to good control of the final molecular weight distribution. One particular advantage of this strategy is that the thermodynamics of analytical ultracentrifugation are well understood which leads to good agreement between simulated MWDs and those produced experimentally. While the use of a sedimenting macroinitiator does somewhat limit this approach, this strategy could be extended to other types of chemical concentration distributions through diffusion or mixing to render this method more synthetically pragmatic.

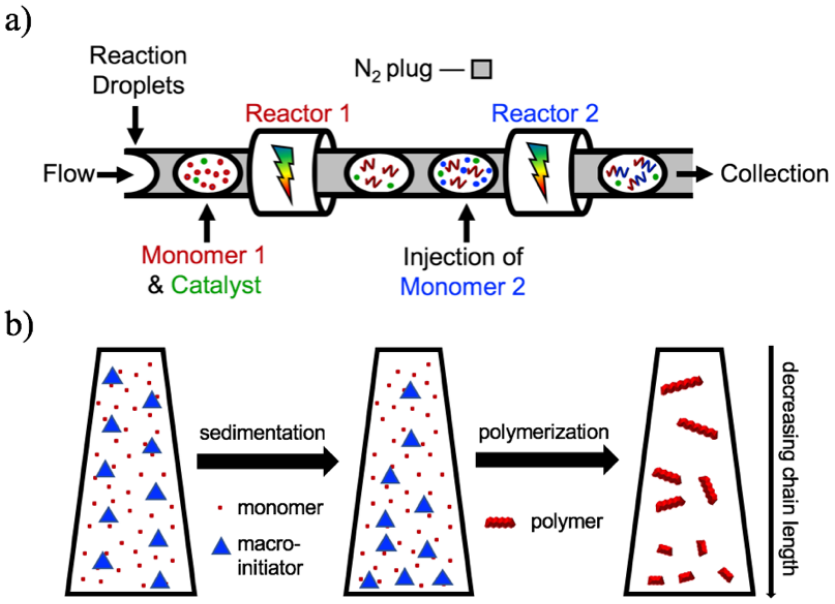

Figure 1.4. Alternative methods for control of polymer MWD shape with photochemical or centrifugal stimuli (a) Modified photoinduced plug flow polymerization reactor setup which enabled the synthesis of block copolymers with compositional gradients. (b) Illustration of MWD control through the use of ultracentrifugation to produce initiator concentration gradients followed by polymerization. Revised from ref. 68 with permission from Angewandte Chemie International Edition.

1.5 Block Copolymer Self-Assembly

Leibler delineated the foundation for the self-assembly of block copolymers and the potential significance of MWD composition on their phase behavior in a transformative theoretical work.[22] Since then, a number of studies have investigated, both theoretically and experimentally, the influence of polymer MWD breadth (specifically *Đ*) on the microphase separation of these hybrid macromolecules.[5-23] Exploration of the effects of MWD shape (skew, etc.) on block copolymer self-assembly has remained unexplored. However, due to the synthetic work outlined above, the community is beginning to investigate the importance of controlling the absolute composition of MWDs. The theoretical investigation of the influence of MWD shape on block copolymer phase behavior has only recently been studied. In this theoretical work, Lynd and Hillmyer compare arbitrary A–B diblock copolymers with the Schulz-Zimm distribution (SZD) to the equilibrium polymerization distribution (EPD) at the same values of *Đ*. It is important to note that the SZD is often used to describe MWDs because it accurately portrays a large number of materials made by various addition polymerizations spanning *Đ* = 1 – 2.[30,31] Conversely, the EPD specifically models the MWDs obtained from the equilibrium polymerization of lactide.[35] These two distributions diverge as the MWD span increases, reaching their maximum difference at *Đ* = 1.5, and converge to similar shapes as *Đ* approaches 2. The domain spacing (d^*) predicted by self-consistent field theory (SCFT) of the aforementioned A–B diblock copolymers was then compared to that of their monodisperse counterparts (d_0) (Figure 1.5a). In these experiments,

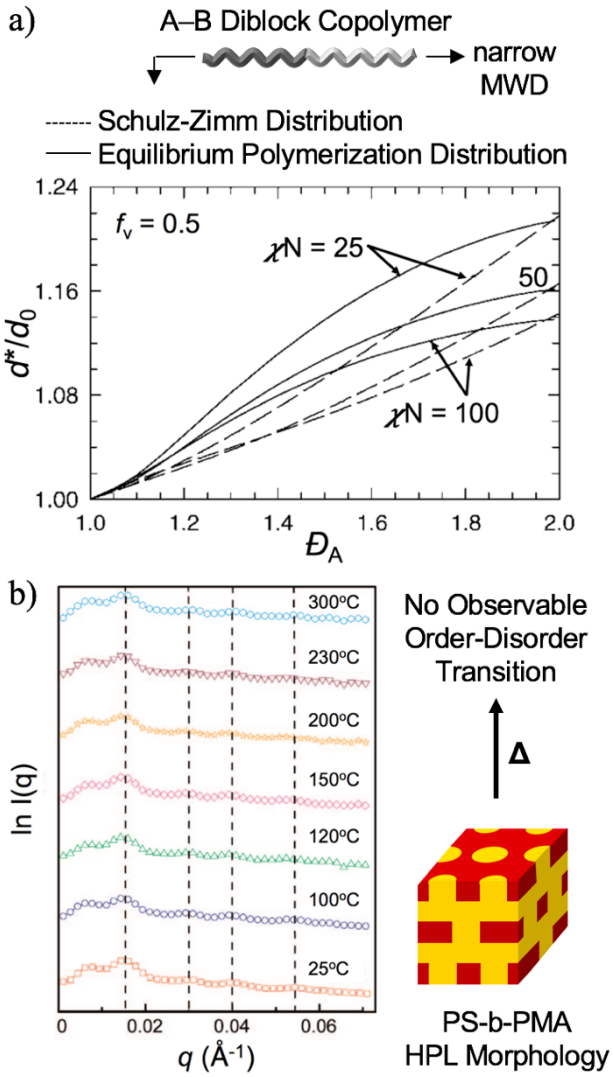

Figure 1.5. Initial experimental and theoretical investigation of the influence of MWD breadth and shape on block copolymer self-assembly (a) Predicted differences in domain spacing between the Schulz-Zimm distributions (dashed lines) and Equilibrium Polymerization distribution (solid lines) in arbitrary A-B diblock copolymers where the A-block MWD breadth and shape are modified. Data is shown for three values of segregation strength (χN). Adapted from ref. 35 with permission from Macromolecules. (b) SAXS measurements of PS-*b*-PMA with a broad and symmetric PS block, showing unprecedented stability of the perforated lamellar phase (P). Dotted lines are indexed to the P phase. Reproduced from ref. 55 with permission from Macromolecules.

only the MWD of the A-block in the A-B diblock copolymer was altered while the B-block remained narrow. The domain spacing of the materials increases with increasing *Đ*. However, there is a striking difference in d^*/d_0 between the two MWD shapes; the largest disparities being seen at *Đ* ≈ 1.5, where the compositions of chain lengths diverge most sharply.

The differences observed in these experiments can be explained by two features. First, the SZD and EPD have different entropic elasticities, namely, the presence of a broad distribution decreases the entropic penalty for stretching a domain because the long chains can more easily fill empty space.[14,21,52,69,70] In this regard, the EPD has a larger relative quantity of long-chain polymers and thus its increased d^*/d_0 with respect to the SZD are in good agreement with theory. Second, domain spacing can increase by having small polymers desorb from the interface and swell the phase of their majority component. This effect is a balance of the gain in entropy by having a short A-block in the B-phase with the loss in enthalpy from surrounding an A-block with dissimilar B-segments. This effect is more pronounced at lower values of the Flory interaction parameter (χ) where the A and B–blocks are more miscible leading to larger A–segments being pulled into the B–phase.[49,52,69,71,72] At *Đ* ≈ 1.5, the EPD also has a significantly larger population of very short polymer chains. Both the domain spacing enhancement mechanisms are in accordance with theoretical predictions.

In addition to the differences in domain spacing between the SZD and EPD, the influence of these distribution shapes was also examined on the phase

diagram of arbitrary A-B diblock copolymers. Interestingly, compared to the relatively large deviations in domain spacing between the two MWDs, only small differences in the phase diagram were predicted by SCFT. For example, when the modified A-block is in the minority phase, the EPD has cylinder and lamellar phase boundaries that are slightly shifted to lower volume fraction (f_v). It was hypothesized that while the decreased entropic stretching penalty induced curvature toward the disperse A-block, this impact can be effectively offset by swelling of the B-domain through chain pull-out of the A-phase, which pushes the phase boundary in the opposite direction.[73]

While simulated studies have suggested that the shape of the MWD has only minor effects on the compositional phase diagram of block copolymers, some experimental work by Matyjaszewski and coworkers have revealed that the skew of the distribution function has a marked impact over self-assembly. The effects of distribution asymmetry on the formation of “metastable” morphologies such as hexagonally perforated layers in diblock copolymers has been explored.[55] As discussed briefly above, reducing the amount of copper catalyst in ATRP enables control over the breadth of the MWD.[54] These dispersity-controlled polymers can be chain extended with another monomer to afford well-defined block copolymers with one narrow block and one broad block. While this process does not offer the ability to govern the precise MWD shape, it does yield polymers whose distribution functions are more symmetric than most synthetically accessible polymers which follow the positively skewed SZD.[32] This synthetic process therefore affords an interesting way to examine

the effects of skew on the self-assembly of block copolymers. The morphological differences were examined between two polystyrene-*block*-poly(methyl acrylate) (PS-*b*-PMA) copolymers with similar block composition ($f_{v,PS}$ = 0.65 and 0.71) and overall molar masses (M_n = 47 and 51 kg/mol) in which the PS block was either narrow or broad and symmetric. Interestingly, it was discovered through small-angle X-ray scattering (SAXS) studies that the polymer with a narrow PS block exhibited a morphology of hexagonally packed cylinders (C) while its counterpart with a broad and symmetric PS block displayed hexagonally perforated layers (P) which is traditionally understood as a metastable morphology.[74] The stability of the P phase block copolymer was then examined in a variety of ways. First, the same sample was subjected to a library of different solvent casting and thermal annealing conditions. Intriguingly, no change in the overall morphology was observed for any of the different sample preparations. In a different experiment, the overall thermal stability of the P phase was examined by temperature-dependent SAXS experiments (Figure 1.5b), where the sample was repeatedly heated to higher temperatures before X-ray data collection. Even up to 300 ^{o}C, no order-order or order-disorder transitions were observed. While these experiments do not provide definitive proof that this P phase is the equilibrium morphology, they do provide strong evidence for the significantly enhanced stability of the P phase in PS-*b*-PMA with a broad and symmetric PS MWDs. This is particularly noteworthy given other examples in the literature which show clearly that the P morphology is metastable in both narrow as well as broadly dispersed block copolymers.[75-77]

The general understanding of the metastability of the P phase is that the mean interfacial curvature has a large standard deviation.[78,79] These large differences in curvature between local environments results in chain packing frustration which typically renders the P phase (as well as other phases such as the double diamond[79]) stable only in a relatively narrow temperature range or close to the order-disorder transition. It was hypothesized that the broad and symmetric distributions compensate for different local environments having large disparities in the mean curvature. Possessing roughly equal portions of large and small polymer chains in the broad distribution may alleviate chain packing frustration more favorably than distribution functions that are skewed, such as the SZD. While additional theoretical and experiment investigation of this phenomenon are needed, this study demonstrates the importance of considering the entire distribution of molar masses in a polymer sample when determining phase behavior.

These studies have been taken a step further by synthesizing a library of block copolymers with systematically deviating MWD shapes in one block by metered addition of initiating species to the anionic polymerizations of styrene.[80] Fors and coworkers then prepared three sets of poly(styrene)-*block*-poly(methyl methacrylate) (PS-*b*-PMMA) copolymers; one with narrow MWDs of both blocks as a control group, a set with a positively skewed PS block but narrow PMMA block, and a set with negatively skewed PS blocks but narrow PMMA blocks. The molar mass and breadth of the PS blocks were held constant to study only the influence of MWD skew, and the amount of PMMA in each block was

increased to explore a range of overall molecular weights. The self-assembly behavior was then examined by grazing-incidence small-angle X-ray scattering measurements (GISAXS) on thermally annealed thin films on silicon wafers. All polymers examined in this study exhibited lamellar morphologies but showed large differences in domain spacing (Figure 1.6a). As expected, the narrow control group with two narrow MWDs showed increases in d^* with overall molar mass in accordance with the generally understood relationship outlined by Matsushita and Papadakis (Figure 1.6a, green).[44,81] However, when the dispersity was broadened and the PS MWDs were skewed to give a high molar mass tail, substantial increases in d^* were observed relative to the narrow MWD counterparts (Figure 1.6a, red). More interestingly, when the dispersity was broadened and the MWD skewed to give a low molar mass tail even greater increases in d^* were revealed (Figure 1.6a, blue). Differences in d^* of over 40% were observed when only the breadth and shape of the PS MWD was modified, holding the overall molar mass and volume fraction constant. The data exposed that both the $Đ$ and the MWD skew are important parameters to consider when determining the lamellar period of block copolymer thin films. Importantly, both MWD shapes have d^* vs. molar mass relationships that deviate considerably from the known correlation between these two variables in narrow polymers, opening the door to utilize MWD shape to tailor the domain spacing of polymers without altering their chemical composition.

The large increases in domain spacing observed in this study are likely due to small PS chains withdrawing from the interface and swelling the PMMA

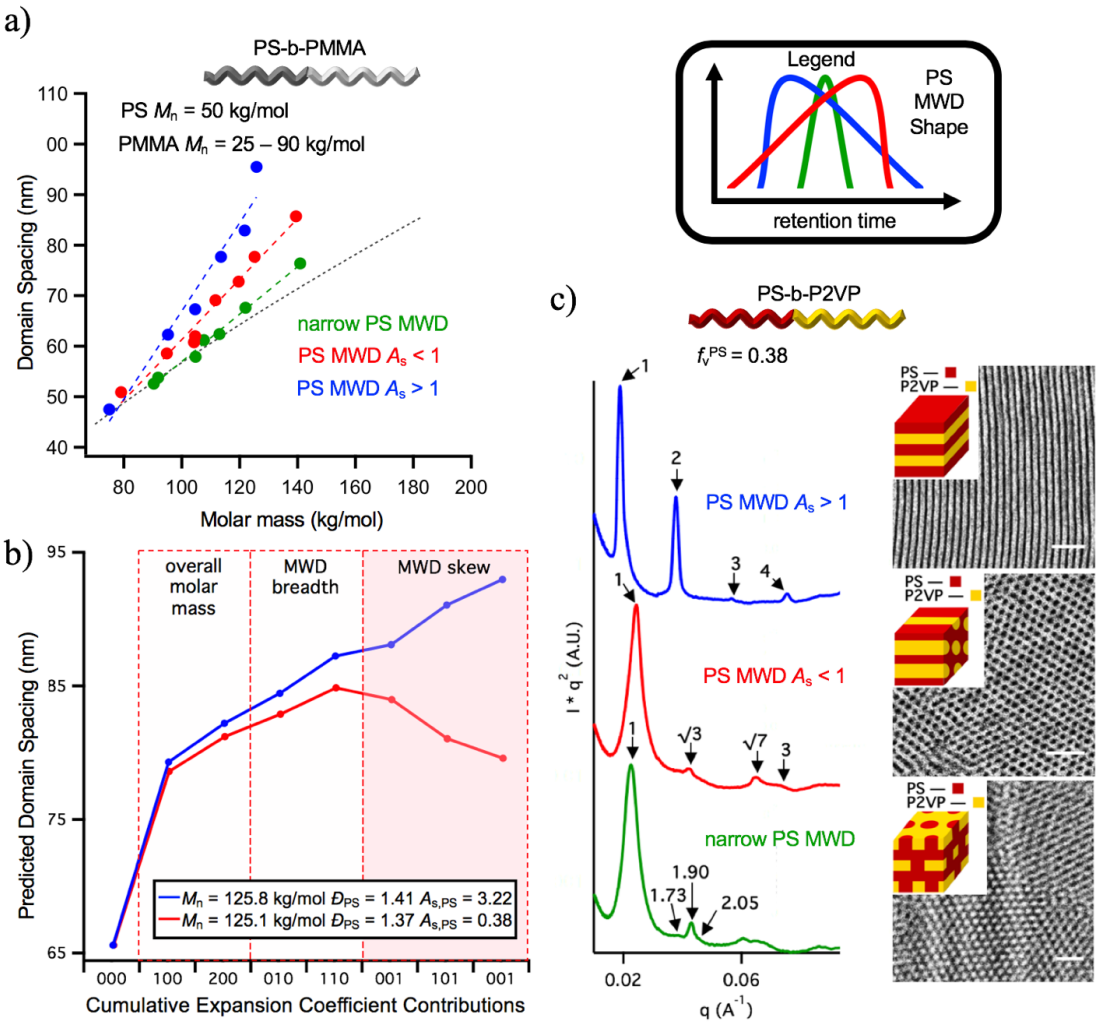

Figure 1.6. The influence of MWD shape on bulk and thin film phase behavior of block copolymers (a) Relationship between *d** and the overall molar mass, PS MWD breadth, and PS MWD skew of lamellar thin films of PS-*b*-PMMA. The black dotted line represents the known relationship between *d** and molar mass in block copolymers with narrow MWDs from ref. 44 and 81 (b) Predicted domain spacing of two polymers with the same M_n, volume fraction, and $Đ$ showing large deviations based on the skew of the PS block. Modified from ref. 80 with permission from the Journal of the American Chemical Society. (c) PS-*b*-P2VP samples with the same M_n and $f_{v,PS}$ display three distinct morphologies based on the shape of the PS MWD. Scale bars are 100 nm. Adapted from ref. 82 with permission from ACS Macro Letters.

phase, as in the chain pull-out mechanism outlined by Matsen and others.[69-72] This hypothesis is supported by the fact that increasing the fraction of PMMA in the overall diblock copolymer increases the deviation in d^* between different MWD shapes. In this swelling mechanism, having larger PMMA blocks enables larger PS segments to desorb from the interface, thus, a higher quantity of PS being pulled into the PMMA phase would result in larger enhancements in lattice spacing. In addition to this observation, the positively skewed PS-*b*-PMMA samples (blue, $A_s > 1$) result in a larger divergence of d^* presumably because they have a larger percentage of very low molar mass PS chains.

Furthermore, population statistics and least-squares analysis were utilized to construct a statistical model for predicting d^* based on overall molar mass, MWD breadth, and MWD skew. This theoretical investigation not only provided a simple process for predicting d^* of block copolymers with high fidelity, but also elucidated fundamental relationships between MWD shape and the lamellar period of block copolymer thin films. In fact, it was discovered that MWD skew has an influence over domain spacing on the same order of magnitude as the breadth of the MWD, demonstrating that the skew is just as important as $Đ$ in determining polymer properties. Figure 1.6b illustrates this crucial aspect by comparing two samples with the same molar mass, volume fraction, and $Đ$. Plotting the cumulative contributions from the statistical model reveals that incorporation of M_n and $Đ$ into the statistical model results in essentially no change in the predicted d^*. However, when the skew components of the PS

MWD are integrated into the model, substantial deviations arise in lamellar periods, accounting for the experimentally observed differences.

Aside from the influence of MWD shape on the d^* of block copolymer thin films, the impact of MWD shape on the bulk phase diagram was also explored for diblock copolymers in which one block had modified MWD shape.[82] In this case, polystyrene-*block*-poly(2-vinylpyridine) (PS-*b*-P2VP) samples were prepared in an analogous fashion to those produced in the study of PS-*b*-PMMA thin films. Again, three sets of samples were prepared with constant M_n of the PS block but with narrow MWD, broad with positively skewed MWD, and broad with negatively skewed MWD. Each sample was chain extended with different amounts of P2VP to investigate a broad range of the phase diagram (Figure 1.6c). Interestingly, no statistically significant differences in d^* were observed for polymers exhibiting the same overall morphology, supporting the hypothesis that the chain pullout mechanism of domain spacing enhancement is not at play in this case. However, based on SAXS measurements, the overall morphology of the samples was altered greatly based on the shape of the PS MWD. In a sample with a low f_v of the PS block, the phase boundary between the lamellar (L) phase and the hexagonally packed cylinder (C) phase was pushed significantly toward higher volume fraction for both broader $Đ$ polymer classes. Additionally, by manipulating the skew of the PS block, the distance of the L/C phase boundary movement could be fine-tuned. Intriguingly, when the modified PS MWD was in the majority component of the block copolymer ($f_{v,PS} > 0.5$), the L/C phase boundaries moved in opposite directions. Positively skewed samples

pushed the L/C boundary toward lower $f_{v,PS}$ while negatively skewed PS blocks induced the L/C boundary to move toward higher $f_{v,PS}$ compared to samples with narrow MWDs. This divergence in phase behavior is exemplified by the fact that three distinct morphologies could be observed in polymer with the same M_n and f_v (Figure 6c). In this instance, the polymer with narrow PS MWD displayed the perforated layer morphology (P) while the positively and negatively skewed samples showed L and C, respectively. These findings provide strong support for the idea that the preferred interfacial curvature of a self-assembled block copolymer is not merely reliant on the span of molar masses in a sample but on the precise mixture of chain lengths, an observation which is in agreement with the hypothesis of Matyjaszewski and coworkers.[55] The materials skewed to low molar mass agree well with previous reports in which it was posited that broad distributions fill empty space more efficiently by possessing decreased entropic stretching penalties, thus curvature toward the disperse block is induced. Alternatively, samples skewed to higher molar mass do not follow this trend, and curvature away from the disperse block was observed. This influence can be explained qualitatively through the different relative quantities of long and short PS chains. The samples skewed to high molar mass have a large portion of high molar mass PS blocks which can more effectively extend to fill empty space as curvature toward the disperse block is increased. On the other hand, materials with PS blocks skewed to low molecular weight have a substantial fraction of extremely low molecular weight material. These small chains prefer not to stretch to fill empty space, instead remaining relaxed at the interface

which reduces the propensity for the disperse block to be on the inside of interfacial curvature. These results demonstrate the promising utility of MWD shape as a means to tailor block copolymer phase behavior, lending the opportunity to manipulate polymer properties in one reactor setup without altering the chemical composition of the final material.

1.6 Rheological and Mechanical Properties

The effects of M_n, M_w, and $Đ$ on physical properties such as tensile strength, toughness, and viscosity have been studied since the 1960s. While early studies have suggested that the influence of MWD shape should influence physical properties, little work has been done to systematically understand how skew affects rheological and mechanical properties. Many of the first theories used to predict rheological behavior assume a monodisperse system.[83-87] However, early experimental evidence indicated that these theories break down with variations in MWD shapes. Middleman's early work on rheological properties lead to one of the first observations that, "undoubtedly, no single average of molecular weight will be sufficient to allow a unique reduced variable correlation to describe precisely the viscosity curves of a wide class of materials, in view of the fact that the curves are sensitive to the shape of the molecular weight distribution, for which [$Đ$] is not a unique measure."[88]

Characterization of polymers through rheological and mechanical measurements is routinely preformed in the polymer industry to understand the processability of the materials in the melt state. Viscosity is the most important

parameter for describing flow of a polymer. Since polymers are non-Newtonian fluids, they often exhibit shear thinning behaviour which means that at higher frequencies, longer polymer chains begin to orient themselves along the direction of the applied stress (flow). *Đ* and skew of the distribution would unsurprisingly have a significant effect on flow behavior due to the dependence of viscosity on chain entanglements. Based on this hypothesis, there have been many attempts to correlate MWD to melt flow index (MFI), typically reported as the mass of polymer that flows out of a capillary in 10 min with a given applied force (inversely proportional to viscosity). By using the power law relating zero shear viscosity (η_0) to M_w as a basis for mathematical models ($\eta_0 \propto M_w^{3.4}$), many theories have attempted to predict the MWD as well as the MWD shape given the MFI. For instance, some work has shown a correlation of 1/MFI with M_w^x (with x = 3.4 – 3.7) for linear polymers while branched polymers tended to best correlate with –ln(MFI) and M_v (the viscosity average molecular weight).[89] More recently, Pérez-Chantaco and coworkers were able to fit a single equation to accurately predict MWD breadths of both linear and branched polyethylenes with *Đ*s ranging from 2-20.[90]

Similarly, the storage modulus (G') and loss modulus (G") of a polymer blend are also of great importance for understanding polymer properties. The point at which G' = G" is known as the crossover point and occurs at a frequency which corresponds to the shift from viscous to elastic behaviour, and has been used as a surrogate for describing a polymer's MWD.[91] Polymers that have a greater weight fraction of high molecular weight chains (*i.e.* a large M_w) tend to

have a cross-over point at lower frequencies than those with lower molecular weight chains. Similarly, narrow *Đ* samples have been shown to hold a crossover point at higher moduli values.[92] MWD effects on the rheology of Ziegler Natta and metallocene derived high density polyethylene (HDPE) samples have also been studied and have supported this inverse correlation between the crossover modulus (G_c) and *Đ*. More importantly, however, it was shown that higher moments of the MWD, such as the z-average molecular weight, as defined by eqn (1.5), give better correlation with the crossover modulus. Plotting M_z/M_w vs. G_c exhibited a much greater linear fit than *Đ* vs. G_c, thus emphasizing that *Đ* alone is not a true measure of polymer properties.[93]

$$M_Z = \frac{\sum M_i^3 N_i}{\sum M_i^2 N_i} \tag{1.5}$$

Others have also noted that *Đ* changes vastly influence rheological properties, showing that non-Newtonian behaviour seemed to occur at higher shear rates for polymers that were monodisperse than for those with broader dispersities.[90] For example, the relationship between *Đ* and viscoelastic behaviour of polystyrene samples was investigated. It was observed that disperse blends of polystyrene tend to fit the “power law” relationship between stress and shear rate better than the monodisperse blends. By measuring the flow curves of each sample, it became apparent that melt viscosity of broad *Đ* polystyrene holds a stronger correlation to M_w at low shear rates but a stronger correlation to M_n at higher shear rates. Furthermore, at low shear rates,

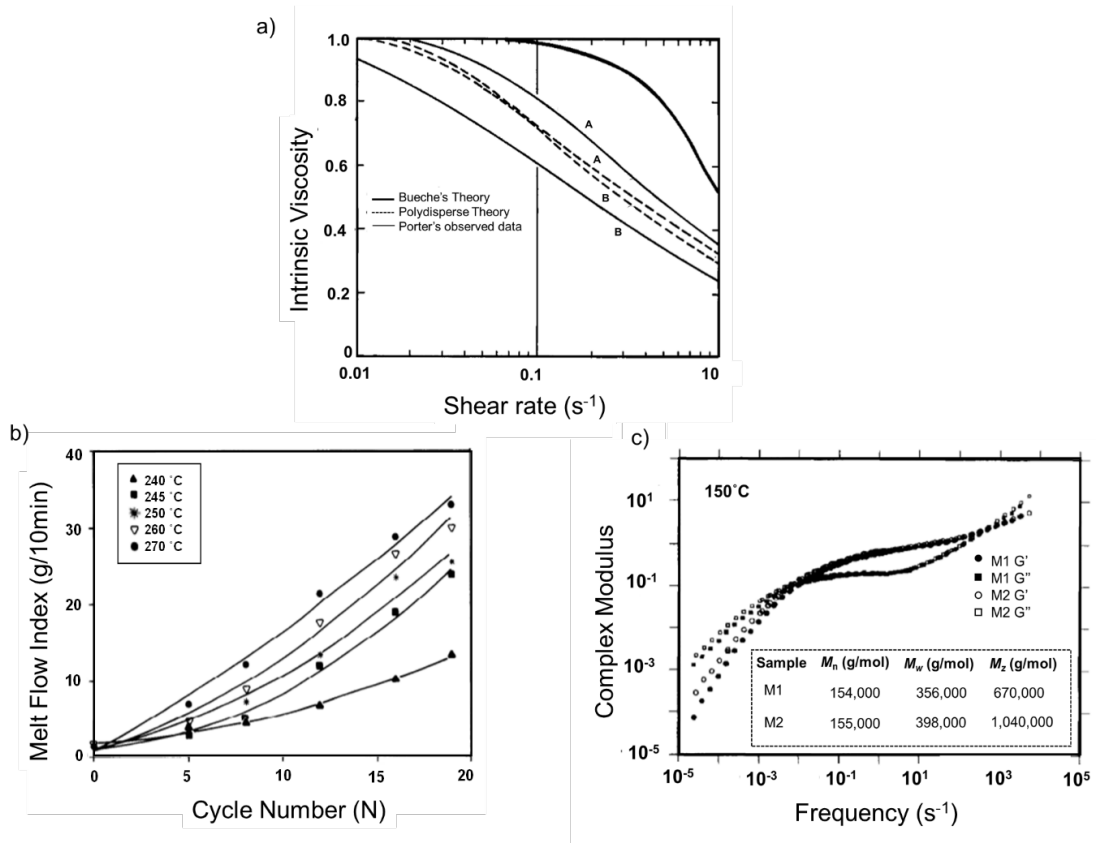

Figure 1.7. Early theoretical and experimental indications that *Đ* and MWD shape have an influence on rheological properties. (a) Intrinsic Viscosity vs. shear rate data for two different solutions of polyisobutylene where B is a more dilute solution than A. Experimental data observed by Porter is compared to Middleman's polydisperse theory and Bueche's original theory. By taking into account dispersity, Middleman's model fits more closely to the experimental data, however, it is still difficult to distinguish between the different isobutylene solutions. Figure adapted from ref. 95 with permission from the Journal of Applied Polymer Science. (b) Melt flow index for polypropylene after N extrusion cycles at various temperatures. Due to an increased amount of chain scission at elevated temperatures, melt flow index increases, corresponding to a decrease in viscosity. Adapted from ref. 98 with permission from Polymer Degradation and Stability (c) comparison of the dynamic modulus master curve for polystyrene blends M1 and M2, showing a large difference in complex modulus (G^*) between M1 and M2 at low frequencies due to the differences in M_z. Figure adapted from ref. 99 with permission from the Journal of Rheology.

polystyrene melts with broader *Đ*s exhibit less temperature sensitive melt viscosities than samples with narrow *Đ*s.[94] To help expand theoretical models in accounting for variations in dispersity, Middleman adapted Bueche's theory to better fit experimental work. By taking dispersity into consideration, Middleman was able to provide a polydisperse model which led to a better correlation to previous experimental viscosity data presented by Porter. While both theoretical models of Bueche and Middleman do not exactly match that of the observed data, the trends are closer when taking into account *Đ* (Figure 1.7a). Most importantly, however, Middleman held one of the earliest observations about the limitations of these theoretical models, explaining that rheological properties are very sensitive to the shape of the MWD and even *Đ* was not a unique measure to explain viscosity curves. [95]

Later mathematical theories were also developed to account for the effects of *Đ* and MWD on the rheological properties of polymer melts. A superposition model was discovered to help define the relationship between MWD and shear viscosity, exemplifying that higher molecular weight fractions dominate viscoelastic behaviour at lower shear rates while low molecular weight fractions are dominant at higher shear rates. This model makes it possible to accurately predict rheological behaviour of blends of homogenous polymers with different MWDs, which is what many earlier models sought to accomplish.[96]

While the first observations about MWD shape and tailing were noted by Middleman, utilizing the change in the MWD to enhance properties has been vastly studied and implemented in developing commercial products through the

technique of polymer blending. Though not in continuous monomodal distributions, blending can be used to alter the MWD by influencing the shape and skew. Incorporation of a small amount of high or low molecular weight chains into a polymer sample can cause considerable variations in processing and properties. For example, taking a narrow polystyrene sample (M_n = 247,000 g/mol, $Đ$ = 1.08) and blending in increasing amounts of low molecular weight polystyrene (M_n = 78,500 g/mol, $Đ$ = 1.08), Rudd was able to show a linear inverse correlation between zero shear viscosity and percent incorporation of low molecular weight PS.[97] Similarly, studies on polypropylene chain-scission have shown that increasing the low molecular weight tail of the MWD can drastically affect rheological properties. At higher extrusion temperatures, chain scission of polypropylene occurs, thus increasing the weight fraction of low molecular polypropylene chains. With a skew towards low molecular weight, fewer entanglements in the polypropylene blend result in a decrease of viscosity as shown by an increase of the melt flow index (Figure 1.7b).[98]

The effects of blending on the rheological behaviour of narrow $Đ$ commercial polystyrene samples were also explored. The dynamic modulus master curves of two blends were measured for narrow PS samples where each blend had roughly the same M_n and M_w but a vastly different M_z, which is especially sensitive to high molecular weight tailing of the MWD. A substantial 3-fold difference in complex modulus between the two blends at low frequencies was observed (Figure 1.7c). This was indicative that the effects of a high molecular weight tail significantly influence the rheological behavior of the

sample.[99] Similarly, industrial production of plastics takes advantage of polymer blending to create materials which allow for easy processing while also rendering the material commercially viable. For example, in industrial processing of polyethylene, blending is used because high molecular weight tailing helps improve material toughness while low molecular weight chains lower viscosity and improve processing. Simply adding a few weight percent of ultra-high molecular weight polyethylene allows for variations in the MWD shape which can improve the stiffness.[100]

More recently, the influence of MWD shape on rheological and tensile properties of poly(styrene-*block*-isoprene) (PS-*b*-PI) was explored where the shape and *Đ* of the PS block varied using the aforementioned method of discrete initiation. Synthesis of these block copolymers allowed for the investigation of the Young's modulus (*E*) of the materials. A library of PS-*b*-PI samples were made in which the PS block was skewed to either high or low molecular weight with varying *Đ.* It was observed that all samples with a PS block skewed to high molecular weight (A_s <1) had consistently higher E values than the corresponding block copolymers with a PS block skewed to low molecular weight (A_s >1). Furthermore, as *Đ* increased and the difference between the A_s values of the corresponding block copolymers widened, the difference in *E* reaches up to 3.5 times greater for the samples with PS skewed to higher molecular weights (Figure 1.8a). This was a clear indication that MWD shape and composition have significant influence over polymer properties.[65]

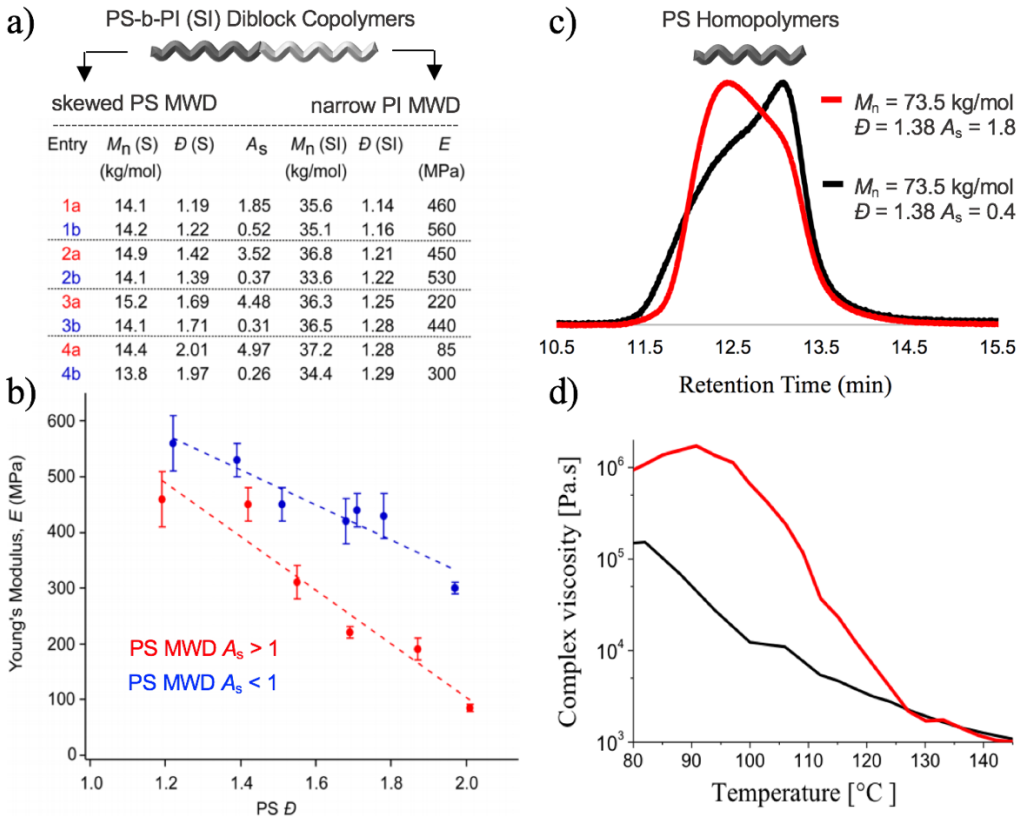

Figure 1.8. The influence of MWD shape on mechanical and rheological properties of homo- and block copolymers while holding M_n and $Đ$ constant. (a) Poly(styrene-*block*-isoprene) block copolymers with the same overall M_n of ~15kg/mol and Young's moduli values for each sample. (b) Plot of polystyrene (PS) $Đ$ vs. E. Blue circles indicate samples with PS blocks that have $A_s < 1$ and red circles indicated samples with PS $A_s > 1$. Amended from ref. 65 with permission from ACS Macro Letters. (c) GPC traces of two polystyrene samples with the same M_n and $Đ$ but opposite skew. (d) Complex viscosity profiles at various temperatures of the two polystyrene samples shown in part (c). Amended from ref. 101 with permission from Macromolecular Rapid Communications.

To further understand the effect of MWD shape on physical properties, rheological testing was performed on polystyrene samples with the same M_n and $Đ$.[101] It was observed that the MWD with a low molecular weight tail (Figure 1.8c, red) held a higher glass transition temperature, an increased stiffness, increased thermal stability and a higher apparent viscosity than the corresponding sample with a high molecular weight tail (Figure 1.8c, black). PS skewed to high molecular weight (Figure 1.8c, black) had a lower T_g of 104 °C relative to the polystyrene sample skewed to low molecular weight (Figure 1.8c, red) (T_g = 111 °C), which is attributed to a variation of chain length composition. A greater amount of smaller molecular weight chains requires less thermal energy to disentangle and flow, thus decreasing the T_g. Furthermore, when looking at the viscosity of the two samples, it was observed that while the shear thinning rates were almost identical between the two samples, the PS samples with MWD tailing toward low molar mass (Figure 1.8d, red) exhibited up to 3 times higher apparent viscosity than that of the PS with skewing toward high molar mass (Figure 1.8d, black) at 25 °C. Even above the T_g, at 150 °C, there was a significant difference between the apparent viscosity of the two samples, with the sample tailing to high molecular weight still maintaining a 2-3 fold increase in the apparent viscosity than the sample tailing to low molecular weight. The observed rheological differences between the two samples is explained through reptation theory where the PS sample which has a higher weight fraction of high molar mass chains retains a greater number of

entanglements, thus reducing the mobility of chains and increasing the viscosity.

Finally, it was shown that by simply changing the shape of the PS sample, the degradation temperature increases by 10 °C between PS samples with opposite MWD shapes, presumably because a larger fraction of high molecular weight chains allowed for the improved thermal stability. By being able to tune the viscosity, T_g, and thermal stability of polymers, optimal processing and property relationships can be achieved. For example, in hot-melt extrusion (HME), very high shear rates and temperatures are used, and the optimal complex viscosity range is 1,000 – 10,000 Pa·s. Since the complex viscosity can be adjusted by changing the shape of the MWD, lower temperatures can be used to reach the same desired viscosity needed for polymer processing.

1.7 Future Outlook

Due to the burgeoning interest in deliberately manipulating polymer properties via molecular weight distributions, a number of methods have been developed to precisely tune the breadth and shape of polymer MWDs for a variety of polymerization processes and monomer types. Reagent feeds as well as controlled initiation and termination processes enable the molar quantities of each chain size in a polymer sample to be precisely controlled.[58-65] Additionally, ultracentrifugation and photocontrolled polymerization strategies offer additional routes to dictating the composition of polymer chain lengths in a given

material.[66-68] Utilizing such synthetic strategies has elucidated that the shape of the distribution function has a profound influence over a vast array of polymer properties. Initial predictions suggested that block copolymer domain spacing should be significantly impacted by the symmetry of the MWD.[5] Experimental studies have shown that domain spacing as well as the overall morphological phase diagram can be predictably manipulated by altering the precise shape and symmetry of the MWD of the final material.[55] In addition to enabling the ability to govern block copolymer self-assembly, the MWD shape also have a significant influence over the rheological and mechanical properties of homo- and block co-polymers. While an impact of MWD shape on these properties has been proposed for decades, only recently have scientists been able to empirically study these structure-property relationships. The entire composition of chain sizes in a polymer alters the viscosity profile, storage and loss moduli, and stiffness of the resultant material.[55,65,80,82]

The studies explored in this review serve as an entry point into the use of MWD shape to tailor polymer properties. This avenue for manipulating polymer function is still in its infancy, but many encouraging opportunities in photonic materials, thermoplastic elastomers, microelectronics, drug-delivery, and plastics await. In this regard, intentionally altering MWDs provides a platform for fine-tuning mechanical properties and processing parameters of commercial polymers without the need to alter the chemical identity of the desired material which renders this strategy promising from an economic perspective. Moreover, the profound influence of MWD on the domain spacing

of block copolymers is highly advantageous for the fabrication of photonic polymers with precisely defined absorption and reflectance windows for applications in energy efficient windows, optical fiber claddings, and coatings for extended material lifetimes.[79,102-106] Additionally, an ability to dictate the phase boundaries of the morphological phase diagram of self-assembled block copolymers using MWDs is promising from the perspective of thermoplastic elastomer applications, materials whose function depends greatly on the physical properties of the constituent monomers as well as the overall microstructure.[65,107-113] Command of the phase behavior of block copolymers in this fashion may also enable more facile access to bicontinuous structures which could find use in microfiltration.[114-117] Furthermore, modifying MWD shape may offer utility to the field of drug-delivery, as the composition of a polymer may provide control over the release of bioactive compounds.[118,119] Lastly, being able to synthetically fine tune polymer MWD shapes could enable the manufacture of an array of polymers with different physical properties but utilizing the same commercial monomers which should have significant industrial and economic benefits in regards to polymer processing and mechanical properties.[120]

Many more fundamental studies are needed to fully elucidate the relationship between molecular weight distribution and polymer structure and function. The ability to extract examples from the literature to investigate the effects of MWD would be greatly beneficial to the realization of this approach and a cohesive theory of MWD shape. In this regard, it would be highly

advantageous for scientists and engineers to report asymmetry factors, skewness, kurtosis, and/or even the higher moments of the distribution function in addition to their molar masses and dispersities. In addition, comparison of MWDs from different SEC instruments poses an additional problem since SEC typically provides *relative* molecular weight information. In this regard, MWDs determined through multi-angle laser light scattering (MALLS) measurements may be more advantageous as they afford *absolute* measurements on polymer molecular weights and MWDs that can be accurately compared across multiple instruments.[121] Moreover, one particularly challenging aspect of this research is the efficient characterization and separation of polymers with distributions of chain lengths or composition in one or multiple blocks by size-exclusion chromatography.[122,123] In this vein, additional effort is necessary in order to expand our analytical toolbox to more effectively characterize complex mixtures of macromolecules. Such efforts are necessary to aid in the advancement of this avenue for dictating polymer function by providing methods for accurate characterization of polymers in which the modified MWD is not in the first block or in which the homo- or block copolymer has multiple MWDs with systematically deviating shapes. Overall, we anticipate that varying polymer MWDs will enable chemists, materials scientists, and engineers to prepare polymers with new properties, previously inaccessible combinations of properties, or to more easily synthesize polymers with desired properties without the need to alter the chemical composition of the target material.

1.8 References

(1) Bates, F. S. et al. Multiblock polymers: panacea or pandora's box? *Science* **336**, 434-440 (2012).

(2) Bates, F. S. et al. Block copolymer thermodynamics: theory and experiment. *Annu. Rev. Phys. Chem.* **41**, 525-557 (1990).

(3) Nichetti, D. et al. Influence of molecular parameters on material processability in extrusion processes. *Polym. Eng. Sci*. **39**, 887-895 (1999).

(4) Collis, N. W. et al. The melt processing of monodisperse and polydisperse polystyrene melts within a slit entry and exit flow. *J. Non-Newtonian Fluid Mech*. **128**, 29-41 (2005).

(5) Lynd, N. A. et al. Polydispersity and block copolymer self-assembly. *Prog. Polym. Sci*. **33**, 875-893 (2008).

(6) Sides, S. W. et al. Continuous polydispersity in a self-consistent field theory for diblock copolymers. *J. Chem. Phys*. *121*, 4974-4986 (2004).

(7) Lynd, N. A. et al. The role of polydispersity in the lamellar mesophase of model diblock copolymers. *J. Polym. Sci., Part B: Polym. Phys*. **45**, 3386-3393 (2007).

(8) Burger C. et al. Polydispersity effects on the microphase-separation transition in block copolymers. *Macromolecules* **23**, 3339-3346 (1990).

(9) Burger C. et al. Polydispersity effects on the microphase-separation transition in block copolymers [Erratum to document cited in CA113(2):7140f] *Macromolecules* **24**, 816 (1991).

(10) Wolff T. et. al Synchrotron SAXS study of the microphase separation transition in diblock copolymers. *Macromolecules* **26**, 1707-1711 (1993).

(11) Fredrickson, G. H. et al. Fluctuation effects in the theory of microphase separation in block copolymers. *J. Chem. Phys*. **87**, 697-705 (1987).

(12) Erukhimovich I. et al. A statistical theory of polydisperse block copolymer systems under weak supercrystallization. *Macromol. Symp.* **81**, 253-315 (1994).

(13) Semenov A., N. Contribution to the theory of microphase layering in block-copolymer melts. *Sov Phys JETP* **61**, 733-742 (1985).

(14) Milner S., T. et al. Effects of polydispersity in the end-grafted polymer brush. *Macromolecules* **22**, 853-861 (1989).

(15) Dobrynin A. et al. Theory of polydisperse multiblock copolymers. *Macromolecule*s, **30**, 4756-4765 (1997).

(16) Spontak R. J. et al. Prediction of microstructures for polydisperse block copolymers, using continuous thermodynamics. *J Polym Sci Part B: Polym Phys* **28**, 1379-1407 (1990).

(17) Bates, F. S. et al. Block copolymers near the microphase separation transition. 3. Small angle neutron scattering study of the homogeneous melt state. *Macromolecules* **18**, 2478-2486 (1985).

(18) Mori, K. et al. Small-angle x-ray scattering from block copolymers in disordered state: 2. Effect of molecular weight distribution. *Polymer* **30**, 1389-1398 (1989).

(19) Sakurai, S. et al. Evaluation of segmental interaction by small-angle x-ray scattering based on the random-phase approximation for asymmetric, polydisperse triblock copolymers. *Macromolecules* **25**, 2679-2691 (1992).

(20) Wolff, T. et al. Synchrotron SAXS study of the microphase separation transition in deblock copolymers. *Macromolecules* **26**, 1707-1711 (1993).

(21) Cooke, D. et al. Effects of polydispersity on phase behavior of diblock copolymers. *Macromolecules* **39**, 6661-6671 (2006).

(22) Leibler, L. Theory of microphase separation in block copolymers. *Macromolecules* **13**, 1602-1617 (1980).

(23) Widin, J. M. et al. Bulk and thin film morphological behavior of broad dispersity poly(styrene-*b*-methyl methacrylate) diblock copolymers. *Macromolecules* **46**, 4472-4480 (2013).

(24) Nguyen, D. et al. Effect of ionic chain polydispersity on the size of spherical ionic microdomains in diblock ionomers. *Macromolecules* **27**, 5173-5181 (1994).

(25) Rane, S. S. et al. Polydispersity index: how accurately does it measure the breath of the molecular weight distribution? *Chem. Mater*. **17**, 926 (2005).

(26) Harrisson, S. The downside of dispersity: why the standard deviation is a better measure of dispersion in precision polymerization. *Polym. Chem*. **9**, 1366-1370 (2018).

(27) Stepto, R. Dispersity in polymer science. *Pure Appl. Chem.* **81**, 351–353 (2009)

(28) Carothers, W. H. Polymerization. *Chem. Rev.* **8**, 353–426 (1931)

(29) Svedberg, T. Sedimentation of molecules in centrifugal fields. *Chem. Rev.* **14**, 1–15 (1934)

(30) Zimm, B. H.; Apparatus and methods for measurement and interpretation of the angular variation of light scattering; preliminary results on polystyrene solutions. *J. Chem. Phys.* **16**, 1099-1116 (1948).

(31) Schulz, G. V. *Z.* About the kinetics of chain polymerization. *Phys. Chem.* **B43**, 25-46 (1939).

(32) Hadjichristidis, N. et al. Polymers with complex architecture by living anionic polymerization. *Chem. Rev*. **101**, 3747-3792 (2001).

(33) Hawker, C. J. et al. New polymer synthesis by nitroxide mediated living radical polymerizations. E. *Chem. Rev*. **101**, 3661-3668 (2001).

(34) Matyjaszewski, K. et al. Atom transfer radical polymerization. *Chem. Rev*. **101**, 2921-2990 (2001).

(35) Lynd, N. A. et al. Theory of polydisperse block copolymer melts: beyond the Schulz-Zimm distribution. *Macromolecules* **41**, 4531-4533 (2008).

(36) Rudin, A. Molecular weight distributions of polymers. *J. Chem. Educ*. **46**, 595 (1969).

(37) Gong, X. et al. Molecular weight distribution characteristics (of a Polymer) derived from a stretched-exponential PGSTE NMR response function-simulation. *Macromol. Chem. Phys.* **213**, 278-284 (2012).

(38) Chem, S-A. et al. The skewness of polymer molecular weight distributions. *J. Poly. Sci.* **21**, 3373-3380 (1983).

(39) Kirkland, J. J. et al. Sampling and extra-column effects in high-performance liquid chromatography; influence of peak skew on plate count calculations. *J. Chromatogr. Sci*. **15**, 303-316 (1977).

(40) Flory, P. J.; Molecular size distribution in linear condensation polymers. *J. Am. Chem. Soc.* **58**, 1877-1885 (1936).

(41) Ryu, J. et al. Molecular weight distribution of branched polystyrene: propagation of Poisson distribution **37**, 8805-8807 (2004).

(42) Peebles, L. H, Jr. In *Molecular Weight Distributions of Polymers*, Interscience, New York (1971).

(43) Noro, A. et al. Effect of composition distribution on microphase-separated structure from BAB triblock copolymers. *Macromolecules* **37**, 3804-3080 (2004).

(44) Matsushita, Y. et al. Molecular weight dependence of lamellar domain spacing of diblock copolymers in bulk. *Macromolecules* **23,** 4313-4316 (1990).

(45) Matsushita Y. et al. Effect of composition distribution on microphase-separated structure from diblock copolymers. *Macromolecules* **36**, 8074-8077 (2003)

(46) Noro A. et al. Effect of molecular weight distribution on microphase-separated structures from block copolymers. *Macromolecules* **38**, 4371-4376 (2005).

(47) Noro A. et al. Chain localization and interfacial thickness in microphase-separated structures of block copolymers with variable composition distributions. *Macromolecules* **39**, 7654-7661 (2006).

(48) Hadziioannou, G. et al. Structural study of mixtures of styrene isoprene two- and three-block copolymers. *Macromolecules* **15**, 267-271 (1982).

(49) Widin, J. M. et al. Unexpected consequences of block polydispersity on the self-assembly of ABA triblock copolymers. *J. Am. Chem. Soc*. **134**, 3834-3844 (2012).

(50) Bendejacq, D. et al. Well-ordered microdomain structures in polydisperse poly(styrene)-poly(acrylic acid) diblock copolymers from controlled radical polymerization. *Macromolecules* **35**, 6645-6649 (2002).

(51) Hustad, P. D. et al. Photonic polyethylene from self-assembled Mesophases of polydisperse Olefin block copolymers. *Macromolecules* **42**, 3788-3794 (2009).

(52) Lynd, N. A. et al. Influence of polydispersity on the self-assembly of diblock copolymers. *Macromolecules* **38**, 8803-8810 (2005).

(53) Lynd, N. A. et al. Effects of polydispersity on the order-disorder transition in block copolymer melts. *Macromolecules* **40**, 8050-8055 (2007).

(54) Plichta, A. et al. Tuning dispersity in diblock copolymers using ARGET ATRP. *Macromol. Chem. Phys.* **213**, 2659-2668 (2012).

(55) Listak, J. et al. Effect of symmetry of molecular weight distribution in block copolymers on formation of “metastable” morphologies. *Macromolecules* **41**, 5919-5927 (2008).

(56) Li, H. et al. Tuning the molecular weight distribution atom transfer radical polymerization using deep reinforcement learning. *Mol. Sys. Des. Eng*. **3**, 496-508 (2018).

(57) Liu, X.; et al. Polymer dispersity control by organocatalyzed living radical polymerization. *Angew. Chem. Int. Ed*. **17**, 5598-5603 (2019).

(58) Meira, G. R. et al. Molecular weight distribution control in continuous “living” polymerizations through periodic operation of the monomer feed. *Polym. Eng. Sci*. **21**, 415-423 (1981).

(59) Alassia, L. M. et al. Molecular weight distribution control in a semibatch living-anionic polymerization. II. Experimental study. *J. Appl. Polym. Sci*. **36**, 481-494 (1988).

(60) Couso, D. A. et al. Molecular weight distribution control in a semibatch living-anionic polymerization. I. Theoretical study *J. Appl. Polym. Sci*. **30**, 3249-3265 (1985).

(61) Farkas, E. et al. Molecular weight distribution design with living polymerization reactions. *Ind. Eng. Chem. Res*. **43**, 7356-7360 (2004).

(62) Seno, K. I. et al. Thermosensitive diblock copolymers with designed molecular weight distribution: Synthesis by continuous living cationic polymerization and micellization behavior. *J. Polym. Sci., Part A: Polym. Chem*. **46**, 2212-2221 (2008).

(63) Litt, M. The effects of inadequate mixing in anionic polymerization: Laminar mixing hypothesis. *J. Polym. Sci*. **58**, 429-454 (1964).

(64) Gentekos, D. T. et al. Beyond dispersity: deterministic control of polymer molecular weight distribution. *J. Am. Chem. Soc*. **138**, 1848-1851 (2016).

(65) Kottisch, V. et al. “Shaping” the future of molecular weight distributions in anionic polymerization. *ACS Macro Lett*. **5**, 796-800 (2016).

(66) Corrigan, N. et al. Controlling molecular weight distributions through photoinduced flow polymerization. *Macromolecules* **50**, 8438-8448 (2017).

(67) Corrigan, N. et al. Copolymers with controlled molecular weight distributions and compositional gradients through flow polymerization. *Macromolecules* **51**, 4553-4563 (2018).

(68) Spinnrock, A. et al. Control of molar mass distribution by polymerization in the analytical ultracentrifuge. *Angew. Chem. Int. Ed*. **57**, 8284-8287 (2018).

(69) Matsen, M. W. Effect of large degrees of polydispersity on strongly segregated block copolymers. *Eur. Phys. J. E: Soft Matter Biol. Phys*. 21, 199-207 (2006).

(70) Woo, S. et al. Domain swelling in ARB-type triblock copolymers *via* self-adjusting effective dispersity. *J. Soft Matter* **13**, 5527-5534 (2017).

(71) Broseta, D. et al. Molecular weight and polydispersity effects at polymer-polymer interfaces. *Macromolecules* **23**, 132-139 (1990).

(72) Fredrickson, G. H. et al. Theory of polydisperse inhomogeneous polymers. *Macromolecules* **36**, 5415-5423 (2003).

(73) Matsen, M. W. Phase behavior of block copolymer/homopolymer blends. *Macromolecules* **28,** 5765-5773 (1995).

(74) Loo, Y.-L. A highly regular hexagonally perforated lamellar structure in quiescent deblock copolymer. *Macromolecules* **38**, 4947-4949 (2005).

(75) Hashimoto, T. et al. Observation of “mesh” and “strut” structures in block copolymer/homopolymer mixtures. *Macromolecules* **25**, 1433-1439 (1992).

(76) Hajduk, D. A. et al. Stability of the perforated layer (PL) phase in diblock copolymer melts. *Macromolecules* **30**, 3788–3795 (1997).

(77) Matsen M. W. Polydispersity-induced macrophase separation in diblock copolymer melts. *Phys Rev Lett* **99**, 148304 (2007).

(78) Matsen, M. W. et al. Unifying weak- and strong-segregation block copolymer theories. *Macromolecules* **29**, 1091-1098 (1996).

(79) Matsen, M. W. et al. Origins of complex self-assembly in block copolymers. *Macromolecules* **29**, 7641-7644 (1996).

(80) Gentekos, D. T. et al. Exploiting molecular meight distribution shape to tune domain spacing in block copolymer thin films. *J. Am. Chem. Soc*. **140**, 4639-4648 (2018).

(81) Busch, P. et al. Lamellar diblock copolymer thin films investigated by tapping mode atomic force microscopy: Molar-mass dependence of surface ordering. *Macromolecules* **36**, 8717-8727 (2003).

(82) Gentekos, D. T. et al. Molecular weight distribution shape as a versatile approach to tailoring block copolymer phase behavior. *ACS Macro Lett*. **7**, 677-682 (2018).

(83) Bueche, F. Influence of rate of shear on the apparent viscosity of A—dilute polymer solutions, and B—bulk polymers. *J. Chem. Phys.* **22**, 1570-1576 (1954).

(84) Rouse P.E. A theory of the linear viscoelastic properties of dilute solutions of coiling polymers. *J. Chem. Phys.* **21**, 1272-1280 (1953).

(85) Pao, Y. H. Dependence of intrinsic viscosity of dilute solutions of macromolecules on velocity gradient. *J. Chem. Phys.* **25**, 1294-1295 (1956).

(86) Pao, Y. H. Hydrodynamic theory for the flow of a viscoelastic fluid. *J. Apply. Phys.* **28**, 591-598 (1957).

(87) Graessley, W.W. Molecular entanglement theory of flow behavior in amorphous polymers. *J. Chem. Phys.* **43**, 2696-2703 (1965).

(88) Dunleavy, J. E. et al. Correlation of shear behavior of solutions of polyisobutylene. *Trans. Soc. Rheol.* **10**, 157-168 (1966).

(89) Bremner, T. et al. Melt flow index values and molecular weight distributions of commercial thermoplastics. *J. Appl. Poly. Sci.* **41**, 1617-1627 (1990).

(90) Rodríguez-Hernández, M.T. et al. Determination of the molecular characteristics of commercial polyethylenes with different architectures

and the relation with the melt flow index. *J. Appl. Poly. Sci.* **104**, 1572-1578 (2007).

(91) Utracki, L.A et al. Linear low density polyethylenes and their blends: Part 2. Shear flow of LLDPE's. *Polym. Eng. Sci.* **27**, 367-379 (1987).

(92) Aho, J. et al. Rheology as a tool for evaluation of melt processability of innovative dosage forms. *Int. J. Pharm.* **494**, 623-642 (2015).

(93) Ansari, M. et al. Rheology of Ziegler-Natta and metallocene high-density polyethylenes: broad molecular weight distribution effects. *Rheol. Acta* **50**, 17-27 (2011).

(94) Ballman, R. L. et al. The influence of molecular weight distribution on some properties of polystyrene melt. *J. Polym. Sci., Part A: Polym. Chem* **2**, 3557-3575 (1964).

(95) Middleman, S. Effect of molecular weight distribution on viscosity of polymeric fluids. *J. Apply. Poly. Sci.* **11**, 417-424 (1967).

(96) Nichetti, D. et al. Viscosity model for polydisperse polymer melts. *J. Rheol.* **42***,* 951-969 (1998).

(97) Rudd J. The effect of molecular weight distribution on the rheological properties of polystyrene. *J. Polym. Sci., Part A: Polym. Chem*, **44**, 459-474 (1960).

(98) González-González, V. A. et al. Polypropylene chain scissions and molecular weight changes in multiple extrusion. *Polym. Degrad. Stab.* **60***,* 33-42 (1998).

(99) Wasserman, S.H. et al. Effects of polydispersity on linear viscoelasticity in entangled polymer melts. *J. Rheol.* **36**, 543-572 (1992).

(100) Stürzel, M. et al. From multisite polymerization catalysis to sustainable materials and all-polyolefin composites. *Chem. Rev.* **116**, 1398-1433 (2016).

(101) Nadgorny, M. et al. Manipulation of molecular weight distribution shape as a new strategy to control processing parameters. *Macromol. Rapid. Commun.* **38**, 1700352 (2017).

(102) Fink, Y. et al. Block copolymers as photonic bandgap materials. *J. Lightwave Technol.* **17**,1963-1969 (1999).

(103) Stefik, M. et al. Block copolymer self-assembly for nanophotonics. *Chem. Soc. Rev.* **44**, 5076-5091 (2015).

(104) Kang, Y. et al. Broad-wavelength-range chemically tunable block-copolymer photonic gels. *Nat. Mater.* **6**, 957-960 (2007).

(105) Kang, C. et al. Full color stop bands in hybrid organic/inorganic block copolymer photonic gels by swelling-freezing. *J. Am. Chem. Soc.* **131**,7538-7539 (2009).

(106) Urbas, A. M. et al. Bicontinuous cubic block copolymer photonic crystals. *Adv. Mater.* **14**, 1850-1853 (2002).

(107) Park, M. et al. Block copolymer lithography: Periodic arrays of ~10^{11} holes in 1 square centimeter. *Science* **276**, 1401-1404 (1997).

(108) Honeker, C. C. et al. Impact of morphological orientation in determining mechanical properties in triblock copolymer systems. *Chem. Mater.* **8**, 1702-1714 (1996).

(109) Bang, J. et al. Block copolymer nanolithography: translation of molecular level control to nanoscale patterns. J. *Adv. Mater.* **21**, 4769-4792 (2009).

(110) Ruiz, R. et al. Density multiplication and improved lithography by directed block copolymer assembly. *Science* **321**, 936-939 (2008).

(111) Kim, S. O. et al. Epitaxial self-assembly of block copolymers on lithographically defined nanopatterned substrates. *Nature* **424**,411-414 (2003).

(112) Chen, L. et al. Robust nanoporous membranes templated by a doubly reactive block copolymer. *J. Am. Chem. Soc.* **129**, 13786-13787 (2007).

(113) Quirk, R. et al. In *Thermoplastic Elastomers*, 2nd ed.; Hanser Publishers: New York 72–100 (1996).

(114) Jackson, E. A. et al. Nanoporous membranes derived from block copolymers; from drug delivery to water filtration. *ACS Nano* **4**, 3548-3553 (2010).

(115) Ahn, H. et al. Nanoporous block copolymer membranes for ultrafiltration: A simple approach to size tunability. *ACS Nano* **8**, 11745-11752 (2014).

(116) Zhao, D. et al. Triblock copolymer syntheses of mesoporous silica with periodic 50 to 300 Angstrom pores. *Science* **279**, 548-552 (1998).

(117) Liang, C. et. al. Synthesis of a large-scale highly ordered porous carbon film by self-assembly of block copolymers. *Angew. Chem. Int. Ed.* **43**, 5785-5789 (2004).

(118) Jeong, B. et al. Biodegradable block copolymers as injectable drug-delivery systems. *Nature* **388**, 860-862 (1997).

(119) Kataoka, K. et al. Block copolymer micelles for drug delivery: Design, characterization and biological significance. *Adv. Drug Deliv Rev.* **64**, 37-48 (2012).

(120) Rubber Industry Sees Value in MWD. Chem. Eng. News 1965, 43, 40.

(121) Wyatt, P. J. Light scattering and the absolute characterization of macromolecules. *Anal. Chim. Acta*. **272**, 1-40 (1993).

(122) Lange, H. et al. Gel permeation chromatography in determining molecular weights of lignins: Critical aspects revisited for improved utility in the development of novel materials. *ACS Sustain. Chem. Eng.* **4**, 5167-5180 (2016).

(123) Determann, H. In *Gel Chromatography · Gel Filtration · Gel Permeation · Molecular Sieves*, 2nd ed.; Springer: New York (1969).

CHAPTER 2
BEYOND DISPERSITY: DETERMINISTIC CONTROL OF POLYMER MOLECULAR WEIGHT DISTRIBUTIONS

2.1 Abstract

The breadth of the molecular weight distributions (MWD) of polymers influences their physical properties; however, no synthetic methods allow precise control of the exact shape and composition of a distribution. We report a modular strategy that enables deterministic control over polymer MWD through temporal regulation of initiation in nitroxide-mediated polymerization reactions. This approach is applicable to any controlled polymerization that uses a discrete initiator, and it allows the use of MWD composition as a parameter to tune material properties.

2.2 Introduction

The dispersity ($Đ$) of a polymer sample, which is the ratio of the weight-average (M_w) and number-average (M_n) molecular weights, has a profound influence on processability[1,2] and block copolymer properties.[3-9] However, $Đ$ is not a rigorous description of the distribution of polymer chain sizes in a given sample and provides information only about the relative span of molecular weights.[10] Importantly, variations in the shape of a molecular weight distribution (MWD) are postulated to have a marked influence on polymer properties as well.[11] Therefore, the development of a strategy to control absolute MWD composition would allow the investigation of the relationship between MWD

shape and polymer function and facilitate the development of more robust materials for applications in areas such as nanolithography, photonics, filtration, and thermoplastic elastomers.[12] Herein, we report a modular synthetic strategy that provides predictable access to functional polymers with precisely defined MWDs.

Based on the importance of MWD on polymer properties, a small number of methods have been developed to govern *Đ*. Blending polymers with various molecular weights is one strategy; however, the preparation of these materials is tedious, requiring the synthesis of multiple polymer samples.[13-15] Moreover, this protocol leads to multimodal compositions, which are undesirable. A second tactic involves the use of uncontrolled polymerizations to give dispersities of ~2. However, these methods provide no control over M_n, *Đ*, or the shape of the distribution.[16-18] Last, by taking advantage of polymer growth kinetics, Matyjaszewski and Hillmyer developed various methods to adjust *Đ* in radical, ring-opening, and anionic polymerization.[19-22] Despite the control achieved by these methods, they modify only the relative breadth of the polymer chain lengths and provide no means for controlling the symmetry and shape of the final molecular composition.

2.3 Results and Discussion

We sought a modular strategy that would allow both fine-tuning of the breadth and shape of a distribution and control of M_n in a wide range of

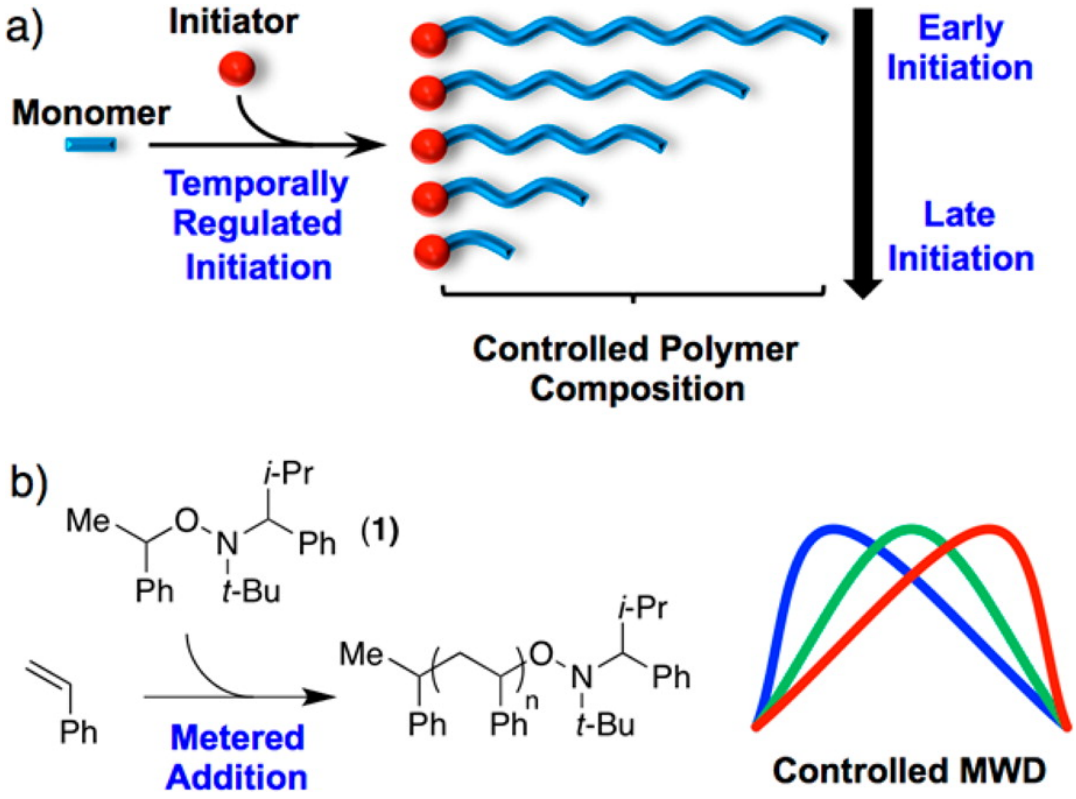

Figure 2.1. (a) Temporal regulation of chain initiation for deterministic control of the shape and composition of polymer molecular weight distributions (MWDs), and (b) the application of this strategy to nitroxide-mediated polymerizations through metered addition of **1**.

monomer types and polymerization classes. We envisaged that precise temporal generation of new polymer chains in a reaction would be a straightforward approach to address this challenge. Specifically, we reasoned that introducing initiators to a controlled polymerization reaction at specific times and rates would allow deterministic control over the exact molar quantities of individual polymer chain lengths in a final sample (Figure 2.1a). Importantly, this modular strategy would be applicable to any controlled polymerization that uses a discrete initiating species and, therefore, would provide well-defined polymer compositions for an extensive set of functional materials.

Nitroxide-mediated polymerization (NMP) was selected to test our hypothesis because of its simplicity, functional group tolerance, and use of stable initiators.[23-25] Preliminary studies focused on regulating *Đ* through metered addition of an alkyl nitroxide initiator (**1**) for the polymerization of styrene (Figure 2.1b).[26] The total molar quantity of initiator and the final conversion of the monomer were held constant for each polymerization, but the time of initiator addition was varied. Introducing the entire amount of **1** at the beginning of the reaction resulted in well-defined polystyrene (PS) with an M_n of 6.0 kg/mol and a *Đ* of 1.17. Intriguingly, adding **1** at constant rates between 0.5 and 2.5 h effectively broadened the *Đ* of the final polymers from 1.29 to 2.02 while maintaining M_n (Figure 2.2a). The size-exclusion chromatography (SEC) traces of these reactions show continuous monomodal MWDs where the molar mass at the peak maximum (M_p) increases with addition time. These results

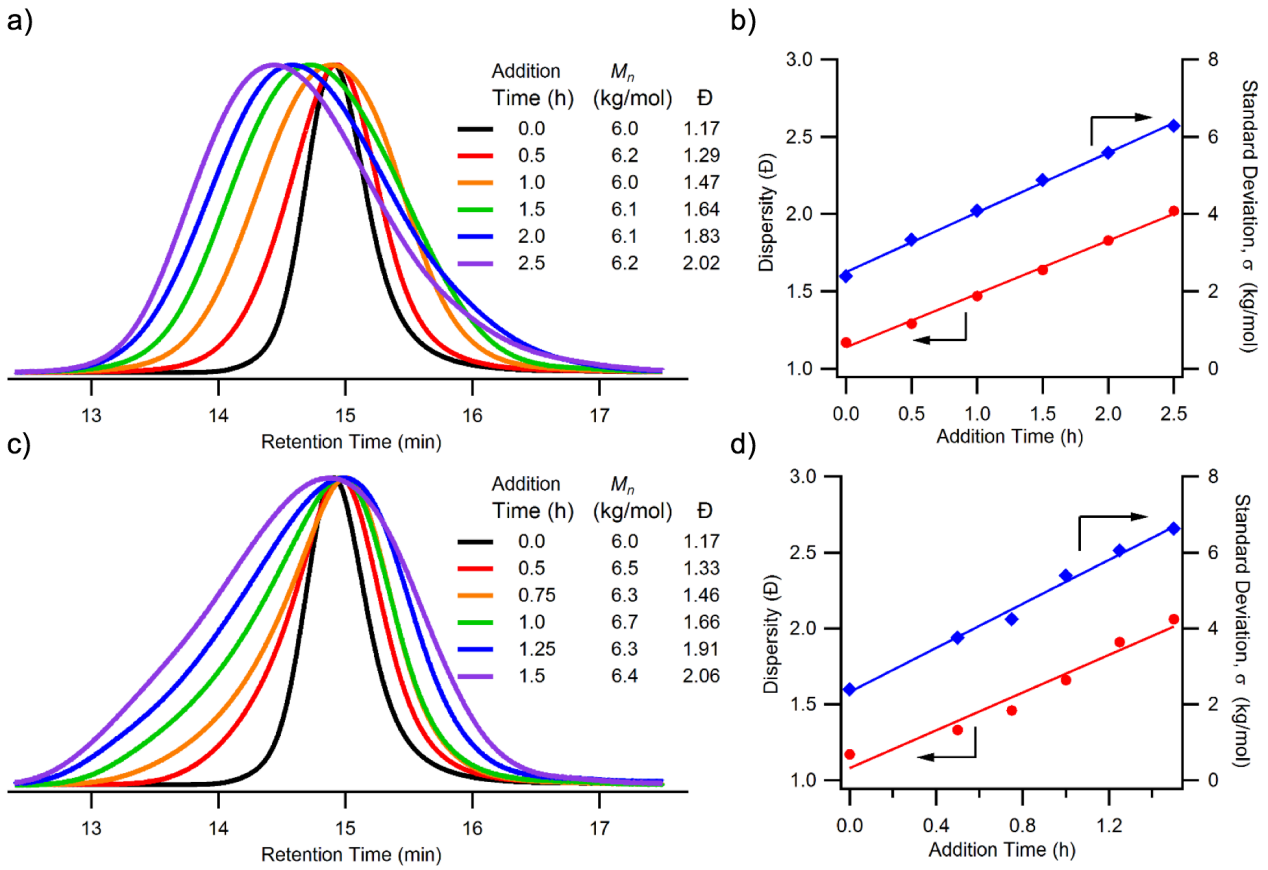

Figure 2.2. Varying the breadth of polystyrene MWDs through (a) constant or (c) linearly increasing addition rates of **1** to tune the shape of the MWDs, and (b,d) show the linear relationship between dispersity/standard deviation with initiator addition time.

clearly demonstrate that the breadth of a MWD can be broadened by controlling the relative rate of initiation to polymerization through metered addition of **1**.

For this same data, plotting *Đ* versus time of initiator addition reveals a linear relationship (Figure 2.2b), which shows that MWD breadth can be predictably tuned. Moreover, because we have demonstrated that we can maintain M_n while regulating *Đ*, we inferred that the absolute breadth of our distribution is precisely controlled.[10,27] In support of this inference, Figure 2.2b shows that standard deviation (σ) increases linearly with addition time.

Encouraged by the excellent control observed when adding **1** at a constant rate, we next investigated the ability to regulate the shape of a MWD. We expected that modulation of the addition rate throughout the course of the reaction would give precise control over the degree of polymerization of the polymer chains in our final material and, therefore, would dictate the shape of the distribution. To investigate this hypothesis, in a procedure analogous to the reactions above, we added a set quantity of **1** at linearly increasing addition rates; we expected that these addition rate profiles would shift the overall peak shape to lower molecular weights. Indeed, all reactions gave polymers with similar M_n values, and *Đ* and σ both increased linearly with addition time (Figure 2.2c,d). More important, the SEC traces revealed that the M_p values for these polymers remain relatively constant; this result is a direct contrast with the values for polymers produced through constant addition rates of **1**, in which M_p shifted to higher molecular weights with increasing *Đ*. These results

illustrate that the shape of a MWD can be systematically varied while M_n and $Đ$ are controlled.

To highlight more thoroughly the differences in MWD shapes that can be accessed with this method, we synthesized more symmetrical distributions by using a nonlinearly increasing addition rate of **1** and compared them to the distributions of the polymers discussed above. Strikingly, gel permeation chromatograph traces of materials from three different addition classes (Figure 2.3a) shows polymers with similar M_n and $Đ$ values but significantly disparate chain length compositions (Figure 2.3b). Clearly these polymers cannot be distinguished by using M_n and $Đ$, and therefore, we used asymmetry factor (A_s) as a metric to identify the MWD differences, where values of ~1 signified symmetrical peaks, and values of >1 or <1 indicated distributions skewed to higher or lower molecular weights, respectively.[28] Figure 2.3b illustrates that A_s accurately depicted the MWD shapes using a single parameter, with the three PS samples having A_s values of 1.5, 1.1, and 0.6. It should be noted that skewness and kurtosis, which are higher moments of the distribution, can also be used to describe MWD shape (see Chapter 2 Appendix).[29]

Importantly, by changing the total molar quantity of **1**, various M_n values can be predictably targeted while maintaining excellent control over the breadth and shape of the MWD (see Chapter 2 Appendix for details). For example, Figure 2.4 shows two polymers with molar masses of 34 kg/mol and $Đ$ values of 1.79 but with variable MWD shapes.

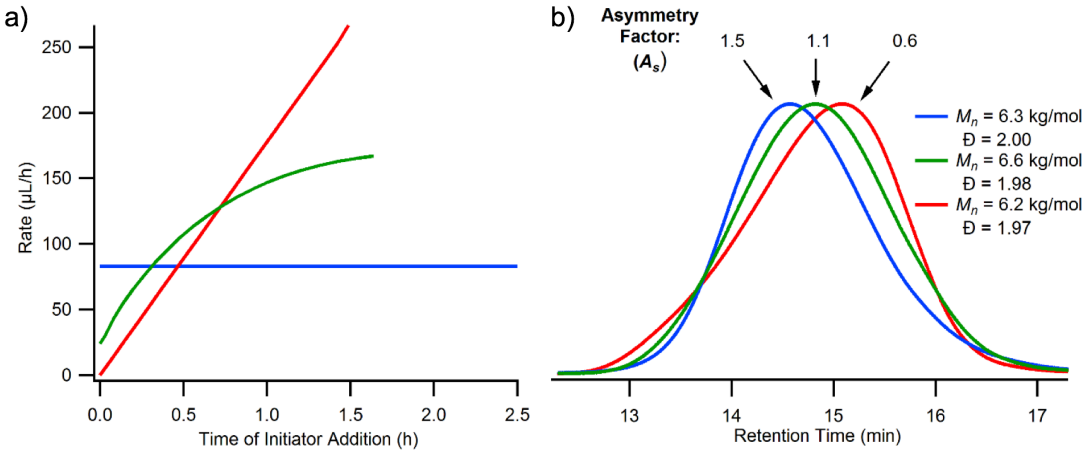

Figure 2.3. Synthesis of polymer samples with similar M_n and $Đ$ values but variable MWD shapes. (a) Addition rate profile of **1** and (b) size-exclusion chromatography (SEC) traces of the three polystyrene samples.

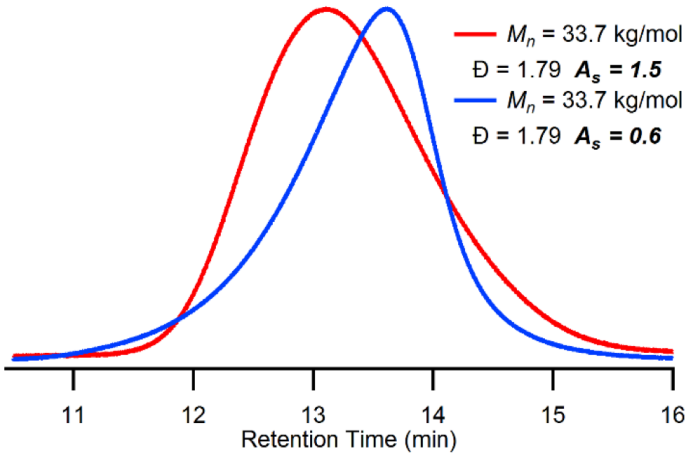

Figure 2.4. Targeting higher-molecular-weight polystyrene while maintaining control over the shape and breadth of the MWD.

The use of living processes in our method is a major advantage that enables further derivatization of the final polymers to form functional materials. Specifically, the excellent chain-end fidelity in NMP reactions gives facile access to block copolymers. To provide evidence that we maintained the nitroxide chain ends in our polymerization reactions, we used two PS samples with identical M_n and $Đ$ values but different MWDs and chain-extended them with isoprene.[30,31] In both cases we observed efficient formation of poly(styrene-*b*-isoprene) block copolymers without remaining macroinitiator (Figure 2.5). In addition, to show the modularity of this approach a bifunctional nitroxide initiator was utilized to grow poly(styrene-*b*-valerolactone) block copolymers while controlling MWD shape (see Chapter 2 Appendix for details).[32]

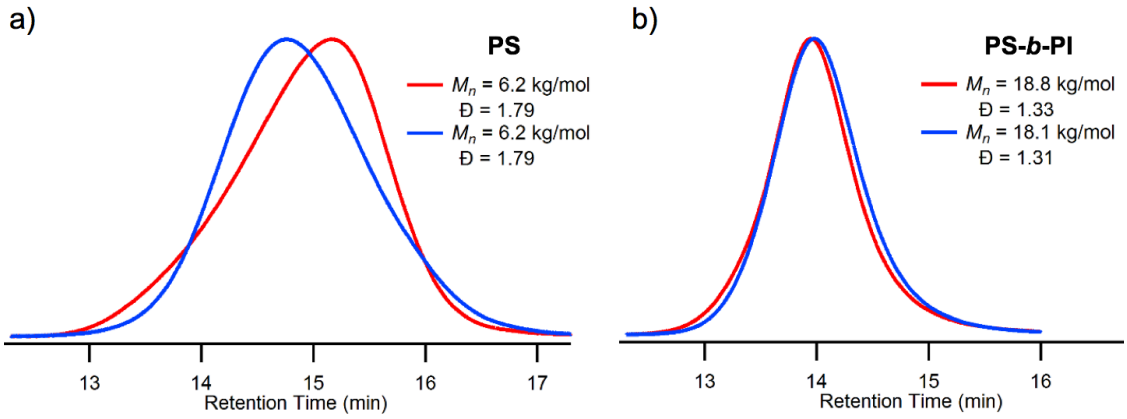

Figure 2.5. Chain extension of polystyrene (PS) macroinitiators synthesized via temporally regulated initiation to give poly(styrene-b-isoprene) (PS-*b*-PI) polymers.

We emphasize that this method is not limited to the synthesis of monomodal polymers with *Đ* values of <2. By adjusting the rate of addition of **1**, we can unambiguously make PS with multimodal distributions or dispersities up to ~4.0 while controlling M_n (Figure 2.6). We anticipate that this adjustability will prove useful in tuning polymer processability, and it further exemplifies the versatility of our approach.

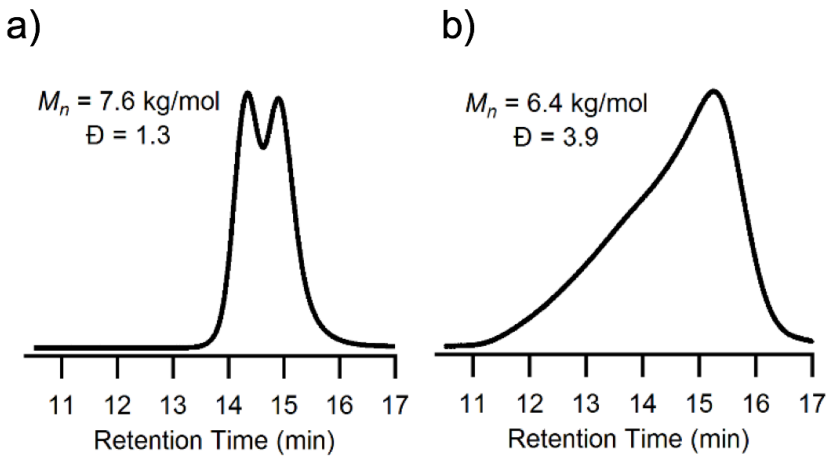

Figure 2.6. Synthesis of polystyrene samples with (a) a bimodal MWD or (b) a *Đ* of 3.9 by using temporally regulated initiation.

2.4 Conclusion

In summary, we have developed a method for precisely controlling the M_n, *Đ*, and shape of a polymer MWD by temporally regulating chain initiation in a controlled NMP process. Using this protocol, we prepared various PS samples that are indistinguishable based solely on the mean and breadth of

their MWDs but have variable chain-length compositions. This modular strategy, which should be applicable in any controlled polymerization process that uses a discrete initiating species,[33] will enable the synthesis of materials that are defined beyond dispersity and will facilitate fundamental studies of polymer MWD shape and physical properties. We anticipate that this general method will change the way MWD is viewed and allow distribution shape to be used as a parameter to tune material function.

2.5 References

(1) Nichetti, D.; Manas-Zloczower, I. *Polym. Eng. Sci.* **1999**, 39, 887.

(2) Collis, N. W.; Mackley, M. R. *J. Non-Newtonian Fluid Mech*. **2005**, 128, 29.

(3) Lynd, N. A.; Meuler, A. J.; Hillmyer, M. A. *Prog. Polym. Sci*. **2008**, 33, 875.

(4) Sides, S. W.; Fredrickson, G. H. *J. Chem. Phys*. **2004**, 121, 4974.

(5) Lynd, N. A.; Hamilton, B. D.; Hillmyer, M. A. *J. Polym. Sci., Part B: Polym. Phys*. **2007**, 45, 3386.

(6) Fredrickson, G. H.; Helfand, E. *J. Chem. Phys*. **1987**, 87, 697.

(7) Cooke, D. M.; Shi, A.-C. *Macromolecules* **2006**, 39, 6661.

(8) Leibler, L. *Macromolecules* **1980**, 13, 1602.

(9) Widin, J. M.; Kim, M.; Schmitt, A. K.; Han, E.; Gopalan, P.; Mahanthappa, M. K. *Macromolecules* **2013**, 46, 4472.

(10) Rane, S. S.; Choi, P. *Chem. Mater*. **2005**, 17, 926.

(11) Lynd, N. A.; Hillmyer, M. A.; Matsen, M. W. *Macromolecules* **2008**, 41, 4531.

(12) Matyjaszewski, K.; Gnanou, Y.; Leibler, L. Macromolecular Engineering: From Precise Macromolecular Synthesis to Macroscopic Materials Properties and Applications; Wiley-VCH: Weinheim, Germany, 2007.

(13) Noro, A.; Iinuma, M.; Suzuki, J.; Takano, A.; Matsushita, Y. *Macromolecules* **2004**, 37, 3804.

(14) Nguyen, D.; Zhong, X.-F.; Williams, C. E.; Eisenberg, A. *Macromolecules* **1994**, 27, 5173.

(15) Hadziioannou, G.; Skoulios, A. *Macromolecules* **1982**, 15, 267.

(16) Hustad, P. D.; Marchand, G. R.; Garcia-Meitin, E. I.; Roberts, P. L.; Weinhold, J. D. *Macromolecules* **2009**, 42, 3788.

(17) Widin, J. M.; Schmitt, A. K.; Schmitt, A. L.; Im, K.; Mahanthappa, M. K. *J. Am. Chem. Soc.* **2012**, 134, 3834.

(18) Bendejacq, D.; Ponsinet, V.; Joanicot, M.; Loo, Y. L.; Register, R. A. *Macromolecules* **2002**, 35, 6645.

(19) Lynd, N. A.; Hillmyer, M. A. *Macromolecules* **2005**, 38, 8803.

(20) Plichta, A.; Zhong, M.; Li, W.; Elsen, A. M.; Matyjaszewski, K. *Macromol. Chem. Phys*. **2012**, 213, 2659.

(21) Listak, J.; Jakubowski, W.; Mueller, L.; Plichta, A.; Matyjaszewski, K.; Bockstaller, M. R. *Macromolecules* **2008**, 41, 5919.

(22) Lynd, N. A.; Hillmyer, M. A. *Macromolecules* **2007**, 40, 8050.

(23) Nicolas, J.; Guillaneuf, Y.; Lefay, C.; Bertin, D.; Gigmes, D.; Charleux, B. *Prog. Polym. Sci*. **2013**, 38, 63.

(24) Hawker, C. J.; Bosman, A. W.; Harth, E. Chem. Rev. 2001, 101, 3661.

(25) Grubbs, R. B. *Polym. Rev*. **2011**, 51, 104.

(26) Benoit, D.; Chaplinski, V.; Braslau, R.; Hawker, C. J. J*. Am. Chem. Soc*. **1999**, 121, 3904.

(27) Rudin, A. The Elements of Polymer Science and Engineering, 2nd ed.; Academic Press: San Diego CA, 1999.

(28) Kirkland, J. J.; Yau, W. W.; Stoklosa, H. J.; Dilks, C. H. J. *J. Chromatogr. Sci.* **1977**, 15, 303.

(29) Rudin, A. *J. Chem. Educ*. **1969**, 46, 595.

(30) Ott, C.; Lohmeijer, B. G. G.; Wouters, D.; Schubert, U. S. *Macromol. Chem. Phys.* **2006**, 207, 1439.

(31) Benoit, D.; Harth, E.; Fox, P.; Waymouth, R. M.; Hawker, C. J. *Macromolecules* **2000**, 33, 363.

(32) Bosman, A. W.; Vestberg, R.; Heumann, A.; Frechet, J. M. J.; Hawker, C. J. *J. Am. Chem. Soc*. **2003**, 125, 715.

(33) To support this claim, we extended the scope of this method to atom transfer radical polymerization; see Chapter 1 Appendix

2.6 Appendix

Experimental

General Reagent Information

All reactions were carried out under a nitrogen atmosphere. Styrene (99+%) and methyl methacrylate (99+%) were purchased from Sigma Aldrich and filtered over a column of basic alumina to remove the stabilizer before use. Isoprene (99%), N,N,N',N",N"- Pentamethyldiethylenetriamine (PMDETA), and ethyl 2-bromoisobutyrate (EBiB) were purchased from Sigma Aldrich and were distilled from calcium hydride under nitrogen prior to use. The initiator, 2,2,5-Trimethyl-3-(1-phenylethoxy)-4-phenyl-3-azahexane (1) and 2,2,5-Trimethyl-4-phenyl-3-azahexane-3-nitroxide (TIPNO) were purchased from Santa Cruz Biotechnology and Sigma Aldrich, respectively, and were used as received. Copper(I) bromide and copper(II) bromide were purchased from Alfa Aesar and Strem Chemical, respectively, and used as received. Toluene was purchased from J.T. Baker and was purified by vigorous purging with argon for 2 h, followed by passing through two packed columns of neutral alumina under argon pressure. Acetone was purchased from Macron and used as received.

General Analytical Information

Polymer samples were analyzed using a Tosoh EcoSEC HLC 8320GPC system with two SuperHM-M columns in series at a flow rate of 0.350 mL/min with THF as the eluting solvent. Number average molecular weight (M_n), weight average molecular weight (M_w), dispersity ($Đ$) values, and asymmetry factors (A_s) were calculated from refractive index chromatograms against TSKgel

polystyrene standards. Conversions were determined from NMR spectra recorded on a Varian Mercury-300 NMR spectrometer in $CDCl_3$.

General Procedure for Styrene Polymerization

A vial, fitted with a screw cap and Teflon septum, was charged with styrene (420 µL, 3.67 mmol). In the case of small scale reactions and longer addition times a small amount of 2,2,5-Trimethyl-4-phenyl-3-azahexane-3-nitroxide (TIPNO radical) was added to reduce autopolymerization (see below for details on individual rate profiles). The styrene was degassed by three freeze-pump-thaw cycles followed by backfilling with a nitrogen atmosphere. A solution of the initiator (1) (36 mg, 0.11 mmol) in styrene (633 µL, 5.52 mmol) was prepared and degassed in the same fashion. 220 µL of the initiator solution was then drawn into a 1 mL syringe that had been flushed with N_2. The syringe was mounted onto a New Era NE-4000 Double Syringe Pump and programmed to the appropriate addition rate profile (see details below). The needle was quickly transferred from the stock solution to the reaction vial. Immediately after introducing the needle tip to the reaction mixture, the vial was submerged into an oil bath at 120 ºC and the syringe pump addition was started. After the desired reaction time, the vial was removed from the oil bath and briefly submerged in liquid nitrogen to stop the reaction. A small aliquot was removed from the reaction mixture and analyzed by GPC and ^1H NMR. The remaining reaction mixture was diluted with toluene (4.0 mL) and then concentrated on a

rotary evaporator. This process was repeated a total of three times and the final white solid was dried on high vacuum overnight.

Procedure for Figure 2.2a:

Constant Addition Rate Profiles Polystyrene samples were prepared according to the general procedure using the following constant addition rates and total volumes. Constant rate additions longer than 1.5 h contained 4 μL of initiator solution prior to degassing.

Table 2.1. Constant Rate Additions

Addition Time (h)	Rate (μL/h)	Total Volume (μL)	Reaction Time (min)
0	N/A	207.0	120
0.5	414.0	207.0	120
1.0	207.0	207.0	120
1.5	138.0	207.0	135
2.0	103.5	207.0	135
2.5	82.8	207.0	150

Procedure for Figure 2.2c: Linearly Ramped Addition Rate Profiles

Polystyrene samples were prepared according to the general procedure using the following linearly ramped addition rates. Addition rates were programmed as a sequence of 20 steps with defined rates and volume added per step into a New Era NE-4000 Double Syringe Pump. Once the syringe pump addition was finished, the needle was left in the reaction mixture until the end of the reaction. In the case of Table 1.4-1.6 a stock solution of TIPNO (6.5 mg, 0.03 mmol) in styrene (1.2 mL, 10.47 mmol) was prepared and 2 μL of the TIPNO solution was distributed to each reaction vessel before degassing.

Table 2.2. 0.5 h Linearly Ramped Rate

Rate (µL/h)	Time (h)	Total Time (h)	Volume per Step (µL)	Total Volume (µL)
40	0.025	0.025	1	1
80	0.025	0.050	2	3
120	0.025	0.075	3	6
160	0.025	0.100	4	10
200	0.025	0.125	5	15
240	0.025	0.150	6	21
280	0.025	0.175	7	28
320	0.025	0.200	8	36
360	0.025	0.225	9	45
400	0.025	0.250	10	55
440	0.025	0.275	11	66
480	0.025	0.300	12	78
520	0.025	0.325	13	91
560	0.025	0.350	14	105
600	0.025	0.375	15	120
640	0.025	0.400	16	136
680	0.025	0.425	17	153
720	0.025	0.450	18	171
760	0.025	0.475	19	190
800	0.021	0.496	17	207

Total Reaction Time : 100 min

Table 2.3. 0.75 h Linearly Ramped Rate

Rate (µL/h)	Time (h)	Total Time (h)	Volume per Step (µL)	Total Volume (µL)
26.67	0.037	0.037	1	1
53.34	0.037	0.075	2	3
80.01	0.037	0.112	3	6
106.7	0.037	0.150	4	10
133.4	0.037	0.187	5	15
160.0	0.037	0.225	6	21
186.7	0.037	0.262	7	28
213.4	0.037	0.300	8	36
240.0	0.037	0.337	9	45
266.7	0.037	0.375	10	55
293.4	0.037	0.412	11	66
320.0	0.037	0.450	12	78
346.7	0.037	0.487	13	91
373.4	0.037	0.525	14	105
400.0	0.037	0.562	15	120
426.7	0.037	0.600	16	136

453.4	0.037	0.637	17	153
480.1	0.037	0.675	18	171
506.7	0.037	0.712	19	190
533.4	0.032	0.744	17	207

Total Reaction Time : 105 min

Table 2.4. 1.0 h Linearly Ramped Rate

Rate (µL/h)	Time (h)	Total Time (h)	Volume per Step (µL)	Total Volume (µL)
20	0.050	0.050	1	1
40	0.050	0.100	2	3
60	0.050	0.150	3	6
80	0.050	0.200	4	10
100	0.050	0.250	5	15
120	0.050	0.300	6	21
140	0.050	0.350	7	28
160	0.050	0.400	8	36
180	0.050	0.450	9	45
200	0.050	0.500	10	55
220	0.050	0.550	11	66
240	0.050	0.600	12	78
260	0.050	0.650	13	91
280	0.050	0.700	14	105
300	0.050	0.750	15	120
320	0.050	0.800	16	136
340	0.050	0.850	17	153
360	0.050	0.900	18	171
380	0.050	0.950	19	190
400	0.043	0.993	17	207

Total Reaction Time : 120 min

Table 2.5. 1.25 h Linearly Ramped Rate

Rate (µL/h)	Time (h)	Total Time (h)	Volume per Step (µL)	Total Volume (µL)
16	0.063	0.063	1	1
32	0.063	0.125	2	3
48	0.063	0.188	3	6
64	0.063	0.250	4	10
80	0.063	0.313	5	15
96	0.063	0.375	6	21
112	0.063	0.438	7	28
128	0.063	0.500	8	36
144	0.063	0.563	9	45

160	0.063	0.625	10	55
176	0.063	0.688	11	66
192	0.063	0.750	12	78
208	0.063	0.813	13	91
224	0.063	0.875	14	105
240	0.063	0.938	15	120
256	0.063	1.000	16	136
272	0.063	1.063	17	153
288	0.063	1.125	18	171
304	0.063	1.188	19	190
320	0.053	1.241	17	207

Total Reaction Time : 120 min

Table 2.6. 1.5 h Linearly Ramped Rate

Rate (µL/h)	Time (h)	Total Time (h)	Volume per Step (µL)	Total Volume (µL)
13.33	0.075	0.075	1	1
26.66	0.075	0.150	2	3
39.99	0.075	0.225	3	6
53.32	0.075	0.300	4	10
66.65	0.075	0.375	5	15
79.98	0.075	0.450	6	21
93.31	0.075	0.525	7	28
106.6	0.075	0.600	8	36
120	0.075	0.675	9	45
133.3	0.075	0.750	10	55
146.6	0.075	0.825	11	66
159.9	0.075	0.900	12	78
173.3	0.075	0.975	13	91
186.6	0.075	1.050	14	105
200	0.075	1.125	15	120
213.3	0.075	1.200	16	136
226.6	0.075	1.275	17	153
239.9	0.075	1.350	18	171
253.3	0.075	1.425	19	190
266.6	0.064	1.489	17	207

Total Reaction Time : 120 min

Procedure for Figure 2.3: Similar M_n and $Đ$ with Different A_s

Polystyrene samples were prepared according to the general procedure using the following addition rates. For rates in Tables 2.7 - 8, a stock solution of

TIPNO (6.5 mg, 0.03 mmol) in styrene (1.2 mL, 10.47 mmol) was prepared and 2 μL of the nitroxide solution was distributed to each reaction vessel before degassing. In the case of Table 2.9, 4 μL of initiator solution was distributed to the reaction vial prior to degassing. After the desired reaction time, the vial was removed from the oil bath and briefly submerged in liquid nitrogen to stop the reaction. A small aliquot was removed from the reaction mixture and analyzed by GPC and ^{1}H NMR. The remaining reaction mixture was diluted with toluene (4.0 mL) and then concentrated on a rotary evaporator. This process was repeated a total of three times and the final white solid was dried on high vacuum overnight.

Table 2.7. 1.42 h Linearly Ramped Rate

Rate (μL/h)	Time (h)	Total Time (h)	Volume per Step (μL)	Total Volume (μL)
14	0.07	0.07	1	1
28	0.07	0.14	2	3
42	0.07	0.21	3	6
56	0.07	0.29	4	10
70	0.07	0.36	5	15
84	0.07	0.43	6	21
98	0.07	0.50	7	28
112	0.07	0.57	8	36
126	0.07	0.64	9	45
140	0.07	0.71	10	55
154	0.07	0.79	11	66
168	0.07	0.86	12	78
182	0.07	0.93	13	91
196	0.07	1.00	14	105
210	0.07	1.07	15	120
224	0.07	1.14	16	136
238	0.07	1.21	17	153
252	0.07	1.29	18	171

266	0.07	1.36	19	190
280	0.06	1.42	17	207

Total Reaction Time : 120 min

Table 2.8. 1.65 h Nonlinearly Ramped Rate

Rate (µL/h)	Time (h)	Total Time (h)	Volume per Step (µL)	Total Volume (µL)
30.26	0.03	0.03	1	1
42.36	0.05	0.08	2	3
53.86	0.06	0.14	3	6
64.75	0.06	0.20	4	10
75.04	0.07	0.26	5	15
85.33	0.07	0.33	6	21
95.01	0.07	0.41	7	28
104.1	0.08	0.49	8	36
112.6	0.08	0.57	9	45
120.4	0.08	0.65	10	55
127.7	0.09	0.73	11	66
134.3	0.09	0.82	12	78
140.4	0.09	0.92	13	91
145.8	0.10	1.01	14	105
150.7	0.10	1.11	15	120
155	0.10	1.22	16	136
158.5	0.11	1.32	17	153
161.6	0.11	1.43	18	171
164	0.12	1.55	19	190
165.8	0.10	1.65	17	207

Total Reaction Time : 120 min

Table 2.9. 2 h Constant Rate

Addition Time (h)	Addition Rate (µL/h)	Addition Volume (µL)
2	103.5	207

Total Reaction Time : 135 min

Supplementary Data for Higher Target Molecular Weight (M_n)

A vial, fitted with a screw cap and Teflon septum, was charged with styrene (420 µL, 3.67 mmol). A stock solution of 2,2,5-trimethyl-4-phenyl-3-azahexane-3-nitroxide (TIPNO, 6.5 mg, 0.0295 mmol) in styrene (1.2 mL, 10.47 mmol) was prepared and 1 µL of the nitroxide solution was transferred to the reaction vessel using a gastight syringe. The solution was degassed by three freeze-pump-thaw cycles followed by backfilling with a nitrogen atmosphere. A solution of the initiator, 1, (18 mg, 0.111 mmol) in styrene (633 µL, 5.52 mmol) was prepared and degassed in the same fashion. In the case of 2 and 3 hour additions a stock solution of TIPNO (6.5 mg, 0.03 mmol) in styrene (1.2 mL, 10.47 mmol) was prepared and 1 µL of the nitroxide solution was distributed to each reaction vessel before degassing. 220 µL of the initiator solution was then drawn into a 1 mL syringe that had been flushed with N_2. The syringe was mounted onto a New Era NE-4000 Double Syringe Pump and programmed to the appropriate constant rate of addition. The needle was quickly transferred from the stock solution to the reaction vial. Immediately after introducing the needle tip to the reaction mixture, the vial was submerged into an oil bath at 120 ºC and the syringe pump addition was started. After the desired reaction time, the vial was removed from the oil bath and briefly submerged in liquid nitrogen to stop the reaction. A small aliquot was removed from the reaction mixture and analyzed by GPC and ^{1}H NMR. The remaining reaction mixture was diluted with toluene (4.0 mL) and then concentrated on a rotary evaporator. This process was repeated a total of three times and the final white solid was dried on high vacuum

overnight. Targeting higher molecular weights in these reactions gave excellent control over Mn and dispersity. See Figure 2.7 and 2.8 for details.

Table 2.10. Addition Rates and Reaction Times for Figure 2.7

Addition Rate (μL/h)	Total Reaction Time (min)
N/A	170
207.0	192
103.5	197
69.00	200

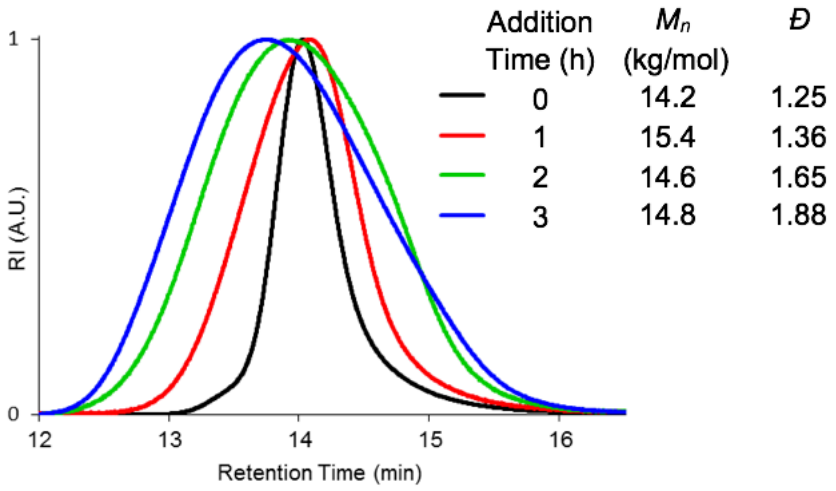

Figure 2.7. Broadening of polystyrene MWD at higher molecular weight using constant rate additions.

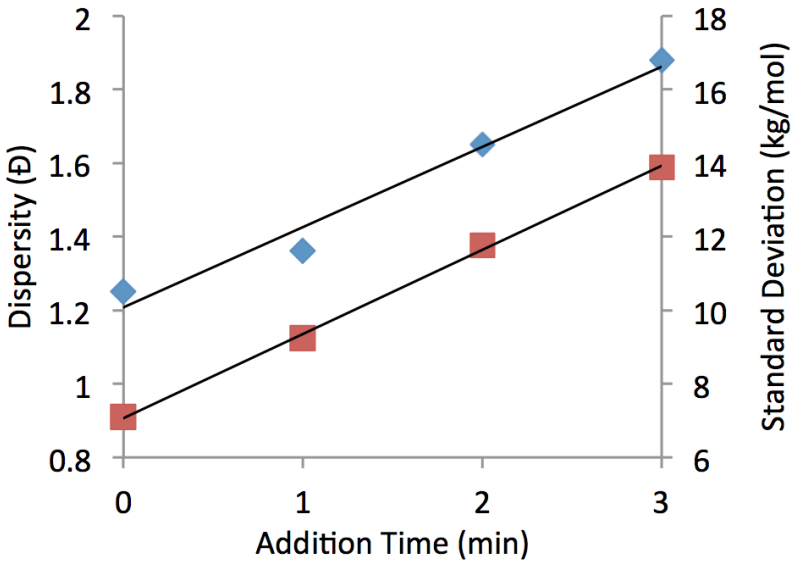

Figure 2.8. Linear relationship of addition time with dispersity and standard deviation.

Procedure for Figure 2.4

A vial, fitted with a screw cap and Teflon septum, was charged with styrene (840 µL, 7.34 mmol). The solution was degassed by three freeze-pump-thaw cycles followed by backfilling with a nitrogen atmosphere. A solution of the initiator, 1, (18 mg, 0.062 mmol) in styrene (1.27 mL, 11.04 mmol) was prepared and degassed by three freeze-pump-thaw cycles. 420 µL of the initiator solution was then drawn into a 1 mL syringe that had been flushed with N_2. The syringe was mounted onto a New Era NE-4000 Double Syringe Pump and programmed to the appropriate addition rate profile (see Tables 2.11 and 2.12). The needle

was quickly transferred from the stock solution to the reaction vial. Immediately after introducing the needle tip to the reaction mixture, the vial was submerged into an oil bath at 120 ºC and the syringe pump addition was started. After the desired reaction time, the vial was removed from the oil bath and briefly submerged in liquid nitrogen to stop the reaction. A small aliquot was removed from the reaction mixture and analyzed by GPC and ^{1}H NMR. The remaining reaction mixture was diluted with toluene (8.0 mL) and then concentrated on a rotary evaporator. This process was repeated a total of three times and the final white solid was dried under vacuum overnight.

Table 2.11. 2 h Constant Rate of Larger Scale

Addition Time (h)	Addition Rate (µL/h)	Addition Volume (µL)
2	207	414

Total Reaction Time : 140 min

Table 2.12. 1.24 h Linearly Ramped Rate

Rate (µL/h)	Time (h)	Total Time (h)	Volume per Step (µL)	Total Volume (µL)
32	0.06	0.06	2	2
64	0.06	0.13	4	6
96	0.06	0.19	6	12
128	0.06	0.25	8	20
160	0.06	0.31	10	30
192	0.06	0.38	12	42
224	0.06	0.44	14	56
256	0.06	0.50	16	72
288	0.06	0.56	18	90
320	0.06	0.63	20	110
352	0.06	0.69	22	132

384	0.06	0.75	24	156
416	0.06	0.81	26	182
448	0.06	0.88	28	210
480	0.06	0.94	30	240
512	0.06	1.00	32	272
544	0.06	1.06	34	306
576	0.06	1.13	36	342
608	0.06	1.19	38	380
640	0.05	1.24	34	414

Total Reaction Time : 140 min

Procedure for Figure 2.5a: Synthesis of Polystyrene Macroinitiators

Polystyrene macroinitiators were prepared according to the general procedure. The linearly ramped rate profile followed Table 2.5, and the 2 h constant addition rate profile was performed according to Table 1.1. For the linearly ramped rate profile a stock solution of TIPNO (6.5 mg, 0.03 mmol) in styrene (1.2 mL, 10.47 mmol) was prepared and 2 μL of the nitroxide solution was distributed to each reaction vessel before degassing. After the desired reaction time, the vial was removed from the oil bath and briefly submerged in liquid nitrogen to stop the reaction. A small aliquot was removed from the reaction mixture and analyzed by GPC and ^{1}H NMR. The remaining reaction mixture was diluted with toluene (4.0 mL) and then concentrated on a rotary evaporator. This process was repeated a total of three times and the final white solid was dried on high vacuum overnight.

Procedure for Figure 2.5b: Synthesis of Poly(styrene-*block*-isoprene)

A representative synthesis of poly(styrene-block-isoprene) is as follows: A polystyrene macroinitiator (M_n = 6.57 kg/mol, 288 mg, 0.0439 mmol) was added

to a schlenk flask. Isoprene (3.51 mL, 35.1 mmol), was then added and the reaction mixture was degassed by three freeze-pump-thaw cycles followed by backfilling with a nitrogen atmosphere and submerged into an oil bath at 120 °C. After 6 h, the reaction was stopped in liquid nitrogen, concentrated on a rotary evaporator, and dried under high vacuum overnight. The resulting polymer was analyzed by ^{1}H NMR and GPC.

Procedure for Figure 2.6a: Multimodal Distributions

The bimodal MWD was prepared according to the general procedure. The initiator solution was added over two injections at a rate of 200 µL/min. 82.8 µL was added at the beginning of the polymerization and after 30 minutes an additional 124.2 µL was injected. After the desired reaction time (2 h), the vial was removed from the oil bath and briefly submerged in liquid nitrogen to stop the reaction. A small aliquot was removed from the reaction mixture and analyzed by GPC and ^{1}H NMR. The remaining reaction mixture was diluted with toluene (4.0 mL) and then concentrated on a rotary evaporator. This process was repeated a total of three times and the final white solid was dried on high vacuum overnight.

Procedure for Figure 2.6b: Synthesis of PS with *Đ* = 3.9

Polystyrene with a dispersity of 3.9 was prepared according to the general procedure. A stock solution of TIPNO (6.5 mg, 0.03 mmol) in styrene (1.2 mL, 10.47 mmol) was prepared and 2 µL of the nitroxide solution was distributed to

each reaction vessel before degassing. After the desired reaction time, the vial was removed from the oil bath and briefly submerged in liquid nitrogen to stop the reaction. A small aliquot was removed from the reaction mixture and analyzed by GPC and ^{1}H NMR. The remaining reaction mixture was diluted with toluene (4.0 mL) and then concentrated on a rotary evaporator. This process was repeated a total of three times and the final white solid was dried on high vacuum overnight. The rate profile for initiator addition followed the exponentially ramped rate below:

Table 2.13. 1.56 h Exponentially Ramped Rate

Rate (µL/h)	Time (h)	Total Time (h)	Volume per Step (µL)	Total Volume (µL)
10	0.100	0.100	1	1
15	0.067	0.167	1	2
20	0.100	0.267	2	4
27.5	0.073	0.339	2	6
35	0.086	0.425	3	9
45	0.067	0.492	3	12
55	0.073	0.565	4	16
67.5	0.059	0.624	4	20
80	0.063	0.686	5	25
95	0.053	0.739	5	30
110	0.109	0.848	12	42
145	0.097	0.945	14	56
185	0.086	1.031	16	72
230	0.078	1.109	18	90
280	0.071	1.181	20	110
335	0.066	1.246	22	132
395	0.061	1.307	24	156
460	0.057	1.364	26	182
530	0.053	1.416	28	210
605	0.050	1.466	30	240
685	0.047	1.513	32	272
770	0.044	1.557	34	306
860	0.042	1.599	36	342
960	0.040	1.638	38	380
1070	0.032	1.670	34	414

Total Reaction Time : 130 min

Supplementary Data for Controlled Addition of a Bifunctional Initiator (2)

Bifunctional initiator (2) was prepared according to a previously developed method by Hawker.[1] A vial, fitted with a screw cap and Teflon septum, was charged with styrene (840 μL, 7.34 mmol). The styrene was degassed by three freeze-pump-thaw cycles followed by backfilling with a nitrogen atmosphere. A solution of the initiator (2) (64.2 mg, 0.19 mmol) in styrene (1.13 mL, 9.9 mmol) was prepared and degassed in the same fashion. 440 μL of the initiator solution was then drawn into a 1 mL syringe that had been flushed with N_2. The syringe was mounted onto a New Era NE-4000 Double Syringe Pump and programmed to the appropriate addition rate profile (see details below). The needle was quickly transferred from the stock solution to the reaction vial. Immediately after introducing the needle tip to the reaction mixture, the vial was submerged into an oil bath at 120 ºC and the syringe pump addition was started. After the desired reaction time, the vial was removed from the oil bath and briefly submerged in liquid nitrogen to stop the reaction. A small aliquot was removed from the reaction mixture and analyzed by GPC and ^{1}H NMR. The remaining reaction mixture was diluted with toluene (4.0 mL) and then concentrated on a rotary evaporator. This process was repeated a total of three times and the final white solid was dried on high vacuum overnight.

Table 2.14. Rate Profile for Controlled Addition of Bifunctional Initiator

Addition Time (h)	Addition Rate (μL/h)	Addition Volume (μL)
2	207	414

Total Reaction Time : 130 min

Supplementary Data for Poly(styrene-block-valerolactone) using a Multifunctional Initiator

A vial, fitted with a screw cap and Teflon septum, was charged with hydroxyl functionalized polystyrene, M_n = 8.1 kg/mol, (81 mg, 0.01 mmol). Valerolactone (104 μL, 1.14 mmol) and dichloromethane (100 μL) were then added followed by a 2 M solution of hydrogen chloride in ether (207 μL, 0.41 mmol) at 0 ºC.[2] After 90 minutes the viscous white solution was diluted in dichloromethane (0.5 mL) and analyzed by GPC.

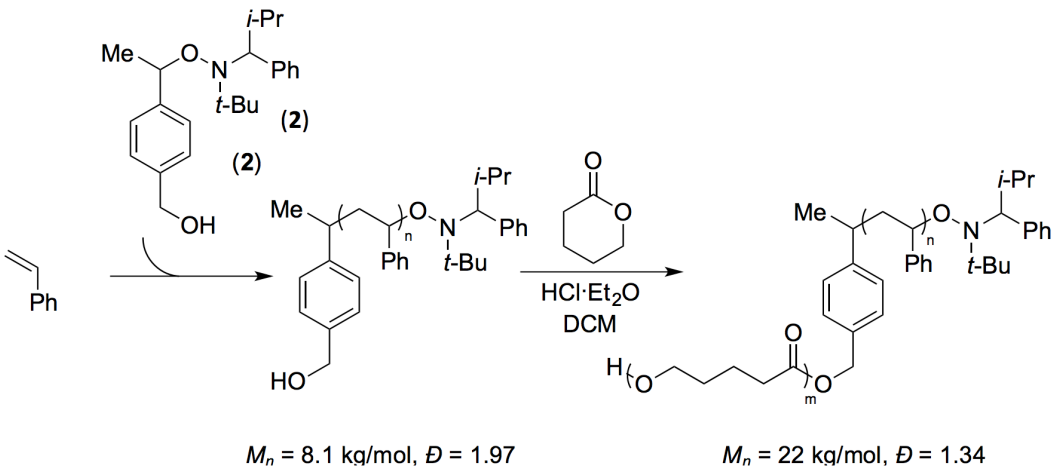

Figure 2.9. Controlled Addition and Block Copolymer Synthesis from a Bifunctional Initiator

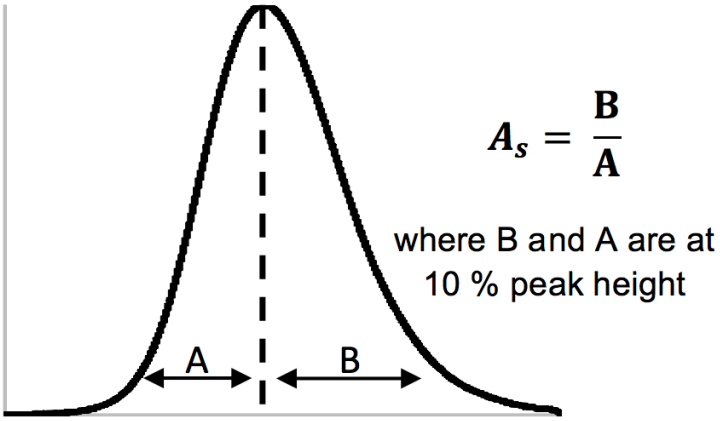

Figure 2.10. Calculation of Asymmetry Factor (A_s)

Supplementary Data for Skewness and Kurtosis of Samples in Figure 2.3

The third and fourth moments about the mean, skewness (α_3) and kurtosis (α_4), respectively, were calculated according to the procedure denoted by Rudin.[3] Briefly, the equations are as follows:

$$\alpha_3 = \frac{M_z M_w M_n - 3M_n^2 M_w + 2M_n^2}{(M_w M_n - M_n^2)^{3/2}} \quad (2.1)$$

$$\alpha_4 = \frac{M_{z+1} M_z M_w M_n - 4M_n^2 M_z M_w + 6M_n^3 M_w - 3M_n^4}{(M_w M_n - M_n^2)^2} \quad (2.2)$$

Table 2.15. Skewness and Kurtosis in Figure 2.3

Addition Profile Type	Skewness (α_3)	Kurtosis (α_4)
Linearly Ramped (Table 1.7)	3.7	26.2
Nonlinearly Ramped (Table 1.8)	2.8	16.3
Constant Rate (Table 1.9)	2.4	14.5

Supplementary Data for Controlled MWD in Atom-Transfer Radical Polymerization (ATRP)

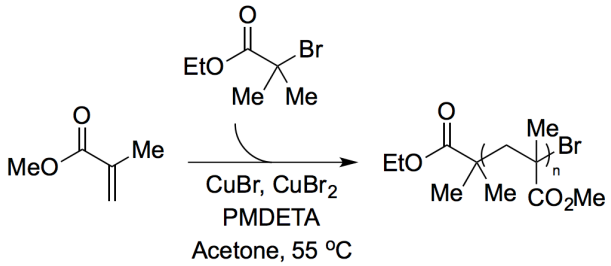

A vial, fitted with a screw cap and Teflon septum, was charged with copper(I) bromide (4.0 mg, 0.03 mmol) and copper(II) bromide (2.7 mg, 0.01 mmol) followed by methyl methacrylate (852 μL, 8.0 mmol), PMDETA (17 μL, 0.08 mmol), and acetone (852 μL). Each reaction mixture was degassed by three freeze-pump-thaw cycles followed by backfilling with a nitrogen atmosphere. A solution of the ethyl 2-bromoisobutyrate (24 μL, 0.16 mmol) in

acetone (400 μL) was prepared and degassed in the same fashion. 220 μL of the initiator solution was then drawn into a 1 mL syringe that had been flushed with N_2. The syringe was mounted onto a New Era NE-4000 Double Syringe Pump and programmed to the appropriate addition rate profile (see details below). The needle was quickly transferred from the stock solution to the reaction vial. Immediately after introducing the needle tip to the reaction mixture, the vial was submerged into an oil bath at 55 ºC and the syringe pump addition was started. After the desired reaction time, the vial was removed from the oil bath and briefly submerged in liquid nitrogen to stop the reaction. A small aliquot was removed from the reaction mixture and analyzed by GPC and ^{1}H NMR.

Table 2.16. Molecular Weight and Dispersity Data for Constant Rate Additions to ATRP

Addition Time (h)	**Addition Rate (μL/h)**	**Reaction Time (h)**	***M*$_n$ (kg/mol)**	***Đ***
0.0	0.0	15	13.2	1.24
1.0	200.0	15	11.8	1.41
2.0	100.0	15	11.8	1.58
3.0	66.67	15	13.3	1.73
4.0	50.0	15	11.8	1.91

2.6 Appendix References

(1) Bosman, A., W., Vestberg, R., Heumann, A., Fréchet, J., M., Hawker, C., J., *J. Am. Chem. Soc*., **2003**, 125, 715.

(2) Lou, X., Detrembleur, C., Jérôme, R., *Macromolecules* **2002**, 35, 1190.

(3) Rudin, A., *J. Chem. Ed*., **1969**, 46, 595.

CHAPTER 3

"SHAPING" THE FUTURE OF MOLECULAR WEIGHT DISTRIBUTIONS IN ANIONIC POLYMERIZATION

3.1 Abstract

Varying molecular weight distributions (MWDs) have the potential to precisely tune polymer properties, but this approach remains relatively unexplored owing to a lack of synthetic methods that provide control over the exact makeup of a distribution. Herein, we report a simple and highly efficient strategy for addressing this challenge through temporal regulation of initiation in the anionic polymerization of styrene. This method yields unprecedented control over the shape of the polymer MWD and facilitates the synthesis of diblock copolymers with controlled MWD compositions. Importantly, we show that the MWD symmetry has a marked influence on the stiffness of poly(styrene-*block*-isoprene) copolymers, which demonstrates that varying MWD shape is an effective method for altering polymer properties.

3.2 Introduction

The dispersity (*Đ*) of a polymer sample is a key parameter in the control of material properties such as viscosity, processability, and all facets of block copolymer self-assembly.[1-14] However, *Đ* is the normalized standard deviation of the molecular weights in a polymer sample and, therefore, describes only the relative breadth of the molecular weight distribution (MWD).[15] Theoretical

studies have looked beyond the breadth of MWD and suggested that distribution shape has a marked influence on polymer physical properties.[16,17] Therefore, synthetic methods that enable deterministic control over the exact distribution of chain lengths in a sample are needed to understand the full influence of MWD composition on polymer properties; these methods have the potential to facilitate the implementation of polymer distribution as a means to develop improved materials.

On this basis, multiple methods have been developed to modify MWDs in controlled polymerizations. The majority of these processes only give control over the relative breadth of the distribution;[9-13] however, a limited number have taken a step toward changing MWD shape. Specifically, Meira and co-workers have demonstrated that variation of monomer and initiator flow rates in continuous flow reactors imparted partial control over MWD shape.[18-21] Further, methods have been developed using pulsed initiation through photolysis or monomer/initiator feeds to give multimodal distributions.[22-24] Additionally, Aoshima and co-workers have tuned polymer composition through controlled termination processes.[25] Although these methods give partial control, new strategies are still needed to give precise regulation of MWD shape in living polymerization processes.

In an effort to realize deterministic control of MWD symmetry, we recently reported a method in which we used temporally controlled initiation in nitroxide-mediated polymerization (NMP) reactions.[26] Specifically, by controlling the addition of an alkyl nitroxide initiator to the polymerization of styrene, we

predictably modulated polymer MWD shape while maintaining excellent control over number-average molecular weight (M_n) and $Đ$. Although this protocol afforded robust command of the MWD, several challenges need to be addressed to make this strategy more powerful and practical. For example, NMP processes inherently produce polymers with broader distributions, which limits how precisely the MWD can be defined through temporally controlled initiation.[27,28] Moreover, these radical polymerizations have limited substrate scopes and can be run only to partial conversions to get reasonable chain-end fidelities. Therefore, we sought a polymerization method that gives more precise control over MWD shape, is applicable to a wider array of monomer types, and provides higher-molecular-weight polymers. Additionally, we wanted a truly living polymerization process that would enable reactions to be run to full conversion, thereby providing access to the one-pot synthesis of block copolymers.

3.3 Results and Discussion

We hypothesized that anionic polymerization would be the ideal reaction class with which to address the above challenges owing to its capacity to give narrow $Đ$s, truly living nature and broad monomer scope.[29-35] Furthermore, for the anionic polymerization of styrene, Lynd and Hillmyer have successfully broadened polymer $Đ$ up to 1.3 through a combination of metered initiator addition and temperature control.[9] BASF also patented a method that enabled the synthesis of broad polystyrene samples through controlled addition of

monomer, initiator, and rate-retarding agents.[36] Although both of these reports did not control the MWD shape, they provided evidence that anionic polymerization would work well in our temporally controlled initiation strategy. Herein, we report the deterministic control of polymer MWDs for the anionic polymerization of styrene (Figure 3.1). This method imparts unprecedented control over MWD shape and opens the door to better understand the relationship between polymer chain-length composition and material properties. Using our new method, we demonstrate that the shape of the MWD in block copolymers has a significant influence on their physical properties, which clearly illustrates that MWD composition can be used to tune polymer function.

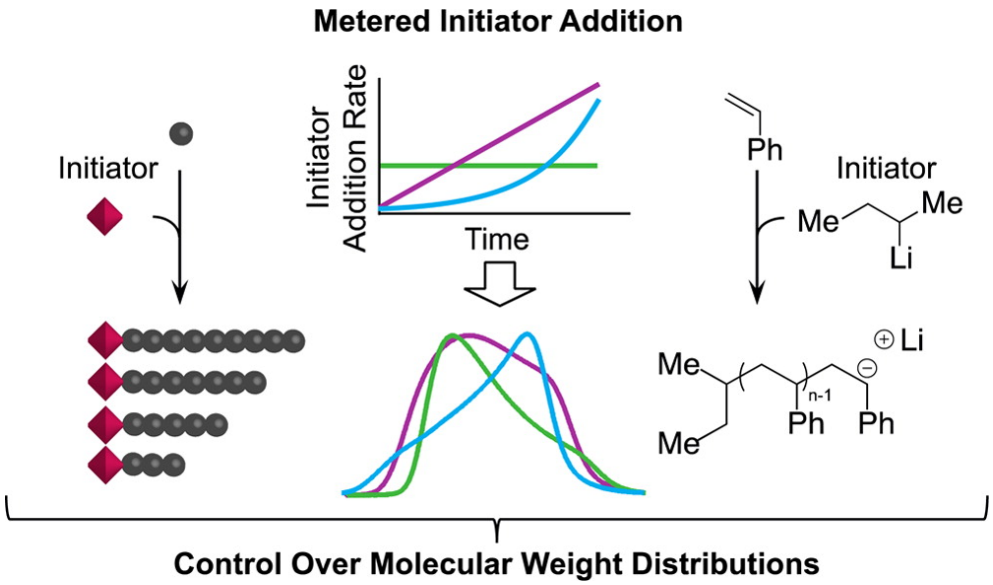

Figure 3.1. Metered addition of sec-butyllithium in the anionic polymerization of styrene to tailor the shape and composition of the molecular weight distribution (MWD).

We began our studies by looking at the temporally controlled initiation of anionic polymerizations of styrene. Metering in a fixed amount of the initiator, *sec*-butyllithium (*s*-BuLi), at a constant rate to a solution of styrene in cyclohexane, we expected to observe the MWD broadening with increasing addition time while M_n remained unchanged (Figure 3.2a). Traditional reaction conditions, in which the full amount of the initiator is added at the beginning of the reaction, yielded a 14.6 kg/mol polystyrene (PS) sample with a narrow $Đ$ of 1.07. In support of our hypothesis, the addition of the same molar quantity of *s*-BuLi at constant rates from 20 to 120 min broadened the $Đ$ from 1.16 to 2.47 without changing M_n (Figure 3.2b). Size exclusion chromatography (SEC) traces of these reactions showed a shift in the peak maximum (M_p) to higher molecular weights and a clear broadening of the distribution as addition time increased (Figure 3.2c). Moreover, a linear relationship between initiator addition time and $Đ$ was observed (Figure 3.2d). These results illustrate that temporally controlled initiation in the anionic polymerization of styrene enables predictable control over polymer $Đ$ and M_n.

Next, we efficiently achieved our goal of controlling the shape of the distribution by modulating the initiator addition rate profile. Compared with polymer samples synthesized with constant rates of initiator addition, those produced with linearly increasing addition rates gave distributions that had less tailing and were significantly broader at 50% peak height (Figure 3.2e–h). Furthermore, drastically different peak shapes were obtained when

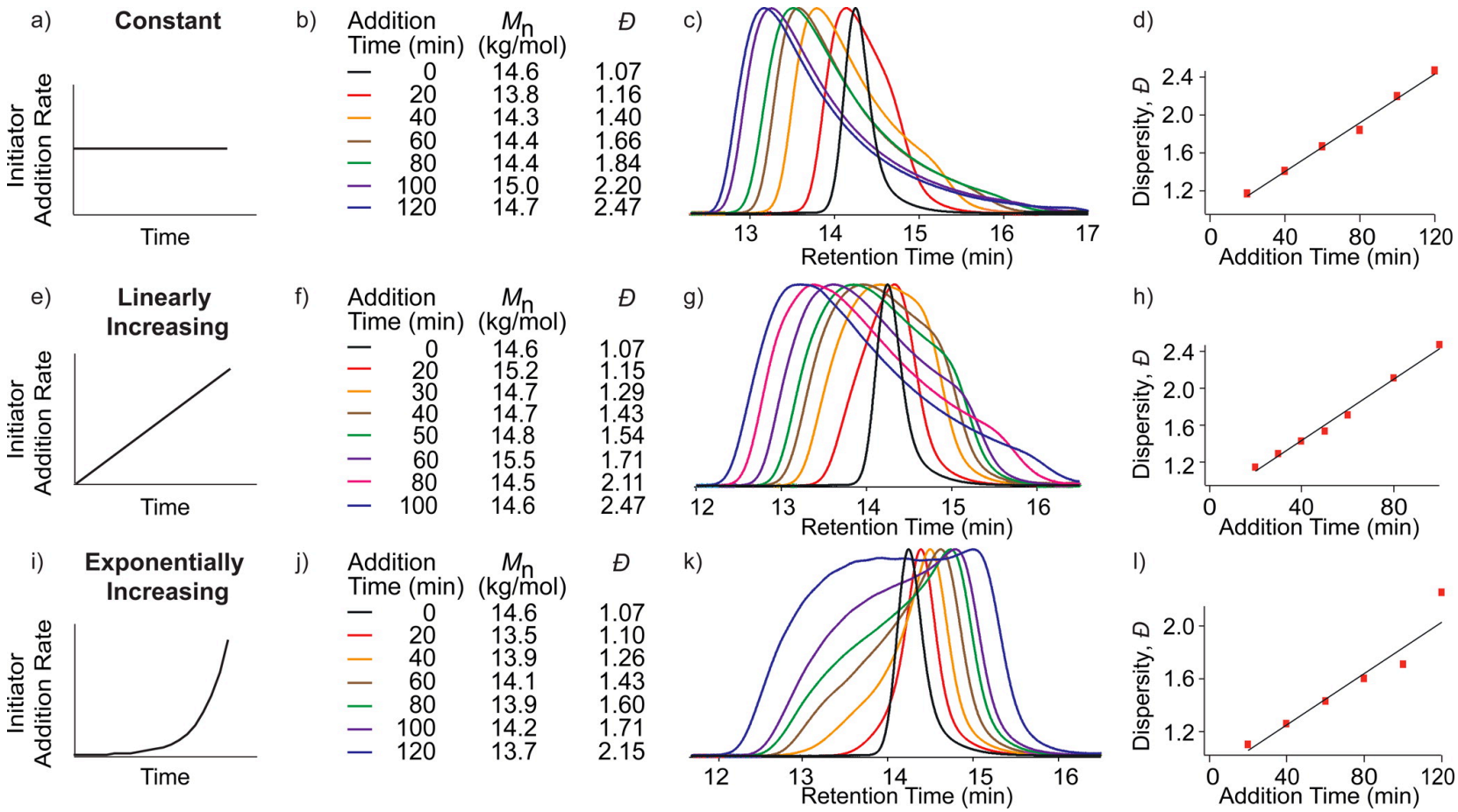

Figure 3.2. Controlling the breadth and shape of polystyrene MWD distributions with constant (a–d), linearly ramped (e–h), and exponentially ramped (i–l) rates of initiator addition (a, e, and i are representative initiator addition profiles).

exponentially increasing rates were used (Figure 3.2i–l). For these addition profiles, the SEC traces showed a decrease in M_p at longer addition times, with a tailing into higher molecular weights. These shapes are the antithesis of the polymer samples prepared with constant rates of addition and demonstrate that our method can be used to achieve drastically different MWD compositions. Notably, for both the linearly and exponentially increasing addition rates, excellent control over M_n was obtained and a linear relationship between $Đ$ and addition time was observed.

A major advantage of using temporally controlled initiation in anionic polymerizations is that vastly different MWD shapes are accessible even at relatively low $Đ$s. We highlight this in Figure 3.3, which shows three SEC curves of PS samples that have $Đ$s of ~1.4 and M_ns of ~14.5 kg/mol but were made with different initiator addition profiles. According to only M_n and $Đ$, these materials would be considered almost identical; however, there is little resemblance among these traces, which have asymmetry factor (A_s) values of 3.6, 1.6, and 0.3 corresponding to polymers made with constant, linearly increasing, and exponentially increasing addition rates, respectively (see Figure 3.3).[37] The overlay of these SEC traces illustrates the drastically variable shapes that can be accessed with our method.

These MWDs can be further described by going beyond M_n and $Đ$ values to the third (skewness, α_3) and fourth (kurtosis, α_4) moments of the distribution function.[38] Skewness describes the symmetry of the curve, whereas kurtosis indicates the amount of tailing on either side of the MWD around M_p. Both of

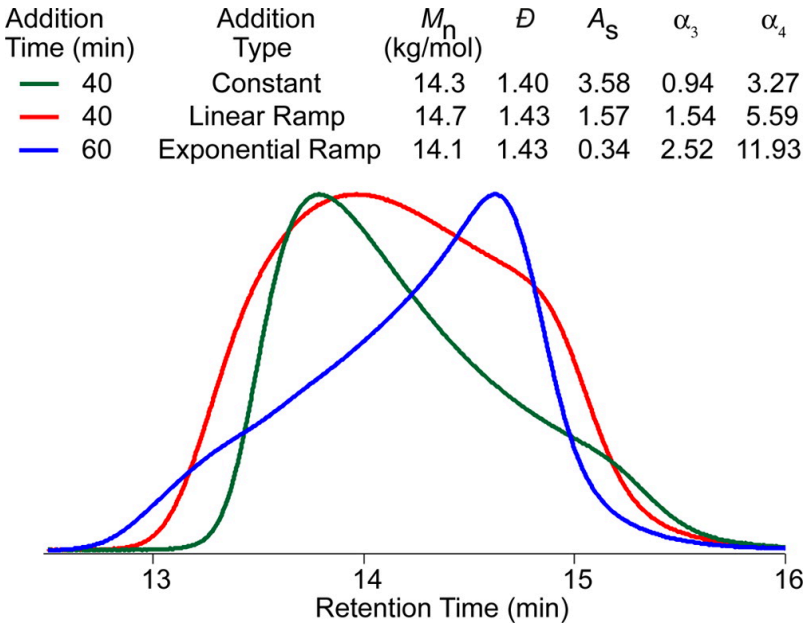

Figure 3.3. Three polymer samples with similar M_n and dispersity ($Đ$) values but drastically variable MWD compositions. α_3, skewness; α_4, kurtosis; A_s, asymmetry factor.

these parameters, which further describe the shape of the distribution, are significantly different among the polymers made with the three initiator addition profiles.

Compared with temporally controlled initiation in NMP reactions, the anionic polymerizations permitted significantly higher levels of control over the shape of the distribution. For example, for PS polymers with $Đ$ values of ~1.4 made with NMP, A_s values ranged from 0.6 to 1.0 (compared with values of 0.3 to 3.6 for anionic polymerizations).[26] These results demonstrate that the inherently narrow MWDs afforded by anionic polymerization enable markedly better command of MWD shape, especially when $Đ$ is below 1.7.

During our studies, we noticed that the majority of the constant and linearly increasing initiator addition rates afforded polymers for which SEC traces showed precipitous peak edges at low molecular weights. We postulated that this outcome was a result of abrupt stops in initiator addition, which caused the distribution to decline sharply to baseline with shorter addition times. To investigate this hypothesis, we monitored one of the polymerizations in which the initiator was added at a constant rate over 40 min. The SEC curves of the polymer before the end of the addition showed a smooth return to baseline (Figure 3.4). However, time points after the addition showed the emergence of the peak edge, which grew as the polymerization proceeded. This experiment provided straightforward evidence to support our hypothesis.

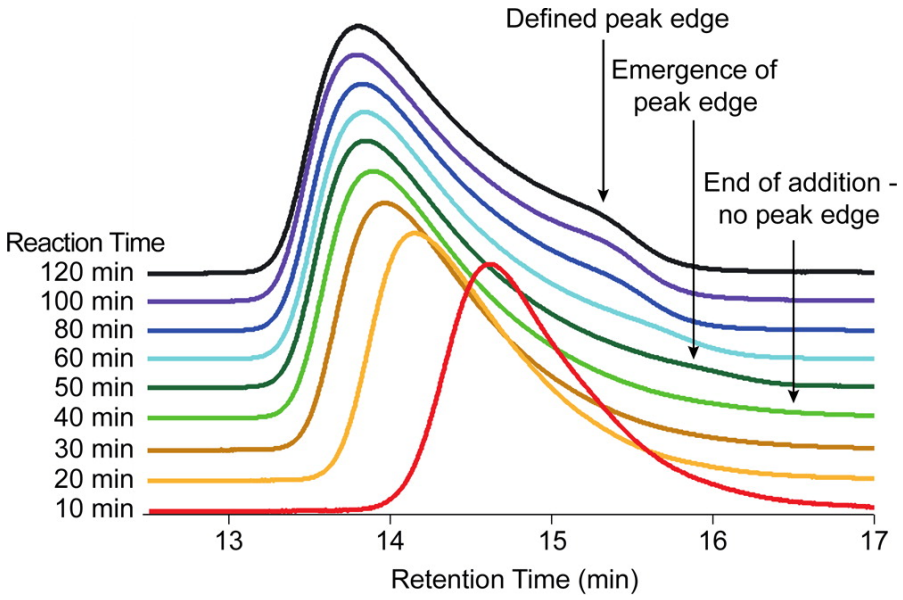

Figure 3.4. Size exclusion chromatography curves at indicated time points with a 40 min constant rate addition.

We reasoned that the observed peak edge could be removed by gradually decreasing the initiator addition rate at the end of the process. Using bell-shaped addition profiles, we obtained nearly symmetrical PS distributions that had no discernible peak edges (Figure 3.5). These data further demonstrate that MWD shape and composition can be precisely tuned by simply modulating the addition profile of the initiator.

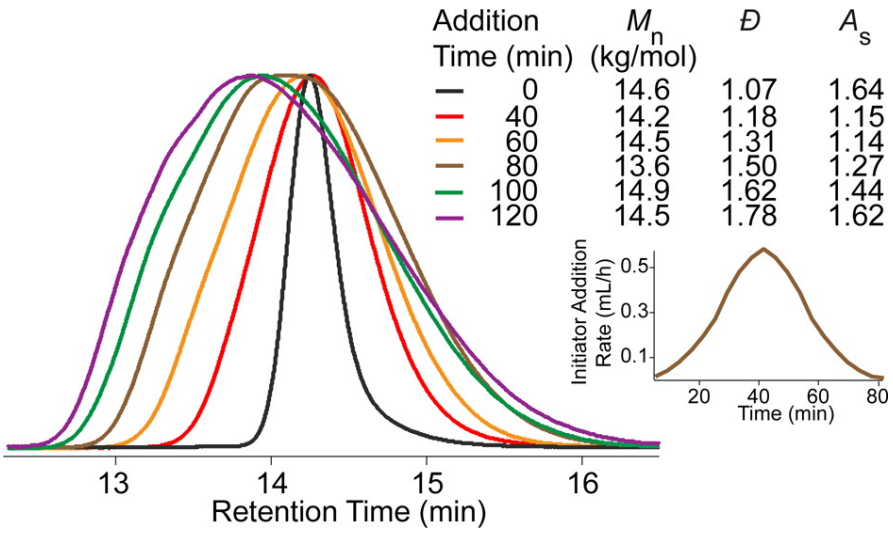

Figure 3.5. Size exclusion chromatography curves of a bell-shaped initiator addition profile. Inset: rate (mL/h) vs time (min) of an 80 min addition profile.

The living nature of anionic polymerizations allows these reactions to run to full conversion and enables the one-pot synthesis of diblock copolymers.[9,39] Taking advantage of these features, we synthesized a series of poly(styrene-*block*-isoprene) copolymers (PS-*b*-PI) in which both the shape and the *Đ* of the PS block varied (Figure 3.6a).[40] In all cases, efficient chain

a)

Entry	M_n (S) (kg/mol)	$Đ$ (S)	A_s	M_n (SI) (kg/mol)	$Đ$ (SI)	E (MPa)
1a	14.1	1.19	1.85	35.6	1.14	460
1b	14.2	1.22	0.52	35.1	1.16	560
2a	14.9	1.42	3.52	36.8	1.21	450
2b	14.1	1.39	0.37	33.6	1.22	530
3a	15.2	1.69	4.48	36.3	1.25	220
3b	14.1	1.71	0.31	36.5	1.28	440
4a	14.4	2.01	4.97	37.2	1.28	85
4b	13.8	1.97	0.26	34.4	1.29	300

b)

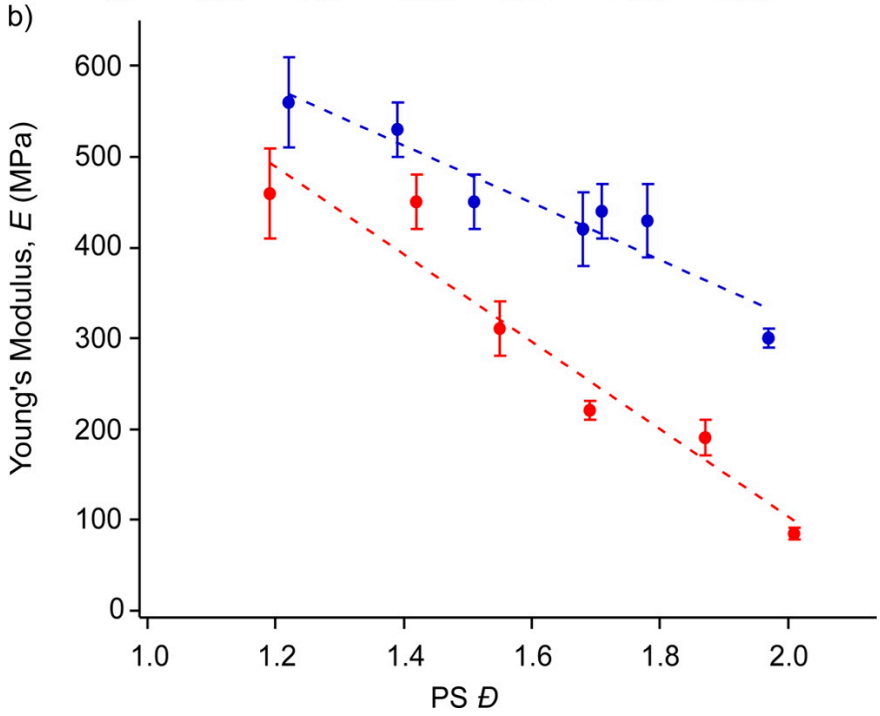

Figure 3.6. (a) Poly(styrene-*block*-isoprene) block copolymers with varying polystyrene (PS) MWD shapes and Young's moduli (E) determined with dynamic mechanical analysis. (b) Plot of PS $Đ$ vs E (MPa): blue circles indicate PS blocks with asymmetry factor (As) values of <1; red circles indicate PS blocks with A_s values of > 1; S = PS; SI = poly(styrene-block-isoprene). Each E value is an average of at least four measurements.

extension of our compositionally controlled PS samples with isoprene gave well-defined PS-*b*-PI copolymers.

With the above series of copolymers in hand, we set out to investigate the influence of MWD shape and breadth on the Young's modulus (E) of the material (Figure 3.6b).[41-44] For all samples, materials in which the PS MWD shape was tailing to higher molecular weights ($A_s < 1$) had E values that were consistently higher than those of samples with shapes tailing to lower molecular weights ($A_s > 1$). This difference in E between the two MWD shapes increased as $Đ$ increased or as the difference in A_s values widened between the samples. For example, two samples in which the $Đ$ of the PS block was ~1.2 with A_s values of 1.9 and 0.5 gave E values of 460 and 560 MPa, respectively; a moderate 1.2-fold increase in E. Remarkably, when we switched to two samples that had PS $Đ$s of ~2.0 with A_s values of 5.0 and 0.3, we observed E values of 300 and 85 MPa, respectively. In this case, the change in E was 3.5-fold between the samples, which clearly shows that the MWD shape and composition have a significant influence. Moreover, these results demonstrate that the MWD shape is just as important, if not more important, than the breadth of the distribution and can effectively be used as a parameter for tuning material function.

3.4 Conclusion

In summary, we have developed a robust method for precisely tailoring MWD shape by temporally regulating initiation in the anionic polymerization of

styrene. The truly living nature of this anionic polymerization allows the synthesis of materials with similar M_n and $Đ$ values but drastically different polymer compositions and provides facile access to block polymers. Taking advantage of our new method, we synthesized a library of PS-*b*-PI copolymers with various PS MWD shapes. Significantly, we found that MWD symmetry had a considerable influence on the stiffness of the material, which shows that MWD shape is a key parameter influencing polymer properties. This simple and modular approach offers unparalleled levels of control and gives access to a wide array of functional materials with systematically deviating polymer compositions. It also provides a platform for further fundamental studies of the influence of MWD shape on polymer properties.

3.5 References

(1) Nichetti, D.; Manas-Zloczower, I. *Polym. Eng. Sci*. **1999**, 39, 887.

(2) Collis, M. W.; Mackley, M. R. *J. Non-Newtonian Fluid Mech*. **2005**, 128, 29.

(3) Lynd, N. A.; Meuler, A. J.; Hillmyer, M. A. *Prog. Polym. Sci*. **2008**, 33, 875.

(4) Sides, S. W.; Fredrickson, G. H. *J. Chem. Phys*. **2004**, 121, 4974.

(5) Bates, F. S.; Hillmyer, M. A.; Lodge, T. P.; Bates, C. M.; Delaney, K. T.; Fredrickson, G. H. *Science* **2012**, 336, 434.

(6) Hillmyer, M. A. *J. Polym. Sci., Part B: Polym. Phys*. **2007**, 45, 3249.

(7) Schmitt, A. K.; Mahanthappa, M. K. *Macromolecules* **2014**, 47, 4346.

(8) Bendejacq, D.; Ponsinet, V.; Joanicot, M.; Loo, Y. L.; Register, R. A. *Macromolecules* **2002**, 35, 6645.

(9) Lynd, N. A.; Hillmyer, M. A. *Macromolecules* **2007**, 40, 8050.

(10) Widin, J. M.; Schmitt, A. K.; Schmitt, A. L.; Im, K.; Mahanthappa, M. K. *J. Am. Chem. Soc*. **2012**, 134, 3834.

(11) Hustad, P. D.; Marchand, G. R.; Garcia-Meitin, E. I.; Roberts, P. L.; Weinhold, J. D. *Macromolecules* **2009**, 42, 3788.

(12) Listak, J.; Jakubowski, W.; Mueller, L.; Plichta, A.; Matyjaszewski, K.; Bockstaller, M. R. *Macromolecules* **2008**, 41, 5919.

(13) Lynd, N. A.; Hillmyer, M. A. *Macromolecules* **2005**, 38, 8803.

(14) Meuler, A. J.; Ellison, C. J.; Evans, C. M.; Hillmyer, M. A.; Bates, F. S. *Macromolecules* **2007**, 40, 7072.

(15) Rane, S. S.; Choi, P. *Chem. Mater*. **2005**, 17, 926.

(16) Lynd, N. A.; Hillmyer, M. A.; Matsen, M. W. *Macromolecules* **2008**, 41, 4531.

(17) Cooke, D. M.; Shi, A.-C. *Macromolecules* **2006**, 39, 6661.

(18) Meira, G. R.; Johnson, A. F. *Polym. Eng. Sci*. **1981**, 21, 415.

(19) Alassia, L. M.; Couso, D. A.; Meira, G. R. *J. Appl. Polym. Sci*. **1988**, 36, 481.

(20) Couso, D. A.; Alassia, L. M.; Meira, G. R. *J. Appl. Polym. Sci*. **1985**, 30, 3249.

(21) Laurence, R. L.; Vasudevan, G. *Ind. Eng. Chem. Process Des. Dev*. **1968**, 7, 427.

(22) Hungenberg, K. D.; Knoll, K.; Wulkow, M. *Macromol. Theory Simul*. **1997**, 6, 393.

(23) Farkas, E.; Meszena, Z. G.; Johnson, A. F. *Ind. Eng. Chem. Res*. **2004**, 43, 7356.

(24) Gosden, R. G.; Meszena, Z. G.; Mohsin, M. A.; Auguste, S.; Johnson, A. F. *Polym. React. Eng*. **1997**, 5, 45.

(25) Seno, K. I.; Kanaoka, S.; Aoshima, S. *J. Polym. Sci., Part A: Polym. Chem*. **2008**, 46, 2212.

(26) Gentekos, D. T.; Dupuis, L. N.; Fors, B. P. *J. Am. Chem. Soc*. **2016**, 138, 1848.

(27) Hawker, C. J.; Bosman, A. W.; Harth, E. *Chem. Rev*. **2001**, 101, 3661.

(28) Grubbs, R. B. *Polym. Rev*. **2011**, 51, 104.

(29) Baskaran, D.; Müller, A. H. E. *Prog. Polym. Sci*. **2007**, 32, 173.

(30) Bywater, S. In Comprehensive Chemical Kinetics; Bamford, C. H., Tipper, C. F. H., Eds.; Elsevier, 1976; Vol. 15, pp 1−65.

(31) Young, R. N.; Quirk, R. P.; Fetters, L. J. In Anionic Polymerization; Springer: Berlin; Heidelberg, 1984; pp 1−90.

(32) Hadjichristidis, N.; Pitsikalis, M.; Pispas, S.; Iatrou, H. *Chem. Rev*. **2001**, 101, 3747.

(33) Hadjichristidis, N.; Iatrou, H.; Pitsikalis, M.; Pispas, S.; Avgeropoulos, A. *Prog. Polym. Sci*. **2005**, 30, 725.

(34) Hirao, A.; Hayashi, M.; Loykulnant, S.; Sugiyama, K.; Ryu, S.; Haraguchi, N.; Matsuo, A.; Higashihara, T. *Prog. Polym. Sci*. **2005**, 30, 111.

(35) Higashihara, T.; Hayashi, M.; Hirao, A. *Prog. Polym. Sci*. **2011**, 36, 323.

(36) Fischer, W.; Knoll, K.; Loth, W.; Warzelhan, V.; Deffieux, A.; Desbois, P.; Fontanille, M.; Latsch, S.; Schade, C.; Gausepohl, H.¨ Anionic Polymerization Process. US6444762 B1, August 18, 1997.

(37) Asymmetry factors (A_s) > 1 describe polymer MWDs tailing into low molecular weights, A_s < 1 describes polymer MWDs tailing into high molecular weights; A_s = 1 indicates a symmetric distribution; see Supporting Information for details;. Kirkland, J. J.; Yau, W. W.; Stoklosa, H. J.; Dilks, C. H. J. *J. Chromatogr. Sci*. **1977**, 15, 303.

(38) Rudin, A. *J. Chem. Educ*. **1969**, 46, 595.

(39) Khandpur, A. K.; Foerster, S.; Bates, F. S.; Hamley, I. W.; Ryan, A. J.; Bras, W.; Almdal, K.; Mortensen, K. *Macromolecules* **1995**, 28, 8796.

(40) Roovers, J. E. L.; Bywater, S. *Macromolecules* **1968**, 1, 328.

(41) Oral, I.; Guzel, H.; Ahmetli, G. *Polym. Bull*. **2011**, 67, 1893.

(42) Nielsen, L. E. *Rheol. Acta* **1974**, 13, 86.

(43) Kenney, J. F. *Polym. Eng. Sci*. **1968**, 8, 216.

(44) Lach, R.; Weidisch, R.; Knoll, K. *J. Polym. Sci., Part B: Polym. Phys*. **2005**, 43, 429.

3.6 Appendix

Experimental

General Reagent Information

All reactions were performed in an Unilab MBraun Glovebox with a nitrogen atmosphere. Styrene (99+%, Sigma Aldrich), isoprene (>99+%, Sigma Aldrich), and cyclohexane (Fischer Scientific, ACS Grade) were dried over calcium hydride (CaH_2) (ACROS organics, 93% extra pure, 0-2 mm grain size) for 12 h. Styrene was vacuum transferred degassed by three freeze-pump-thaw cycles. Cyclohexane and isoprene were distilled under nitrogen and degassed by vigorously sparging with nitrogen for 30 minutes or three freeze-pump-thaw cycles, respectively. *Sec*-butyllithium (Sigma Aldrich, 1.4 M in cyclohexane) and isopropanol (anhydrous, 99.5%) were used as received.

General Analytical Information

All polymer samples were analyzed using a Tosoh EcoSEC HLC 8320GPC system with two SuperHM-M columns in series at a flow rate of 0.350 mL/min. THF was used as the eluent and all number-average molecular weights (M_n), weight-average molecular weights (M_w), dispersities ($Đ$), asymmetry factors (A_s), M_z and M_{z+1} were calculated from refractive index chromatograms against TSKgel polystyrene standards. Conversions were determined on a Varian 400 MHz NMR spectrometer in $CDCl_3$. Tensile properties of compression molded block copolymer samples were analyzed by dynamic

mechanical analysis using a TA Instruments DMA Q800 Dynamic Mechanical Thermal Analysis (DMA) instrument.

General Procedure for Styrene Polymerizations

A 20 mL scintillation vial equipped with a magnetic stirrer was flame dried, brought into the glove box, and charged with 6.9 mL of cyclohexane and 0.8 mL of styrene (6.98 mmol). A *sec*-butyllithium stock solution in cyclohexane (0.16 M) was prepared for the reactions and a total volume of 360 μL of the solution was drawn into a 1mL syringe and then mounted onto a New Era NE-4000 Double Syringe Pump. The pump was programmed according to the appropriate rate profile, which would dispense a total volume of 320 μL (0.0512 mmol of *s*-BuLi) of the initiator solution. Once the needle was submerged into the reaction mixture, the addition program was started. The reaction turned slowly bright orange over the course of the addition due to the formation of the polystyryl anion. The reaction was allowed to reach full conversion and was quenched with excess isopropanol until the solution was clear and colorless. The polymer was isolated by removing the solvent under vacuum overnight to afford a white solid.

For the 80 min, 100 min, and 120 min additions of exponentially increasing rates a 0.0533 M initiator solution was prepared. The total initiator solution volume and cyclohexane volume were adjusted to 960 μL (0.0512 mmol) and 6.1 mL, respectively.

Procedure for Figure 3.2a-c: Constant Addition Rate Profiles

The synthesis was performed according to the general procedure and the New Era NE-4000 Double Syringe Pump was programmed to the following addition rate profiles for the constant rates shown in Table 3.1.

Table 3.1. Constant Rate Addition Profiles

Addition Time (min)	Rate (µL/h)	Total Volume (µL)
20	960	320
40	480	320
60	320	320
80	240	320
100	192	320
120	160	320

Procedure for Figure 3.2d-f: Linearly Ramped Addition Rate Profiles

The synthesis was performed according to the general procedure. All linearly increasing addition rate profiles were programmed as a sequence of 20 step increments with each step corresponding to a phase in the New Era NE-4000 Double Syringe Pump program. See Table 2.2 for detailed rates and volumes.

Table 3.2. Linearly Ramped Rate Addition Profile

Step #	Rate (µL/h)							Volume per Step (µL)
	20min	30min	40min	50min	60min	80min	100min	
1	167	111	83	67	56	42	33	2.8
2	250	167	125	100	83	62	50	4.2
3	334	223	167	134	111	83	67	5.6
4	417	278	209	167	139	104	84	7.0
5	501	334	250	200	167	125	100	8.3
6	584	390	292	234	195	146	117	9.7
7	668	445	334	267	223	167	134	11.1
8	751	501	376	301	250	188	150	12.5
9	835	557	417	334	278	209	167	13.9
10	918	612	459	367	306	230	184	15.3
11	1002	668	501	401	334	250	200	16.7
12	1085	724	543	434	362	271	217	18.1
13	1169	779	584	468	390	292	234	19.5
14	1252	835	626	501	417	313	250	20.9
15	1336	890	668	534	445	334	267	22.3
16	1419	946	710	568	473	355	284	23.7
17	1503	1002	751	601	501	376	301	25.0
18	1586	1057	793	634	529	397	317	26.4
19	1670	1113	835	668	557	417	334	27.8
20	1753	1169	877	701	584	438	351	29.2

Procedure for Figure 3.2g-i: Exponentially Ramped Addition Rate Profiles

The synthesis was performed according to the general procedure. All exponentially increasing addition profiles were programmed as a sequence of 20 step increments with each step corresponding to a phase in the New Era

NE-4000 Double Syringe Pump program. See Table 3.3 for detailed rates and volumes. For 80, 100, and 120 min long exponentially ramped additions, the total addition volume had to adjusted to 960 µL due to a more dilute initiator solution (0.0533 M) (Table 3.4).

Table 3.3. Exponentially Ramped Rate Addition Profile for 20 – 60 min

Step #	**Rate (µL/h)**			**Volume per Step (µL)**
	20min	40min	60min	
1	9.2	4.6	3.1	0.2
2	12.9	6.4	4.3	0.2
3	18.0	9.0	6.0	0.3
4	25.2	12.6	8.4	0.4
5	35.3	17.7	11.8	0.6
6	49.4	24.7	16.5	0.8
7	69.2	34.6	23.1	1.2
8	96.9	48.5	32.3	1.6
9	135.6	67.8	45.2	2.3
10	189.9	95.0	63.3	3.2
11	265.9	132.9	88.6	4.4
12	372.2	186.1	124.1	6.2
13	521.1	260.6	173.7	8.7
14	729.5	364.8	243.2	12.2
15	1021	510.7	340.4	17.0
16	1430	715.0	476.6	23.8
17	2002	1001	667.3	33.4
18	2803	1401	934.2	46.7
19	3924	1962	1308	65.4
20	5493	2747	1831	91.6

Table 3.4. Exponentially Ramped Rate Addition Profile for 80 – 120 min

Step #	Rate (µL/h)			Volume per Step (µL)
	80min	100min	120min	
1	6.9	5.5	4.6	0.5
2	9.7	7.7	6.4	0.6
3	13.5	10.8	9.0	0.9
4	18.9	15.1	12.6	1.3
5	26.5	21.1	17.7	1.8
6	37.1	29.7	24.7	2.5
7	51.9	41.5	34.6	3.5
8	72.7	58.1	48.4	4.8
9	101.7	81.4	67.8	6.8
10	142.4	113.9	95.0	9.5
11	199.4	159.5	132.9	13.3
12	279.1	223.3	186.1	18.6
13	390.8	312.6	260.6	26.1
14	547.1	437.7	364.8	36.5
15	765.9	612.7	510.7	51.1
16	1072	857.8	715.0	71.5
17	1501	1201	1001	100.1
18	2102	1681	1401	140.1
19	2942	2354	1962	196.2
20	4119	3295	2747	274.6

Procedure for Figure 3.4: Bell-Shaped Addition Rate Profiles

The synthesis was performed according to the general procedure. All bell-shaped addition profiles were programmed as a sequence of 20 step

increments with each step corresponding to a phase in the New Era NE-4000 Double Syringe Pump program. See Table 3.5 for detailed rates and volumes.

Table 3.5: Bell-Shaped Rate Addition Profile

Step #	**Rate (µL/h)**					**Volume per Step (µL)**
	20min	40min	60min	80min	100min	
1	25.6	17.0	12.8	10.2	8.5	0.9
2	76.7	51.1	38.3	30.7	25.6	2.6
3	153.4	102.2	76.7	61.3	51.1	5.1
4	255.6	170.4	127.8	102.2	85.2	8.5
5	383.4	255.6	127.8	153.4	127.8	12.8
6	536.8	357.8	191.7	214.7	178.9	17.9
7	766.8	511.2	268.4	306.7	255.6	25.6
8	945.7	630.5	383.4	378.3	315.2	31.5
9	1074	715.7	472.9	429.4	357.8	35.8
10	1150	766.8	536.8	460.1	383.4	38.3
11	1074	715.7	575.1	429.4	357.8	35.8
12	945.7	630.5	536.8	378.3	315.2	31.5
13	766.8	511.2	472.9	306.7	255.6	25.6
14	536.8	357.8	383.4	214.7	178.9	17.9
15	383.4	255.6	268.4	153.4	127.8	12.8
16	255.6	170.4	191.7	102.2	85.2	8.5
17	153.4	102.2	76.7	61.3	51.1	5.1
18	76.7	51.1	38.3	30.7	25.6	2.6
19	25.6	17.0	12.8	10.2	8.5	0.9
20	12.8	8.5	6.4	5.1	4.3	0.4

Description of MWD shape by asymmetry factor (A_s), skewness (α_3) and kurtosis (α_4)

The asymmetry factors (A_s) of our MWDs were calculated using the EcoSEC Analysis program. A_s is defined as the ratio of the distance from the peak maximum to the right edge of the peak and the distance from the peak maximum to the left edge of the peak at 10 % peak height. A graphical description is provided in Figure 3.7.

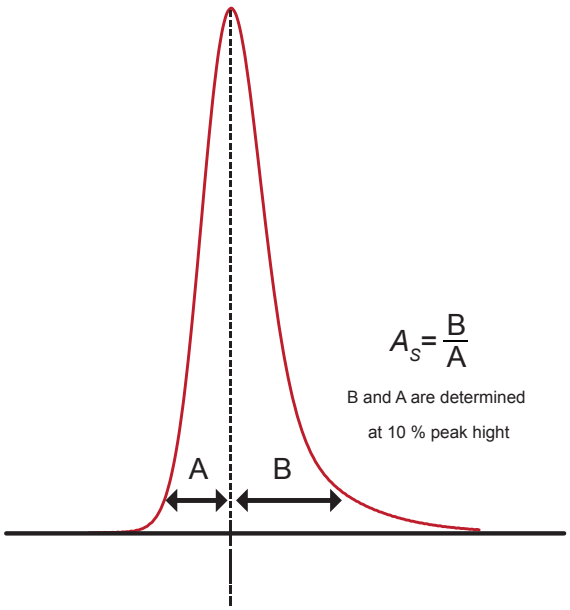

Figure 3.7. Graphical Illustration of the Calculation of Asymmetry Factor A_s

The third and fourth moments about the mean, skewness (α_3) and kurtosis (α_4), respectively, were calculated according to the method described by Rudin.[1] The equations are shown below:

$$\alpha_3 = \frac{M_z M_w M_n - 3M_n^2 M_w + 2M_n^2}{(M_w M_n - M_n^2)^{3/2}} \quad (3.1)$$

$$\alpha_4 = \frac{M_{z+1} M_z M_w M_n - 4M_n^2 M_z M_w + 6M_n^3 M_w - 3M_n^4}{(M_w M_n - M_n^2)^2} \quad (3.2)$$

General Procedure for Poly(styrene-b-isoprene) (PS-*b*-PI) Polymerizations and Sample Preparation for Dynamic Mechanical Analysis

Polystyryllithium was prepared according to the general procedure. After approximately 5 hours, 1 mL (9.99 mmol) of isoprene was added to the stirring reaction mixture. The solution turned colorless. The reaction was allowed to stir for 6 hours to allow for full conversion according to ^{1}H NMR. See Table 3.6 from details on block polymer compositions.

Preparation of PS-*b*-PI samples for Dynamic Mechanical Analysis

0.2 wt% BHT as a stabilizer was added as a solution in DCM followed by concentrating on a rotary evaporator and vacuum overnight. After densifying at 120 ^{o}C and 2000 lbs. for 5 min using a Carver Press, samples were compression molded into dog bones (16 mm, 2.5 mm, 0.6 mm) at the same temperature and pressure for 5 minutes.

Table 3.6: PS-*b*-PI samples for dynamic mechanical analysis; f_{PI} indicates the weight fraction of polyisoprene

entry	PS M_n	PS $Đ$	PS A_s	PSPI M_n	PS-PI $Đ$	f_{PI}
1a	14.1	1.19	1.85	35.6	1.14	0.60
1b	14.2	1.22	0.52	35.1	1.16	0.60
2a	14.9	1.42	3.52	36.8	1.21	0.60
2b	14.1	1.39	0.37	33.6	1.22	0.58
3a	15.2	1.69	4.48	36.3	1.25	0.58
3b	14.1	1.71	0.31	36.5	1.28	0.61
4a	14.4	2.01	4.97	37.2	1.28	0.61
4b	13.8	1.97	0.26	34.4	1.29	0.60
5a	15.1	1.55	4.14	37.7	1.21	0.60
5b	14.9	1.51	0.33	35.5	1.23	0.60
6a	14.2	1.87	4.71	34.8	1.30	0.59
6b	15.5	1.78	0.29	36.3	1.32	0.57
7a	14.5	1.68	0.32	35.9	1.27	0.60

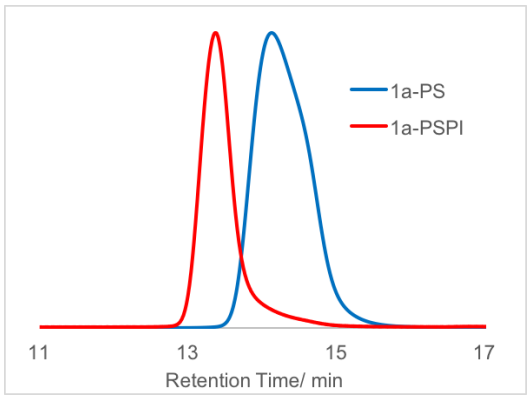

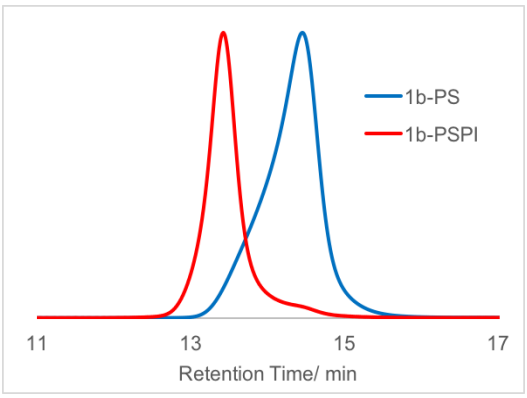

Figure 3.8. Size-exclusion chromatograms of polydisperse PS block and the corresponding PS-*b*-PI block copolymers corresponding to entries 1a,b in Figure 3.6.

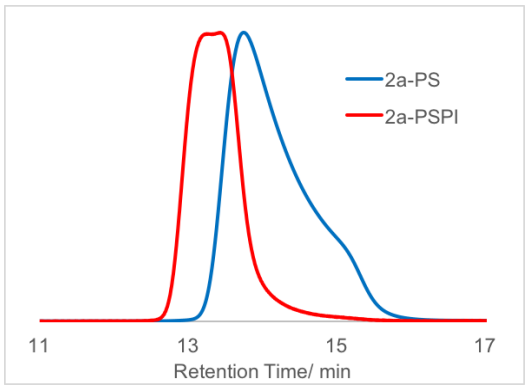

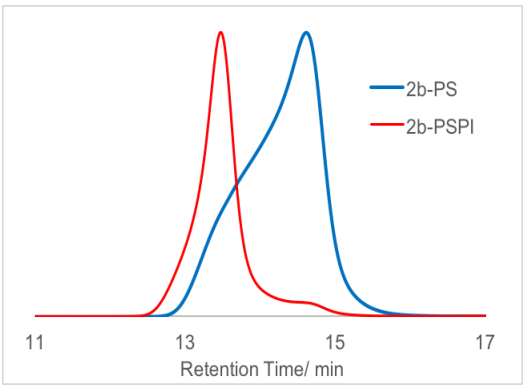

Figure 3.9. Size-exclusion chromatograms of polydisperse PS block and the corresponding PS-*b*-PI block copolymers corresponding to entries 2a,b in Figure 3.6.

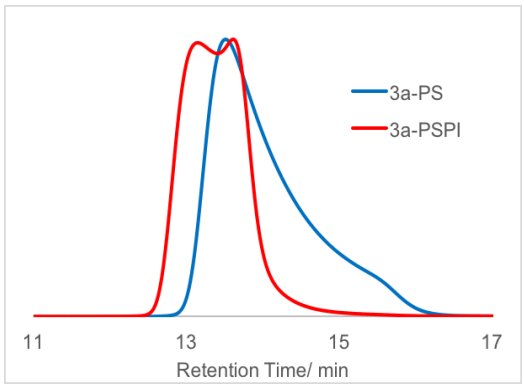

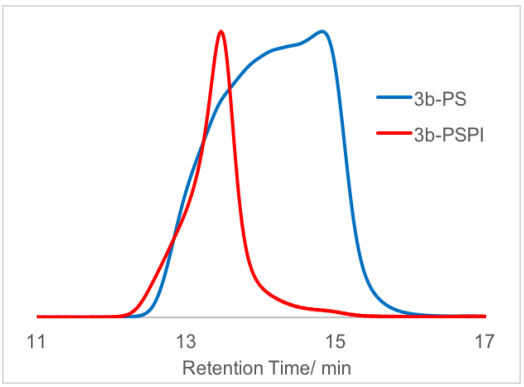

Figure 3.10. Size-exclusion chromatograms of polydisperse PS block and the corresponding PS-*b*-PI block copolymers corresponding to entries 3a,b in Figure 3.6.

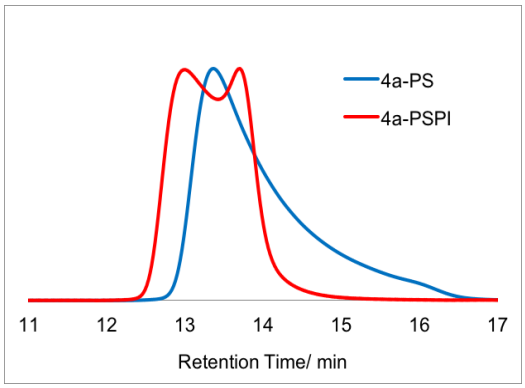

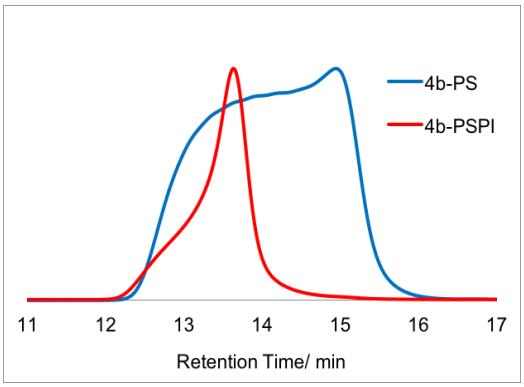

Figure 3.11. Size-exclusion chromatograms of polydisperse PS block and the corresponding PS-*b*-PI block copolymers corresponding to entries 4a,b in Figure 3.6.

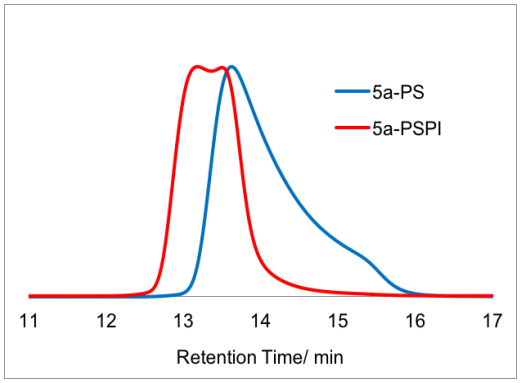

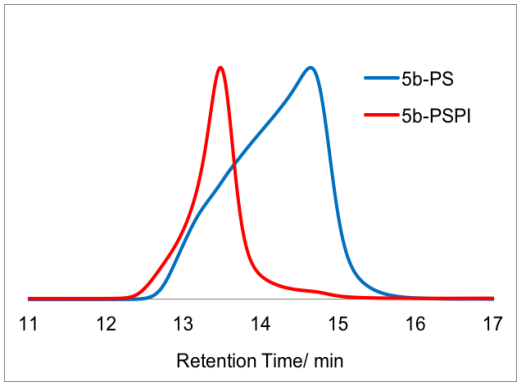

Figure 3.12. Size-exclusion chromatograms of polydisperse PS block and the corresponding PS-*b*-PI block copolymers corresponding to entries 5a,b in Figure 3.6.

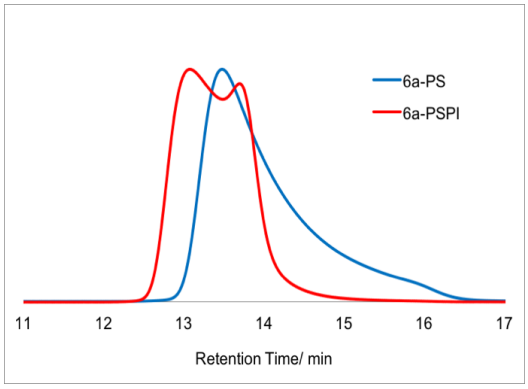

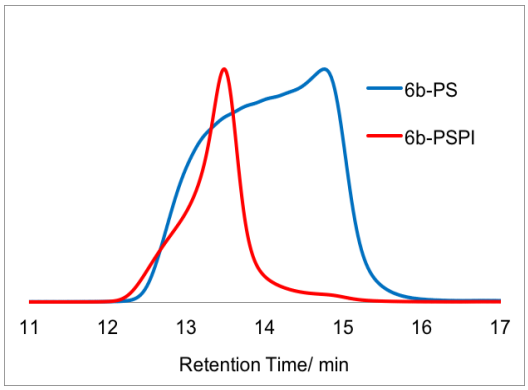

Figure 3.13. Size-exclusion chromatograms of polydisperse PS block and the corresponding PS-*b*-PI block copolymers corresponding to entries 6a,b in Figure 3.6.

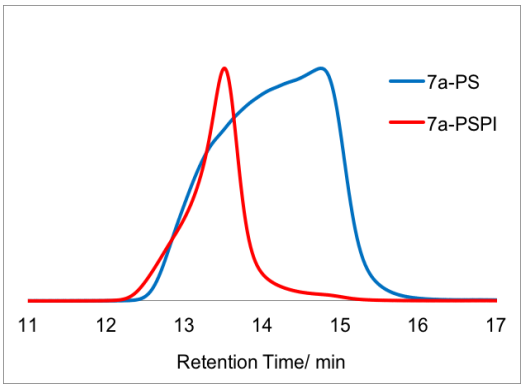

Figure 3.14. Size-exclusion chromatograms of polydisperse PS block and the corresponding PS-*b*-PI block copolymers corresponding to entry 7a in Figure 3.6.

Measurement of Young's Moduli of PS-*b*-PI samples

Stress/strain curves were obtained in tension with force control of 1.0 N/min and Young's moduli were obtained by evaluating the slope of the stress/strain curve at low strain values.

3.6 Appendix References

(1) Rudin, A., *J. Chem. Ed.*, **1969**, 46, 595.

CHAPTER 4

MANIPULATION OF MOLECULAR WEIGHT DISTRIBUTION SHAPE AS A NEW STRATEGY TO CONTROL PROCESSING PARAMETERS

4.1 Abstract

Molecular weight and dispersity (*Đ*) influence physical and rheological properties of polymers, which are of significant importance in polymer processing technologies. However, these parameters provide only partial information about the precise composition of polymers, which is reflected by the shape and symmetry of molecular weight distribution (MWD). In this work, the effect of MWD symmetry on thermal and rheological properties of polymers with identical molecular weights and *Đ* is demonstrated. Remarkably, when the MWD is skewed to higher molecular weight, a higher glass transition temperature (T_g), increased stiffness, increased thermal stability, and higher apparent viscosities are observed. These observed differences are attributed to the chain length composition of the polymers, easily controlled by the synthetic strategy. This work demonstrates a versatile approach to engineer the properties of polymers using controlled synthesis to skew the shape of MWD.

4.2 Introduction

Understanding the thermal and viscoelastic properties of polymers is critical for the engineering and determination of processing conditions in important industrial technologies, such as hot-melt extrusion (HME), injection

molding, and 3D printing (3DP).[1-4] It is well known that rheological properties of polymers are strongly influenced by their chemical structure, molecular weight, and polydispersity (*Đ*).[2,5-10] In particular, variations in *Đ* change the relaxation profiles of polymers by shifting their crossover point, and affect the range of deformation rates and temperatures required for melt processing.[2,5] However, *Đ* provides only partial information about the relative distribution of polymer chain sizes, being defined as a ratio of the weight-average (M_w) and the number-average (M_n) molecular weights. Therefore, *Đ* does not provide information about the symmetry and shape of molecular weight distribution (MWD), which also influences polymer properties.[11,12] Previous studies on MWD effects on polymer properties have been limited in their rigor due to insufficient technology to precisely control the shape and symmetry of the distribution. A simple approach to tuning polymer processability without changing its chemical characteristics is highly desirable.

Recently, we developed a synthetic strategy to control the MWD shape of polymers with identical M_n and *Đ* by feeding the initiation species into a controlled polymerization process at predetermined rates and times. This temporal control of chain initiation dictates the molar quantities of each chain length in the final material.[11,12] This simple and scalable synthetic method to control the symmetry (skewness) of MWDs enables the next generation of structure property investigations. Of particular interest is the effect of molecular composition, or skewness of the distribution, on the rheological properties of polymers. This modular approach enables the preparation of polymers with

complementary (opposite) skewness, and therefore enables the extension of systematic investigations of the classical effects of M_n and $Đ$ on rheological properties of polymers.

In this work, we investigate and compare thermal and rheological properties of linear polymers with identical M_n and $Đ$, but with distinctly different skewness of MWDs. We demonstrate that a facile synthetic technique to control the symmetry of MWD enables the tuning of thermal and rheological properties of polymers towards desired performances, such as enhanced thermal stability or lowered processing temperatures.

4.3 Results and Discussion

Two different linear polystyrene samples were prepared by a previously reported method demonstrated in Figure 4.1a (initiation profiles are shown in Figure 4.5 of the Chapter 4 Appendix).[11] The M_n and M_w of the synthesized polymers were identical (73.5 and 101.4 kg/mol, respectively, $Đ$ = 1.38), as indicated by SEC. However, the MWD skew of these polymers was opposite. Asymmetry factor (A_s) was used as a relative measure of sample skewness and is defined as the distance of the center line (peak max) to the back slope divided by the center line to the front slope at 10% peak height.[11-13] One sample with a positive skew (PS_{high}, high molecular weight skew, A_s = 1.8) and one with a negative skew (PS_{low}, low molecular weight skew, A_s = 0.4) were synthesized.[11] The distinctly different MWD symmetries are evident by SEC traces shown in Figure 4.1b.

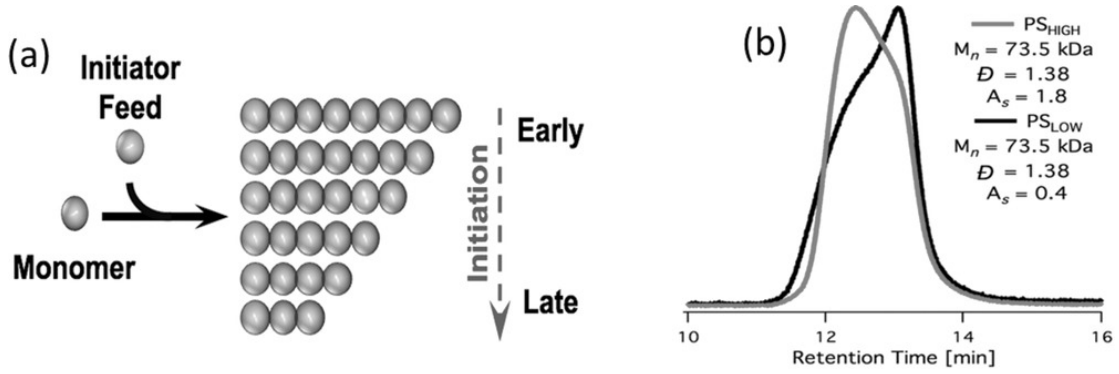

Figure 4.1. Preparation and characterization of polymers with skewed MWD. a) General strategy for controlling MWD shape through temporally regulating polymer chain initiation. b) SEC traces of polymers PS_{high} and PS_{low}, which exhibit a distinctly different skewness of their MWD. Regardless of identical M_n and $Đ$, PS_{low} contains a larger fraction of low molecular weight polymer chains, and PS_{high} has a higher fraction of high molecular weight polymer chains.

The glass transition temperature (T_g) is a fundamental and critical parameter to investigate in any polymer system. Below the T_g, the stiffness of polymers, associated with their dominant solid-like nature, limits their ability to disentangle and flow.[1, 2] Therefore, the tan delta characteristic is crucial, as it determines the lowest temperature for an efficient melt processing. The effect of M_n and $Đ$ on T_g is well known,[1, 9, 10] however the effect of skewness has yet to be explored. DMA results indicate noticeable differences between T_g values of PS_{low} and PS_{high}, with the average values of 104.0 and 110.6 °C for PS_{low} and PS_{high}, respectively. A representative loss tangent curve is demonstrated in Figure 4.2a (statistical data is shown in Figure 4.6 of the Chapter 4 Appendix). The results are also supported by DSC (Figure 4.7, Chapter 4 Appendix). The

differences between the T_g values obtained by both methods can be attributed to the differences between the methodologies. While much larger amounts of polymer are used for DMA (gram scale); only a few milligrams of materials are used for DSC. Therefore, DMA provides a higher accuracy by taking into consideration mass attributions.[1] These differences are attributed to the variation in chain length composition of these polymers. Since shorter polymer chains require less thermal energy to disentangle and flow, the increase in their relative content decreases the transition temperature. These differences clearly demonstrate the effect of MWD symmetry on flow properties. Therefore, the ability to skew the symmetry of polymers by choosing the precise synthetic methodology,[11, 12] gives direct control over the operating temperatures available for the melt processing of a specific polymer.

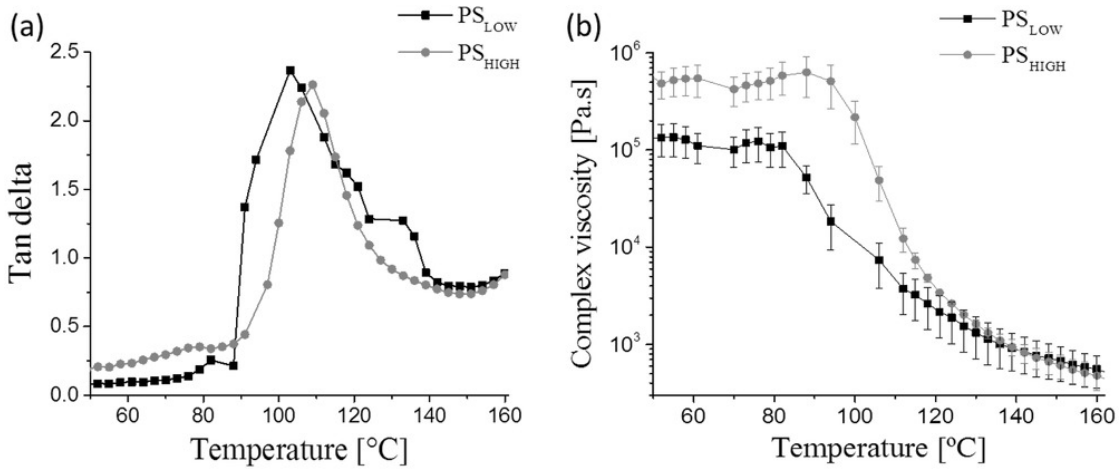

Figure 4.2. Evaluation of temperature-dependent flow characteristics of PS_{high} and PS_{low}. a) A representative tan delta curve demonstrates differences between the T_gs of PS_{high} and PS_{low}. b) Complex viscosities of PS_{high} and PS_{low} illustrate significantly higher stiffness of PS_{high} in low temperatures region.

Viscosity is another essential property to be considered, which describes the dynamic response of viscoelastic materials to subjected temperatures and shears.[1] Viscosity profiles are crucial for polymer processing, since exceedingly high viscosities generate high torques during HME, and as a result may resist or even prevent the rotation of the screw.[1, 2] When the viscosity is exceedingly low, extruded filaments fail to retain their desired shape.[2] Therefore, it is essential to establish a well-defined operational window for melt processability. Complex viscosity of PS_{high} is significantly higher than that of PS_{low} between 50 and 127 °C (Figure 4.2b). With the increase in temperature, the complex viscosity of polymers PS_{low} and PS_{high} gradually decreases as expected, and when the examined temperatures exceed 127 °C, the viscosity profiles of both polymers overlap and reach almost identical values. These observations can be attributed to the thermal relaxation achieved by polymers of different chain lengths at different temperatures. Above a critical temperature, all polymer compositions become sufficiently fluidic, exhibiting similar flow characteristics.

The optimal complex viscosity range for polymers used in HME has been previously reported as ≈ 1000 – 10,000 Pa s.[1,2] Adjusting the HME temperature accordingly allows a facile scalability of the process.[1] Therefore, these values define the recommended operational window for HME. While PS_{low} reaches optimal complex viscosity values between 106 and 138 °C, the optimal operational window of PS_{high} requires elevated temperatures of 115–138 °C. As a result, the temperature range required for processing of PS_{low} is significantly broadened. Although both polymer samples exhibit identical M_n and $Đ$,

differences in their molar mass compositions affect their processing temperature regime.

The examination of apparent viscosity indicates that both polymers exhibit shear thinning with almost identical shear thinning rates. However, both below and above the T_g of PS_{high} has a higher apparent viscosity. We demonstrate this at 25 and 150 °C, Figure 4.3a,b, respectively. At 25 °C, the apparent viscosity of PS_{high} is about 3 times higher than the apparent viscosity of PS_{low}. Significant differences are more obvious at the low shear region, but become less pronounced when shear rates reach ≈1000 /s (Figure 4.3a). Surprisingly, upon the increase in temperature to 150 °C, which is well above the T_g of both polymer samples, differences between the apparent viscosities were still observed (Figure 4.3b). The apparent viscosity of PS_{high} remained 2 – 3 times higher than the apparent viscosity of PS_{low}. With the increase in shear rates above 300 /s, apparent viscosity profiles of both polymers became similar.

These findings indicate that even well above the T_g, where both short and long chain polymers are provided with sufficient energy to flow, chain length composition continues to contribute to physical properties. The ability to process polymers at decreased shear rates by implementing a simple synthetic approach can be harnessed to enhance the processability of polymers, especially when the availability of powerful high shear equipment is limited.

Macromolecular responses to stress and strain are time dependent, owing to the viscoelastic nature of the material at study.[2] To obtain an insight

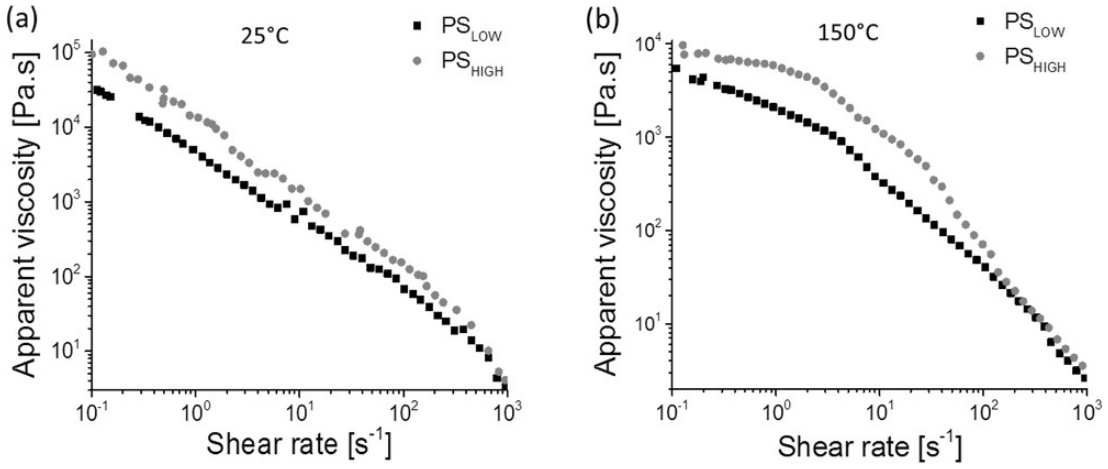

Figure 4.3. Apparent viscosity of polymers PS_{high} and PS_{low} as a function of shear rate at a) 25 °C and b) 150 °C. The apparent viscosity of PS_{high} is higher than the apparent viscosity of PS_{low}.

into the stiffness of PS_{high} and $PS_{low,}$ dynamic moduli and complex viscosity were examined at 25, 120, and 150 °C (Figure 4.4). For all the examined temperatures, the storage modulus and the complex viscosity of PS_{high} were consistently higher than those of PS_{low}, indicating its increased stiffness. The complex viscosities of PS_{high} and PS_{low} gradually decreased with the increase in frequencies, as expected, for all the examined temperatures. At 25 °C storage moduli of both PS_{high} and PS_{low} exhibited very weak frequency dependence, which can be attributed to their exceedingly dominant solid-like nature at room temperature within the examined frequencies range (Figure 4.4a). With further increase in temperature above the T_g (120 and 150 °C), storage moduli decreased and exhibited strong frequency-dependent behavior. At 120 °C and high frequencies region, the storage modulus of PS_{high} was higher by almost

one order of magnitude than the storage modulus of PS_{low}. Despite the reduction in the observed differences between PS_{high} and PS_{low} moduli at the low frequencies region, the storage modulus of PS_{high} remained up to 2 times higher than the storage modulus of PS_{low} (see Figure 4.4b for representative data and Figure 4.8 of the Chapter 4 Appendix for statistical data). The observed differences are attributed to the different chain length compositions of the polymers. PS_{high} contains a larger fraction of high molecular weight polymers than PS_{low}; therefore its response to the induced oscillatory deformation at shorter time scales is more limited, which is associated with a strong elastic response, represented by high storage modulus values. Although a similar trend is observed at the low frequencies region, with the gradual increase in provided relaxation time the effect of the molecular weight composition decreases, indicating less pronounced long term differences between the polymers. When the temperature increased to 150 °C, only small differences between the storage moduli and complex viscosities of PS_{high} and PS_{low} were observed, which can be explained by sufficiently high energy provided to all polymer chain length compositions (Figure 4.4c). Frequency sweep results indicate that polymer stiffness is affected by polymer chain length composition, which was tuned by controlling the shape of MWD.

Another important characteristic for consideration during HME is thermal degradation temperature (T_d), which should not be exceeded during thermal processing of polymers in order to retain their function.[1] TGA shows differences between T_d values of PS_{high} and PS_{low}, demonstrated in Figure 4.9 (Chapter 4

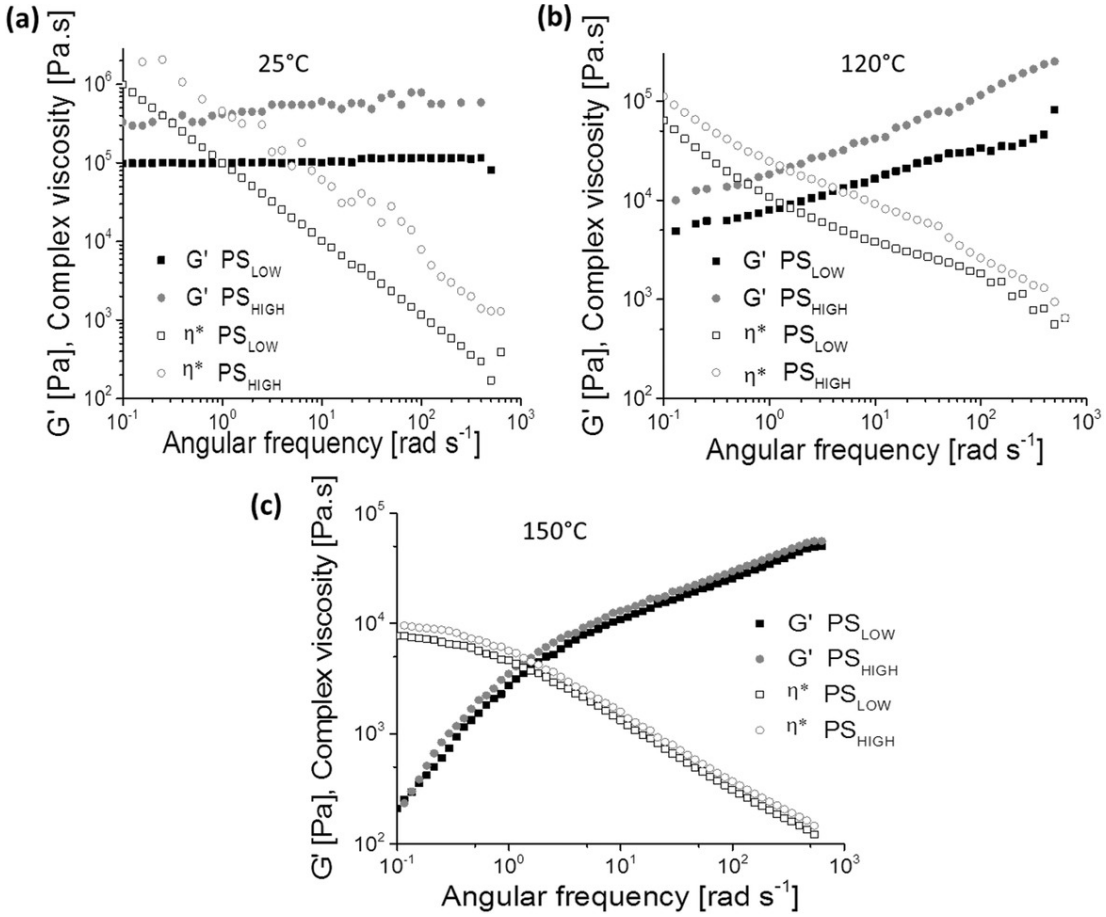

Figure 4.4. PS_{high} and PS_{low} storage modulus and complex viscosity as a function of frequency at a) 25 °C, b) 120 °C, and c) 150 °C. PS_{high} storage modulus and complex viscosity are consistently higher than PS_{low}.

Appendix). The clearly observed differences in T_d (≈10 °C) and the degradation profiles of PS_{high} and PS_{low} could be attributed to the different compositions of these polymers. The larger fraction of long chain polymers results in an improved thermal stability, which shifts the T_d to higher temperatures.[14]

Rheological differences between PS_{high} and PS_{low} can be explained by the well-known reptation theory.[15] In the melted state, polymer chains are closely packed and their random motion is constrained by the neighboring chains. In the entangled systems the relaxation time of polymers is a function of the number of monomer units, reflected by their molecular weight, and strongly affecting their rheological properties. With the increase in molecular weight the number of entanglements increases, which reduces the mobility of polymer chains.[15] Therefore, skewing the MWD of polymers toward higher or lower molecular weights has a direct effect on their relaxation ability, providing a precise control over their rheological properties.

4.4 Conclusions

In summary, we have demonstrated that molecular composition of polymers, reflected by the shape and the symmetry of MWD, has a significant impact on their thermal and rheological properties. While the effect of M_n and $Đ$ on polymer processability has been broadly explored, these parameters provide only partial description of polymers viscoelastic and thermal properties. Shifting the symmetry of MWD toward a larger content of short chain polymers enables an efficient reduction of temperatures and shear rates

required for polymer processing, which allows milder processing conditions and a broader operational window. When improved thermal stability is a major consideration, MWD symmetry shift toward a larger content of long chain polymers is favorable. We have demonstrated that MWD shape can serve as a powerful tool for the optimization of polymer processing parameters.

4.5 References

(1) S. S. Gupta, A. Meena, T. Parikh, A. T. Serajuddin, J. *Excipients Food Chem.*, **2014**, 5, 32.

(2) J. Aho, J. P. Boetker, S. Baldursdottir, J. Rantanen, *Int. J. Pharm.,* **2015**, 494, 623.

(3) M. Nadgorny, Z. Xiao, C. Chen, L. A. Connal, *ACS Appl. Mater. Interfaces* **2016**, 8, 28946.

(4) M. Nadgorny, Z. Xiao, L. A. Connal, *Mol. Syst. Des. Eng.*, **2017**, DOI: 10.1039/C7ME00023E.

(5) X. Ye, T. Sridhar, *Macromolecules* **2005**, 38, 3442.

(6) M. Ansari, S. G. Hatzikiriakos, A. M. Sukhadia, D. C. Rohlfing, *Rheol. Acta*, **2011**, 50, 17.

(7) S. H. Wasserman, W. W. Graessley, *J. Rheol.,* **1992**, 36, 543.

(8) H. Watanabe, T. Sakamoto, T. Kotako, *Macromolecules* **1985**, 18, 1008.

(9) D. Nichetti, I. Manas-Zloczower, *Polym. Eng. Sci.,* **1999**, 39, 887.

(10) N. W. Collis, M. R. Mackley, *J. Non-Newtonian Fluid Mech*., **2005**, 128, 29.

(11) D. T. Gentekos, L. N. Dupuis, B. P. Fors, *J. Am. Chem. Soc*., **2016**, 138, 1848.

(12) V. Kottisch, D. T. Gentekos, B. P. Fors, *ACS Macro Lett*., **2016**, 5, 796.

(13) J. J. Kirkland, W. W. Yau, H. J. Stoklosa, C. H. J. Dilks, *J. Chromatogr. Sci.,* **1977**, 15, 303.

(14) M. E. Calahorra, M. Cortazar, J. I. Eguiazabal, J. M. Guzman, *J. Appl. Polym. Sci.*, **1989**, 37, 3305.

(15) J. M. Piau, J. F. Agassant, Rheology for Polymer Melt Processing, Elsevier, Amsterdam, The Netherlands 1996, p. 5.

4.6 Appendix

Experimental

Anionic Polymerization of Skewed Polystyrenes (PS_{low}, PS_{high})

All reactions were performed in a Unilab MBraun Glovebox. Styrene (99%, Sigma Aldrich) was stirred over calcium hydride (CaH_2) overnight and vacuum transferred into a flame dried Schlenk bomb followed by three freeze–pump–thaw cycles. Cyclohexane (Fisher Scientific, ACS Grade) was distilled under argon after stirring over a 1:1 mixture of sec-butyllithium (*s*-BuLi) and diphenylethylene (deep red) for 1 h followed by three freeze–pump–thaw cycles. s-BuLi (1.4 M, Sigma Aldrich) and isopropanol (Sigma Aldrich) were used as received. Polystyrene samples PS_{high} and PS_{low} were synthesized by previously described procedure.[1,2] Briefly, PS_{high} was prepared by slow addition of *s*-BuLi (516 µL, 35×10^{-3} mol) at constant rate of 516 µL/h to a solution of styrene (1 mL) in cyclohexane (8 mL). PS_{low} was prepared in a similar manner with an exponentially ramped addition rate of *s*-BuLi over 2.5 h. Each reaction was quenched with a few drops of isopropanol after 6 h. These polymers were isolated by removing the solvent under reduced pressure to yield a white solid.

Size Exclusion Chromatography (SEC)

All polymer MWDs were characterized using a Tosoh EcoSEC HLC 8320GPC system with two SuperHM-M columns in series and a flow rate of 0.350 mL/min with tetrahydrofuran as the eluent. Number-average molecular weights, weight-average molecular weights, dispersities, and asymmetry

factors, were calculated from refractive index chromatograms against TSKgel polystyrene standards.

Rheological Measurements

Rheological characterization was conducted on a controlled stress rheometer with parallel plates geometry (40 mm diameter, AR-G2, TA Instruments). For all the rheological tests, solid samples were used by compressing and melting polystyrene powder into 40 mm diameter uniform slabs.[1] Dynamic mechanical analysis (DMA) was performed by ramping up the temperature at constant increments of 3 °C from 50 to 160 °C, at a constant angular frequency of 6.283 rad/s and 0.5% strain. Apparent viscosity measurements were conducted by a continuous ramp up of the shear rate from 0.1 to 1000 /s at a constant temperature (25 and 150 °C). Frequency sweep tests were performed by scanning angular frequencies from 0.1 to 628.3 rad/s under 1.0% strain at various temperatures (25, 120, and 150 °C). The rheological measurements were repeated (n = 3) to assure reproducibility.

Thermogravimetric Analysis (TGA)

The analysis was performed on a PerkinElmer Diamond instrument (Pyris Diamond TG-DTA, High Temp 115). The sample was placed in an alumina crucible and heated from 30 to 600 °C at a constant rate of 10 °C/min under nitrogen flow. The degradation temperature was indicated as a transition point where the sharpest change in the curve occurred (a point of a

drastic change in the slope). The measurements were repeated (n = 3) to assure reproducibility.

Differential Scanning Calorimetry (DSC)

The tests were conducted on a PerkinElmer DSC8500, with a scanning rate of 10 °C/min, in the temperature range of 25–200 °C.

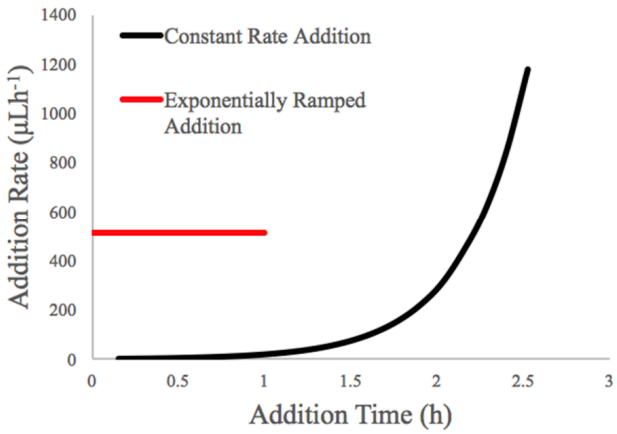

Figure 4.5. *s*-BuLi initiator addition profiles for PS_{high} (constant rate, red) and PS_{low} (exponentially ramped rate, black) to produce polymers with the same M_n and $Đ$ but with different MWD shapes

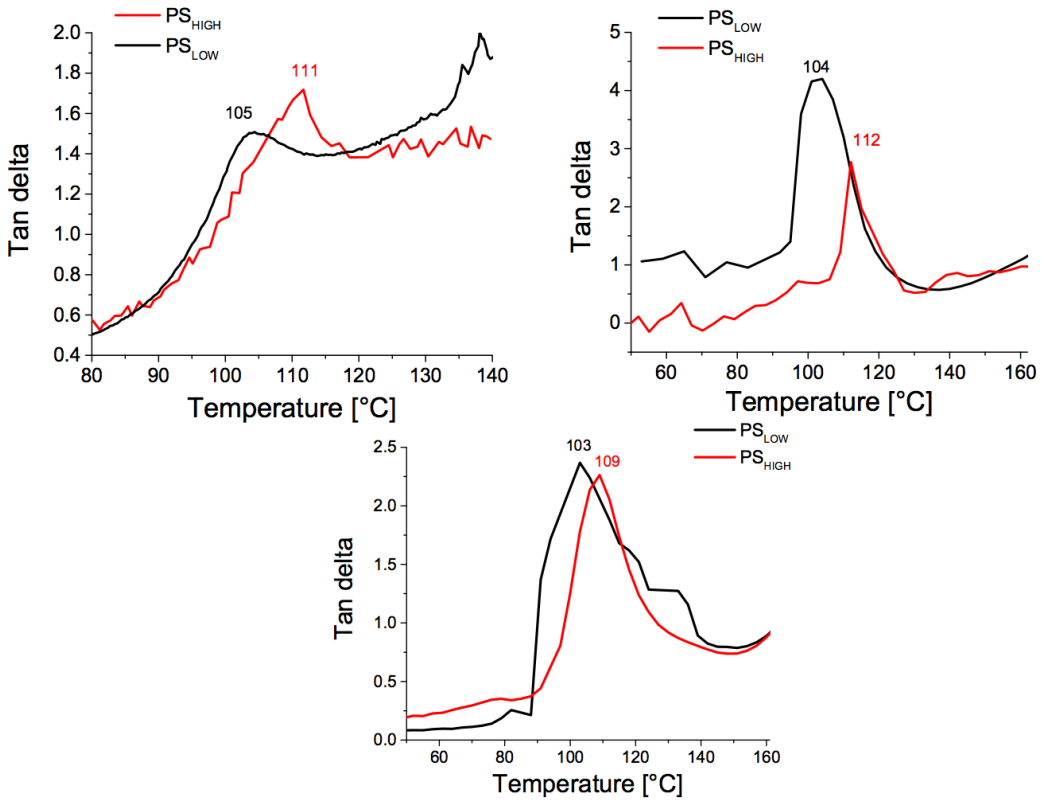

Figure 4.6. PS_{high} and PS_{low} tan delta curves. Three independent sets of DMA results are shown. T_g is represented by the peak of tan delta curve. T_g values of PS_{high} are shifted towards higher temperatures compared to T_g values of PS_{low} due to an increased content of longer polymer chains. T_g values are (average ± σ):

$$T_g\,(PS_{high}) = 110.6 \pm 1.5\ °C$$

$$T_g\,(PS_{low}) = 104.0 \pm 1.0\ °C$$

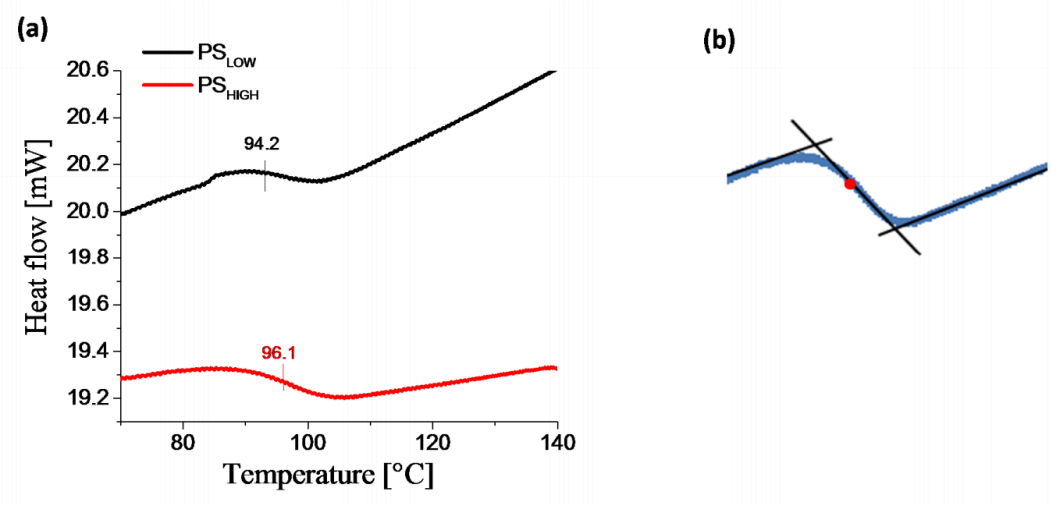

Figure 4.7. DSC profiles of PS_{high} and PS_{low}. (a)The results indicate ~2°C difference between the T_gs of PS_{high} and PS_{low}. (b) Demonstration of the method used to determine the T_gs. T_g is represented by the midpoint of the line with a distinct slope (red dot).

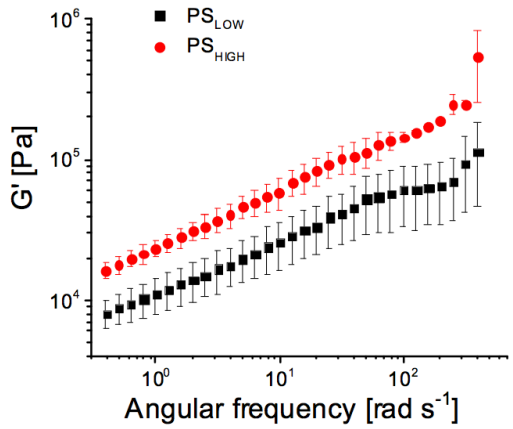

Figure 4.8. Frequency sweep curves of PS_{high} and PS_{low} at 120°C (average ± σ). Both polymers exhibit strong frequency dependence. Average storage modulus values of PS_{high} are consistently higher than the storage modulus values of PS_{low} at all the examined frequencies range. Differences of almost one order of magnitude are observed at the high frequencies region, which gradually decrease. At the low frequencies region the storage modulus of PS_{high} is up to 2 times higher than the storage modulus of PS_{low}.

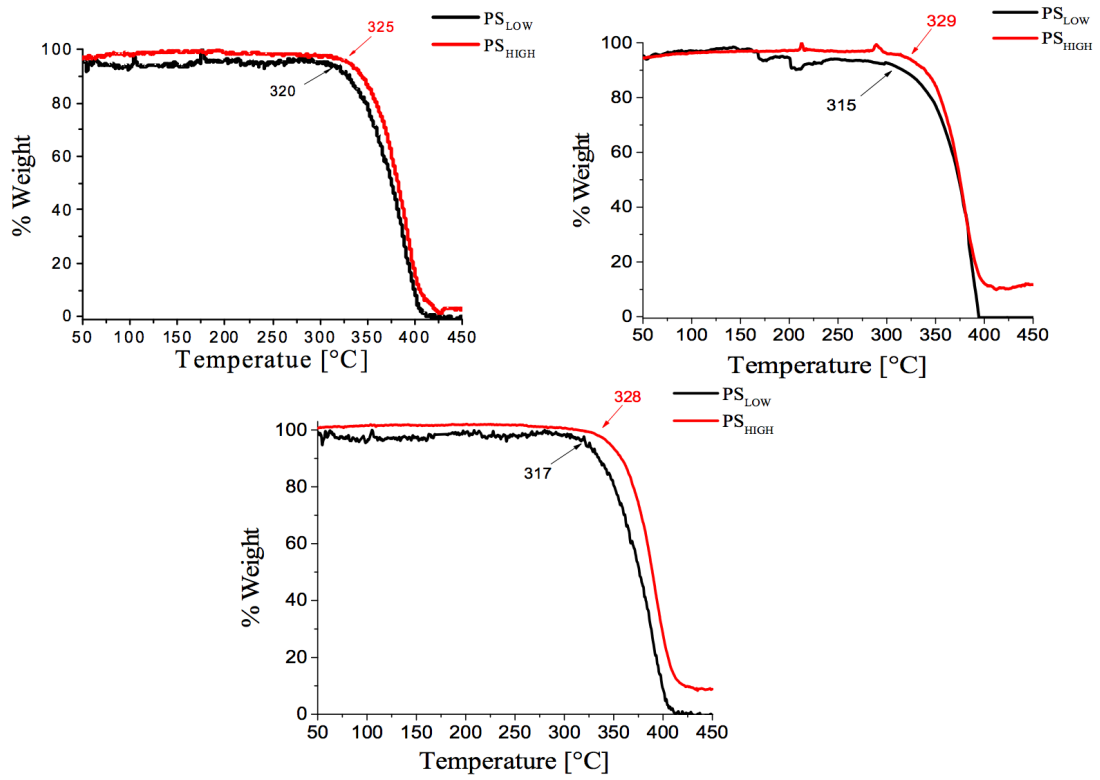

Figure 4.9. TGA curves of polymers PS_{high} and PS_{low} (3 independent scans are demonstrated). In all the examined cases, the degradation temperature of PS_{high} is consistently shifted towards higher temperatures relatively to PS_{low}, due to a higher content of long polymer chains, which are more thermally stable. (T_d is indicated as a point of a sharp change in the slope). Moreover, PS_{high} exhibits a more moderate degradation profile. T_d values are (average ± σ):

$$T_d\ (PS_{high}) = 327.3 \pm 2.1\ °C$$

$$T_d\ (PS_{low}) = 317.3 \pm 2.5\ °C$$

4.6 Appendix References

(1) D. T. Gentekos, L. N. Dupuis, B. P. Fors, *J. Am. Chem. Soc*., **2016**, 138, 1848.

(2) V. Kottisch, D. T. Gentekos, B. P. Fors, *ACS Macro Lett*., **2016**, 5, 796.

CHAPTER 5

EXPLOITING MOLECULAR WEIGHT DISTRIBUTION SHAPE TO TUNE DOMAIN SPACING IN BLOCK COPOLYMER THIN FILMS

5.1 Abstract

We report a method for tuning the domain spacing (D_{sp}) of self-assembled block copolymer thin films of poly(styrene-block-methyl methacrylate) (PS-*b*-PMMA) over a large range of lamellar periods. By modifying the molecular weight distribution (MWD) shape (including both the breadth and skew) of the PS block via temporal control of polymer chain initiation in anionic polymerization, we observe increases of up to 41% in Dsp for polymers with the same overall molecular weight ($M_n \approx 125$ kg/mol) without significantly changing the overall morphology or chemical composition of the final material. In conjunction with our experimental efforts, we have utilized concepts from population statistics and least-squares analysis to develop a model for predicting D_{sp} based on the first three moments of the MWDs. This statistical model reproduces experimental D_{sp} values with high fidelity (with mean absolute errors of 1.2 nm or 1.8%) and provides novel physical insight into the individual and collective roles played by the MWD moments in determining this property of interest. This work demonstrates that both MWD breadth and skew have a profound influence over D_{sp}, thereby providing an experimental and conceptual platform for exploiting MWD shape as a simple and modular handle for fine-tuning D_{sp} in block copolymer thin films.

5.2 Introduction

The use of block copolymers has become pervasive in the fields of chemistry, materials science, and engineering over the past few decades. With the propensity to rapidly self-assemble into highly ordered nanostructures, block copolymers have played an integral role in the development of novel photonic applications, lithographic materials, filtration membranes, and thermoplastic elastomers.[1-21] However, the ability to control and selectively tune the properties of block copolymers over a broad range without changing their chemical composition remains a challenge to date.[22-25] For this objective to be addressed, modifying the molecular weight distribution (MWD) of the final material has recently emerged as a promising path forward.[26-51] In this regard, a comprehensive understanding of how the MWD shape (e.g., the breadth/spread, skew, etc.) influences the phase behavior and physical properties of block copolymers is still in its infancy and will be fundamental to the future success of this approach.

Polymers are typically characterized using the following statistical quantities: the number-average molar mass (M_n), the weight-average molar mass (M_w), and the dispersity ($Đ$), which is defined as the ratio M_w/M_n. The effects of molecular weight on copolymer phase behavior are fairly well understood.[51,52] However, in many instances, such as the fabrication of photonic polymers with very large domain spacing (D_{sp}), increasing M_n is not an effective strategy due to the likelihood of chain scissions and other difficulties with the preparation and processing of high molecular weight materials.[54-59] In

these cases, it becomes crucial to look at other avenues for tuning phase behavior such as altering the polymer MWDs. To date, only a few research groups have investigated the influence of MWD, or more accurately the *Đ,* on the self-assembly of di- and triblock copolymers.[10,35,36,39,40,44,45,60-62] Lynd and Hillmyer found that increasing the *Đ* of one block (of a diblock copolymer) results in shifted phase boundaries in block copolymer melts, and Matyjaszewski and co-workers have shown that traditionally metastable morphologies, such as hexagonally perforated layers, can be stabilized with high values of *Đ*. Moreover, Mahanthappa and co-workers reported that triblock copolymers with a disperse midblock (*Đ* ≈ 2) prepared by uncontrolled methods have composition-dependent morphology windows that differ considerably from those of their counterparts with narrow distributions (*Đ* ≈ 1). Quite interestingly, it has been demonstrated that the incorporation of blocks with large *Đ* influences the D_{sp} of bulk materials.[10,35,39]

However, the manipulation of *Đ* is only the first step in harnessing the shape of the MWD in the control and fine-tuning of block copolymer properties. In this regard, the use of *Đ* as the sole statistical quantity to describe a MWD is quite limited as it only defines the relative breadth of molar masses in a polymer sample and therefore provides an incomplete and oversimplified description of the MWD shape. To proceed forward, a more comprehensive characterization of MWD shape will require quantities that incorporate statistical information from higher moments of the distribution such as skewness and kurtosis, which describe the relative degree of asymmetry and population in the tails in a given

MWD. Although such quantities have been proposed to heavily influence polymer properties,[22,26-28,34,63-65] experimental validations for such hypotheses have been hindered due to the lack of modular synthetic strategies for gaining predictive control over chain length composition in a MWD. With these synthetic challenges in mind, we have recently reported that temporal regulation of chain initiation in controlled polymerizations does indeed impart deterministic control of the breadth and skew of polymer MWDs (Figure 5.1), thereby providing an experimental platform for exploiting MWD shape as a simple and modular handle to fine-tune polymer properties.[26-28]

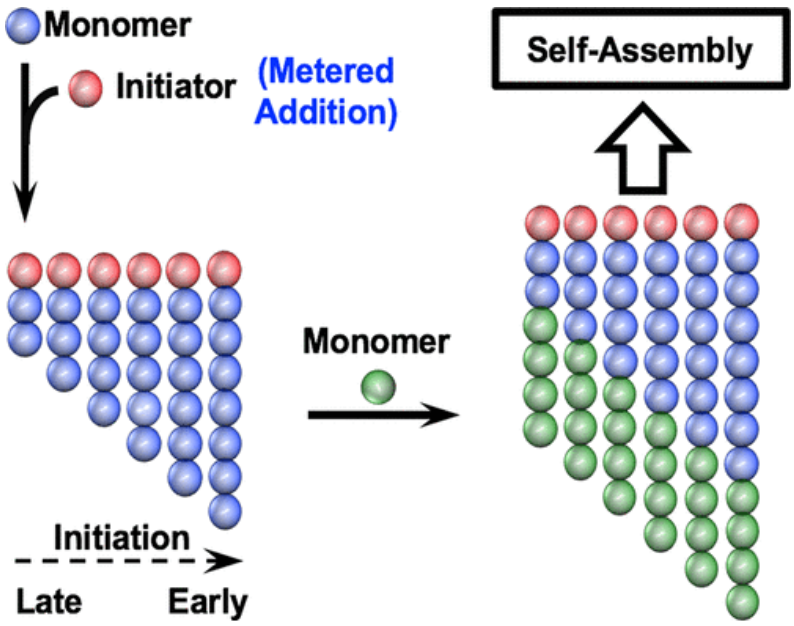

Figure 5.1. General synthetic strategy for the preparation of block copolymers with controlled MWD breadth and skew via temporal regulation of polymer chain initiation of the first block (blue) followed by chain extension with a second monomer (green) to afford well-defined diblock copolymers.

In this study, we employ the aforementioned synthetic strategy to investigate the self-assembly of poly(styrene-*block*-methyl methacrylate) (PS-*b*-PMMA) thin films in which the PS blocks have systematically varied MWD breadths and skews. The general approach is shown in Figure 5.1. Quite interestingly, we demonstrate that the PS MWD skew has a substantial influence over the phase behavior of PS-*b*-PMMA with effects that are of the same order of magnitude as the breadth/spread. By only modifying the breadth and skew of the PS block MWD, we observed unprecedented increases in D_{sp} of more than 40% without significantly changing the overall morphology or chemical composition of the final material. To quantify and further differentiate the individual and collective roles played by the MWD breadth and skew in determining D_{sp}, we have also developed a highly accurate statistical model for predicting this quantity based on the first three moments of the MWDs. We anticipate that the findings reported herein on the tailoring of D_{sp} in block copolymers will have significant ramifications in the development of novel photonic polymers, which require atypically large periodicities to scatter light.[5,54,55] More broadly speaking, we also hope that this work will provide an experimental and conceptual framework for exploiting MWD shape as a simple and modular handle for fine-tuning the phase behavior and physical properties of block copolymer thin films.

5.3 Results and Discussion

5.3.1 Design and Thin Film Self-Assembly

The preparation of PS-b-PMMA via anionic polymerization was chosen as a model system due to its living nature, i.e., high chain-end fidelity and the excellent control of molecular weight for both blocks in the polymerization, which allowed the chain-length heterogeneity to be confined to the PS block.[35,66−69] Figure 2 shows the general synthetic strategy and representative size-exclusion chromatography (SEC) traces of the diblock copolymers. Slow addition of an alkyllithium initiating species (*s*-BuLi) to a monomer solution at predetermined rates and times (see Tables 5.4 and 5.5) allows for precise temporal control of polymer chain initiation and skews the MWD to either high or low molar mass (Figure 5.2b). More precisely, a negative skew, or skewing to high molar mass (red PS trace; Figure 5.2b), represents tailing into the high molecular weight region of the SEC trace while the distribution is tilted toward lower molecular weight (the mode is shifted toward lower molecular weight). Likewise, a positive skew, skewing to low molecular weight (blue PS trace in Figure 5.2b), describes the shape of a chain length distribution that tails into the low molecular weight region of the SEC trace while the mode is shifted toward higher molecular weight. The M_n of the PS block of all polymers in this study was held constant at ~50 kg/mol, which is controlled via the ratio of monomer to total initiator added to the reaction mixture. Each PS block was subsequently chain-extended with varying amounts of methyl methacrylate until the final block copolymers reached overall M_n values from 75 to 140 kg/mol (Figure 5.2c).

Initially, a series of polymers with narrow PS MWDs (Table 5.1, samples 1–7) and increasing fractions of PMMA was prepared as a control group. Subsequently, a repertoire of polymers with similar overall M_n values and block compositions but with PS blocks with broader distributions ($Đ \approx 1.4$) and either negative or positive skewing (see Table 5.1, samples 8–15 and samples 16–21,

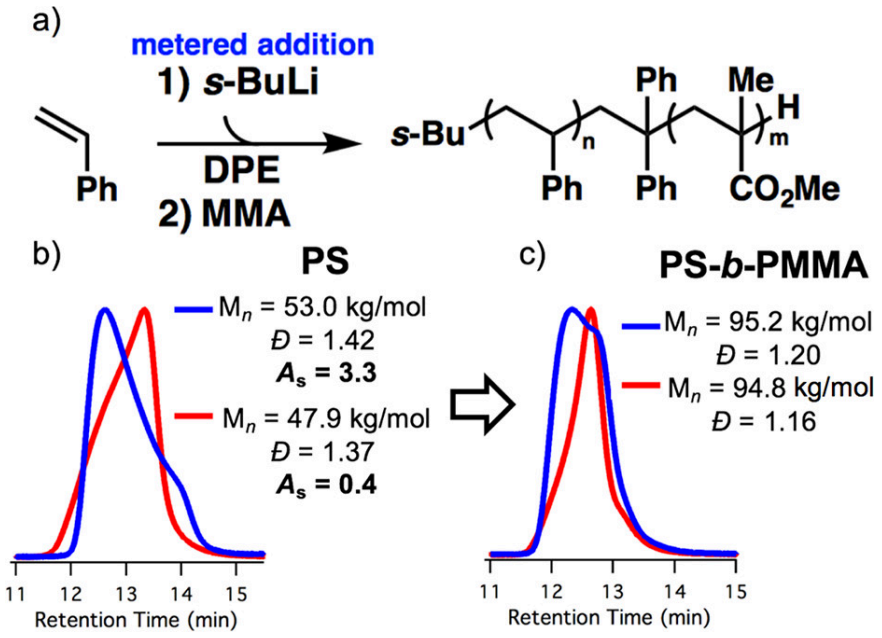

Figure 5.2. (a) General synthetic approach to PS-*b*-PMMA diblock copolymers through metered addition of *s*-BuLi and representative size-exclusion chromatography traces of (b) starting PS blocks and (c) PS-*b*-PMMA showing the controlled MWD shape of the PS block (DPE, diphenylethylene; PMMA, poly(methyl methacrylate); PS, polystyrene).

respectively). We note in passing that the asymmetry factor ($A_{s,PS}$) is included as a qualitative descriptor for the skew of each PS MWD, where $A_{s,PS}$ values of

Table 5.1. Molecular and Morphological Characteristics of PS-*b*-PMMA Diblock Copolymers

Sample (p)	$M_{n,\,PS}$ (kg/mol)	$Đ_{PS}$	$A_{s,\,PS}$[a]	$M_{n,\,PS\text{-}b\text{-}PMMA}$ (kg/mol)	$Đ_{PS\text{-}b\text{-}PMMA}$	$f_{v,PS}$[b]	$D_{sp,\,expt}$[c] (nm)	M_1[d] (min)	M_2[d] (min)	M_3[d] (min)	$D_{sp,\,pred}$[d] (nm)
1	52.6	1.10	N/A	90.3	1.08	0.54	52.6	12.61	0.269	0.280	53.8
2	54.1	1.08	N/A	91.8	1.10	0.55	53.8	12.60	0.227	0.266	54.0
3	52.6	1.10	N/A	104.7	1.10	0.46	57.9	12.48	0.269	0.280	58.4
4	54.1	1.08	N/A	107.6	1.10	0.46	61.2	12.44	0.227	0.266	59.4
5	52.6	1.10	N/A	113.0	1.09	0.43	62.4	12.40	0.269	0.280	62.5
6	54.1	1.08	N/A	122.0	1.11	0.40	67.6	12.31	0.227	0.266	66.5
7	54.1	1.08	N/A	140.9	1.13	0.34	76.4	12.16	0.227	0.266	77.9
8	55.7	1.45	0.35	79.0	1.28	0.67	50.9	12.71	0.584	–0.307	50.9
9	47.9	1.37	0.38	94.8	1.16	0.46	58.6	12.60	0.528	–0.227	55.9
10	53.8	1.38	0.42	104.2	1.17	0.48	60.8	12.48	0.514	–0.219	61.7
11	47.9	1.37	0.38	104.6	1.15	0.42	62.0	12.45	0.528	–0.227	63.4
12	53.8	1.38	0.42	111.6	1.17	0.44	69.1	12.37	0.514	–0.219	68.7
13	55.7	1.45	0.35	119.6	1.18	0.43	72.8	12.32	0.584	–0.307	72.4
14	47.9	1.37	0.38	125.1	1.20	0.35	77.7	12.24	0.528	–0.227	79.6
15	47.9	1.37	0.38	139.4	1.16	0.35	85.7	12.19	0.528	–0.227	84.4
16	53.0	1.42	3.30	74.9	1.27	0.67	47.5	12.73	0.559	0.474	47.4
17	53.0	1.42	3.30	95.2	1.20	0.52	62.3	12.54	0.559	0.474	60.3
18	53.0	1.42	3.30	104.6	1.20	0.47	67.3	12.44	0.559	0.474	69.3
19	51.3	1.41	3.22	113.5	1.20	0.41	77.7	12.35	0.556	0.483	78.6
20	53.0	1.42	3.30	121.7	1.20	0.40	82.9	12.30	0.559	0.474	84.4
21	51.3	1.41	3.22	125.8	1.24	0.37	95.5	12.23	0.556	0.483	93.0

[a] Asymmetry factor (A_s) of the polystyrene (PS) block (vide supra). [b] Volume fraction ($f_{v,PS}$) of the PS block calculated from tabulated homopolymer densities. [c] Experimental and predicted domain spacings ($D_{sp,expt}$ and $D_{sp,pred}$, respectively) of perpendicularly oriented PS-*b*-PMMA lamellae. [d] M_1, M_2, and M_3 denote the descriptors employed in our statistical model that describe the molecular weight distribution shape (first three moments).

>1 and <1 describe skewing to low and high molar mass, respectively.[70,71] The fraction of PMMA content was varied across these three sets of polymers to investigate the impact of PS MWD shape on self-assembly at different total molecular weights and block compositions ($f_{v,PS}$ of 0.35–0.65).

Using the library of PS blocks with systematically deviating compositions of chain lengths and increasing fractions of the PMMA blocks between samples, we prepared thin films on silicon wafers and performed grazing-incidence small-angle X-ray scattering (GISAXS) studies to determine the morphological characteristics of each block copolymer (Figure 5.3). As anticipated, polymers with narrow PS MWDs showed modest increases in D_{sp} from 52.6 to 76.4 nm with increasing molar mass from 90.3 to 140.9 kg/mol (Figure 5.3a, green entries). Specifically, an extension in molecular weight of 50.6 kg/mol (a 56% increase of overall M_n) resulted in a 23.8 nm increase in D_{sp} (a 45% expansion of the lamellar period). Notably, when $Đ$ was broadened to 1.4 and skewed to high molar mass (Figure 5.3a, red entries), large increases in D_{sp} were observed relative to those seen for the narrow PS MWD control group. In contrast to block polymers with narrow PS distributions, polymers with negative skew and M_n values from 79.0 to 139.4 kg/mol showed remarkable increases in D_{sp} from 50.9 to 85.7 nm. This corresponds to a 67% rise over the range of molar masses studied here. Among polymers with similar M_n values (see Table 5.1, entries 6 and 14), a $Đ$ of 1.4 and MWD skewing of the PS block to high molar mass resulted in increases in block periodicities of up to 15% compared with those of samples with narrow MWDs. These data show that broadening the MWD of one block to a $Đ$ of 1.4 has a strong

influence on this aspect of phase behavior, resulting in a large increase in the window of available domain periods for polymers with almost identical molar mass and volume fraction.

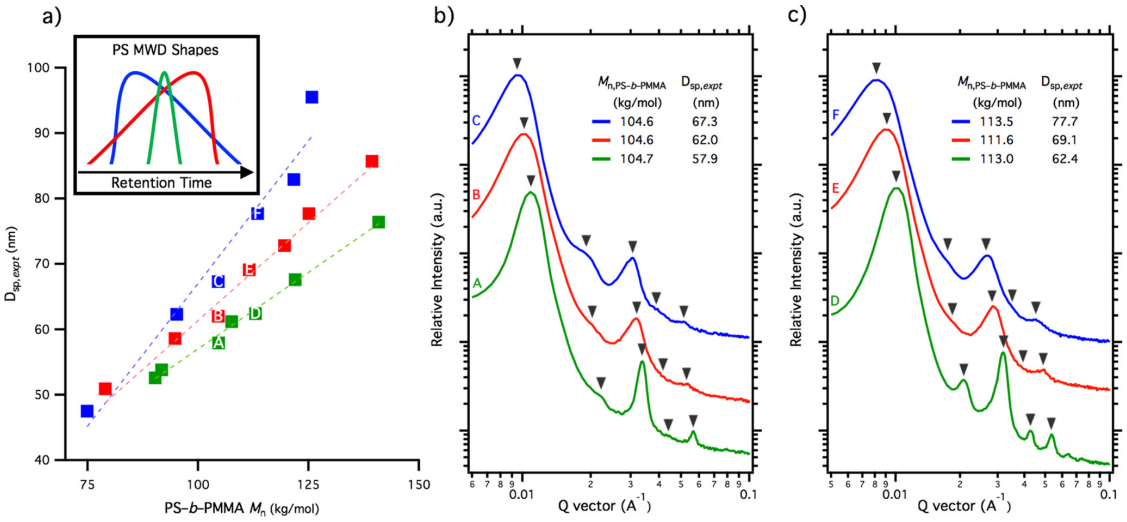

Figure 5.3. (a) D_{sp} versus overall PS-*b*-PMMA M_n for positively skewed (blue), negatively skewed (red), and narrow MWD (green), which shows vastly different lamellar periods dependent on PS MWD skew. (b, c) Analogous GISAXS line cuts along the Yoneda band plotted versus log *q*-vector show strong shifts in the primary reflection (first triangle) used to find D_{sp} in (a). Line cuts have been indexed to lamellae.

Most intriguing, when the $Đ$ of the PS block was broadened to 1.4 and low molar mass skewing was imparted on the MWD (Figure 5.3a, blue entries), even larger increases in lamellar periods from 47.5 to 95.5 nm were observed, a 100% expansion in D_{sp} for polymers with M_n values between 74.5 and 125.8 kg/mol.

Remarkably, relative to narrow MWD polymers with similar M_n values (see Table 5.1, entries 6 and 21), polymers with PS blocks skewed to low molar mass showed a 41% enhancement in D_{sp}, which is almost 30 nm. This type of skewing allowed access to a D_{sp} of 95.5 nm in a polymer of only 125.8 kg/mol. Moreover, compared with polymers skewed to high molar mass, those skewed to low molar mass showed a D_{sp} increase of up to 23% at the same $Đ$ (entries 14 and 21), demonstrating clearly that PS MWD skew has a profound role in the self-assembly of lamellar domains. We envision that these findings will provide a platform from which to use MWD skew as a useful tool for manipulating the phase behavior of block copolymers.

As an important aside, we note that preparing materials with very large D_{sp} by solely increasing molecular weight has significant fundamental and practical limits. First, the Gaussian chain model for lamellar systems suggests that D_{sp} increases sublinearly with M_n in symmetric diblock copolymers.[52,53] Though this effect is not apparent as plotted in Figure 5.3 (presumably due to the narrow range of molecular weights and increasing asymmetry in the volume fraction of the polymers in this study, see Chapter 5 Appendix), the model brings to light the fact that there exists a plateauing effect on D_{sp}. That is to say, as the M_n increases, its influence on D_{sp} is reduced. Thus, the molecular weight cannot simply be increased to attain arbitrarily high D_{sp}. Moreover, high molecular weight block copolymer chains can have a limited ability to diffuse to form an equilibrium morphological structure and are often trapped in a nonequilibrium state.[54-57] In addition to the above inherent limits, high molecular

weights pose critical processing challenges for two practical reasons. First, high molecular weight materials with narrow MWD often have very high viscosities, requiring a correspondingly high energy input for sufficient melt-processing, and second, these large polymers are prone to chain scissions during such energy-intensive processing, which considerably damages the material and alters its intended physical properties.[58,59,72] Regarding these problems, we envision that our approach will help bridge some of this gap and will, therefore, be the subject of future work.

Further visualization of this change in D_{sp} with changing PS MWD spread and skew is shown in Figure 5.3b and c, which present the horizontal GISAXS line cuts of two sets of polymers with similar molar masses but different MWDs of the PS block. Plots of relative intensities versus log of the q-vector distinctly illustrate large shifts in the primary reflection. The position of these Bragg peaks embodies the extreme influence of the PS MWD shape on D_{sp}, which falls to lower q as PS MWD is broadened and positively skewed. The broadening of the primary and higher-order reflections indicates that some degree of long-range order is lost (or decreasing grain size) as the PS MWD is broadened and/or skewed. However, in most cases, three scattering peaks are observed, demonstrating that the films remain well-ordered. All of the samples we have evaluated here had quantifiable scattering in only the Yoneda band of the two-dimensional scattering pattern (with scattering in the horizontal direction suggesting that the block copolymer interface is primarily oriented normal to the substrate surface). These scattering results reveal only integer value vertical reflections that are characteristic of

perpendicular lamellar morphology (see Figure 5.13 for representative 2D GISAXS data).[53,74-80] Notably, this was the only morphology observed in all of the polymers studied here. More interesting, however, is that these modifications to the PS MWD breadth and skew result primarily in large changes to D_{sp} that are not accompanied by a simultaneous phase transition. Apart from reduced grain size, the fact that large variations in MWD shape of the PS block left the overall morphology predominantly intact indicates that this should be a rather durable way to modulate D_{sp} in block copolymer thin films.

Atomic force microscopy studies also lend support to the fact that the overall morphology remains intact (Figure 5.4) by showing the expected fingerprint pattern for perpendicular meandering lamellae. These micrographs demonstrate that, in addition to the internal morphology, the surface morphology also remains well ordered when the MWD shape of the PS block has been significantly altered.

The origin of domain spacing expansion in samples with large $Đ$ has been of considerable interest both experimentally and theoretically. The observed increase in lattice spacing of bulk samples with relatively large $Đ$ has been attributed to the tendency for individual polymer chains to withdraw from the interface and swell the domain of their majority-like segment.[10,30,45,81,82] In general, it is enthalpically most favorable to surround both the A and B blocks by their like segments, which is only possible when each chain is confined to the interface. However, although confining all chains to the 2-dimensional

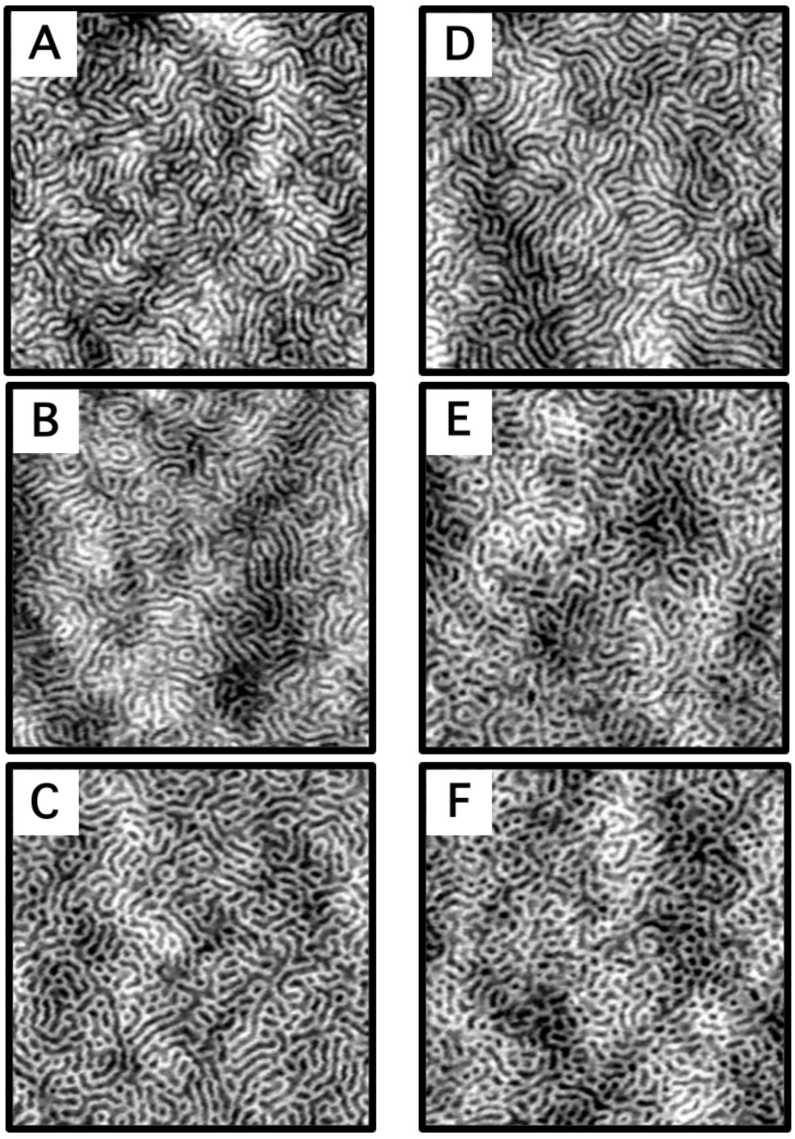

Figure 5.4. Atomic force microscopy (AFM) height images (2 × 2 μm) of unaligned perpendicular lamellae. Sample names (A–F) correspond to those labeled in Figure 5.2. Fast Fourier Transforms (FFTs) are shown in the Chapter 5 Appendix.[73]

interface minimizes unfavorable A-B contacts, it also imposes a stringent entropic penalty on the polymer chain ensemble. Thus, in a polymer sample with large enough disparities in A-B block lengths (e.g., short A blocks bound to long B blocks, such as found in samples with large $Đ$), more stabilization is gained entropically by surrounding small A blocks with dissimilar B segments than is gained enthalpically by confining these chains to the domain interface. Such asymmetric polymer chains, therefore, preferentially diffuse away from the interface and swell the majority B domain, increasing the overall D_{sp}.

We propose that such polymer chain desorption from the interface is a major contributing mechanism to domain swelling in our samples with diverse PS MWD shapes. This hypothesis is initially supported by the fact that broadening the PS MWD to a $Đ$ of 1.4 results in increased lattice spacing for both positively and negatively skewed samples. Hence, in contrast to narrow MWDs (Table 5.1, samples 1–7), the presence of low molecular weight PS species in the broad distributions (Table 5.1, samples 8–21) allows swelling of the PMMA domain to take place. More interesting, the data shown here also clearly demonstrate that this driving force is quite sensitive to the PS MWD shape or the absolute composition of long, medium, and short chains. Because the positively skewed samples have a larger portion of relatively low molecular weight material, the influence of chains withdrawing from the interface is expected to be amplified in these samples relative to those with negatively skewed PS MWDs. Moreover, this hypothesis is also reinforced through the observation that increasing the molecular weight of the PMMA block increases the difference in D_{sp} of positively

versus negatively skewed samples. In this case, the growth in molecular weight of the PMMA block would result in the propensity for larger PS chains to be pulled away from the interface, thus permitting a greater number of PS chains to be pulled into the center of the PMMA domain. Because the positively skewed samples have a larger relative portion of low molecular weight species, the disparate rise in D_{sp} for such samples is consistent with the aforementioned hypothesis. Moreover, the observed coalescence of D_{sp} values at lower molecular weights in Figure 5.3a further supports this proposition and denotes the point at which the PMMA block is too small to drive short PS chains away from the interface. These observations illustrate the sensitivity of domain spacing to the relative population of low molecular weights chains and, consequently, the promising potential of using MWD skew to precisely control such properties.

Lastly, large $Đ$ has also been proposed to influence the overall lamellar spacing by decreasing the entropic cost of stretching an ensemble of chains due to the combination of large and small chains being able to fill space more efficiently. This allows an ensemble of chains to stretch further than its narrow MWD counterpart. More experimental and theoretical evidence is needed to determine the degree to which this mechanism is contributing to the overall D_{sp} with respect to the MWD shape of the PS block.[40,45,46,83,84]

5.3.2 Statistical Modeling and Least Squares Analysis

An accurate and reliable quantitative description of how MWD shape influences block copolymer phase behavior would not only provide key physical

insight into fundamental quantities such as D_{sp} but also further enable the rational design of block copolymers with new and improved physical properties. As a first step toward achieving this goal, we have employed concepts from population statistics and linear least-squares analysis to construct a model that correlates the statistical descriptors of MWD shape to D_{sp} in block copolymer thin films.[85,86] We envision the use of more sophisticated machine learning-based techniques[87-92] to further enrich our understanding of the physical consequences of MWD shape in the future when more data becomes available.

To start, we used the unprocessed elution profiles (traces) obtained from size exclusion chromatography (SEC) instead of the differential distributions in an effort to eliminate any potential ambiguities due to post processing of the raw SEC data. In our statistical model, we utilized three descriptors (M_1, M_2, and M_3) derived from the first three moments of the unprocessed SEC traces to describe the physical MWD variables that have been experimentally modified in this study (i.e., the size of the PS-*b*-PMMA, the spread of the PS block, and the skew of the PS block).

For the M_1 statistical descriptor, we employed the first moment of the diblock copolymer SEC trace, which represents the overall molecular weight of the PS-*b*-PMMA. This choice is tantamount to quantifying the increase of PMMA in this diblock copolymer because the M_n of the PS block remained constant throughout this study (with an M_n of 50 kg/mol; see Table 5.1). Because the next quantity of interest was the breadth/spread of the PS block, we took the square root of the second central moment (i.e., the standard deviation) of the PS SEC

trace as the M_2 statistical descriptor. For the changes in the skew of the PS block to be captured, the cubic root of the third central moment was used as the M_3 statistical descriptor. The functional form chosen for the $M_2$and M_3 descriptors (i.e., the square and cubic roots of the corresponding central moments, respectively) yields a set of statistical quantities with units that are consistent with M_1. We note in passing that the use of consistent units is one of the requirements for quantifying the relative importance of each of these MWD shape descriptors in determining properties of interest such as D_{sp}.

Letting ρ(t) represent the fractional elution rate at time t from a given SEC trace, we know that

$$\int \rho(t)\, dt = 1 \tag{5.1}$$

due to normalization. As such, the first, second, and third *central moments* of a SEC trace are given by:

$$\mu_1 = \int \rho(t) \times t\, dt, \tag{5.2}$$

$$\mu_2 = \int \rho(t) \times (t - \mu_1)^2\, dt, \tag{5.3}$$

and

$$\mu_3 = \int \rho(t) \times (t - \mu_1)^3\, dt, \tag{5.4}$$

respectively. As described above, we seek to construct a set of statistical descriptors that can be used to correlate D_{sp} with the overall molecular weight of the PS-*b*-PMMA, the breadth/spread of the PS block, and the skew of the PS block. In order to do so (and still maintain a set with consistent units), the M_1, M_2, and M_3 statistical descriptors were taken as:

$$M_1 = \mu_1^{\text{PS-}b\text{-PMMA}}, \tag{5.5}$$

$$M_2 = \sqrt[2]{\mu_2^{\text{PS}}}, \tag{5.6}$$

and

$$M_3 = \sqrt[3]{\mu_3^{\text{PS}}}, \tag{5.7}$$

respectively (see Table 5.1). Note that the M_3 statistical descriptor above in Eq. (5.7) is not equivalent to the statistical definition of skewness (which is also known as the Pearson's moment coefficient of skewness) given by $\alpha_3 = \mu_3/\mu_2^{3/2}$. In theory, higher central moments could also be used as statistical descriptors. In practice, however, one is often faced with a limited data set and care must be taken to employ the minimal number of descriptors in a statistical model (*i.e.*, to prevent overfitting). With access to an increased number of samples in the future (in this work we have $N = 21$ polymer samples), it would be very interesting to

explore how such higher central moments are correlated with physical properties of interest.

Using these three statistical descriptors, the experimental D_{sp} for a given polymer sample, p, were fit to the following power series expansion:

$$\mathrm{D}_{\mathrm{sp},expt}^{(p)} \approx \sum_{ijk} c_{ijk} \left(\Lambda_1^{(p)}\right)^i \left(\Lambda_2^{(p)}\right)^j \left(\Lambda_3^{(p)}\right)^k = \mathrm{D}_{\mathrm{sp},pred}^{(p)} , \tag{5.8}$$

in which the c_{ijk} are the targeted expansion coefficients, and the sum starts with $i = j = k = 0$ and includes all terms such that $i + j + k \leq \Gamma$, where Γ is the truncation order (which is usually taken to be 1 or 2 in this work). For the p-th polymer sample, $\Lambda_1^{(p)}$, $\Lambda_2^{(p)}$, and $\Lambda_3^{(p)}$ are the normalized deviations for each statistical descriptor from the corresponding *population mean*, *i.e.*,

$$\Lambda_q^{(p)} = \frac{M_q^{(p)} - \langle M_q \rangle}{\langle M_q \rangle} \tag{5.9}$$

for $q = 1, 2, 3$ and $\langle \cdot \rangle$ denotes an average over *all* of the samples in the training set. In other words, $\langle M_1 \rangle$ represents the mean retention time across *all* of the PS-*b*-PMMA SEC traces and $\Lambda_1^{(p)}$ represents the normalized deviation of the p-th sample from the population mean; $\langle M_2 \rangle$ represents the mean spread in the retention time across *all* of the PS SEC traces and $\Lambda_2^{(p)}$ represents the normalized deviation of the p-th sample from the population mean spread; $\langle M_3 \rangle$ represents

the mean skew in the retention time across *all* of the PS SEC traces and $\Lambda_3^{(p)}$ represents the normalized deviation of the p-th sample from the population mean skew.

The simplest statistical model for D_{sp} in the form of Eq. (5.8) would have $\Gamma = 1$, and would include a constant offset (c_{000}), which is analogous to the y-intercept in linear regression analysis, and a term that is linear in each of the statistical descriptors ($c_{100}, c_{010}, c_{001}$). In this work, we will explore the $\Gamma = 2$ statistical model, which also accounts for bilinear coupling between statistical descriptors ($c_{110}, c_{101}, c_{011}$), *e.g.*, coupling between the spread and skew, as well as quadratic contributions from individual descriptors ($c_{200}, c_{020}, c_{002}$).

To determine the optimal expansion coefficients in our statistical model (Eq. (4.8)), we minimize the sum of squared residuals (errors) between the experimental and predicted D_{sp} values over all training samples, *i.e.*,

$$\{c_{ijk}\} = \arg\min_{\{c_{ijk}\}} \left\{ \sum_{p=1}^{N} \left(\mathrm{D}_{\mathrm{sp},expt}^{(p)} - \mathrm{D}_{\mathrm{sp},pred}^{(p)} \right)^2 \right\}. \tag{5.10}$$

To complete our statistical model for D_{sp} in these block copolymers, each term in Eq. (5.8) must be normalized over all of the samples in the training set, which results in a transformation of the $\{c_{ijk}\}$ into their final normalized form $\{\bar{c}_{ijk}\}$. This additional level of normalization allows for a quantitative assessment of the relative importance of each term in our statistical model *via direct comparison of*

the final expansion coefficients. For a detailed derivation of this additional normalization procedure, see the Chapter 5 Appendix. We stress here that this final normalization is crucial for the *physical interpretation* of the individual and collective influences that each of these MWD shape descriptors have in determining D_{sp} in these block copolymers.

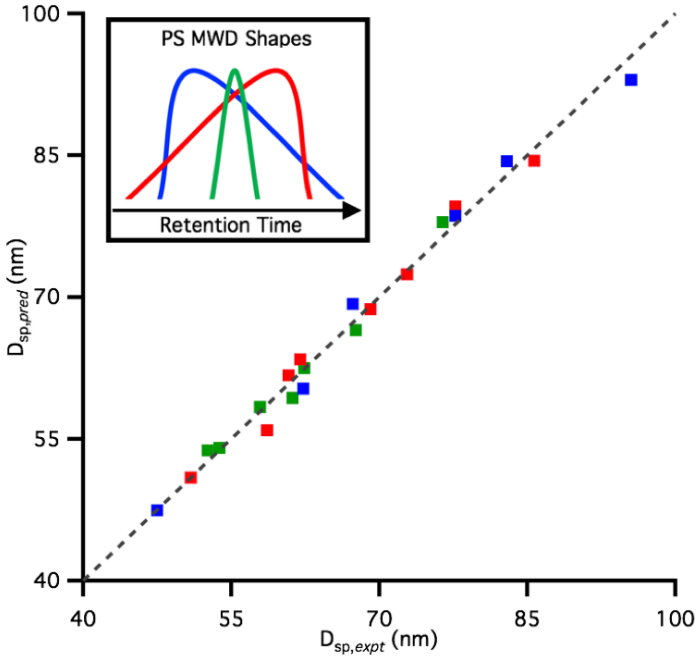

Figure 5.5. Correlation plot between predicted ($D_{sp,pred}$) and experimental ($D_{sp,expt}$) values based on the statistical model defined in Eq. (5.8). The dashed line represents a perfect correlation.

To minimize the number of fitting parameters in our statistical model and prevent overfitting, we only use a limited number of terms in the power series

expansion formula in Eq. (5.8). In doing so, our statistical model reproduces the experimentally observed D_{sp} values with extremely high fidelity, as shown in the correlation plot in Figure 5.5 (listed in Table 5.1). Error analysis including the mean signed error (MSE), mean absolute error (MAE), root-mean-squared error (RMSE), and maximum error (MAXE) are provided in Table 5.2. With a MSE of 0.0 nm, our statistical model shows no systematic error in the prediction of D_{sp} in this data set. Furthermore, the ability to reproduce experimental D_{sp} values to within 1.2 – 1.4 nm on average (MAE–RMSE) further demonstrates the accuracy and reliability of this approach. We attribute the error remaining in this model to the limited sample size (N = 21) and it is expected that these residual errors will decrease with a larger and more comprehensive sample of polymer MWDs.

Table 5.2. Errors in the Prediction of Domain Spacing (D_{sp})

	error (nm)
MSE	0.0
MAE	1.2
RMSE	1.4
MAX	2.7

The final set of optimized expansion coefficients is provided in Table 5.3. The first term included in our statistical model is $\bar{c}_{000} = +65.6$, which represents a *constant* (global offset) D_{sp} value corresponding to a reference polymer sample whose statistical descriptors are given by the population means: $M_1 = \langle M_1 \rangle = 12.426$, $M_2 = \langle M_2 \rangle = 0.446$, and $M_3 = \langle M_3 \rangle = 0.134$. In other words, the reference polymer sample in this statistical model is not an idealized MWD with an

exceedingly narrow spread (and no skew) centered around a single M_n, and instead has a slightly broader spread (and small positive skew) that represents the *average* polymer MWD in our sample set.

Table 5.3. Values and Physical Meanings of the Expansion Coefficients Included in the Statistical Model of (Eq. (5.8))

i	*j*	*k*	$\bar{c}_{ijk}$	**Physical Meaning**
0	0	0	+65.6	*constant* (global offset)
1	0	0	–21.2	*linear* (mean, Λ_1)
0	1	0	+4.48	*linear* (spread, Λ_2)
0	0	1	+1.08	*linear* (skew, Λ_3)
1	1	0	–7.44	*bilinear* (mean & spread, $\Lambda_1\Lambda_2$)
1	0	1	–5.50	*bilinear* (mean & skew, $\Lambda_1\Lambda_3$)
0	1	1	+3.02	*bilinear* (spread & skew, $\Lambda_2\Lambda_3$)
2	0	0	+6.98	*quadratic* (mean, $\Lambda_1^2 = \Lambda_1\Lambda_1$)

Consider now the first *linear* term in our expansion, $\bar{c}_{100} = -21.2$, which represents the correlation between D_{sp} and the mean retention time (of the total diblock copolymer). To physically interpret this finding, note that a negative sign in an expansion coefficient (in the statistical model employed herein) denotes that D_{sp} (*i.e.*, the property of interest) increases with a decrease in the corresponding statistical descriptor. As such, this finding indicates that D_{sp} increases with decreasing retention time. Due to the inverse relationship between retention time and molecular weight, this corresponds to an increase in D_{sp} with increasing molecular weight. This finding aligns well with our current understanding that D_{sp} and polymer molecular weight are positively correlated.[37,38] We note in passing that a quadratic term in the mean retention time ($\bar{c}_{200}$) was also included because

this statistical descriptor is the most important parameter for determining D_{sp}, and therefore decreases the statistical error in our predictions of this property of interest.

The second linear term in our expansion ($\bar{c}_{010} = +4.48$) accounts for the influence of the spread/breadth in the PS SEC trace and indicates that D_{sp} increases with increasing *spread* in the retention time. Since this statistical descriptor correlates very well with $Đ_{PS}$, this finding is again consistent with previous observations that there exists a positive correlation between D_{sp} and $Đ$.[8] Interestingly, we note that the magnitude of $\bar{c}_{010}$ (which can be directly compared to the magnitude of $\bar{c}_{100}$ in this statistical model) suggests that while molecular weight has the largest influence on D_{sp}, the influence of MWD spread on this property of interest is also quite substantial. In the same breath, we find that the skew of the PS MWD also has a noteworthy influence over D_{sp} as demonstrated by the fact that $\bar{c}_{001} = +1.08$.

In moving beyond $\Gamma = 1$, we found that the bilinear couplings in our statistical model (as weighted by the $\bar{c}_{110}$, $\bar{c}_{101}$, and $\bar{c}_{011}$ expansion coefficients; see Table 4.3) are *all* substantial in magnitude. This finding is strongly indicative of important *collective* roles played by these MWD descriptors in determining D_{sp}. In particular, we note the relatively large bilinear coupling between the mean and skew (with $\bar{c}_{101} = -5.50$) and between spread/breadth and skew of the PS block MWD (with $\bar{c}_{011} = 3.02$), which suggests that MWD skew has an even more pronounced influence over D_{sp} when the molecular weight *and/or* MWD spread is also large, as observed experimentally in Figure 5.3a.

In fact, significant deviations in D_{sp} for polymer samples that have the same overall molecular weight and breadth can be solely attributed to the terms that involve the skew of the PS block MWD. Figure 5.6 demonstrates this critical finding by plotting the cumulative influence of each term in our statistical model for three samples comprised of similar molecular weights and volume fractions. Importantly, our model demonstrates that a narrow PS MWD breadth (Figure 5.6 green; $\bar{c}_{010}$ and $\bar{c}_{110}$) results in a decrease in D_{sp} relative to the population average. Further, both positively and negatively skewed PS MWDs have the same distribution breadth (Figure 5.6 red and blue) and therefore result in similar contributions from the terms containing the distribution mean and spread, as expected. Most interesting, however, are the influences from terms containing a skew component ($\bar{c}_{001}$, $\bar{c}_{101}$, and $\bar{c}_{011}$). Initially, in the narrow MWD sample with slight positive skew ($M_3 = 0.266$) close to the population mean ($\langle M_3 \rangle = 0.134$) there is almost no influence of skew in determining the overall D_{sp}, consistent with the magnitude of $\bar{c}_{011}$. Conversely, when the PS MWD is modified and skewed to high (red) or low (blue) molecular weight, the profound influence of MWD shape becomes evident. In this striking example, the predicted D_{sp} values remain essentially the same when only the terms which do not contain a skew component are included. However, once the terms that do account for the PS block skew are included, substantial deviations of approximately 15 nm emerge in the predicted D_{sp} values. More precisely, a positively skewed PS MWD which contains a significant portion of low molecular weight polymer chains leads to an expansion of D_{sp} while negatively skewed samples that lack such a fraction of PS chains

result in decreased D_{sp} values. These observations are consistent with the hypothesis that domain swelling *via* chain desorption is sensitive to the relative fraction of low molecular weight chains in the final material, which is governed by MWD skew.

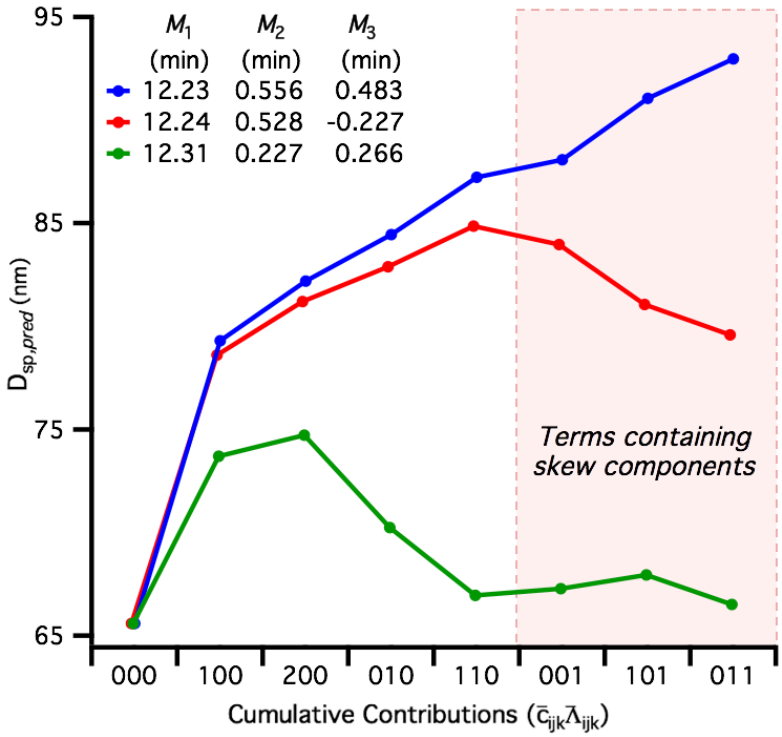

Figure 5.6. Cumulative contributions to the predicted D_{sp} values for samples 6 (green), 14 (red), and 21 (blue) based on the statistical model defined in Eq. (5.8). All samples have the same overall M_n while samples 14 and 21 have the same MWD breadth, and therefore illustrate that large deviations in D_{sp} can be attributed to the skew of the PS block MWD.

5.4 Conclusion

In this work, we have demonstrated a general approach to using MWD shape (breadth *and* skew) as a parameter for fine-tuning the D_{sp} of block copolymer thin films. The synthetic process for doing so allows predictable increases in D_{sp} of up to 40% for fairly low molecular weights and relatively narrow dispersity values. GISAXS and AFM studies establish that by tuning the MWD shape of *only* one block, D_{sp} can be systematically varied across a large window of lamellar periods, even at values of the same molecular weight *and* dispersity. These data illustrate that modulation of the *entire* MWD may be used as an ever-present handle to fine-tune the phase behavior of the final material. We accompany these experimental results with a robust statistical model which provides a quantitative estimate of the influence of the first three central MWD moments on domain spacing. This theoretical model illustrates that both breadth and skew have a substantial influence over this property of interest and reproduces the experimental D_{sp} values with high fidelity (to within 1.2 – 1.4 nm on average). These results show that higher moments of MWDs play an important role in the self-assembly process, and to the best of our knowledge, this work is the first attempt at simultaneously determining the individual and collective influences of MWD mean, spread, and skew on D_{sp} in block copolymers. This joint experimental and theoretical endeavor further expands our fundamental understanding of the critical role played by MWDs in the determination of polymer physical properties. In doing so, we provide an experimental and conceptual platform for exploiting MWD shape as a general and modular handle to fine-tune

properties of increasing interest such as D_{sp} in block copolymer thin films. We anticipate that these findings will enable the development of a general and scalable strategy for designing and synthesizing polymers with atypically large periodicities for next-generation photonic materials.

5.5 References

(1) Bates, F. S.; Hillmyer, M. A.; Lodge, T. P.; Bates, C. M.; Delaney, K. T.; Fredrickson, G. H. *Science* **2012**, *336*, 434.

(2) Kim, H.-C.; Park, S.-M.; Hinsberg, W. D. *Chem. Rev.* **2010**, *110*, 146.

(3) Bates, F. S.; Fredrickson, G. H. *Annu. Rev. Phys. Chem.* **1990**, *41*, 525.

(4) Leibler, L. *Macromolecules* **1980**, *13*, 1602.

(5) Fink, Y.; Urbas, A. M.; Bawendi, M. G.; Joannopoulos, J. D.; Thomas, E. L. *J. Lightwave Technol.* **1999**, *17*, 1963.

(6) Stefik, M.; Guldin, S.; Vignolini, S.; Wiesner, U.; Steiner, U. *Chem. Soc. Rev.* **2015**, 44, 5076.

(7) Kang, Y.; Walish, J. J.; Gorishnyy, T.; Thomas, E. L. *Nat. Mater.* **2007**, *6*, 957.

(8) Kang, C.; Kim, E.; Baek, H.; Hwang, K.; Kwak, D.; Kang, Y.; Thomas, E. L. *J. Am. Chem. Soc.* **2009**, *131*, 7538.

(9) Urbas, A. M.; Maldovan, M.; DeRege, P.; Thomas, E. L. *Adv. Mater.* **2002**, *14*, 1850.

(10) Hustad, P. D.; Marchand, G. R.; Garcia-Meitin, E. I.; Roberts, P. L.; Weinhold, J. D. *Macromolecules* **2009**, *42*, 3788.

(11) Park, M. *Science* **1997**, *276*, 1401.

(12) Bang, J.; Jeong, U.; Yeol Ryu, Du; Russell, T. P.; Erren, T. C.; Hawker, C. J. *Adv. Mater.* **2009**, *21*, 4769.

(13) Ruiz, R.; Kang, H.; Detcheverry, F. A.; Dobisz, E.; Kercher, D. S.; Albrecht, T. R.; de Pablo, J. J.; Nealey, P. F. *Science* **200**8, *321*, 936.

(14) Kim, S. O.; Harun, H. S.; Stoykovich, M. P.; Ferrier, N. J.; de Pablo, J. J.; Nealey, P. F.; *Nature* **2003**, 424, 411.

(15) Chen, L.; Phillip, W. A.; Cussier, E. L.; Hillmyer, M. A.; *J. Am. Chem. Soc.* **2007**, 129, 13786.

(16) Jackson, E. A.; Hillmyer, M. A. *ACS Nano* **2010**, *4*, 3548.

(17) Ahn, H.; Park, S.; Kim, S.-W.; Yoo, P. J.; Ryu, D. Y.; Russell, T. P. *ACS Nano* **2014**, *8*, 11745.

(18) Zhao, D.; Feng, J.,; Huo, Q.; Melosh, N.; Fredrickson, G. H.; Chmelka, F.; Stucky, G. D.; *Science* **1998**, 279, 548.

(19) Liang, C.; Kunlun, G.; Guiochon, G. A.; Mays, J. W.; Sheng, D. *Angew. Chem. Int. Ed.* **2004**, 43, 5785.

(20) Honeker, C. C.; Thomas, E. L. *Chem. Mater.* **1996**, 8, 1702.

(21) Quirk, R. P.; Morton, M. In *Thermoplastic Elastomers*; 2nd ed.; Hanser Publishers: New York, **1996**; pp 72-100.

(22) Lynd, N. A.; Meuler, A. J.; Hillmyer, M. A. *Prog. Polym. Sci.* **2008**, *33*, 875.

(23) Grubbs, R. B.; Grubbs, R. H. *Macromolecules*, **2017**, 50, 6979.

(24) Rubber Industry Sees Value in MWD. *Chem. Eng. News.* **1965**, 43, 40.

(25) Peplow, M.; *Nature* **2016**, 556, 266.

(26) Gentekos, D. T.; Dupuis, L. N.; Fors, B. P. *J. Am. Chem. Soc.* **2016**, *138*, 1848.

(27) Kottisch, V.; Gentekos, D. T.; Fors, B. P. *ACS Macro Lett.* **2016**, *5*, 796.

(28) Nadgorny, M.; Gentekos, D. T.; Xiao, Z.; Singleton, S. P.; Fors, B. P.;

Connal, L. A. *Macromol. Rapid Commun.* **2017**, 38, 1700352.

(29) Sides, S. W.; Fredrickson, G. H. *J. Chem. Phys.* **2004**, *121*, 4974.

(30) Widin, J. M.; Schmitt, A. K.; Schmitt, A. L.; Im, K.; Mahanthappa, M. K. *J. Am. Chem. Soc.* **2012**, *134*, 3834.

(31) Matsen, M. W. *Phys. Rev. Lett.* **2007**, *99*, 148304.

(32) Leibler, L.; Benoit, H. *Polymer* **1981**, *22*, 195.

(33) Burger, C.; Ruland, W.; Semenov, A. N. *Macromolecules* **1990**, *23*, 3339.

(34) Meuler, A. J.; Ellison, C. J.; Evans, C. M.; Hillmyer, M. A.; Bates, F. S. *Macromolecules* **2007**, *40*, 7072.

(35) Lynd, N. A.; Hillmyer, M. A. *Macromolecules* **2007**, *40*, 8050.

(36) Widin, J. M.; Kim, M.; Schmitt, A. K.; Han, E.; Gopalan, P.; Mahanthappa, M. K. *Macromolecules* **2013**, *46*, 4472.

(37) Bendejacq, D.; Ponsinet, V.; Joanicot, M.; Loo, Y. L.; Register, R. A. *Macromolecules* **2002**, *35*, 6645.

(38) Kennemur, J. G.; Yao, L.; Bates, F. S.; Hillmyer, M. A. *Macromolecules* **2014**, *47*, 1411.

(39) Schmitt, A. K.; Mahanthappa, M. K. *Macromolecules* **2014**, *47*, 4346.

(40) Lynd, N. A.; Hillmyer, M. A. *Macromolecules* **2005**, *38*, 8803.

(41) Vanderlaan, M. E.; Hillmyer, M. A. *Macromolecules* **2016**, *49*, 8031.

(42) Li, S.; Register, R. A.; Weinhold, J. D.; Landes, B. G. *Macromolecules* **2012**, *45*, 5773.

(43) Schmitt, A. L.; Repollet-Pedrosa, M. H.; Mahanthappa, M. K. *ACS Macro Letts* **2012**, *1*, 300.

(44) Ruzette, A.; Tence-Girault, S.; Leibler, L.; Chauvin, F.; Bertin, D.; Guerret, O.; Gerard, P. *Macromolecules* **2006**, *39*, 5804.

(45) Matsen, M. W. *Eur. Phys. J. E* **2007**, *21*, 199.

(46) Cooke, D. M.; Shi, A. *Macromolecules* **2006**, *39*, 6661.

(47) Jiang, Y.; Yan, X.; Liang, H.; Shi, A.-C. *J. Phys. Chem. B* **2005**, *109*, 21047.

(48) Jiang, Y.; Huang, R.; Liang, H. *J. Chem. Phys.* **2005**, *123*, 124906.

(49) Pandav, G.; Ganesan, V. *J. Chem. Phys.* **2013**, *139*, 214905.

(50) Doncom, K. E. B; Blackman, L. D.; Wright, D. B.; Gibson, M. I.; O'Reilly R. K. *Chem. Soc. Rev.* **2017**, 46, 4119.

(51) Oschmann, B.; Lawrence, J.; Schulze, M. W.; Ren, J. M.; Anastasaki, A.; Luo, Y.; Nothling, M. D.; Pester, C. W.; Delaney, D. R.; Connal, L. A.; McGrath, A. J.; Clark, P. G.; Bates, C. M.; Hawker, C. J. *ACS Macro Lett.* **2017**, 6, 668.

(52) Matsushita, Y.; Mori, K.; Saguchi, R.; Nakao, Y.; Noda, I.; Nagasawa, M. *Macromolecules* **1990**, *23*, 4313.

(53) Busch, P.; Posselt, D.; Smilgies, D. M.; Rheinländer, B.; Kremer, F.; Papadakis, C. M. *Macromolecules* **2003**, *36*, 8717.

(54) Runge, M. B.; Bowden, N. B.; *J. Am. Chem. Soc.* **2007**, 129, 10551.

(55) Yoon, J.; Lee, W.; Thomas, E. L.; *Adv. Mater.* **2006**, 18, 2691.

(56) Kim, E.; Ahn, H.; Park, S.; Lee, H.; Lee, M.; Lee, S.; Kim, T.; Kwak, E.; Lee, J. H.; Lei, X.; Huh, J.; Bang, J.; Lee, B.; Ryu, D. Y. *ACS Nano* **2013**, 7, 1952.

(57) Grubbs, R. B.; Grubbs, R. H. *Macromolecules*, **2017**, 50, 6979.

(58) Nichetti, D.; Manas-Zloczower, I. *Polym. Eng. Sci.* **1999**, *39*, 887.

(59) Perego, G.; Cella, G. D.; Bastioli, C. *J. Appl. Polym. Sci.* **1996**, 37.

(60) Broseta, D.; Fredrickson, G. H.; Hefland, E.; Leibler, L. *Macromolecules* **1990**, 23, 132.

(61) Anastasiadis, S. H.; Gancarz, I.; Koberstein, F. T. *Macromolecules* **1988**, 21, 2980.

(62) Peters, A. J.; Lawson, R. A.; Ludovice, P. J.; Henderson, C. L. *Proc. SPIE 8680*, *Alternative Lithographic Technologies V*, **2013**, 868020.

(63) Williamson, L. D.; Nealey, P. F. *Macromolecules* **2015**, 48, 3997.

(64) Noro, A.; Iinuma, M.; Suzuki, J.; Takano, A.; Matsushita, Y. *Macromolecules* **2004**, 37, 3804.

(65) Listak, J.; Jakubowski, W.; Mueller, L.; Plichta, A.; Matyjaszewski, K.; Bockstaller, M. R. *Macromolecules* **2008**, *41*, 5919.

(66) Widin, J. M.; Kim, M.; Schmitt, A. K.; Han, E.; Gopalan, P.; Mahanthappa, M. K. *Macromolecules* **2013**, *46*, 4472.

(67) Lynd, N. A.; Hillmyer, M. A.; Matsen, M. W. *Macromolecules* **2008**, *41*, 4531.

(68) Baskaran, D.; Müller, A. H. E. *Prog. Polym. Sci.* **2007**, *32*, 173.

(69) Young. R. N.; Quirk, R. P; Fetters, L. J. In *Anionic Polymerization*; Springer: Berlin; Heidelberg, 1984.

(70) Hadjichristidis, N.; Pitsikalis, M.; Pispas, S.; Iatrou, H. *Chem. Rev.* **2001**, *101*, 3747.

(71) Hadjichristidis, N.; Iatrou, H.; Pitsikalis, M.; Pispas, S.; Avgeropoulos, A. *Prog. Polym. Sci.* **2005**, *30*, 725.

(72) Kirkland, J. J.; Yau, W. W.; Stoklosa, H. J.; Dilks, C. H., Jr. *J. Chromatogr. Sci.* **1977**, *15*, 303.

(73) Rudin, A. *J. Chem. Educ.* **1969**, *46*, 595.

(74) Gonzalez-Gonzalez, V. A.; Neira-Velazquez, G.; Angulo-Sanchez, J. L.; *Polym. Degrad. Stab.* **1998**, 60, 33.

(75) Zhang, X.; Berry, B. C.; Yager, K. G.; Kim, S.; Jones, R. L.; Satija, S.; Pickel, D. L.; Douglas, J. F.; Karim, A. *ACS Nano* **2008**, *2*, 2331.

(76) Zhang, J.; Dorthe, P.; Smilgies, D. M.; Perlich, J.; Kyriakos, K.; Jaksch, S.; Papadakis, C. M. *Macromolecules* **2014**, 47, 5711.

(77) Sepe, A.; Hoppe, E. T.; Jaksch, S.; Magerl, D.; Zhong, Q.; Perlich, J.; Posselt, D.; Smilgies, D.-M.; Papadakis, C. M.; *J. Phys.: Condens. Matter* **2011**, 23, 254213.

(78) Walton, D. G.; Kellogg, G. J.; Mayes, A. M.; Lambooy, P.; Russell, T. P. *Macromolecules*, **1994**, 27, 6225.

(79) Zhang, X.; Douglas, J. F.; Jones, R. L. *Soft Matter*, **2012**, 8, 4980.

(80) Matsen, M. W.; Bates, F. S. *Macromolecules*, **1996**, 29, 1091

(81) Broseta, D.; Fredrickson, G. H.; Hefland, E.; Leibler, L.; *Macromolecules* **1990**, 23, 132.

(82) Fredrickson, G. H.; Sides, S. W. *Macromolecules* **2003**, 36, 5415.

(83) Woo, S.; Shin, T. J.; Choe, Y.; Lee, H.; Huh, J.; Bang, J. *Soft Matter* **2017**, *13*, 5527.

(84) Milner, S. T.; Witten, T. A.; Cates, M. E.; *Macromolecules* **1989**, 22,853.

(85) Devore, J. L. In *Probability and Statistics for Engineering and the Sciences*; Cengage Learning: Boston, Massachusetts, **2015**.

(86) Taylor, J. R. In *Introduction to Error Analysis: The Study of Uncertainties in Physical Measurements*; University Science Books: South Orange, New Jersey, **1997**.

(87) Rupp, M.; Tkatchenko, A.; Müller, K.-R.; Lilienfeld, von, O. A.; *Phys. Rev. Lett.* **2012**, *108*, 058301.

(88) Bartók, A. P.; Payne, M. C.; Kondor, R.; Csányi, G.; *Phys. Rev. Lett.* **2010**, 104, 136403.

(89) Rajan, K. *Mater. Today* **2005**, *8*, 38.

(90) Behler, J.; Parrinello, M.; *Phys. Rev. Lett.* **2007**, *98*, 146401.

(91) Hamdia, K. M.; Lahmer, T.; Nguyen-Thoi, T.; Rabczuk, T. *Comput. Mater. Sci.* **2015**, *102*, 304.

(92) Pilania, G.; Wang, C.; Jiang, X.; Rajasekaran, S.; Ramprasad, R. *Sci. Rep.* **2013**, *3*, 2810.

5.6 Appendix

Experimental

General Reagent Information

All reactions were carried out in an Unilab MBraun Glovebox with nitrogen atmosphere. Styrene (99+%, Sigma Aldrich) and methyl methacrylate (99%, Sigma Aldrich) were dried over calcium hydride (CaH_2) overnight and vacuum transferred into a flame dried Schlenk flask followed by three freeze-pump-thaw cycles. Methyl methacrylate was further purified by adding trioctylaluminum (25% in hexanes, Sigma Aldrich) until a yellow color persisted and then vacuum transferred to a flame dried Schlenk flask. Cyclohexane (Fisher Scientific, ACS Grade) was dried by stirring over a 1:1 solution of diphenylethylene and *s*-butyllithium (*s*-BuLi) followed by distilling under positive pressure of argon. Diphenylethylene was stirred over *n*-BuLi (2.5 M in hexanes, Sigma Aldrich) for 1 hour before distilling into a flame dried Schlenk flask under vacuum. Tetrahydrofuran was purchased from J.T. Baker and was purified by vigorous purging with argon for 2 h, followed by passing through two packed columns of neutral alumina under argon pressure. *S*-butyllithium (1.4 M in cyclohexane), butylated hydroxyltoluene (BHT, Alfa Aesar), methanol (Sigma Aldrich), and LiCl (Sigma Aldrich) were used as received.

General Analytical Information

Polymer samples were analyzed using a Tosoh EcoSEC HLC 8320GPC system with two SuperHM-M columns in series at a flow rate of 0.350 mL/min with THF

as the eluting solvent. Number average molecular weight (M_n), weight average molecular weight (M_w), dispersity (Đ) values, and asymmetry factors (A_s) were calculated from refractive index chromatograms against TSKgel polystyrene standards. NMR spectra, recorded on a Varian Mercury-300 NMR spectrometer in $CDCl_3$, and tabulated homopolymer densities were used to determine volume fractions ($f_{v,PS}$).

Preparation of Block Copolymers with Skewed PS Blocks

A 20 mL scintillation vial with a Teflon-coated magnetic stir bar was charged with 8 mL of cyclohexane and 2 mL of styrene (17.5 mmol). Stock solutions of *s*-BuLi were diluted with cyclohexane to a concentration of 0.1136 M for all reaction. A total volume of 380 μL was drawn into a 1 mL syringe before mounting on a New Era NE-4000 Double Syringe Pump. The syringe pump was programmed according to the appropriate rate profile to dispense 340 μL of the stock *s*-BuLi solution into the polymerization. The syringe pump was started immediately after the needle was submerged into the reaction mixture. During initiator addition, the polymerization reaction slowly turned bright orange. After full conversion, diphenylethylene (1.05 equiv) was added and stirred for 1 h until the solution turned deep red.

Chain Extension with MMA and Polymer Isolation

A flame-dried Schlenk bomb was brought into the glovebox and charged with LiCl (40 mg, 0.9 mmol). Each Schlenk flask was removed from the glovebox,

and 40 mL of tetrahydrofuran was added under positive pressure of argon. Once the LiCl dissolved, the solution was cooled to –78 °C in a dry ice/acetone bath and a few drops of *s*-BuLi (1.4 M in cyclohexane) were added until a yellow color persisted. After stirring for 1 h, the solution was warmed to room temperature and maintained until the yellow color dissipated completely. Each Schlenk flask was then brought back into the glovebox, and 2 mL of the living diphenylethyllithium end-capped PS polymerization mixture was added. The flasks were then removed from the glovebox and cooled to –78 °C with dry ice/acetone. Once cooled, the appropriate amount of methyl methacrylate was added under positive pressure of argon, and the flask was sealed and allowed to stir at –78 °C for 1 h before quenching with vigorously degassed methanol. Each polymer was then precipitated into cold methanol, and small amounts of terminated PS homopolymer were removed via Soxhlet extraction with cyclohexane.

Self-Assembly of PS-*b*-PMMA Thin Films

Silicon wafers were cut to 2 cm × 2 cm, submerged overnight in a piranha solution, rinsed several times with distilled water, and blown dry with nitrogen to remove all visible dust. The wafers were then plasma-treated for 60 s immediately before spin-coating. Each silicon wafer was spun dry from toluene for 30 s at 3000 rpm and an acceleration of 400 /s. Then, solutions of each polymer in toluene (25 mg/mL) were spun under the same conditions to light blue films, each approximately 160 nm as measured with a spectroscopic reflectometer (FilMetrics F20). All samples were then annealed in a vacuum oven at 180 °C for

15 h. Longer annealing times did not result in any significant further changes to the surface morphology as observed by AFM.

Grazing Incidence Small Angle X-ray Scattering

All X-ray experiments were conducted at the D1 beamline of the Cornell High Energy Synchrotron Source (CHESS) with a multilayer monochromator (λ = 1.17 Å) and a two-dimensional area detector distance of 1.82 m. The critical angle for PS-*b*-PMMA used in this study was about $\alpha_{c,Sample}$ = 0.11° and varied slightly from sample to sample. Scattering measurements were obtained at an incident angle of α_I = 0.13°, which is between the critical angle of the polymer film and the SiO_2/Si substrate ($\alpha_{c,Substrate}$ = 0.17°) where the structure throughout the entire film thickness contributes significantly to the scattering signal via coherent interference.[1-3] All D_{sp} values were measured at the position of the primary reflection in the GISAXS data from line cuts of the Yoneda band.[4,5] All GISAXS data was analyzed using Igor's Nika software package.[6]

Statistical Modelling and Least-Squares Analysis

All of the statistical modeling and linear least-squares analyses utilized in this work were performed using an in-house script written in MATLAB 2017b. In order to compute the central moments for each MWD, the SEC traces (which contained intensity *vs*. time data) were mapped *via* cubic spline interpolation onto an equispaced grid that consisted of 10,000 points and spanned the relevant

elution time interval of 9-15 min. All negative intensities from the SEC traces were baseline corrected to zero.

The optimized expansion coefficients in Eq. (5.10) were trained on the entire data set (N = 21) using least-squares analysis followed by testing on the same data set (with an associated error profile provided in Table 5.2). To further quantify the error associated with this statistical model, we have also performed leave-one-out (LOO) cross validation within the existing data set.[7] In particular, we separated the 21 samples considered herein into 21 distinct training sets (each containing 20 samples) and testing sets (each containing 1 sample). The stability and robustness of our model is confirmed by minimal variation observed in the optimized expansion coefficients during LOO cross validation (with an associated error profile provided in Table 5.8). To further demonstrate the transferability of our optimized expansion coefficients, we utilized ridge regression (*via* the introduction of a regularization parameter) during the LOO cross validation study and observed no further reduction in the D_{sp} prediction error.[8,9]

Procedure for Polystyrene Skewed to Low Molecular Weight (Table 5.1, Entry 16-21)

Living polystyrenes were prepared according to the general procedure (see manuscript) using the following constant addition rate profiles:

Table 5.4. 50 min Constant Rate of *s*-BuLi Addition

Step Number	Rate (μL/h)	Volume per Step (μL)
1	408	340

Procedure for Polystyrene Skewed to High Molecular Weight (Table 5.1, Entry 8-15)

Living polystyrenes were prepared according to the general procedure using the following exponentially ramped addition rate profiles:

Table 5.5. 85 min Exponentially Ramped Rate of *s*-BuLi Addition

Step Number	Rate (μL/h)	Volume per Step (μL)
1	2.4	0.2
2	3.3	0.2
3	4.6	0.3
4	6.4	0.4
5	9.0	0.6
6	12.5	0.9
7	17.5	1.3
8	24.5	1.7
9	34.3	2.4
10	48.1	3.4
11	67.3	4.7
12	94.2	6.6
13	131.9	9.2
14	184.7	12.9
15	258.5	18.1
16	361.9	25.3
17	506.7	35.5
18	709.3	49.6
19	993.1	69.5
20	1390	97.3

Procedure for Narrow MWD Polystyrene (Table 5.1, Entry 1-7)

Living polystyrenes were prepared according to the general procedure. The syringe pump was not used in the case of narrow MWD polystyrenes. 340 μL of *s*-BuLi (0.1136 M) was added instantaneously to the cyclohexane/styrene mixture.

Calculation of Asymmetry Factor (A_s)

The Tosoh ECOSEC analysis program was used to calculate asymmetry factors. Figure 5.7 illustrates A_s, which describes the ratio of the distance from the peak max to the front of the peak over the distance from the peak max line to the back of the peak at 10% peak height.

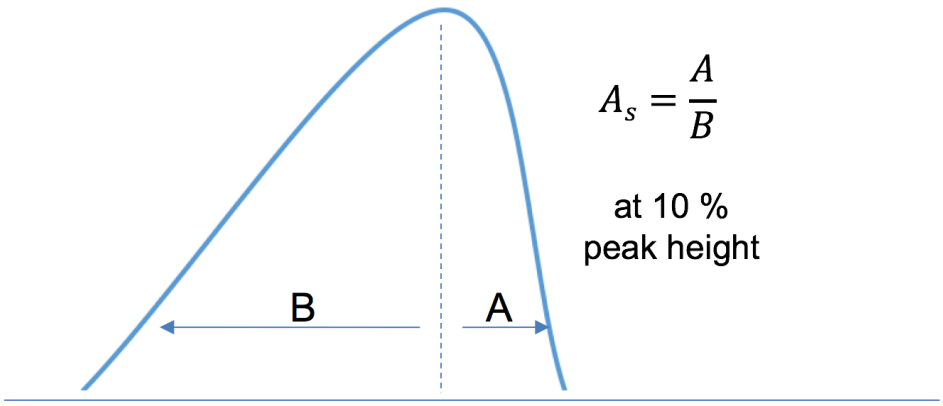

Figure 5.7. Calculation of Asymmetry Factor (A_s)

Characterization by Atomic Force Microscopy with Fast Fourier Transforms and Height Images from Figure 5.4

Atomic Force Microscopy (AFM) images were obtained using an Asylum-MFP3D-Bio-AFM-SPM in tapping mode and flattened in Igor Pro. Fast Fourier Transforms (FFTs) are shown below.

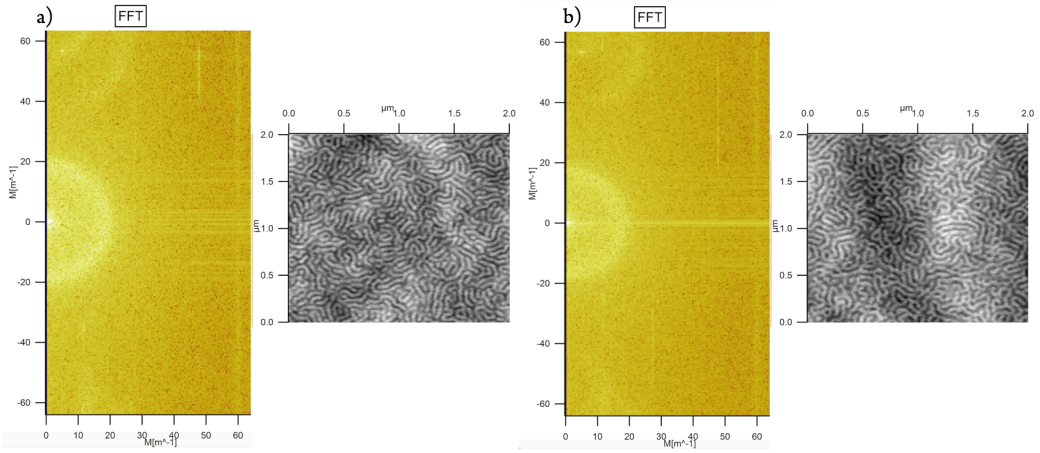

Figure 5.8. FFT and Height Image for Figure 4.4a and 4.4b

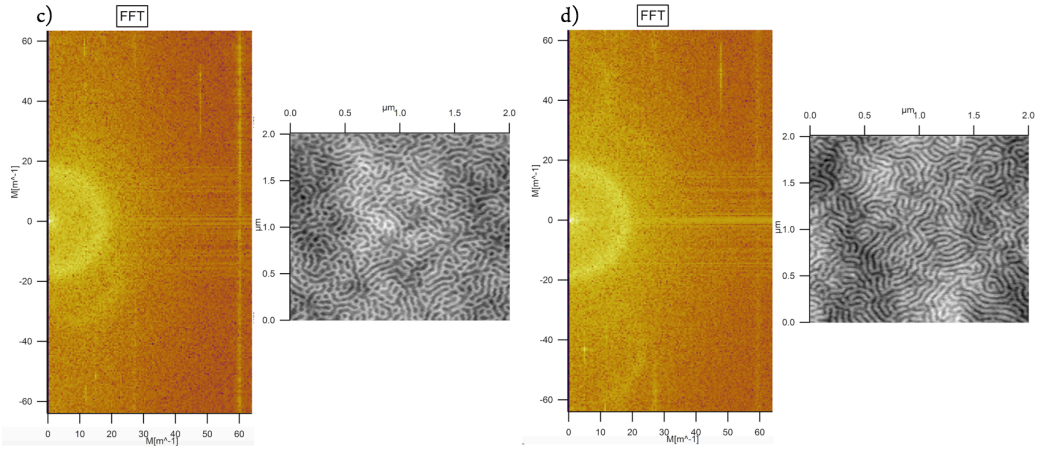

Figure 5.9. FFT and Height Image for Figure 4.4c and 4.4d

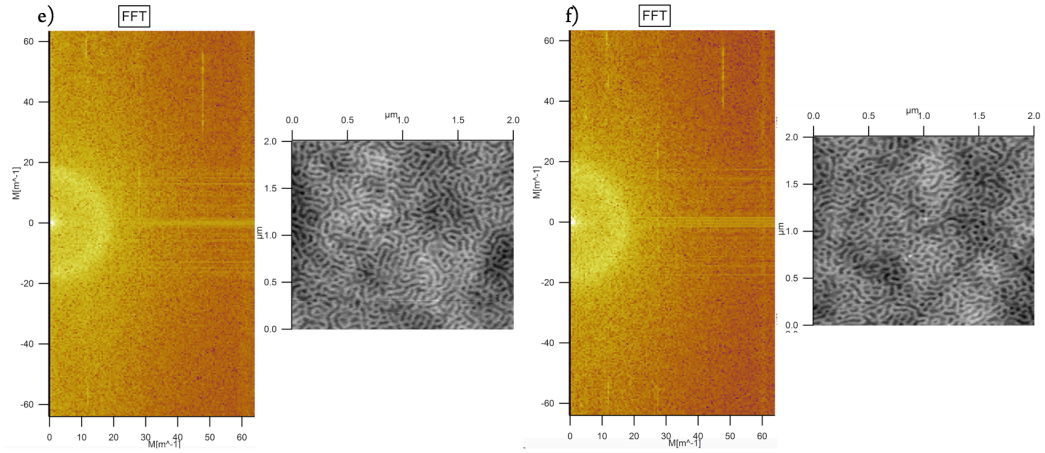

Figure 5.10. FFT and Height Image for Figure 4.4e and 4.4f

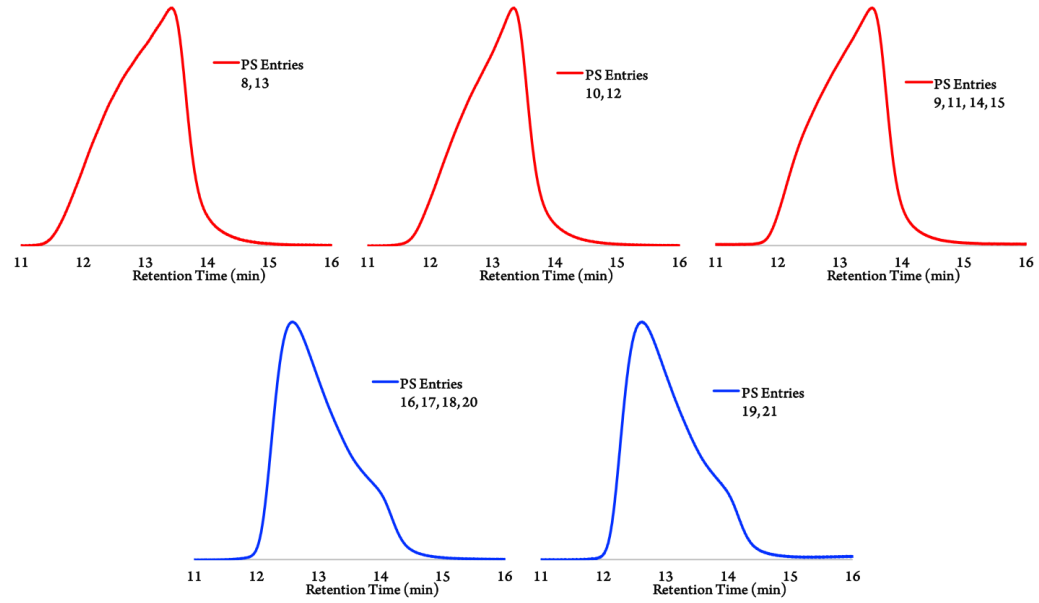

Figure 5.11. Skewed PS Blocks from Table 5.1 where MWDs skewed to high molecular weight are shown in red (entries 8 – 15) and MWDs skewed to low molecular weight in blue (entries 16 – 21).

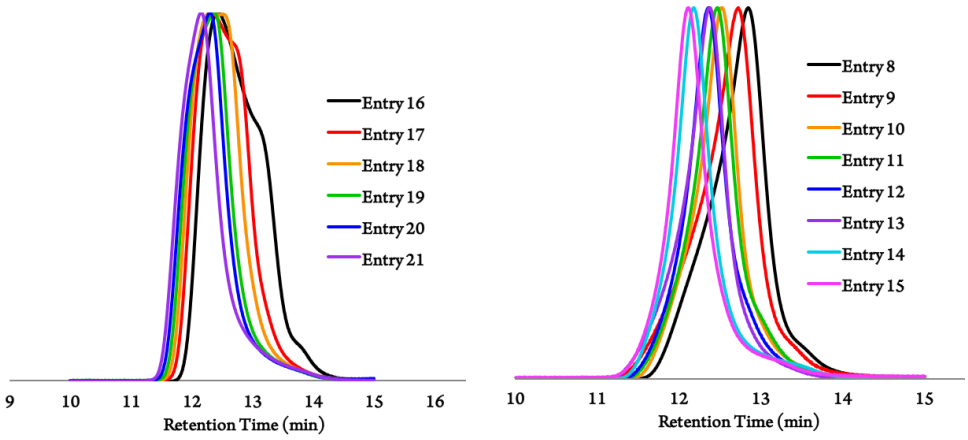

Figure 5.12. Skewed PS-b-PMMA Diblock Copolymers Used in D-spacing Study. Entries correspond to those in Table 5.1.

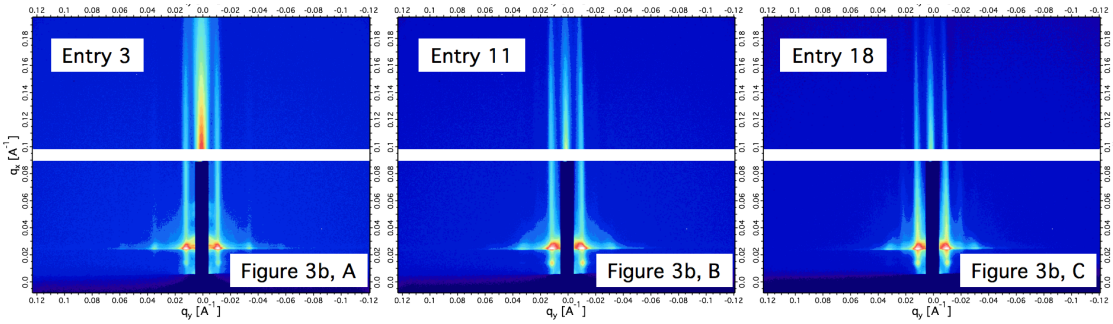

Figure 5.13. Representative 2D GISAXS Images Showing Perpendicular Orientation of Lamellae.

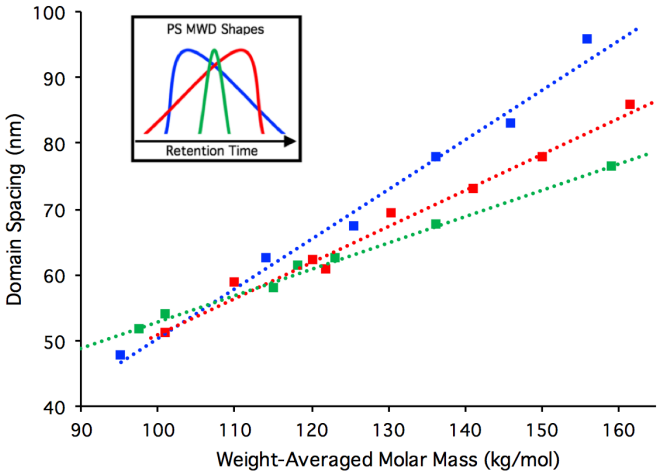

Figure 5.14. Domain Spacing Plotted Against M_w of PS-b-PMMA Block Copolymers.

The trends observed in D_{sp} with respect to M_n in Figure 5.3 are conserved when plotted against M_w. The narrow control group (green squares) are offset to lower M_w in this plot due to the fact that they have narrower MWDs (*i.e.*, $Đ = M_w/M_n$).

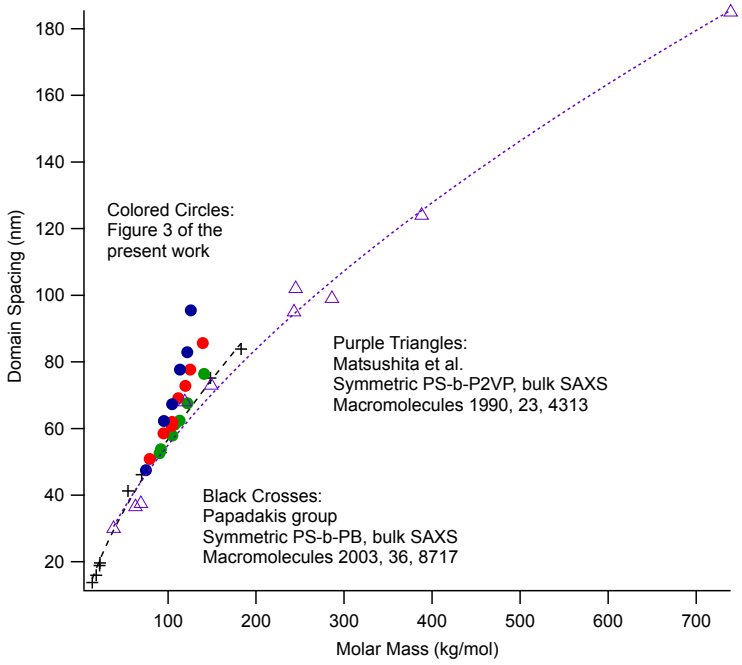

Figure 5.15. Comparison of D_{sp} vs. M_n Between the Current Work and Literature Examples of Symmetric Block Copolymers.

Based on previous experimental efforts by Matsushita and Papadakis, there is reasonable agreement between the control group (green circles) in the current study and the established relationship between domain spacing and molar mass of narrow MWD block copolymers. It is important to note that the present study alters both molar mass and volume fraction, and, therefore, may not follow the power law that has been established for block copolymers at constant block compositions.

Additional Normalization Procedure Utilized in Statistical Modeling and Least-Squares Analysis

As mentioned in the main text, an additional transformation is required to allow for a quantitative assessment of the relative importance of each term in our statistical model *via direct comparison of the final expansion coefficients*. To derive this transformation (which is simply another level of normalization), we start with the statistical model given in given in Eq. (4.8) and define

$$\Lambda_{ijk}^{(p)} = \left(\Lambda_1^{(p)}\right)^i \left(\Lambda_2^{(p)}\right)^j \left(\Lambda_3^{(p)}\right)^k \tag{5.11}$$

such that

$$\mathrm{D}_{\mathrm{sp},expt}^{(p)} \approx \sum_{ijk} c_{ijk} \left(\Lambda_1^{(p)}\right)^i \left(\Lambda_2^{(p)}\right)^j \left(\Lambda_3^{(p)}\right)^k = \sum_{ijk} c_{ijk} \Lambda_{ijk}^{(p)} = \mathrm{D}_{\mathrm{sp},pred}^{(p)} \tag{5.12}$$

We then normalize each term in this power series expansion by the corresponding statistical maximum over all of the samples in the training set, *i.e.*,

$$\Lambda_{ijk}^{\max} = \left| \max_{\{p\}} \left\{ \Lambda_{ijk}^{(p)} \right\} \right| \tag{5.13}$$

which leads to the final expression for our statistical model for D_{sp}:

$$\mathrm{D}_{\mathrm{sp},expt}^{(p)} \approx \sum_{ijk} c_{ijk} \Lambda_{ijk}^{(p)} = \sum_{ijk} \bar{c}_{ijk} \bar{\Lambda}_{ijk}^{(p)} = \mathrm{D}_{\mathrm{sp},pred}^{(p)} \,, \tag{5.14}$$

in which

$$\bar{\Lambda}_{ijk}^{(p)} = \frac{\Lambda_{ijk}^{(p)}}{\Lambda_{ijk}^{\max}} \tag{5.15}$$

and

$$\bar{c}_{ijk} = c_{ijk} \Lambda_{ijk}^{\max}. \tag{5.16}$$

Eq. (5.14) is the final working expression for computing the predicted values of D_{sp} and can be used with either (i) $\{c_{ijk}\}$ and $\left\{\Lambda_{ijk}^{(p)}\right\}$ or (ii) $\{\bar{c}_{ijk}\}$ and $\left\{\bar{\Lambda}_{ijk}^{(p)}\right\}$.

Table 5.6. Population Means Utilized in Eq. (5.9)

$\langle \boldsymbol{M_1} \rangle$	$\langle \boldsymbol{M_2} \rangle$	$\langle \boldsymbol{M_3} \rangle$
12.426	0.446	0.134

Table 5.7. Normalization Factors Defined in Eq. (5.13)

i	j	k	$\Lambda_{ijk}^{\max}$
0	0	0	1.0000
1	0	0	0.0244
0	1	0	0.4908
0	0	1	3.2961
1	1	0	0.0104
1	0	1	0.0761
0	1	1	1.0147
2	0	0	0.0006

Table 5.8. Errors in the LOO Cross-Validated Predictions of Domain Spacing (D_{sp})

	error (nm)
MSE	0.0
MAE	1.6
RMSE	2.1
MAXE	4.4

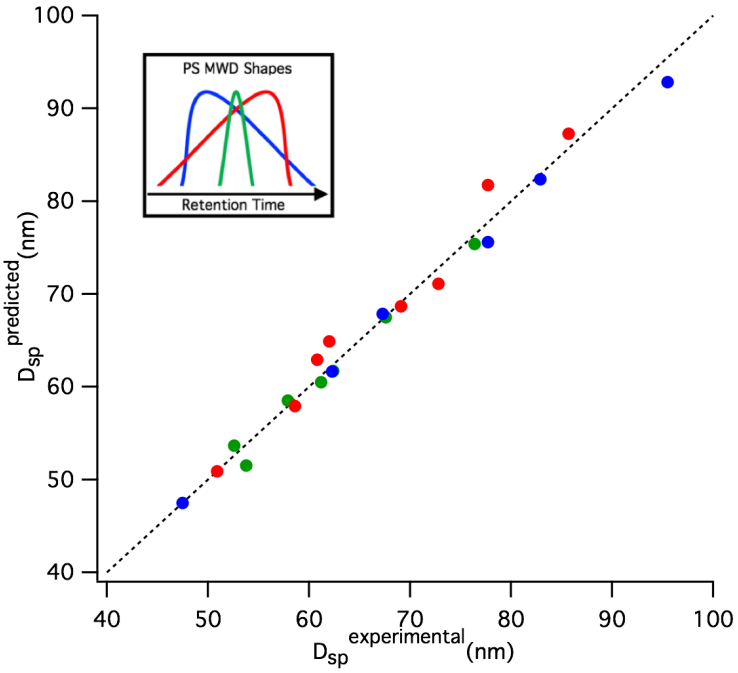

Figure 5.16. Predicted D_{sp} Values from the Statistical Model in Eq. (5.8) Based on the MWD Shape of the Final PS-b-PMMA Copolymer.

A comparison between Figure 5.5 and Figure 5.16 demonstrate good agreement, which supports the fact that modifications to the MWD shape are confined to the PS block and the PMMA block remains narrow and monodisperse.

Table 5.9. Values of the Expansion Coefficients and Normalization Factors for the D_{sp} Prediction in Figure 5.16.

i	j	k	$\bar{c}_{ijk}$	Λ_{ijk}^{max}
0	0	0	65.9	1.0000
1	0	0	–18.6	0.0252
0	1	0	8.91	0.3949
0	0	1	1.04	1.1572
1	1	0	–3.34	0.0072
1	0	1	–8.17	0.0135
0	1	1	9.46	0.2364
2	0	0	–2.36	0.0006

5.6 Appendix References

(1) Smilgies, D. M.; Busch, P.; Papadakis, C. M.; Posselt, D. *Synchrotron Radiat. News* **2002**, *15*, 35.

(2) Chavis, M. A; Smilgies, D.-M.; Weisner, U. B.; Ober, C. K. *Adv. Funct. Mater.* **2015**, 25, 3057.

(3) Kim S. H.; Misner M. J.; Xu T.; Kimura M.; Russell T. P. *Adv. Mater.* **2004**, 16, 226.

(4) Lee, B.; Park, I.; Yoon, J.; Park, S.; Kim, J.; Kim, K.-W.; Chang, T.; Ree, M. *Macromolecules* **2005**, *38*, 4311.

(5) Busch, P.; Rauscher, M.; Smilgies, D. M.; Posselt, D.; Papadakis, C. M. *J. Appl. Cryst.* **200**6, *39*, 433.

(6) Ilavsky, J. *J. Appl. Cryst.* **2012**, *45*, 324.

(7) Arlot, S.; Celisse, A. *Statist. Surv.* **2010**, *4*, 40.

(8) Hoerl, A. E.; Kennard, R. *Technometrics* **1970**, 12, 55.

(9) Seber, G.; Lee, A. J.; In *Linear Regression Analysis*; New Jersey, **2003.**

CHAPTER 6

MOLECULAR WEIGHT DISTRIBUTION AS A VERSATILE APPROACH TO TAILORING BLOCK COPOLYMER PHASE BEHAVIOR

6.1 Abstract

The molecular weight distributions (MWDs) of block copolymers significantly impact their morphological phase behavior, but exploiting these features as a means to tune material properties has been limited to the MWD breadth, or dispersity (*Đ*). Manipulation of the entire MWD has promising potential to address this challenge by providing a convenient and versatile route toward tailoring polymer nanostructure. Herein, we describe the self-assembly of poly(styrene)-*block*-poly(2-vinylpyridine) (PS-*b*-P2VP) where the PS blocks have systematically deviating compositions of molecular weights. We find that controlling the MWD shape—breadth and skew—afforded access to different morphologies in samples with the same molecular characteristics, including *Đ*. As such, we illustrate the generality and effectiveness of this strategy, and anticipate that it will facilitate the increased deployment of disperse polymer compositions in advanced materials applications.

6.2 Introduction

The controlled synthesis of block copolymers, a class of self-organizing hybrid macromolecules, has facilitated the development of many advanced materials applications such as microelectronics, pho-tonic materials, filtration

membranes, and drug delivery systems.[1-12] The general notion has persisted that uniform polymers with narrow molecular weight distributions (MWDs) are required for robust self-assembly. However, recent evidence has shown that broad polymers form well-defined nanostructures, inspiring the deliberate manipulation of MWDs as a useful new approach to dictating block copolymer function.[13-27] In this respect, there is important practical utility in governing material properties without the need to alter their chemical composition.[28,29] In fact, command of the entire MWD provides a uniquely versatile handle for tuning phase behavior on the grounds that there is, in principle, infinite variability of the MWD shape.[13-15] Furthermore, numerous contemporary polymerization strategies produce materials with non-uniform MWDs and their full realization in future technologies rests upon a deep fundamental understanding of the relationship between MWD shape and block copolymer self-assembly.[17,30]

A number of studies have explored the influence of dispersity (*Đ*), or the relative span of chain lengths, on the microphase separation of block copolymers. Preliminary work revealed that well-ordered morphologies could be achieved and demonstrated a dependence of domain spacing (D_{sp}) on *Đ*. Moreover, it was discovered that the observed morphologies—lamellae (L), perforated lamellae (PL), gyroid (G), cylinders (C), spheres (S)—of samples with large *Đ* diverged from their narrow counterparts at the same block compositions. Thus, *Đ* affects can alter the position and size of the morphology composition windows.[17] However, *Đ* is not a complete description of the composition of polymer chain lengths in a given sample, and as such it is only the

first stage of exploiting the full potential of MWDs. Theoretical studies have, indeed, proposed that the higher moments of the distribution function should profoundly impact phase behavior, claims which have remained underexplored due to the lack of general synthetic strategies for dictating the precise molar quantities of each chain length.[30] We have recently demonstrated that polymers with distinct MWD shapes were readily accessible through a temporally controlled initiation process. In fact, we found that holding the number-averaged molar mass (M_n), volume fraction (f_v), and $Đ$ constant, with opposite skews, the D_{sp} of lamellar thin films could be varied predictably.[31] Coupled with our previous work in which the MWD skew enforced substantial control over Young's modulus,[14,15] we envision the ability to govern both microphase and macroscale polymer properties. Additionally, this process may allow simultaneous and independent control of volume fraction and morphology, parameters which are tightly coupled in monodisperse samples. However, in order to discover the full reach of this strategy, fundamental studies of the influence of MWD shape on bulk phase behavior over several morphologies are critical.

In this work, we explore the morphological characteristics of poly(styrene)-*block*-poly(2-vinylpyridine) (PS-*b*-P2VP) copolymers where the MWD shape (breadth and skew) of the poly(styrene) (PS) block was systematically varied. We demonstrate that the precise MWD breadth and skew have strong influences over self-assembly. Specifically, in copolymers with disperse and skewed blocks as the minority component, the L/C phase boundary is shifted toward higher volume fraction. When the disperse block is

the majority component we observe an interesting new phenomenon; the L/C phase boundaries diverge, shifting to lower PS content for negatively skewed samples and to higher PS content in positively skewed samples. These changes demonstrate the potential for using this strategy to tune phase behavior, and gives new physical insight into how the entire MWD influences block copolymer self-assembly.

6.3 Results and Discussion

We commenced our investigation with the synthesis of three sets of PS-*b*-P2VP copolymers with overall Mn values ranging from 31.8 – 96.5 kg/mol (Figure 6.1). All polymers contain PS blocks with M_n values of ~ 25 kg/mol but variable MWD compositions. The first series of samples was comprised of narrow MWDs ($Đ$ < 1.1) in both blocks and functioned as a control group (Table 6.1, entries 1 – 6). The second (Table 6.1, entries 7 – 14) and third (Table 6.1, entries 15 – 23) sample sets possessed PS blocks with broadened MWDs ($Đ$ ~ 1.4) with either a positive or negative skew, respectively.

Specifically, the PS blocks were prepared by temporally controlled initiation through metered addition of *s*-BuLi to the anionic polymerization of styrene (Figure 6.1a). When the initiator was added at a constant rate during the polymerization, the PS sample includes a larger fraction of high molar mass polymers, giving a negatively skewed MWD (Figure 6.1b and 6.1c, blue). Conversely, if the addition occurs at an exponential rate, the majority of the polymer chains are initiated at a later stage of the reaction, yielding a MWD that

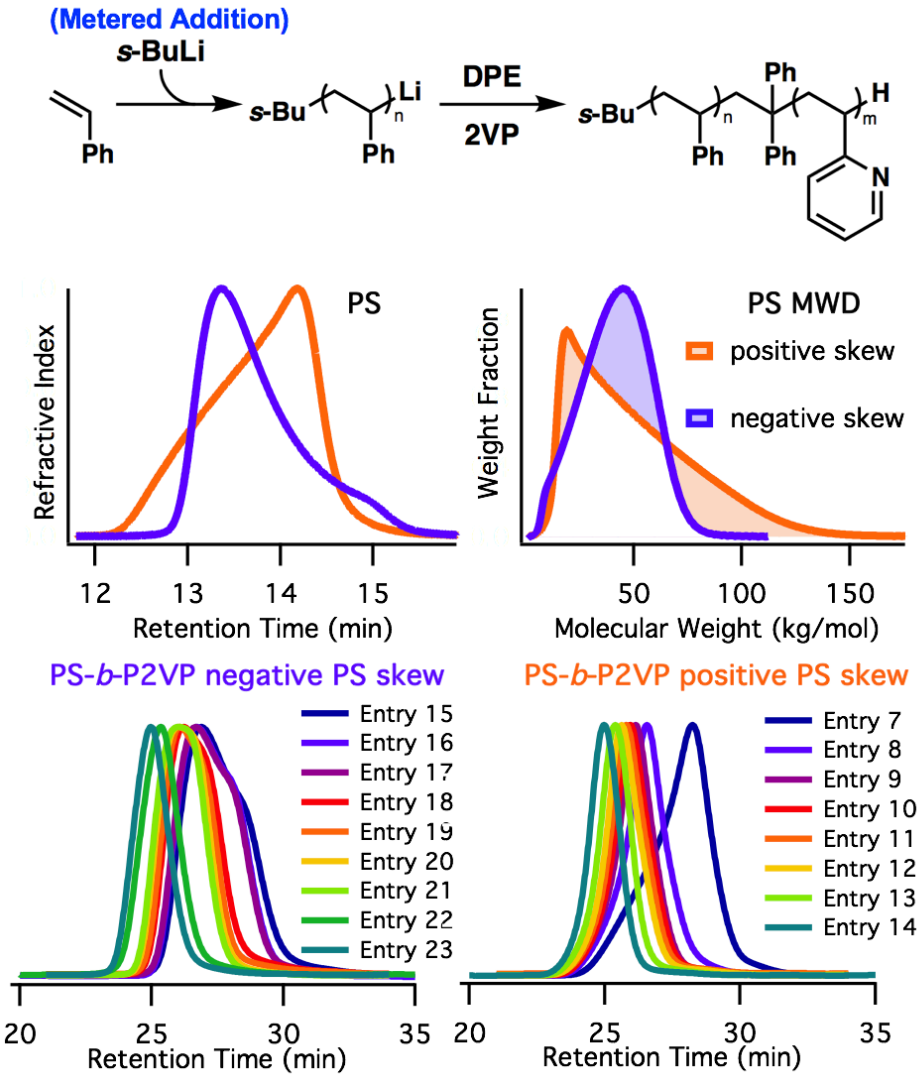

Figure 6.1. (a) Reaction scheme for the anionic polymerization of PS-*b*-P2VP copolymers with skewed PS blocks, (b) PS SEC traces, (c) normalized differential MWDs, and SEC traces of final diblock copolymers with (d) negatively and (e) positively skewed PS blocks (DPE = diphenylethylene; 2VP = 2-vinylpyridine).

is positively skewed (Figure 6.1b and 6.1c, orange). Interestingly, the peak molar mass (M_p) of these PS samples provides a measure of how mass is distributed in a given sample. In the positively skewed PS (Figure 6.1c; orange trace), this value was shifted below the mean (M_n ~ 25 kg/mol) to an M_p ~ 18 kg/mol, while it was transferred far above the mean to M_p ~ 45 kg/mol when skewed negatively (Figure 6.1c; blue trace). More quantitatively, we use the coefficient of skewness (α_3) to describe the distribution asymmetry.[32] We then proceeded to chain extend these PS samples with varying amounts of 2VP to span a range of different morphologies.[33] We observed a drop in the *Đ* values upon chain extension, and the SEC traces retained the shape of their parent PS homopolymer, providing strong evidence that the second block was well-controlled and any differences in MWD were con-strained to the PS block (Figure 6.1d and 6.1e).To characterize the morphological phase behavior of these polymers we performed small-angle X-ray scattering (SAXS) measurements of all 23 PS-b-P2VP samples (Table 6.1).[33]

Significantly, the distribution has a strong effect on the morphological behavior of PS-*b*-P2VP. We started at the higher end of molar masses that we explored, where PS was the minority component of the final block copolymer (Figure 6.2). Specifically, a copolymer sample possessing a $f_{v,\,PS}$ = 0.35 with a narrow MWD, exhibited a lamellar (L) morphology (Table 6.1, entry 5), characterized by a combination of SAXS and transmission electron microscopy (TEM). Against this baseline, we examined the morphological phase behavior

Table 6.1. Molecular and Morphological Characteristics of Poly(styrene)-*block*-poly(2-vinylpyridine) Copolymers

Entry	$M_{n,\,PS}$ [a] (kg/mol)	$Đ_{PS}$ [a]	$M_{p,\,PS}$ [a] (kg/mol)	$\alpha_{3,\,MWD}$ [b]	$M_{n,\,PSP2VP}$ [c] (kg/mol)	$Đ_{PSP2VP}$ [a]	$f_{v,\,PS}$ [c]	D_{sp} [d] (nm)	*phase* [e]
1	24.1	1.08	28.1	N/A	31.8	1.03	0.75	23.6	C
2	24.1	1.08	28.1	N/A	36.3	1.03	0.67	27.5	PL
3	24.3	1.09	28.4	N/A	56.4	1.03	0.41	38.2	L
4	24.8	1.09	28.7	N/A	64.2	1.03	0.37	41.3	L
5	24.8	1.09	28.7	N/A	68.0	1.02	0.35	42.0	L
6	24.4	1.09	28.6	N/A	75.2	1.02	0.31	41.2	L’
7	25.0	1.45	18.9	2.2	36.7	1.21	0.67	25.7	C
8	24.7	1.45	18.8	2.1	50.8	1.12	0.47	38.2	L
9	24.7	1.45	18.8	2.1	61.2	1.10	0.39	40.6	L
10	24.0	1.39	19.7	1.7	63.4	1.08	0.36	42.2	C
11	24.7	1.45	18.8	2.1	67.9	1.08	0.35	42.4	C
12	24.0	1.39	19.5	1.7	70.3	1.07	0.33	44.0	C
13	24.0	1.39	19.5	1.7	73.3	1.07	0.31	44.4	C
14	24.6	1.42	19.7	1.8	92.5	1.05	0.25	46.5	C
15	24.2	1.41	44.7	0.8	34.7	1.17	0.69	33.2	L
16	24.2	1.41	44.7	0.8	39.8	1.13	0.60	34.1	L
17	24.2	1.41	44.7	0.8	43.4	1.13	0.54	34.3	L
18	24.0	1.41	43.8	0.9	50.7	1.11	0.46	41.3	L
19	24.0	1.41	43.8	0.9	54.4	1.08	0.42	41.4	L
20	24.1	1.43	46.1	0.8	67.1	1.07	0.34	41.8	C
21	24.1	1.43	46.1	0.8	69.8	1.07	0.33	42.2	C
22	24.2	1.40	44.9	0.8	84.7	1.06	0.27	46.6	C
23	24.2	1.40	44.9	0.8	96.7	1.05	0.24	49.0	C

[a] Determined by SEC against PS standards; [b] Computed from differential PS MWDs; [c] Calculated using NMR spectroscopy and tabulated homopolymer densities; [d] Calculated from the position of the principle scattering wavevector (q^*); [e] (C = hexagonally packed cylinders; PL = perforated lamellae; L = lamellae; L’ = minor C in primarily L)

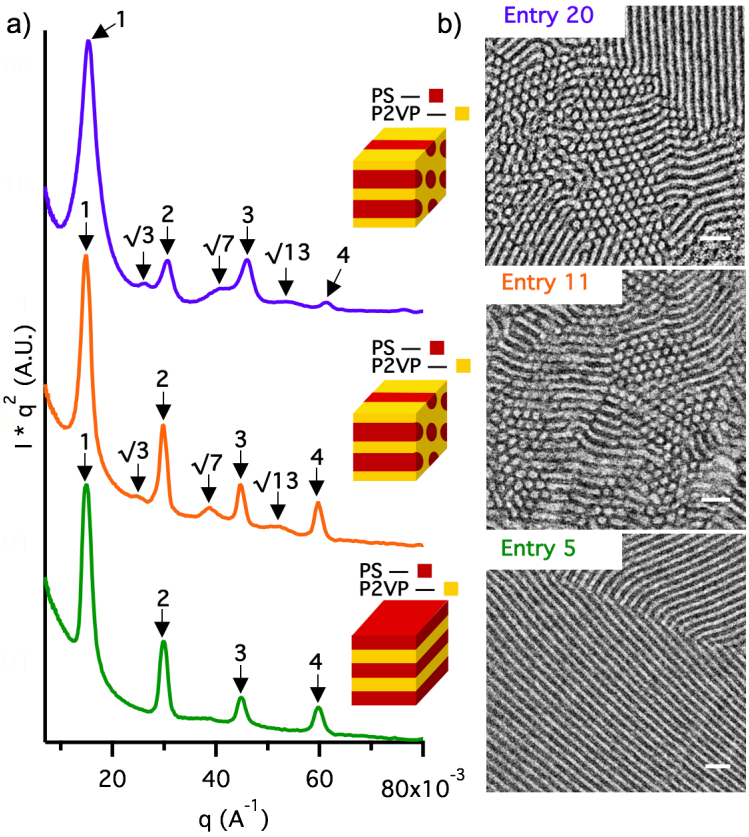

Figure 6.2. (a) 1D SAXS profiles for three copolymers at $f_{v,\,PS}$ = 0.34 – 0.35 having PS MWDs with $Đ$ < 1.1 (green), $Đ$ ~ 1.4 and α_3 = 2.1 (orange), and $Đ$ ~ 1.4 and α_3 = 0.8 (blue), and (b) the corresponding TEM images. Scale bars are 100 nm

of two block copolymers having similar M_n and $f_{v,\,PS}$ values but with either positive (Table 6.1, entry 11) or negative (Table 6.1, entry 20) PS skews. Interestingly, both samples showed a shift to C from the observed L of the sample with a narrow PS distribution. Since all other molecular characteristics apart from MWD were held constant, this morphological transition from L to C exemplifies the effects of varying the PS MWD.

Subsequently, as the copolymers' PS content was increased to $f_{v,\,PS}$ = 0.41 – 0.60, each sample adopted the L structure. However, as the PS block composition was further increased, the PS–rich samples of varying MWDs exhibited morphologies that diverged from one another at the same $f_{v,\,PS}$ (Figure 6.3). At a $f_{v,\,PS}$ = 0.67, the narrow PS MWD yielded well-defined perforated lamellae (PL) (Table 6.1, entry 2), confirmed *via* SAXS through the characteristic reflection at q^* = 1.9 (Figure 6.3a and 6.3b) as well as the lamellar perforations which were visible by TEM (Figure 6.3e). A subsequent sample with PS MWD that was expanded to $Đ$ ~ 1.4 and positively skewed produced a cylindrical morphology of P2VP in a PS matrix (Figure 6.3c and 6.3f). Interestingly the same sample with a negatively skewed PS block resulted in well-defined lamellae (Figure 6.3d and 6.3g). These majority PS copolymers show divergent morphologies based on the MWD skews, which is unlike what was observed when the PS is the minority phase.

There are currently two proposed mechanisms to explain how dispersity influences phase behavior. The first effect is that exceedingly short and asymmetric chains can desorb from the interface as long as the enthalpic penalty for surrounding a short block with unlike segments is not greater than the entropic cost of confining these chains to the interface.[17,25,34-38] This ability for individual chains to desorb from the interface swells the domain of that individual chain's majority component, increasing the D_{sp} relative to narrow counterparts.[31,34,35] In the present work, we would expect to see increasing deviations in D_{sp} with decreasing $f_{v,\,PS}$ based on previous studies with

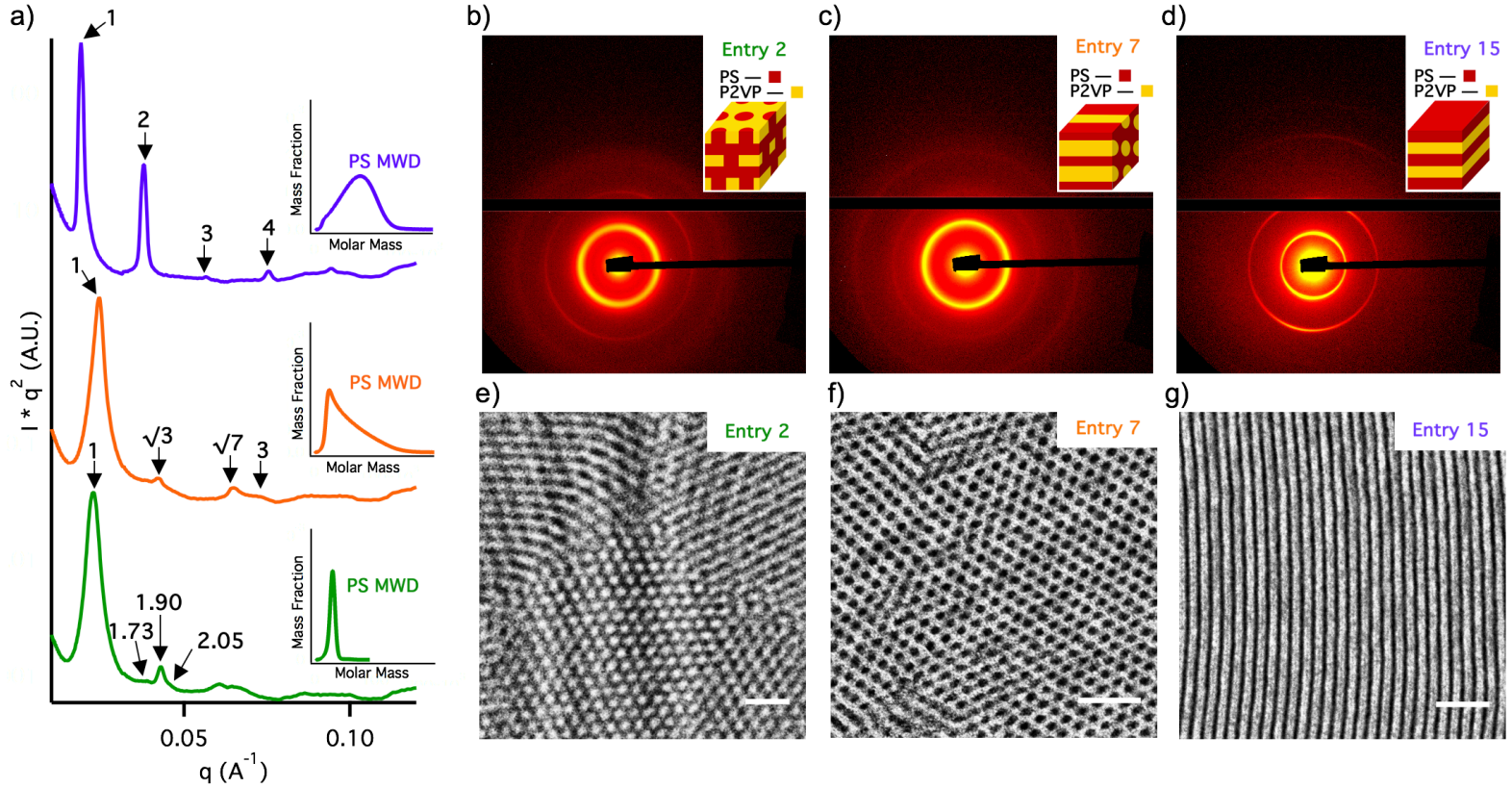

Figure 6.3. Three different morphologies exhibited by three polymers with similar M_n at $f_{v,\,PS}$ = 0.67 – 0.69 but either monodisperse (green), positively skewed (orange), or negatively skewed (blue) PS MWDs with (a) reduced SAXS intensity profiles and corresponding PS MWDs as in-sets, (b – d) 2D SAXS patterns, and (e – g) TEM images where the dark and light regions are the P2VP and PS domains, respectively. Scale bars are 100 nm

polystyrene-*block*-poly(methyl methacrylate).[31] Considering that this effect is more pronounced at lower χ values and that we observe little influence on D_{sp}, it is unlikely that this mechanism is contributing significantly to the current work (see Chapter 6 Appendix).

The second driving force is that heterogeneous mixtures of chain lengths (increased breadth or $Đ$) in an A-B diblock copolymer allow chains to fill space more efficiently; long chains can fill open space while short chains remain relaxed at the interface. This characteristic decreases the entropic burden of stretching the broadened A–block and allows the narrow B–block to relieve chain crowding by curving the interface away from itself and toward the block with increased $Đ$.[25,36-40] Since PS-*b*-P2VP copolymers with the same degree of immiscibility (χN) and $f_{v,\ PS}$ yielded an assortment of morphologies, consideration of trends in the curvature of each morphological interface with respect to MWD shape provides insight about the specific contributions of MWD breadth and skew.

Figure 6.4 shows a modified compositional phase diagram which demonstrates how MWD skew triggers significant movement of the phase boundaries from the perspective of the entire sample library. The initial change when the PS is the minority block from L to C corresponds to an increase in interfacial curvature. This result is in qualitative agreement with previous reports, and likely arises from the fact that the PS block has many chain lengths

present (Figure 6.4, i – iii). This allows the disperse block to stretch further and induces curvature toward the PS.

More intriguing, the same trend is not repeated in the PS–rich region of the phase diagram. The narrow MWD control at a $f_{v, PS}$ = 0.67 (Figure 6.4, iv) afforded a PL structure which suggests that the PS–rich lamellar phase boundary occurs at a slightly lower $f_{v, PS}$ of 0.65.[33,44-46] The transition from PL to L with $Đ$ ~ 1.4 and negative skewing is also in good qualitative agreement boundary occurs at a slightly lower $f_{v, PS}$ of 0.65.[33,44-46] The transition from PL to L with $Đ$ ~ 1.4 and negative skewing is also in good qualitative agreement with the literature (Figure 6.4, v). However, a complete reversal of interfacial curvature away from the disperse PS block was observed when the majority block was positively skewed (Figure 6.4, vi). This divergence suggests that the effect of dispersity on interfacial curvature is not purely reflective of samples with mixtures of different chain lengths, but it is more intricately coupled to the relative quantities of large and small chains. Samples with negative skew have a high M_p of about 45 kg/mol and thus contain almost 60% of polymer chains above the M_n. These samples agreed with the general trend of previous reports where curvature occurs toward the disperse block due to its enhanced ability to stretch. In stark contrast however, the positively skewed majority PS sample has over 60% of its polymer chains below the M_n (M_p ~ 18 kg/mol). Long polymer chains have a greater number of degrees of freedom and thus have an enhanced capacity to stretch to fill open space, while short chains prefer to

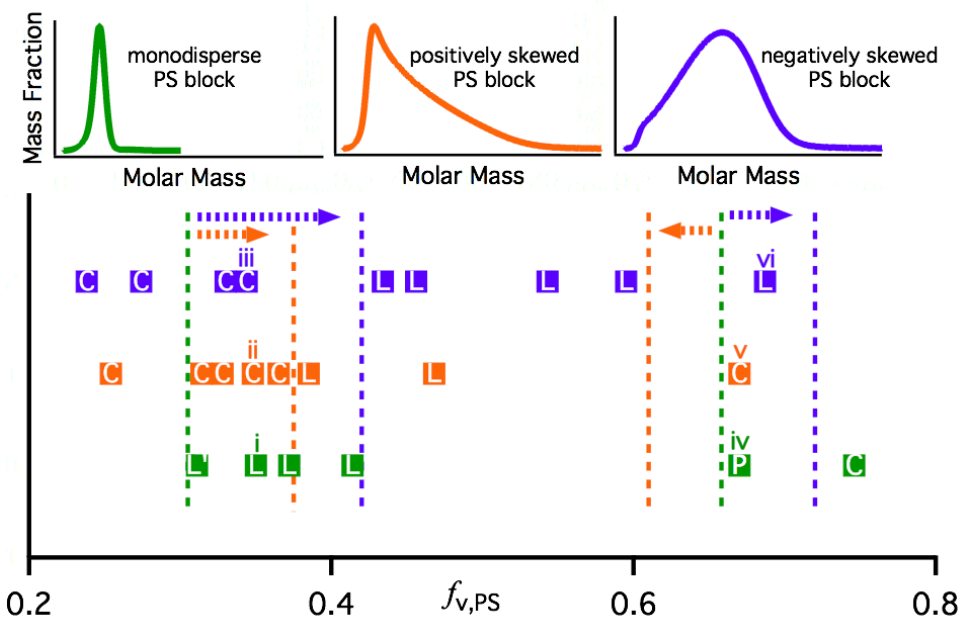

Figure 6.4. PS-*b*-P2VP phase diagram of MWD shape versus block composition, omitting χN for visual clarity, where dashed lines and arrows show the motion and tentative position of the lamellar phase boundaries (L = lamellae; C = hexagonally close packed cylinders; P = hexagonally perforated layers; L' = primarily lamellae with minor cylinders).[41-43]

remain relaxed at the interface. Since the positively skewed PS blocks in the majority component contain a substantial fraction of very low molecular weight chains, we propose that the entropic penalty for stretching these short PS chains outweighs the penalty for stretching the P2VP phase. Thus, curvature toward the disperse block is no longer favorable, and curvature away from the PS is observed. This induces a shift in the L/C phase boundary toward lower PS content for positively skewed sample. Conversely, the negatively skewed PS MWDs resulted in opposite trend, presumably due to its larger fraction of high

molar mass material which allows the disperse block to stretch further, flattening the interface and pushing the L/C phase boundary toward higher PS content. These changes correspond to a shift of the lamellar composition window in negatively skewed PS samples, and a significant narrowing for positively skewed PS MWDs. Based on these results, MWD should enable increased control of polymer properties and access to novel materials, as polymer microstructure can be modified while all other molecular characteristics are held constant, including *Đ*.

6.4 Conclusion

In this work, we have demonstrated that modulating the higher moments of the molecular weight distribution influences the bulk morphological phase behavior of PS-*b*-P2VP. Varying the MWD breadth and skew of the PS block enabled significant control over the width of the lamellar composition windows and allowed three distinct morphologies to be prepared via solely changing the MWD breadth and skew of the constituent blocks. These data suggest that different molar quantities of each chain length contribute distinctly and significantly to the capacity for a polymer chain ensemble to stretch, which alters the resultant morphologies by increasing or decreasing the preferred interfacial curvature. Interestingly, these effects persisted even when the MWD breadth, or *Đ*, was held constant. We propose that this general strategy provides a new means to tailor the microphase behavior of block copolymers, and anticipate

that it will facilitate the implementation of disperse polymers in next generation materials

6.5 References

(1) Bates, F. S.; Hillmyer, M. A.; Lodge, T. P.; Bates, C. M.; Delaney, K. T.; Fredrickson, G. H. *Science* **2012**, 336, 434.

(2) Bates, F. S.; Fredrickson, G. H. *Annu. Rev. Phys. Chem*. **1990**, 41, 525.

(3) Park, M.; Harrison, C.; Chaikin, P. M.; Register, R. A.; Adamson, D. H. *Science* **1997**, 276, 1401

(4) Bang, J.; Jeong, U.; Ryu, D. Y.; Russell, T. P.; Erren, T. C.; Hawker, C. J. *Adv. Mater*. **2009**, 21, 4769.

(5) Ruiz, R.; Kang, H.; Detcheverry, F. A.; Dobisz, E.; Kercher, D. S.; Albrecht, T. R.; de Pablo, J. J.; Nealey, P. F. *Science* **2008**, 321, 936.

(6) Fink, Y.; Urbas, A. M.; Bawendi, M. G.; Joannopoulos, J. D.; Thomas, E. L. *J. Lightwave Technol*. **1999**, 17, 1963.

(7) Kang, Y.; Walish, J. J.; Gorishnyy, T.; Thomas, E. L. *Nat. Mater*. **2007**, 6, 957.

(8) Urbas, A. M.; Maldovan, M.; DeRege, P.; Thomas, E. L. *Adv. Mater*. **2002**, 14, 1850.

(9) Ahn, H.; Park, S.; Kim, S.-W.; Yoo, P. J.; Ryu, D. Y.; Russell, T. P. *ACS Nano* **2014**, 8, 11745.

(10) Zhao, D.; Feng, J.; Huo, Q.; Melosh, N.; Fredrickson, G. H.; Chmelka, F.; Stucky, G. D. *Science* **1998**, 279, 548.

(11) Rosler, A.; Guido, W. M.; Klok, H.-A. *Adv. Drug Deliv. Rev.* **2001**, 53, 95.

(12) Kataoka, K.; Harada, A.; Nagasaki, Y. *Adv. Drug Deliv. Rev*. **2001**, 47, 113.

(13) Gentekos, D. T.; Dupuis, L. N.; Fors, B. P. *J. Am. Chem. Soc.* **2016**, 138, 1848.

(14) Kottisch, V.; Gentekos, D. T.; Fors, B. P. *ACS Macro Lett*. **2016**, 5, 796.

(15) Nadgorny, M.; Gentekos, D. T.; Xiao, Z.; Singleton, S. P.; Fors, B. P.; Connal, L. A. *Macromol. Rapid Commun*. **2017**, 38, 1700352.

(16) Sides, S. W.; Fredrickson, G. H. *J. Chem. Phys.* **2004**, 121, 4974.

(17) Widin, J. M.; Schmitt, A. K.; Schmitt, A. L.; Im, K.; Mahanthappa, M. K. *J. Am. Chem. Soc*. **2012**, 134, 3834.

(18) Matsen, M. W. *Phys. Rev. Lett*. **2007**, 99, 148304.

(19) Meuler, A. J.; Ellison, C. J.; Evans, C. M.; Hillmyer, M. A.; Bates, F. S. *Macromolecules* **2007**, 40, 7072.

(20) Lynd, N. A.; Hillmyer, M. A. *Macromolecules* **2007**, 40, 8050.

(21) Widin, J. M.; Kim, M.; Schmitt, A. K.; Han, E.; Gopalan, P.; Mahanthappa, M. K. *Macromolecules* **2013**, 46, 4472.

(22) Bendejacq, D.; Ponsinet, K.; Joanicot, M.; Loo, Y. L.; Register, R. A. *Macromolecules* **2002**, 35, 6645.

(23) Kennemur, J. G.; Yao, L.; Bates, F. S.; Hillmyer, M. A. *Macromolecules* **2014**, 47, 1411.

(24) Schmitt, A. K.; Mahanthappa, M. K. *Macromolecules* **2014**, 47, 4346.

(25) Lynd, N. A.; Hillmyer, M. A. *Macromolecules* **2005**, 38, 8803.

(26) van Genabeek, B.; de Waal, B. F. M.; Ligt, B.; Palmans, A. R. A.; Meijer, E. W. *ACS Macro Lett*. **2017**, 6, 674

(27) van Genabeek, B.; Lamers, B. A. G.; de Waal, B. F. M.; van Son, M. H. C.; Palmans, A. R. A.; Meijer, E. W. *J. Am. Chem Soc.* **2017**, 139, 14869.

(28) Grubbs, R. B.; Grubbs, R. H. *Macromolecules*, **2017**, 50, 6979.

(29) Rubber Industry Sees Value in MWD. *Chem. Eng. News*. **1965**, 43, 40.

(30) Lynd, N. A.; Meuler, A. J.; Hillmyer, M. A. *Prog. Polym. Sci*. **2008**, 33, 875.

(31) Gentekos, D. T.; Jia, J.; Tirado, E. S.; Barteau, K. P.; Smilgies, D.-M.; DiStasio Jr., R. A.; Fors, B. P. *J. Am. Chem. Soc*. **2018**, 140, 4639.

(32) Rudin, A. *J. Chem. Educ*. **1969**, 46, 595.

(33) Schulz, M. F.; Khandpur, A. K.; Bates, F. S.; Almadal, K.; Mortensen, K.; Hajduk, D. A.; Gruner, S. M. *Macromolecules*, **1996**, 29, 2857.

(34) Lynd, N. A., Hamilton, B. D., and Hillmyer, M. A. *J. Polym. Sci. B* **2007**, 45, 3386.

(35) Hustad, P. D.; Marchand, G. R.; Garcia-Meitin, E. I.; Roberts, P. L.; Weinhold, J. D. *Macromolecules* **2009**, 42, 3788.

(36) Matsen, M. W. *Eur. Phys. J. E* **2007**, 21, 199.

(37) Cooke, D. M.; Shi, A. *Macromolecules* **2006**, 39, 6661.

(38) Broseta, D.; Fredrickson, G. H.; Hefland, E.; Leibler, L. *Macromolecules* **1990**, 23, 132.

(39) Fredrickson, G. H.; Sides, S. W. *Macromolecules* **2003**, 36, 5415.

(40) Woo, S.; Shin, T. J.; Choe, Y.; Lee, H.; Huh, J.; Bang, J. *Soft Matter* **2017**, 13, 5527.

(41) The L to C border for the monodisperse samples was assigned at $f_{v, PS}$ ~ 0.31 supported by the fact that entry 6 was primarily L but contained a minor C component.

(42) Entry 9 and 10 show a rapid transition from L to C at significantly higher PS content than the series of samples with narrow PS, which supported the assignment of $f_{v, PS}$ = 0.38 as the C to L phase boundary in positively skewed PS MWDs at a Đ = 1.4.

(43) The L/C boundary in negatively skewed minority–PS samples is likely shifted towards higher PS fractions than both the narrow and positively skewed materials, consistent with our explanation of the effects observed in samples with high PS content (vide supra).

(44) Loo, Y.-L.; Register, R. A. *Macromolecules*, **2005**, 38, 4947.

(45) Listak, J.; Jakubowski, W.; Mueller, L.; Plichta, A.; Matyjaszewski, K.; Bockstaller, M. R. *Macromolecules* **2008**, 41, 5919.

(46) Beardsley, T. M.; Matsen, M. W. *Macromolecules* **2011**, 44, 6209.

6.6 Appendix

Experimental

General Reagent Information

All reactions were performed in an MBraun glovebox with a nitrogen atmosphere or in freshly flame-dried glassware under positive pressure of argon unless otherwise stated. The purification of all polymerization materials was concluded by degassing with three freeze-pump-thaw cycles and all reagents were stored in a glovebox. *s*-Butyllithium (*s*-BuLi) (1.4 M in cyclohexane, Sigma Aldrich), *n*-butyllithium (*n*-BuLi) (1.6M in hexanes, ACROS Organics), methanol (MeOH) (Fisher Scientific), trioctylaluminum (25 wt% in hexanes, Sigma Aldrich), hexanes (Fisher Scientific), and toluene (Fisher Scientific) were used as received. Styrene (Sigma Aldrich) was purified by vacuum transfer after stirring over calcium hydride until a grey/blue color persisted. 2-Vinylpyridine (2VP) (Sigma Aldrich) was first purified in the same manner as styrene. It was then purified an additional time directly prior to use by adding (Oct_3Al) until a yellow/orange color persisted with at least 1 h stirring to scavenge any remaining reactive species followed by vacuum transfer to a flame-dried Schlenk bomb. Diphenylethylene (DPE) (ACROS Organics) was purified *via* short-path vacuum distillation after stirring over *n*-BuLi for 1 h. Cyclohexane (Fisher Scientific) was dried by adding a premade mixture of 1:1 *s*-BuLi:DPE (0.5M in cyclohexane) and distilled under argon. Tetrahydrofuran (THF) (Fisher Scientific) was vigorously sparged with argon for 2 h and passed through two packed columns of neutral alumina under positive pressure. Directly prior to the

polymerization reactions, THF was dried further by adding *s*-BuLi at –78 °C until a light yellow/green color persisted and stirred for 1 h before being warmed to room temperature and transferred to a glovebox.

General Analytical Information

All polystyrene (PS) samples were analyzed using a Tosoh EcoSEC HLC 8320GPC system with two SuperHM-M columns in series and THF as eluent at a flow rate of 0.350 mL/min at 40 °C. Number-averaged molar masses (M_n), weight-averaged molar masses (M_w), and dispersity values ($Đ$) for PS were determined against TSKgel PS standards. All poly(styrene)-b-poly(2-vinylpyridine) (PS-*b*-P2VP) copolymers were analyzed using a Waters Ambient-Temperature GPC with three PSS GRAM columns in series running dimethylformamide (DMF) with 0.10% lithium bromide (LiBr) as the eluent, and all traces were obtained at 35 °C at a flow rate of 1.0 mL/min. Volume fractions ($f_{v,\,PS}$) were determined by nuclear magnetic resonance (NMR) spectroscopy and recorded on a Bruker Avance III HD 500 MHz instrument.

Preparation of Poly(styrene)-*block*-poly(2-vinylpyridine) with Skewed PS Blocks

To prepare living PS blocks with skewed MWDs, *s*-BuLi (790 μL, 0.091M in cyclohexane) was added to a vigorously stirring solution of styrene (2 mL) in cyclohexane (2.18 M) at predetermined rate profiles using a New Era NE–4000 Double Syringe Pump (see Table 6.2 and 6.3). Once the initiator addition was

finished and full monomer conversion was reached, DPE (14 μL, 1.1 equiv.) was added, and the polymerization mixture became deep red over the course of 1 h. Aliquots of the PSLi solution (14.5 μmol Li) were then added to a series of Schlenk bombs containing THF (40 mL), sealed, and attached to a Schlenk line under positive argon pressure. Once the bright red reaction mixture was cooled to –78 °C in a dry-ice/acetone bath, the appropriate amount of 2VP was added dropwise and resealed. Each polymerization was allowed to react for an additional 2 h before being quenched with degassed MeOH. Each polymer was then concentrated on a rotary evaporator, redisolved in THF (10 mL) and precipitated into rapidly stirring hexanes (200 – 400 mL) to afford a white powder. Any samples containing small amounts of terminated PS homopolymer were purified by Soxhlet extraction in cyclohexane and subsequently precipitated into hexanes an additional time. All polymers were then dried in a vacuum oven at 120 °C for 12 h.

Sample Preparation and Morphological Characterization

PS-b-P2VP samples for small-angle X-ray scattering (SAXS) were prepared by first, compression molding the dry powder into the center of a stainless steel washer (4.42 mm I.D., 9.53 mm O.D., 0.79 mm thickness) between two Mylar sheets at 180 °C and 2000 psi for 2 min using a Carver Press. The solid diblock copolymer samples were then sealed within the washer using Kapton tape and further thermally annealed at 180 °C in a vacuum oven for 15 h before cooling to room temperature under vacuum. These washers

were used directly for the small-angle X-ray scattering measurements which were performed at the G1 beamline at Cornell High Energy Synchrotron Source (CHESS). 2D-SAXS patterns were recorded with a Dectris Eiger 1M detector (1030 $\times$ 1065 pixels, 77 $\times$ 80 mm^2 active area) at a sample to detector distance of 2.027 m and an X-ray wavelength (λ) of 1.252 Å. The data was corrected for detector response, calibrated with silver behenate, and, using the Nika package in Igor Pro,[1] reduced by azimuthally integrating the 2D pattern to acquire a 1D plot of intensity versus the scattering wavevector (q).

For imaging *via* transmission electron microscopy (TEM), the glassy polymer samples were removed from the stainless steel washer, embedded in a microscopy resin (Embed 812, Electron Microscopy Sciences), and allowed to cure in an oven at 60 °C for 24 h. The sample blocks were trimmed with a razor blade and sectioned using a Leica Ultracut UCT Ultramicrotome equipped with a DiATOME Ultra Diamond Knife. Thin sections (< 70 nm) were floated onto 300-mesh hexagonal Cu grids and placed in an iodine chamber (a selective stain for P2VP) for 1 h prior to imaging with an FEI Tecnai 12 BioTwin TEM operating at 120 kV. All electron micrographs were processed in ImageJ to enhance and normalize contrast.

Table 6.2. Addition Rates of s-BuLi for the Preparation of Skewed PS Blocks for Entries 7 – 14

Step Number	Rate [μL/h]	Volume per Step [μL]
1	1337	790

Table 6.3. Addition Rates of s-BuLi for the Preparation of Skewed PS Blocks for Entries 15 – 23

Step Number	Rate [μL/h]	Volume per Step [μL]
1	5.5	0.5
2	7.6	0.5
3	10.5	0.7
4	14.6	0.8
5	20.6	1.4
6	28.6	2.1
7	40.0	3.0
8	56.1	3.9
9	78.5	5.6
10	110.1	7.9
11	154.0	10.9
12	215.6	15.3
13	301.8	21.4
14	422.7	30.0
15	591.6	42.0
16	828.2	58.8
17	1160	82.5
18	1623	115.2
19	2273	161.4
20	3181	226.0

Calculation of Skewness

Using the differential molecular weight distributions (MWDs), the following equation was used to calculate the central moments (μ_n) of the distribution function:

$$\mu_n = \int_{-\infty}^{\infty} (x - \mu)^n f(x) dx \qquad (6.1)$$

The skewness was then calculated according the Pearson's coefficient moment of skewness (α_3), which is the third standardized moment defined as:

$$\alpha_3 = \frac{\mu_3}{\mu_2^{3/2}} \tag{6.2}$$

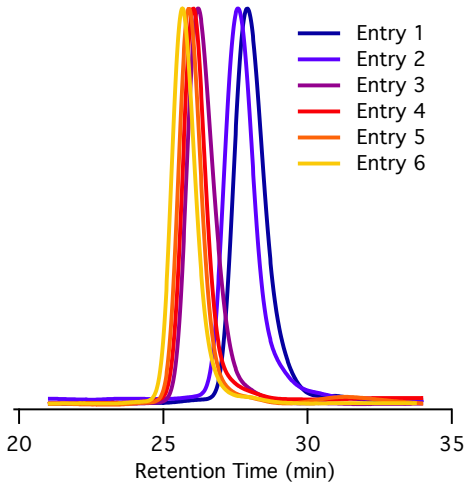

Figure 6.5. Size Exclusion Chromatographs of PS-b-P2VP with Narrow MWDs for Entries 1 – 6

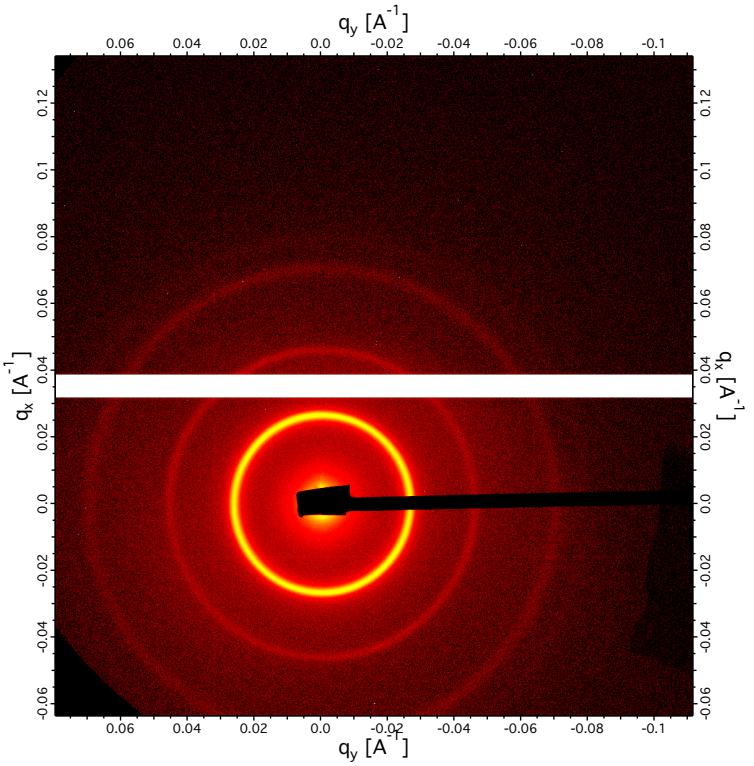

Figure 6.6. 2D SAXS Scattering Profile for Table 6.1 Entry 1

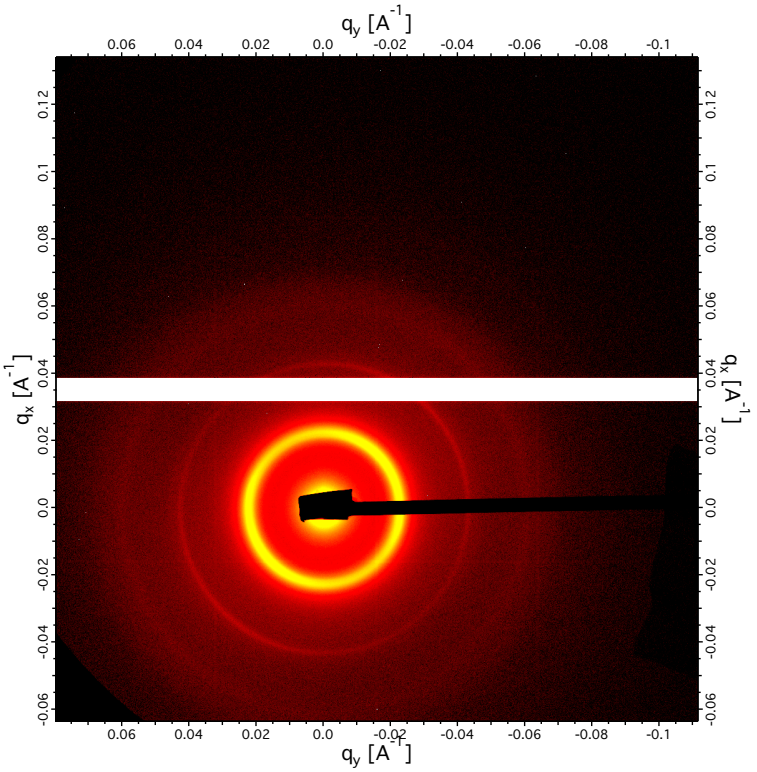

Figure 6.7. 2D SAXS Scattering Profile for Table 6.1 Entry 2

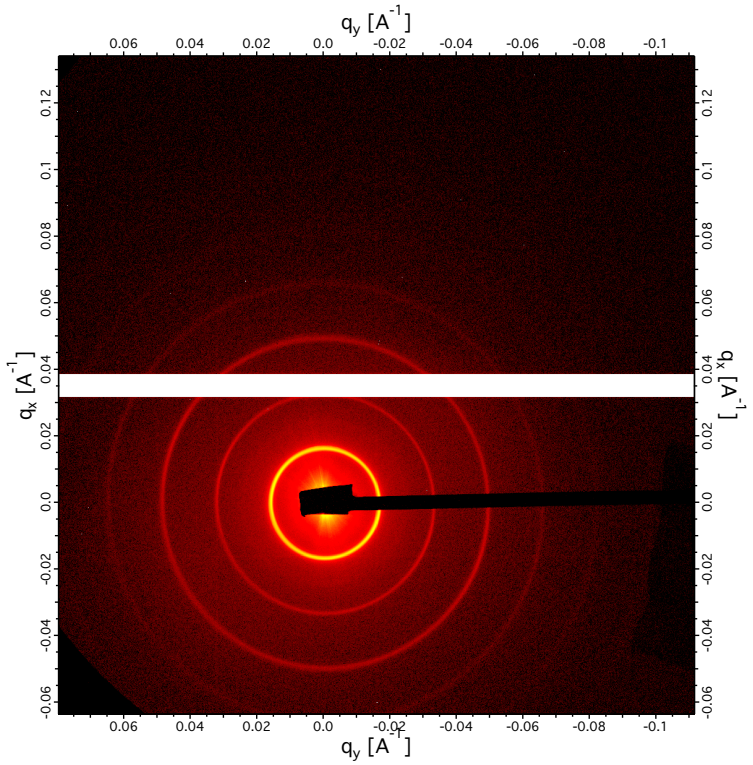

Figure 6.8. 2D SAXS Scattering Profile for Table 6.1 Entry 3

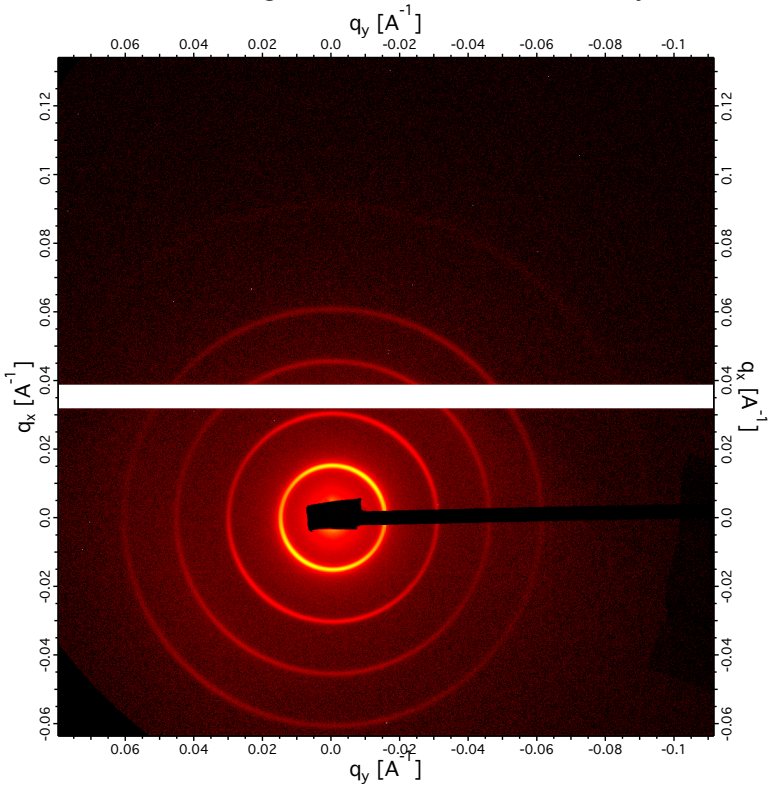

Figure 6.9. 2D SAXS Scattering Profile for Table 6.1 Entry 4

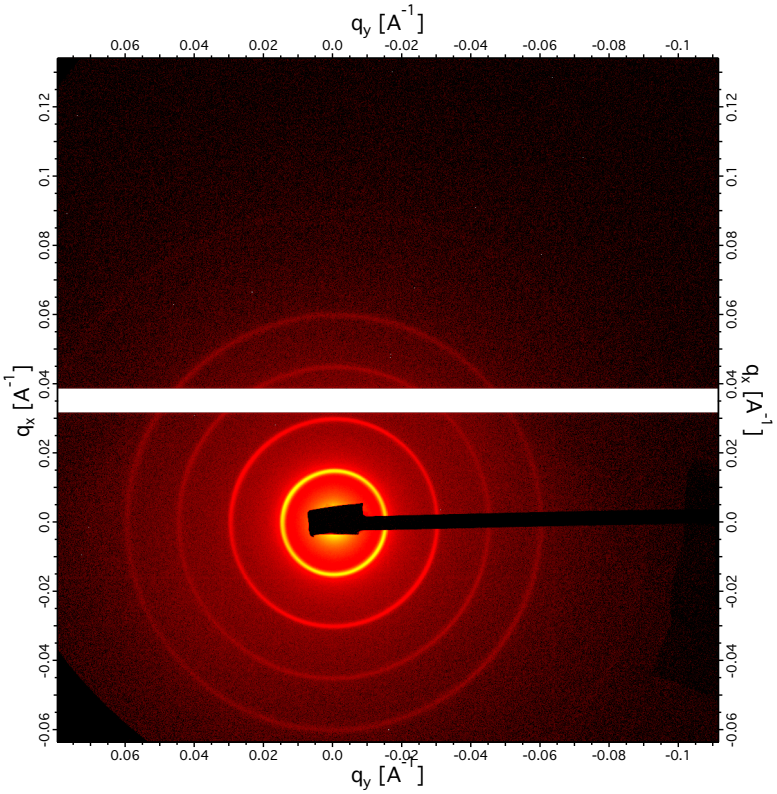

Figure 6.10. 2D SAXS Scattering Profile for Table 6.1 Entry 5

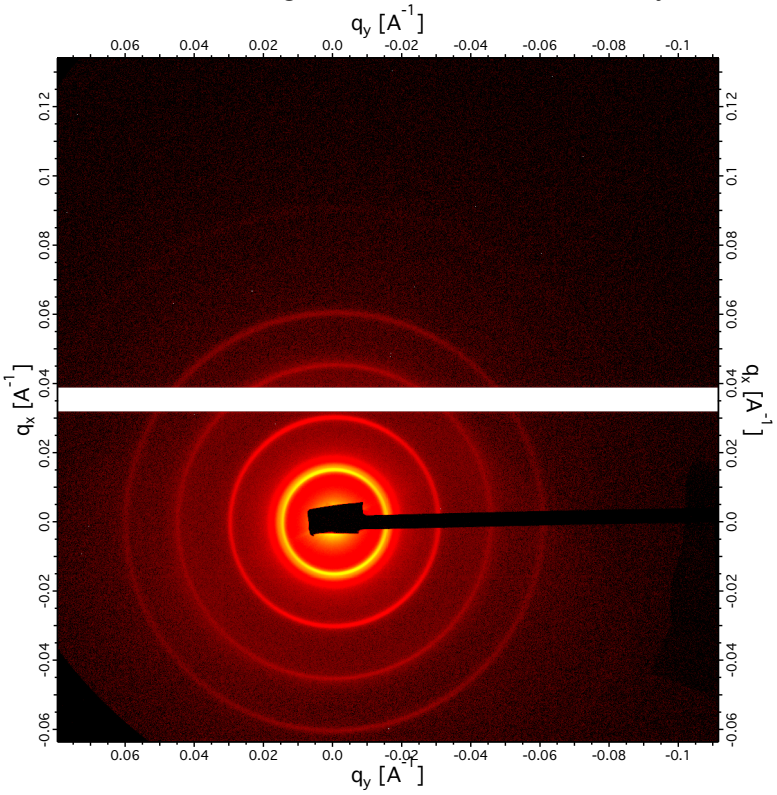

Figure 6.11. 2D SAXS Scattering Profile for Table 6.1 Entry 6

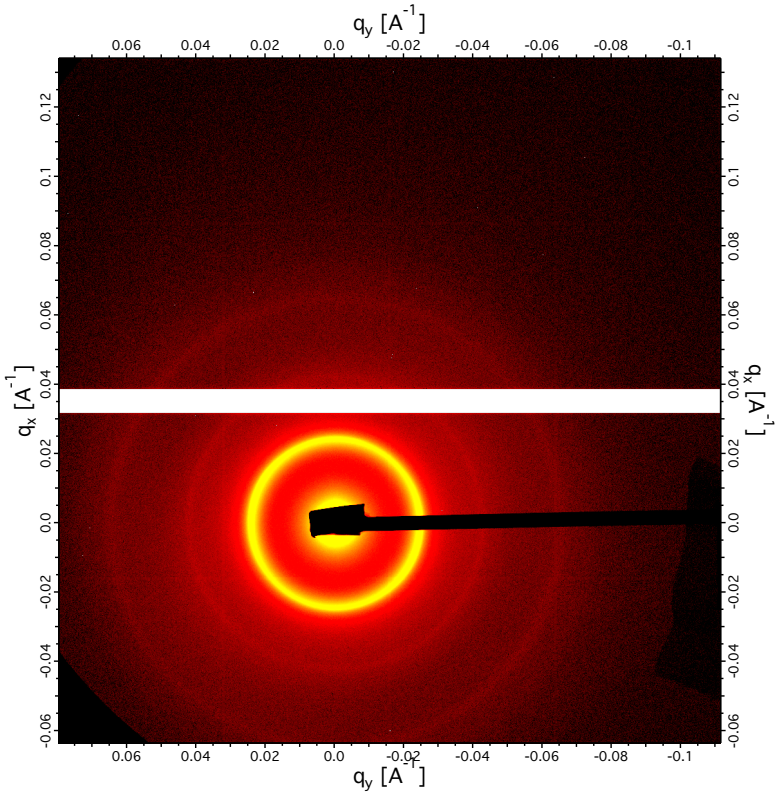

Figure 6.12. 2D SAXS Scattering Profile for Table 6.1 Entry 7

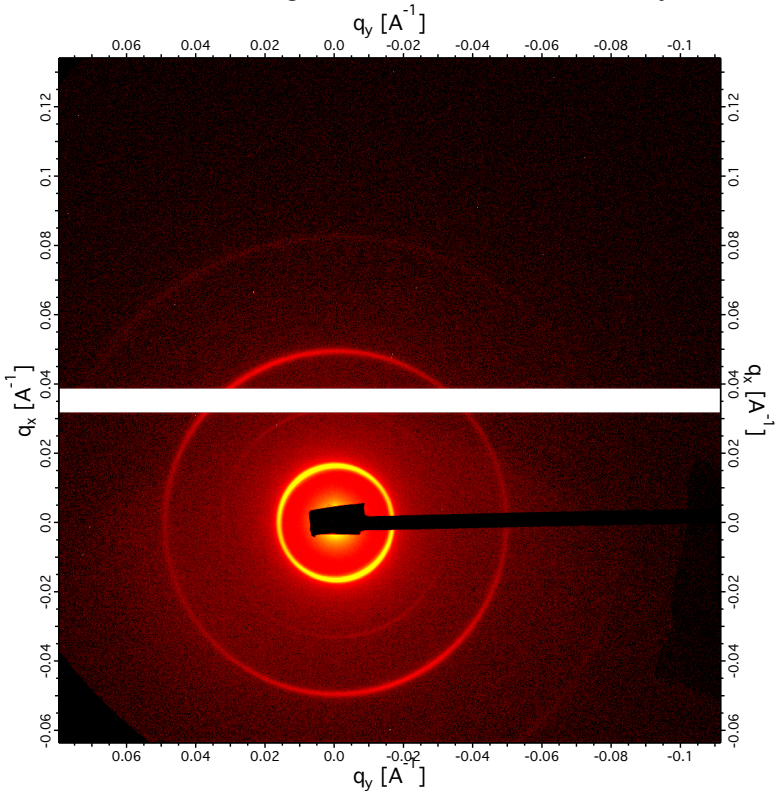

Figure 6.13. 2D SAXS Scattering Profile for Table 6.1 Entry 8

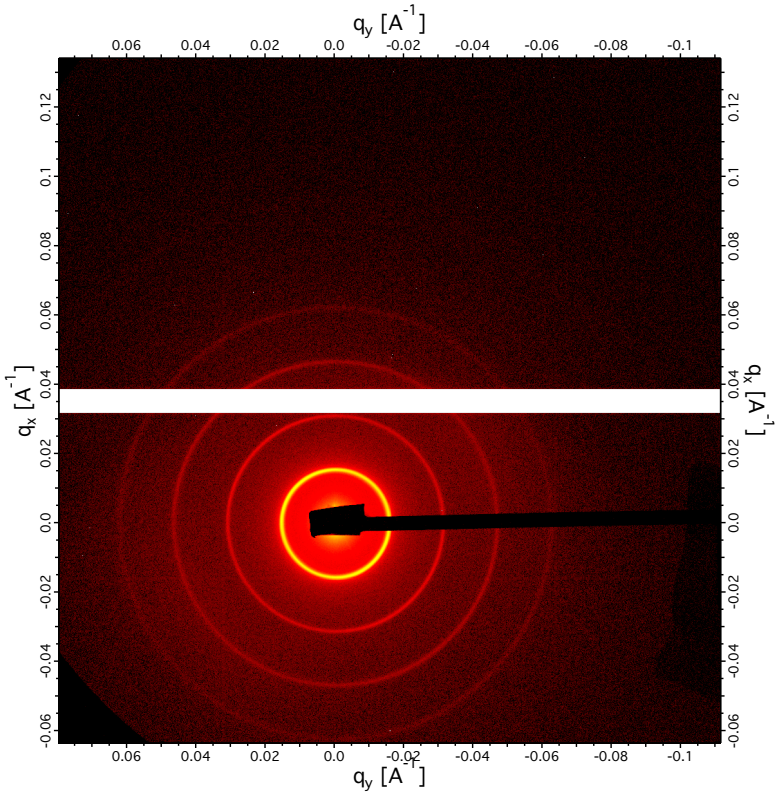

Figure 6.14. 2D SAXS Scattering Profile for Table 6.1 Entry 9

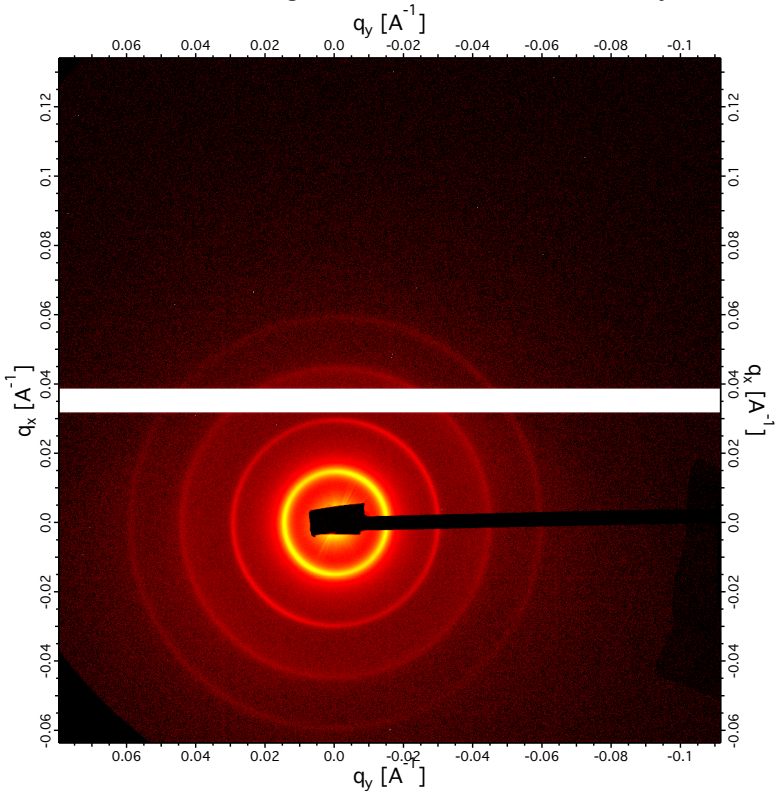

Figure 6.15. 2D SAXS Scattering Profile for Table 6.1 Entry 10

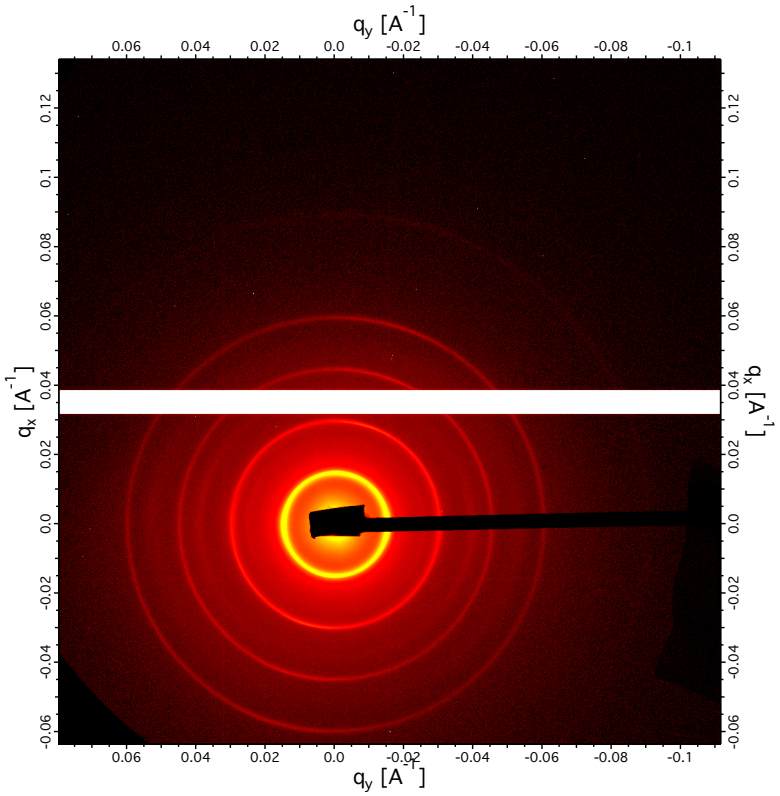

Figure 6.16. 2D SAXS Scattering Profile for Table 6.1 Entry 11

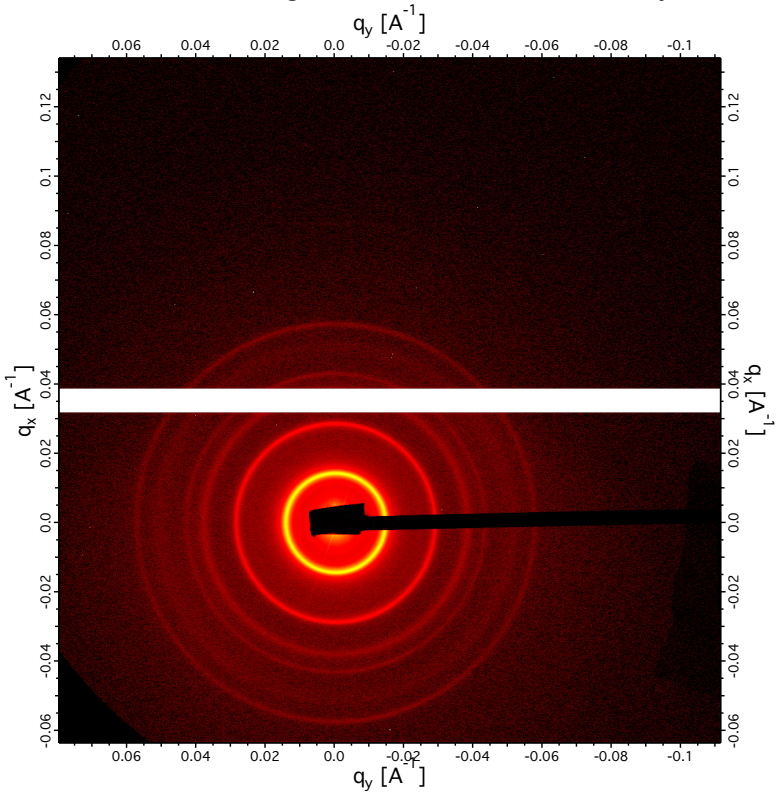

Figure 6.17. 2D SAXS Scattering Profile for Table 6.1 Entry 12

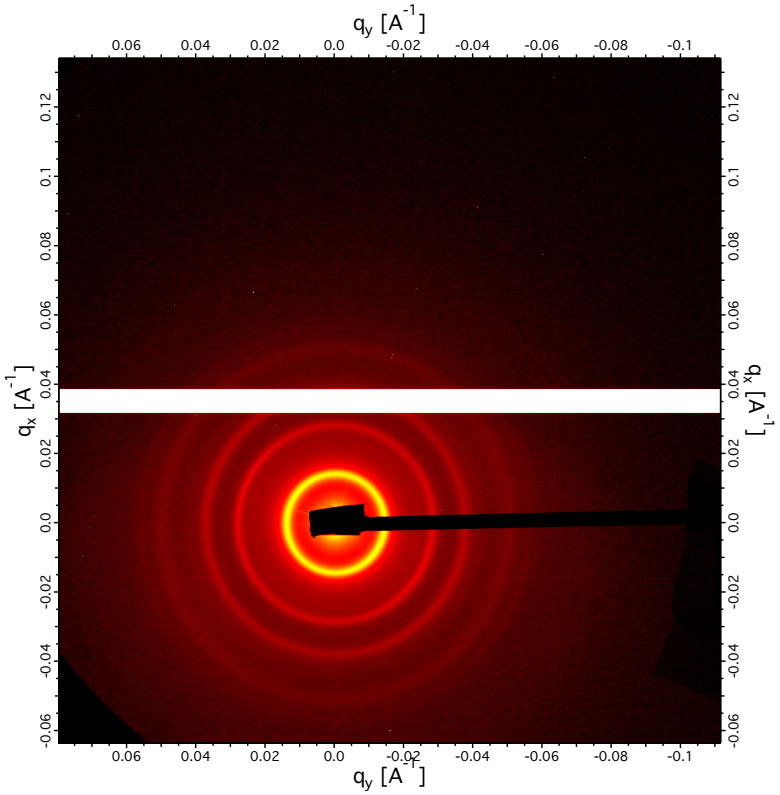

Figure 6.18. 2D SAXS Scattering Profile for Table 6.1 Entry 13

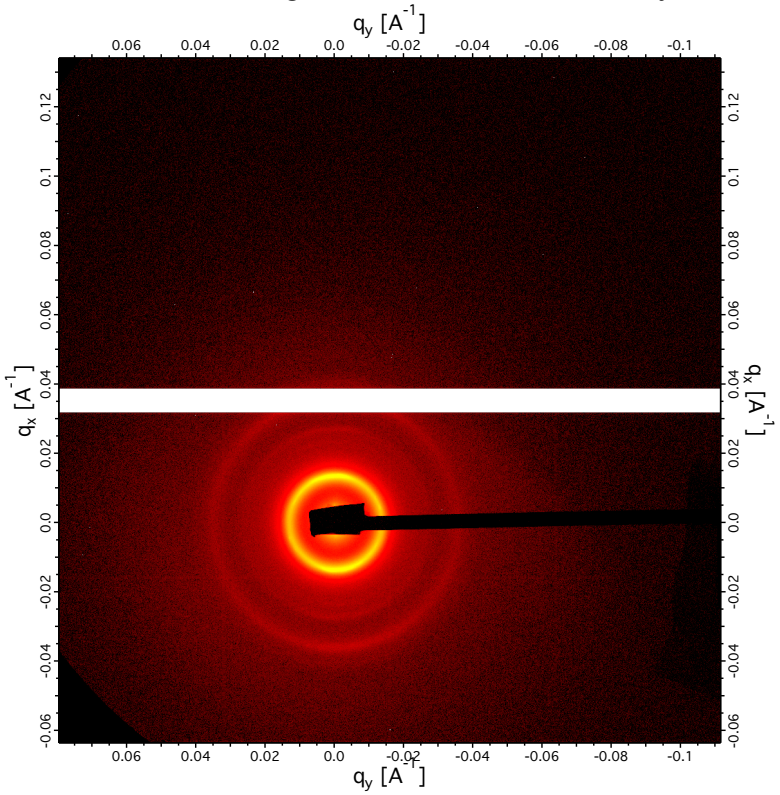

Figure 6.19. 2D SAXS Scattering Profile for Table 6.1 Entry 14

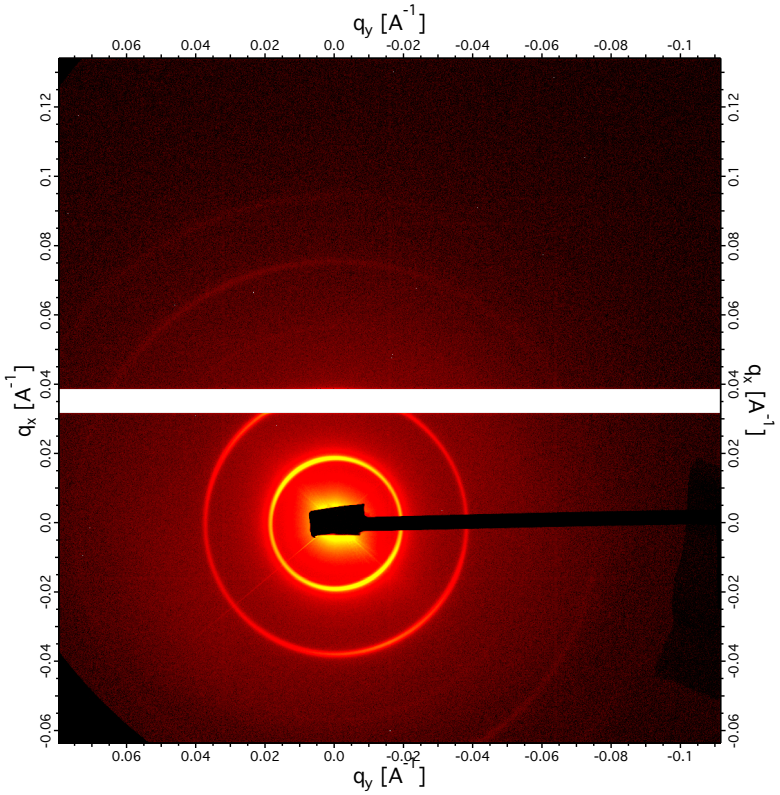

Figure 6.20. 2D SAXS Scattering Profile for Table 6.1 Entry 15

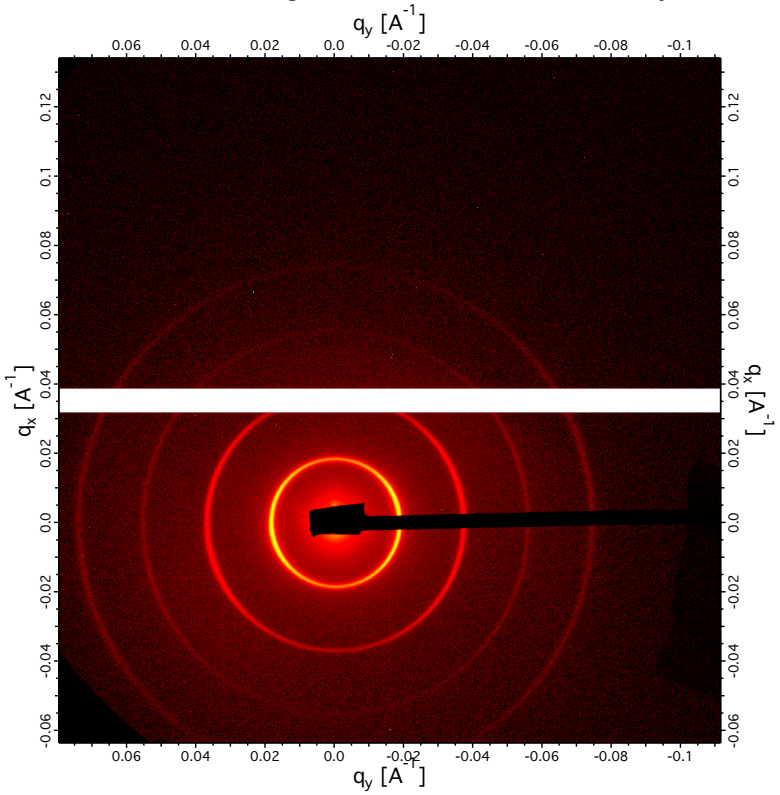

Figure 6.21. 2D SAXS Scattering Profile for Table 6.1 Entry 16

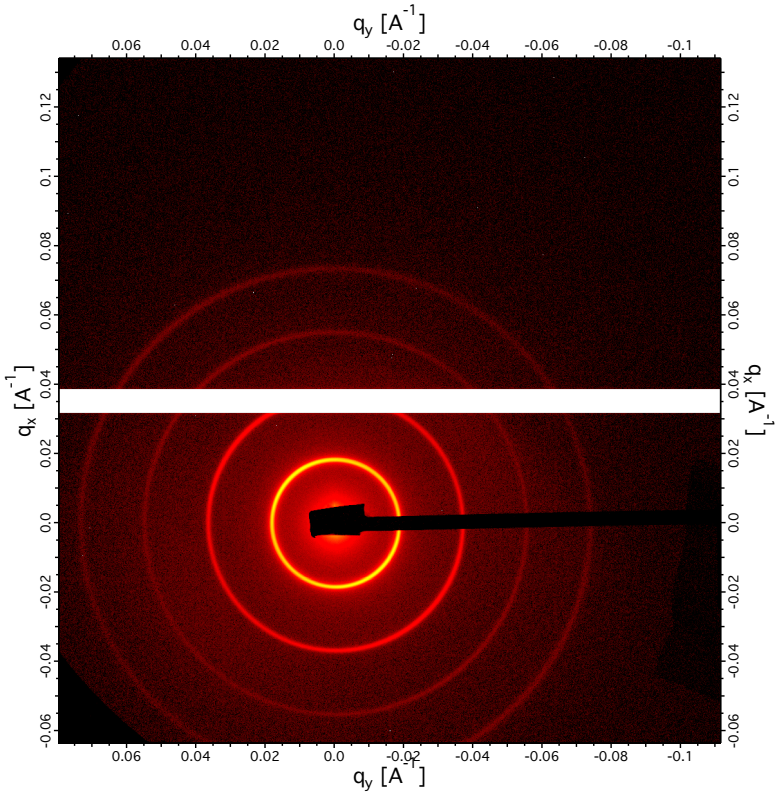

Figure 6.22. 2D SAXS Scattering Profile for Table 6.1 Entry 17

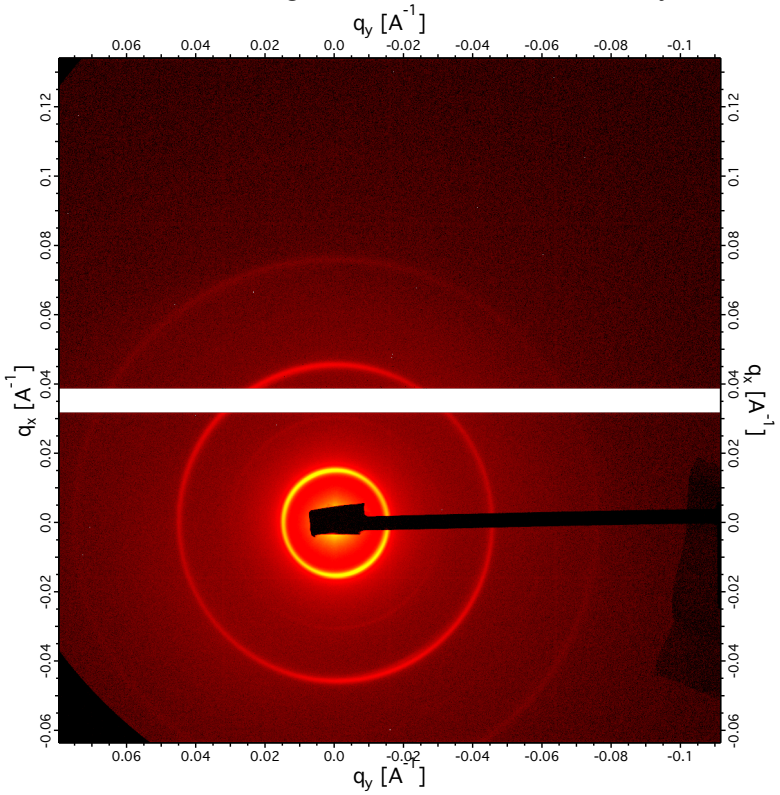

Figure 6.23. 2D SAXS Scattering Profile for Table 6.1 Entry 18

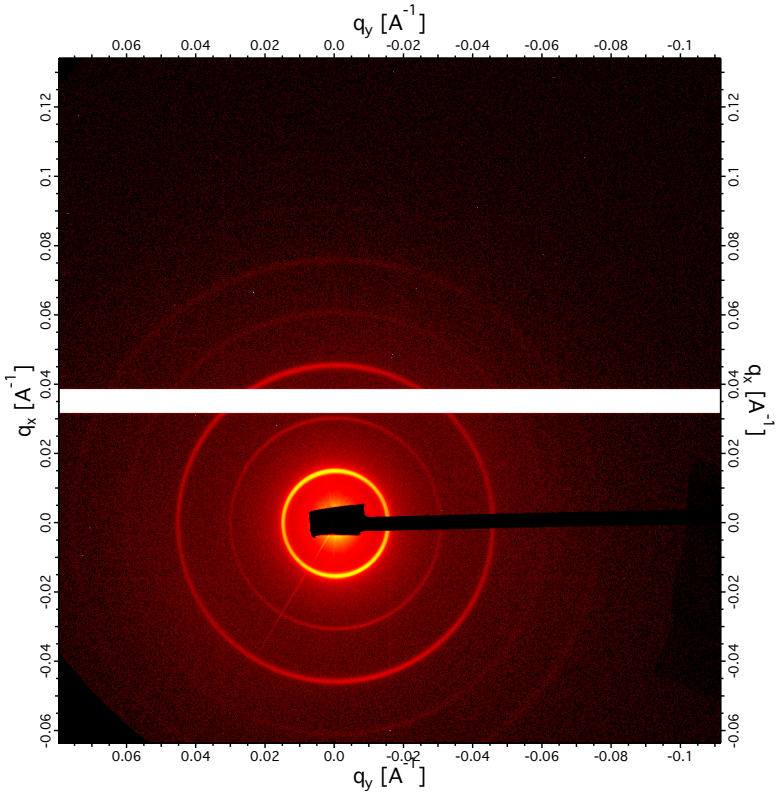

Figure 6.24. 2D SAXS Scattering Profile for Table 6.1 Entry 19

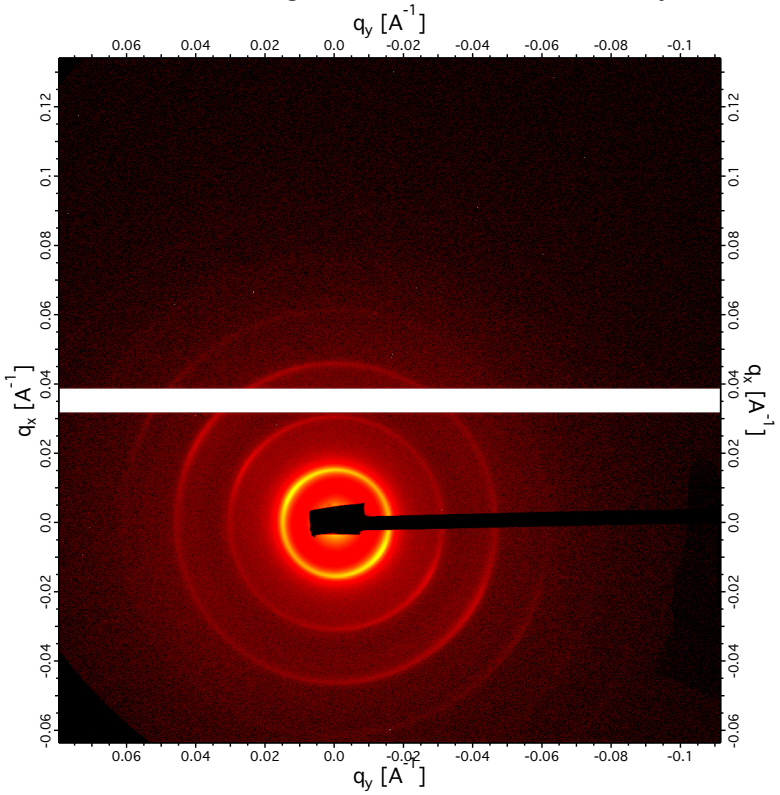

Figure 6.25. 2D SAXS Scattering Profile for Table 6.1 Entry 20

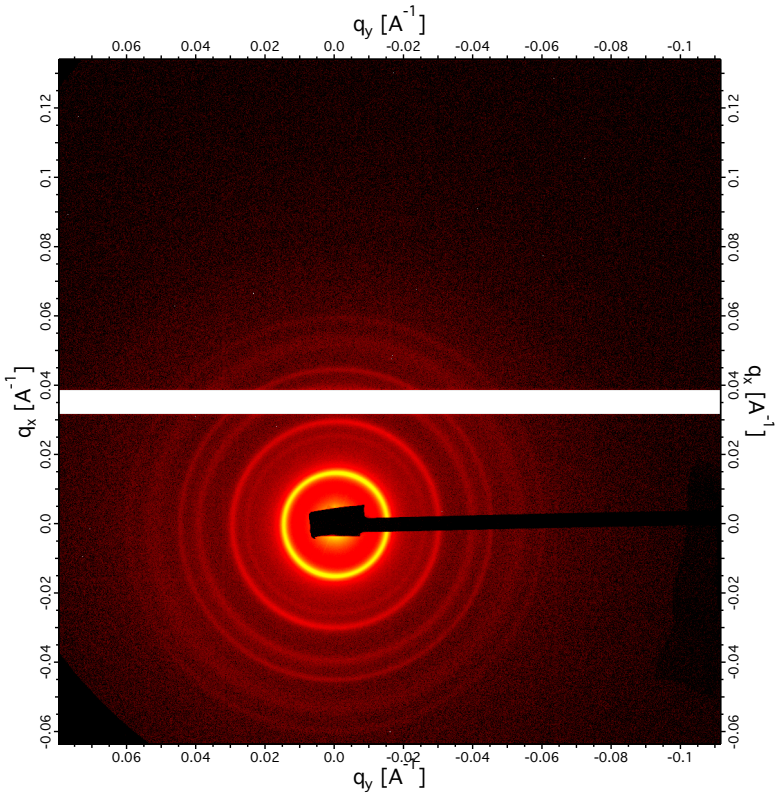

Figure 6.26. 2D SAXS Scattering Profile for Table 6.1 Entry 21

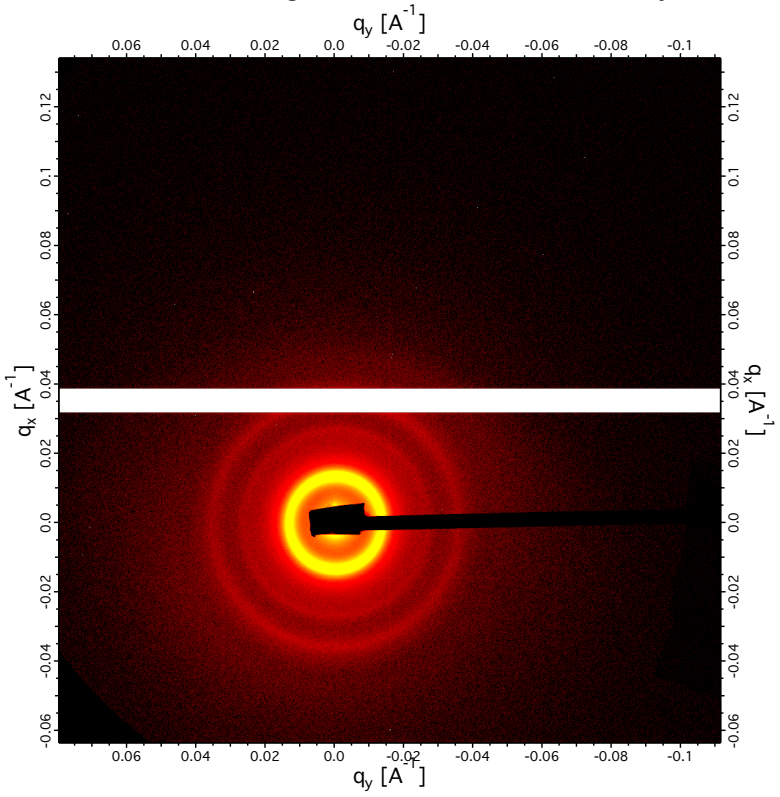

Figure 6.27. 2D SAXS Scattering Profile for Table 6.1 Entry 22

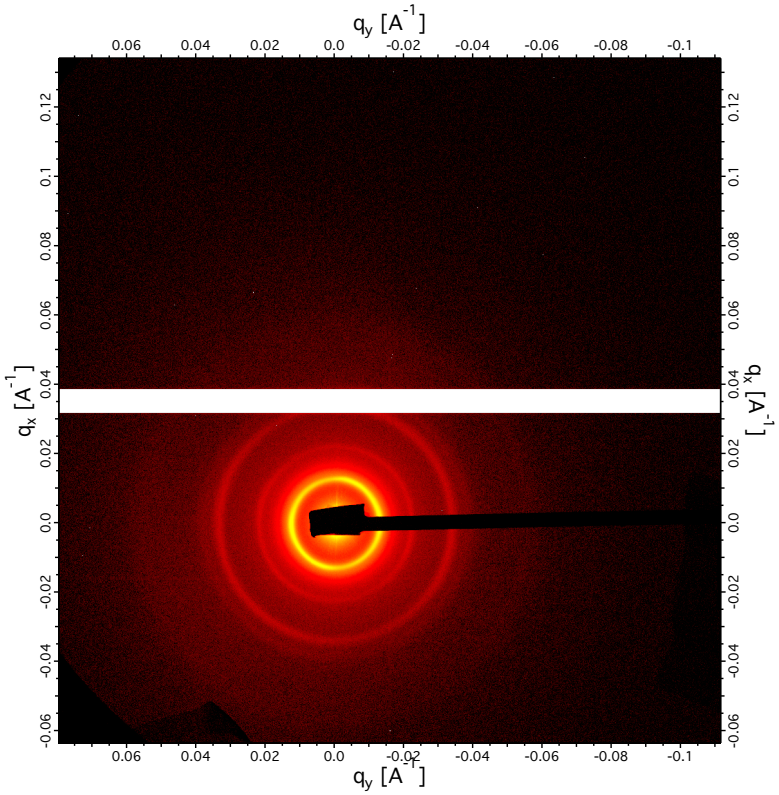

Figure 6.28. 2D SAXS Scattering Profile for Table 6.1 Entry 23

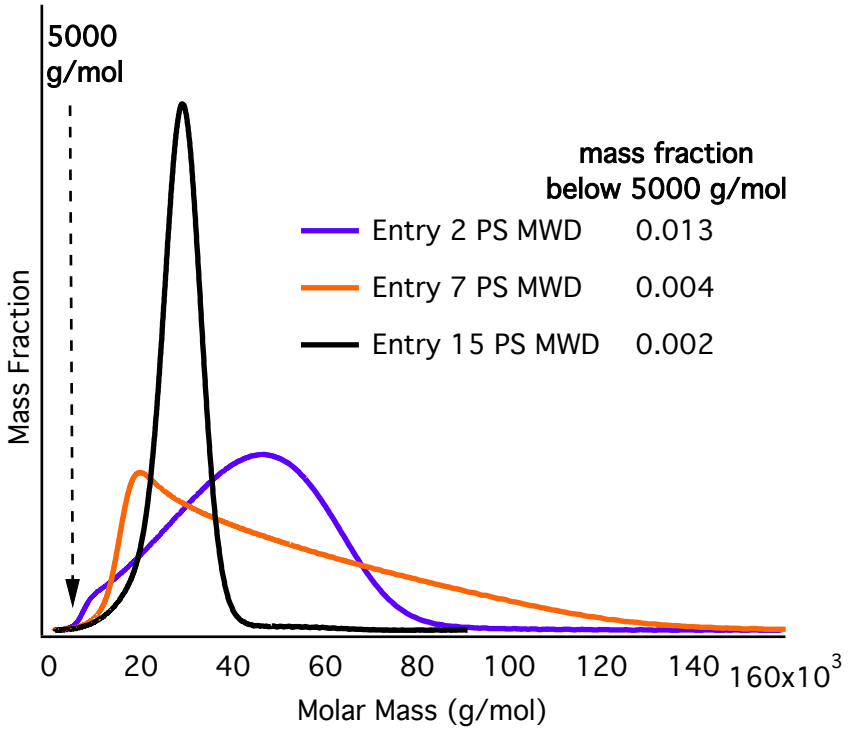

Figure 6.29. Fraction of PS Mass Below 5 kg/mol for Three Types of MWD Shapes.

All MWD shapes have the vast majority of their mass above 5000 g/mol. This fraction of polymers are above their order-disorder transition at the annealing temperatures used in this study. Such chains presumably desorb from the interface and increase the domain spacing. This number is exceptionally low and supports the claim that effects of chain desorption are minimized in this study and do not contribute significantly to the morphological phase behavior.

6.6 Appendix References

(1) Ilavsky, J. *J. Appl. Cryst.* **2012**, *45*, 324.

(2) Chintapalli, M.; Chen, C.; Thelen, J. L.; Teran, A. A.; Wang, X.; Garetz, B. A.; Balsara, N. P. *Macromolecules* **2014**, *47*, 5424.

CHAPTER 7

PREDICTIVE DESIGN OF MOLECULAR WEIGHT DISTRIBUTIONS IN ANIONIC POLYMERIZATION

7.1 Abstract

Molecular weight distributions (MWD) have a substantial impact on a diverse set of polymer physical and rheological properties, from processability and stiffness to many aspects of block copolymer microphase behavior. The precise MWD compositions of these polymers can be modularly controlled through temporal initiation in anionic polymerizations by metered addition of a discrete initiating species. With the technique described in this work, we identify initiator addition profiles through theoretical modeling which can be used to prepare any desired arbitrary MWD. This kinetic model reproduces experimental MWDs with high fidelity. Our modeling strategy incorporates a detailed kinetic description of polymer initiation and propagation, including the association and dissociation equilibria of the living polymer chain ends. We simplify the kinetic model by incorporating the aggregation phenomena into an effective propagation rate constant k_p, allowing it to vary with the polymer chain length (i). Importantly, this model also yields the ability to predict MWDs at any arbitrary value of monomer conversion during the polymerization. Lastly, we simulate MWDs for a variety of new, yet unmeasured, initiator addition profiles, demonstrating the predictability of this approach.

7.2 Introduction

The molecular weight distribution (MWD) of polymers has a profound influence over their physical properties, from processability and bulk macroscale properties to nearly all aspects of block copolymer phase behavior.[1–15] Research in this area has been largely restricted to studying only the effects of dispersity (*Đ*), a parameter which describes the relative span of chains lengths in a given sample. However, morphological and rheological properties of polymers have a significant dependence on the shape and symmetry of their component MWDs. The impact of the MWD shape on such a diverse set of polymer properties clearly demonstrates that modulation of the entire distribution of chain sizes is a promising avenue for fine-tuning the function of polymeric materials without the need to change their chemical structure.[3–8,13] However, until recently this approach has remained largely unexplored due to the lack of general methods that enable the synthesis of polymers with systematically deviating MWDs. In this regard, a general predictive model for targeting any prespecified MWD shape would provide a platform from which scientists and engineers can exploit such phenomena.

Several methods have gained synthetic control of polymer *Đ*.[11,16-24] Although most of these polymerization methods provide excellent control over the relative span of molar masses, they offer only limited control of the absolute shape of polymer MWDs. Our group has recently reported a method for deterministic control of polymer MWD shapes in anionic polymerizations, where the molar quantities of each chain size are dependent on the time at which each

chain is initiated.[6–8,25–28] Using this strategy, enabled through the temporal addition of initiator,[7] it has been demonstrated that precise control of the shape and composition of the distribution function profoundly affects polymer physical properties. In further studies of the anionic polymerization of styrene[6] this simple and highly efficient strategy allows the synthesis of functional poly(styrene-*block*-isoprene) copolymers with controlled MWDs, showing that MWD symmetry has a profound influence over the stiffness of these materials.[7] Moreover, in a subsequent study, the thin film domain spacing as well as the bulk morphologies of self-assembled block copolymers could be varied over a wide range simply through modulating the MWD shape of one block.[25] Although this approach is universal and broadly applicable to an array of different monomers and polymerization classes, the resultant MWD derived from any initiator addition rate profile cannot be known *a priori*—a desired MWD must be achieved through a trial and error process. Consequently, in order to fully utilize the shape of polymer MWDs as a handle to control polymer properties, a predictive model that facilitates access to any arbitrary distribution of chain lengths would offer significant advantages.

To be able to predict MWD composition from a specific initiator addition profile, we began by looking at kinetic models that have been previously developed for anionic polymerization. A simplified model of living and irreversible anionic polymerization kinetics,[29] as well as models developed to simulate MWD in semi-batch living anionic polymerizations were available.[19,30-32] However, we found these systems did not accurately predict the final MWDs

in our polymerizations with controlled initiator additions. We hypothesized that the discrepancies in the theoretical and experimental MWDs were because these models did not take into account chain end aggregation, which we believed to be a key kinetic parameter in our system. Theoretical and experimental studies for anionic polymerizations have shown that the rate of polymerization is highly dependent on the degree of polymerization.[33,34] The general consensus for the anionic polymerization of styrene in hydrocarbon solvents is that the growing species exist primarily as dormant associated dimers with a small amount of active dissociated monomeric polystyryllithium species.[35-37] It was proposed that this change in rate was a result of the chain ends existing in equilibrium as inactive associated dimers or active monomers and that this equilibrium would change based on the chain length of the polymer (Scheme 7.1).[38] In this study, we develop a model that takes the dynamic aggregation equilibrium into account for the anionic polymerization of styrene and enables the accurate prediction of MWD composition for a wide array of initiator addition profiles. Importantly, we believe this strategy will be applicable

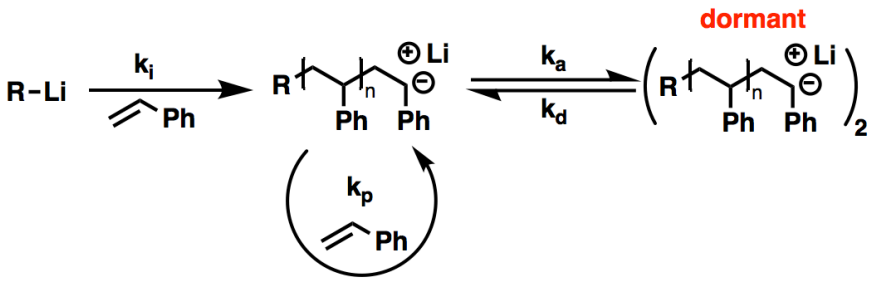

Scheme 7.1. Initiation, propagation, and aggregation equilibrium in anionic polymerization of styrene used in this theoretical model.

to a variety of anionic polymerization methods where chain end aggregation can influence propagation rates.

7.3 Theoretical Modeling

In this study, we develop a kinetic model of anionic polymerization of styrene which enables the prediction of any arbitrary MWD prepared by adding initiating species, *sec*-butyllithium (*s*BuLi), at predetermined rates and times throughout the polymerization reaction. In order to theoretically model MWDs of arbitrary shape based on the temporal initiation of polymer chains, the kinetics of initiation and propagation need to be understood. Below, we give a description of our approach to this kinetic behavior, describing first the simple kinetic model which neglects the complex phenomena of alkyllithium aggregation and subsequently a more detailed picture that includes aggregation which was required to accurately reproduce the experimental MWDs in this study. Processing of the raw SEC retention time data is described in detail in the Supporting Information (Figure 7.12 and 7.13, Equations 7.9–7.13)

In a polymerization mixture of styrene, M, in a hydrocarbon solvent, the typical structure of *s*BuLi is that of a tetrameric aggregate,[38,39,41] $\tilde{I}$, which dissociates into the active initiating species , I.

$$\tilde{I} \underset{k_a}{\overset{k_d}{\rightleftarrows}} 4I \tag{7.1}$$

Subsequently, active dissociated initiator is rapidly consumed by styrene present in the reaction mixture in the polymer chain initiation step,

$$I + M \overset{k_0}{\rightarrow} N_1 \tag{7.2}$$

where k_0 is the chain initiation rate constant. The dissociation of aggregated initiator is expected to be slower than that the first monomer addition and initiator association, thus the rate constant k_a, is neglected. Moreover, chain initiation is expected to be much shorter than chain propagation.[34]

$$N_i + M \overset{k_p}{\rightarrow} N_{i+1} \tag{7.3}$$

Equations (2) and (3) constitute a simplified understanding of anionic polymerization which is not sufficient to accurately model our data. This simplified description was studied by Sanchez and coworkers where k_0 and k_p are taken constant, and provided a limited ability to determine the shape of MWDs when the entire quantity of initiator was added at once.[29] Our preliminary study, not detailed here, revealed that no single pair of these two parameters were able to fit at least a subset of our experimental data (several different initiator addition profiles). Therefore, alkyllithium aggregation of living polymer chain ends during chain growth (Scheme 7.1) has to be accounted for.

The straightforward modeling approach is to assume the rate constant of chain propagation, k_p, that enters Equation (7.3) uniform for all chain lengths (the innate reactivity of the anionic chain end is constant), while the chains can temporarily form inactive dimers with the rate parameter $\tilde{k}_a(i,j)$,

$$N_i + N_j \underset{\tilde{k}_d}{\overset{\tilde{k}_a(i,j)}{\rightleftarrows}} \widetilde{N}_{i,j} \tag{7.4}$$

where i and j are the degrees of polymerization of the two reacting polymer chains. The associated dimers are dormant and must dissociate before chain propagation can occur, in a process with the dissociation rate constant $\tilde{k}_d$.The dependence of $\tilde{k}_a$ on i and j is non-trivial and unknown, however, shorter chains presumably have a higher probability of creating dormant dimers due to their higher mobility and more accessible active anionic chain ends from the lack of steric bulk; similar to the decreased chain mobility leading to the Trommsdorff-Norrish effect.[42] The short chains can also form dimers with longer chains, and each combination of chain lengths has its own distinct equilibrium constant. Consequently, long chains are expected to dimerize at a much lower rate than shorter chains and thus remain active for longer periods of time than short polymers. Strictly speaking, the *observed* propagation rate constant appears to be dynamic, but this is likely due to the complex aggregation behavior being dependent on the entire statistical distribution of chain lengths, $\{N_{j\geq 1}(t)\}$, which also varies with time and renders the system dynamics challenging to solve. By

absorbing the process of association and dissociation of the polystyryllithium dimers into an average effective rate constant of chain propagation, a function of the chain length, *i*,

$$k_p = \kappa \cdot k_p(i) \tag{7.5}$$

we avoid solving a complex matrix of equations related to $\widetilde{N}_{i,j}$, mentioned above, setting $\tilde{k}_a(i,j) = 0$. In addition, we reserve a monomer-concentration-dependent parameter, κ, to account for a potential dependence on the concentration. Incorporation of such an average rate constant into the reactions in Equations (7.1)-(7.3) makes modeling feasible and is approximated by the standard differential rate equations:

(7.6)

$$\frac{d\tilde{I}}{dt} = -k_d\tilde{I}$$

$$\frac{dI}{dt} = 4k_d\tilde{I} - k_0IM$$

$$\frac{dM}{dt} = -k_0IM - \sum_{i=1}^{\infty} k_p(i)N_iM$$

$$\frac{dN_{i\geq 1}}{dt} = \delta_{1i}k_0IM + (1-\delta_{1i})k_p(i-1)N_{i-1}M - k_p(i)N_iM$$

where δ_{1i} is the Kronecker delta symbol, 0 when $i \neq 1$ and 1 when $i = 1$.

It is important to note that the system description that includes Equation (7.4), i.e. constant propagation rate and complex dimers aggregation behavior,

is not equivalent to an effective rate approach summarized in Equation (7.6). This question requires a search for functions $\tilde{k}_a$ and $\tilde{k}_d$ which themselves may depend on multiple parameters. Nonetheless, the following sections show that the effective rate approach is suitable for describing our system for a variety of experimental conditions.

7.4 Initiator Addition Rates

In order to test the accuracy of the above kinetic model in predicting MWD shapes, we explore a variety of initiator addition profiles shown below. The alkyllithium initiating species was added at various rates and times to the reaction mixture to start the polymerization process. The total amount of the initiator and monomer in each experiment was kept the same, I_0 and M_0, respectively, such that the final M_n values of the polymers remained constant. We carried out our studies by employing initiator addition profiles from earlier work,[6,7] and also designing two types of complementary profiles. Figure 7.1 contains initiator addition rates as a function of time. Data from the experiments corresponding to Figure 7.1B–F are used for demonstration of the predictive power of the model (see Results and Discussion).

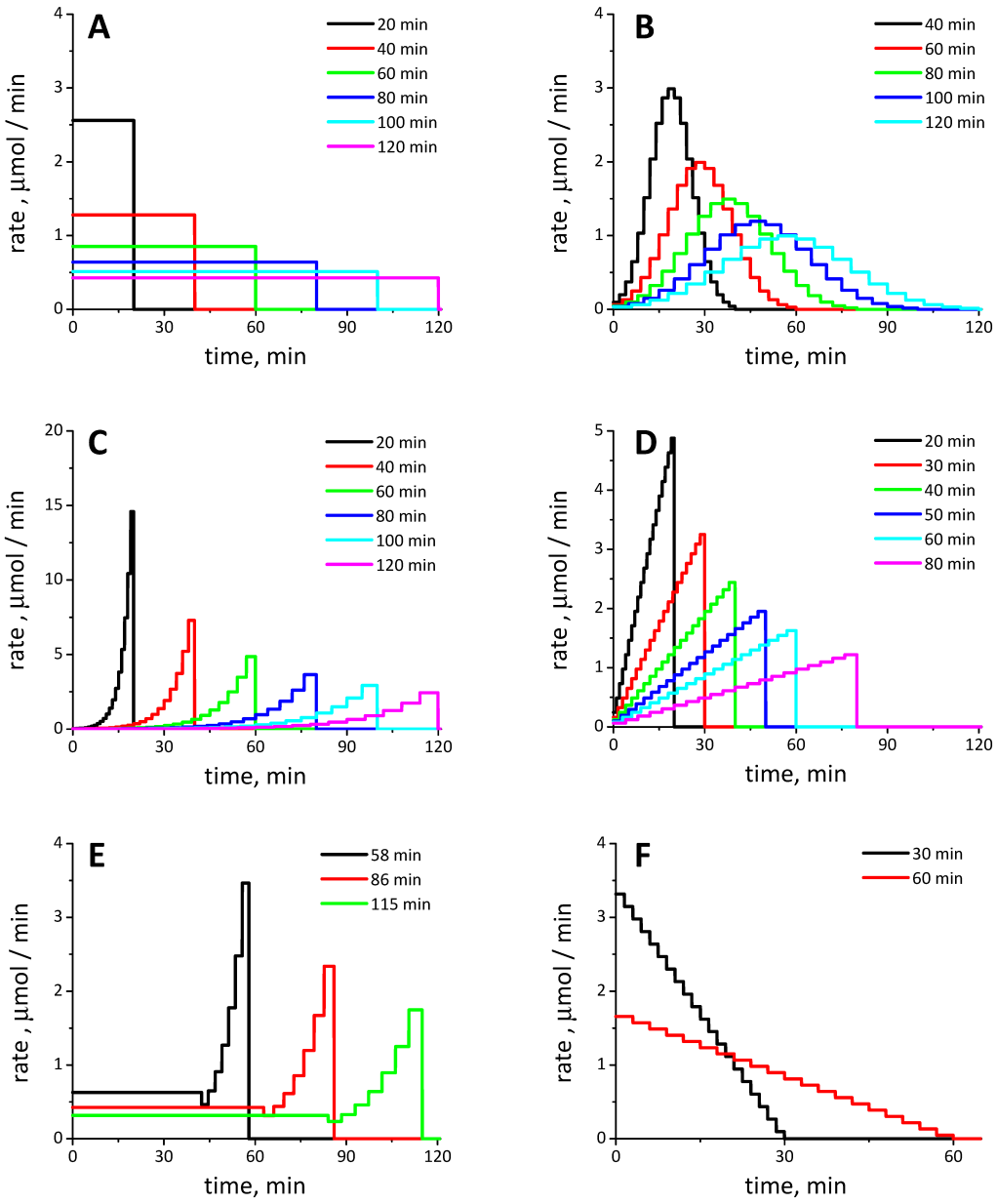

Figure 7.1. Initiator addition rates following four shapes: (A) constant rate, (B) bell-shaped rate, (C) exponentially increasing rate, and (D) linearly increasing rate, (E) partly constant and then exponentially increasing rate (See Appendix)

7.5 Results and Discussion

Data Fitting and Theoretical Model Parameter Investigation

In the preceding section, we outlined a modeling approach that can be applied to the grand challenge of predicting MWDs for any arbitrary initiator addition profile. Here we show how to utilize it and fit the experimental data. The overall process starts with the development of the theoretical model on a training data set, in this case, the constant rates of initiator addition (Figure 7.1A). Then, all of the rate parameters in Equation (7.6) were calculated and optimized. This model was then used to fit the MWDs of all other initiator addition profiles not within the training set, i.e. Figure 7.1B–F. Initially, as we mentioned previously, the process of the initiator association is neglected, $k_a = 0$, due to fast initiation of the dissociated species. The rate for the initiation process cannot be precisely determined from the considered experimental data due to large differences in the timescales of chain initiation and propagation. Setting the rate k_d to be an order of magnitude larger than the propagation rate for the chains after one monomer addition is sufficient to describe the data. In this work, we set $k_d = 7\ \mathrm{min}^{-1}$ and $k_0 = 8.06\ \mathrm{M}^{-1}\mathrm{min}^{-1}$, determined by optimization during the fitting procedure. The parameter κ is dependent on the initial monomer concentration, M_0, and set to unity except for the dilution experiments in Figure 7.9. To solve Equation (6), we utilize a standard Runge-Kutta-Fehlberg method (RKF45),[43,44] an algorithm for the numerical solution of differential equations. The resulting MWDs are compared to the preprocessed experimental data. The nonlinear least squares method is used to find the unknown parameters (rate constants).

The last rate parameter we determined was k_p. We hypothesized that larger polymer chains, having decreased mobility and increased steric bulk, would result in a lower affinity for aggregation to the dormant species and thus have a higher rate of propagation. Therefore, for each experiment with the constant initiator addition rate, the training set described above, we simulated the polymerization process with an unknown dependence of $k_p(i)$ on i, Equation (7.5), which was initially chosen as a first order polynomial, $k_p(i) = a \cdot i + b$, where a and b are unknown parameters. A simple linear dependence was found insufficient to fit parameters a and b simultaneously for the entire training set. For this reason, we chose to further explore the relationship between $k_p(i)$ and i. The function found to best fit these data is shown in Figure 7.2, which illustrates a nonlinear dependence of $k_p(i)$ on *i* (Equation 7.13). Importantly, this rate of propagation is in good qualitative agreement with previous studies,

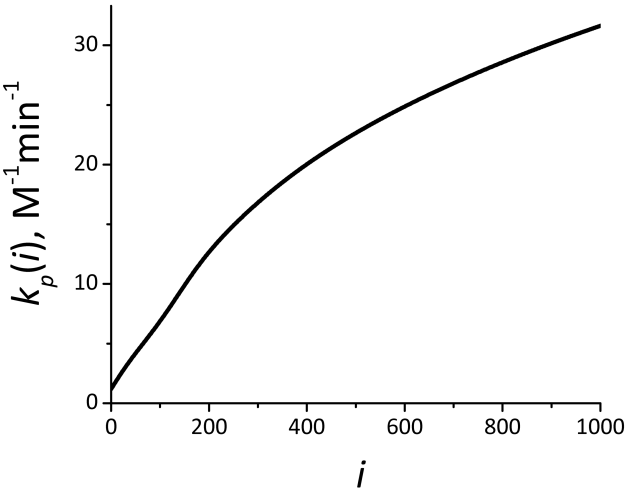

Figure 7.2. Numerically determined *effective* rate constant as a function of chain length, Equation (7.13), that fits the experimental MWDs for the constant rates of initiator addition, Figure 7.1A.

which found that the apparent propagation rate constant increases with increasing chain length.[34]

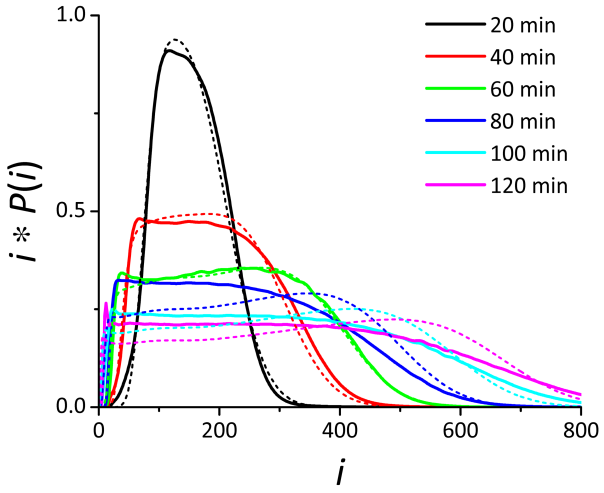

Figure 7.3. Experimental data (solid lines) and calculated curves (dashed lines) for the constant rate, Figure 7.1A, used as a training set to determine the average *effective* propagation rate, shown in Figure 7.2.

7.6 Model Validation

Without any modification, the effective propagation rate (Figure 7.2) was found to accurately describe the MWDs derived from the other rate profiles not within the training data set used to develop the theoretical model (Figure 7.1B, 1C, and 1D), with the bell-shaped, exponentially increasing, and linearly increasing initiator addition rates. The modeling curves along the experimental data are shown in Figure 7.4. This model provides a good fit of the experimental MWDs, closely following the shape of each type of initiation profile. Moreover, it is important to note that as the initiation time increases, so does the deviation between experimentally determined MWDs (Figure 7.4, solid lines) and those

that were determined through theoretical modeling (Figure 7.4, dotted lines). Interestingly, the fits are about equally accurate for each type of initiator addition profile, from constant and linearly increasing rates of addition to more complex profiles such as exponentially increasing and bell-shaped rates. This observation exemplifies the robustness and modularity of this theoretical approach.

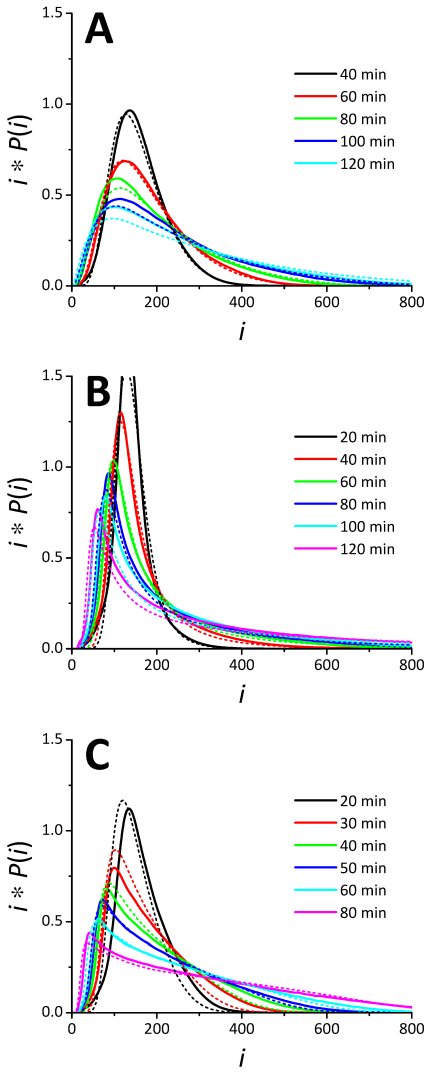

Figure 7.4. Experimental data (solid lines) and calculated curves (dashed lines) for the average *effective* rate, kept the same for all curves in this plot: (A) bell-shaped rate, (B) exponentially increasing rate, and (C) linearly increasing rate.

One case, where all the initiator was added at once at the beginning of the polymerization reaction, was suboptimal if simulated with the effective rate profile in Figure 7.2, (Figure 7.5). However, in this experiment, the initiator is added instantaneously, resulting in a much larger concentration of initiator at the beginning of the reaction and therefore giving different kinetics. This is in contrast to the experiments in which the initiator was added continuously into the system on the order of an hour or longer. As noted by Sanchez, the concentration of initiator has been shown to dramatically influence the polymerization kinetics as the MWDs are highly dependent on initial conditions.[29,39,40] The small amount of error shown in Figure 7.5 likely arises from these differences, and a more detailed analysis may require incorporation of the aggregation behavior of the alkyllithium initiator from Equation (7.1) into the model. However, the fit from the current model is quite reasonable and a more complex discussion of the dynamics in such systems is beyond the scope of the present work.

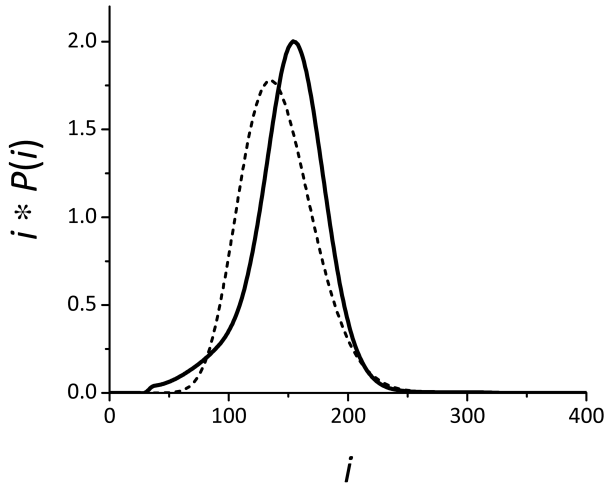

Figure 7.5. 0-min initiator addition time experimental data (solid line) and a calculated curve (dashed line) for the average *effective* rate shown in Figure 7.2.

Furthermore, we improved the fits for the data sets Figure 7.3 and (A),(B) in Figure 7.4 where the model-experiment discrepancy was the largest for longer initiator addition times. Due to the fact that aggregation is a dynamic process which is dependent on the concentration of each chain size in solution, we determined customized $k_p(i)$ relationships for each type of addition profile and used them to better model the resultant MWDs. The improved distribution fits and the corresponding experimental data are shown in Figure 7.6. The modified chain propagation rates are available as insets. Notably, the fits for longer addition times are significantly improved using the optimized $k_p(i)$ vs i profile. The source of the deviations of the optimized rates from the effective rate in Figure 7.5 likely originates from the specific contribution of each chain length present in solution for different initiator addition profiles since different molar quantities of each chain length will result in distinct association equilibria. In this regard, it is interesting to point out that Figure 7.6 demonstrates that the customized effective $k_p(i)$ follow the same trend as the relationship found in the training data set. Also notable, increasing addition times, in general, induced a slight drop in $k_p(i)$, presumably due to a larger fraction of small polymer chains being present, which would shift the aggregation equilibrium marginally toward dormant species.

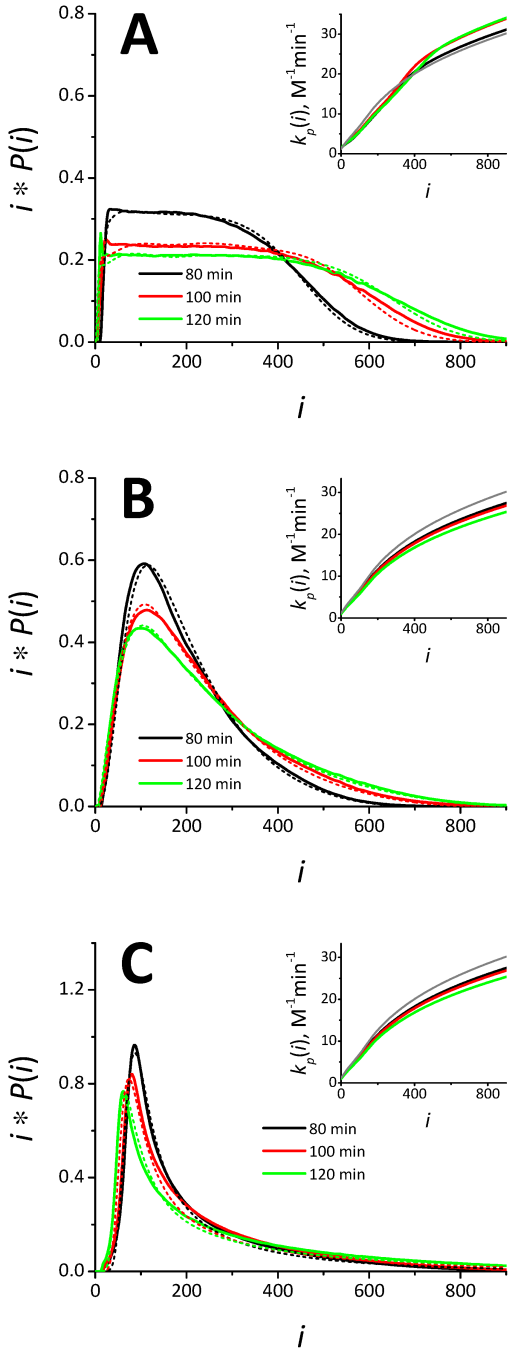

Figure 7.6. Experimental data (solid lines) and calculated curves (dashed lines) for the improved chain propagation rates, different for each curve in this Figure, see text for detail: (A) constant rate, (B) bell-shaped rate, and (C) exponentially increasing rate. Insets contain the chain propagation rates color-coded to the distributions generated from these rates. The solid grey lines in all insets are identical to Figure 7.2.

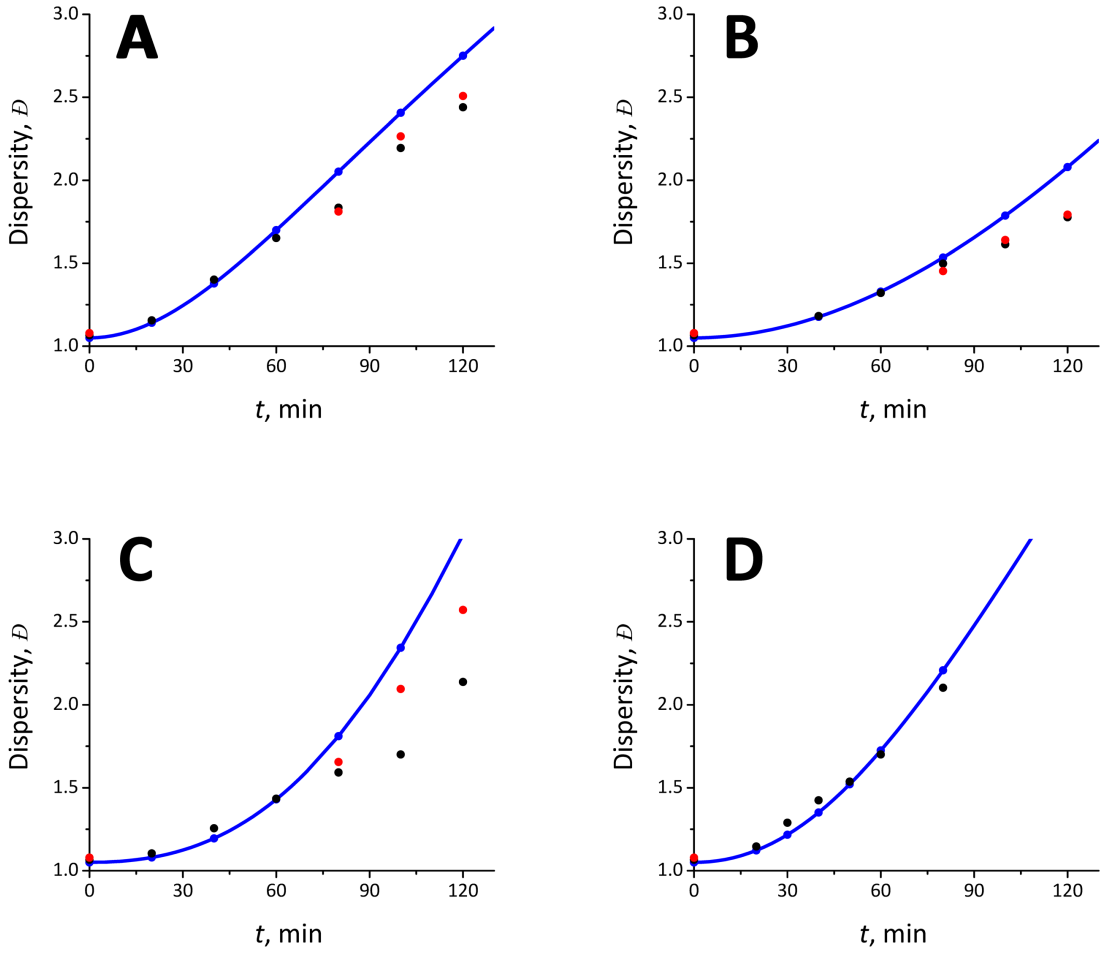

Figure 7.7. Dispersity (*Đ*), calculated for all the experiments discussed above: (A) constant rate, (B) bell-shaped rate, (C) exponentially increasing rate, and (D) linearly increasing rate. Solid blue lines (with selected cases magnified as blue circles) correspond to the effective rate constant, $k_p(i)$, given in Figure 7.2. Black circles represent dispersity calculated from the experimental data, whereas red circles are for the improved model fits as in Figure 7.6.

We then calculated dispersity (*Đ*), an important molecular weight distribution parameter, for various initiator addition times and compared these results to the values obtained directly from the size-exclusion chromatography data (Figure 7.7). The panels (A)-(D) of this Figure correspond to the initiator

addition rates of the type shown in Figure 7.1(A)-(D). Solid blue lines with selected dots magnified in blue are obtained from the model, in a similar way to Figure 7.4, whereas the black dots correspond to the experimental data, and red dots are the improved fits from Figure 7.5 and 7.6. Interestingly, at shorter addition times the general model predicts dispersity values with high precision. However, the comparison between experimental and theoretical dispersity values shows a decreased accuracy of the general *effective* rate constant determined from the training set without any further modification (Figure 7.2). Modelling addition times of 80 min or higher results in larger deviations from experimental values. However, this can be substantially improved by using customized *effective* rate profiles. It is important to briefly note that the experimentally determined dispersity values may be slightly overestimated compared to the true dispersity values, though this effect is minimal.[45]

We then proceeded to examine the predictive behavior of our strategy by modeling MWDs prepared by more complex initiator addition profiles (shown in Figure 7.1E and F) which have not been previously reported, and in which the experimental MWDs were obtained after simulation. Similarly to the bell-shaped, exponentially increasing and linearly increasing initiator addition rates, without any modification, the effective propagation rate was found to satisfactory describe the more complex constant-then-exponentially-increasing rates of initiator addition demonstrated in Figure 7.8A. The predicted (calculated) curves using the standard $k_p(i)$ vs *i* profile in Figure 7.2 retain the same shape as those achieved experimentally. The modeling of constant-then-exponentially-

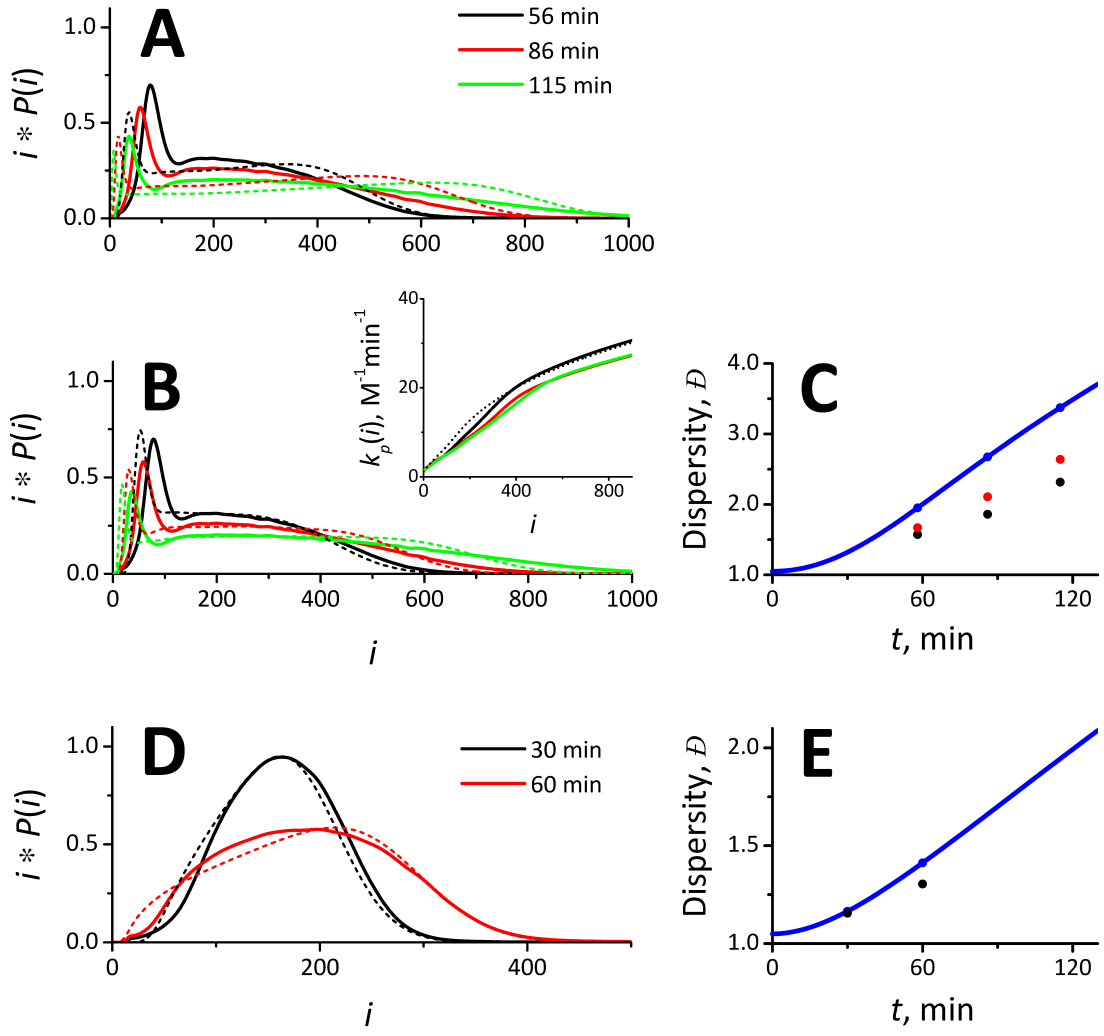

Figure 7.8. (A) Experimental data (solid lines) and model curves (dashed lines) calculated with the generic k_p from Figure 7.2 for the initiator addition rate in Figure 7.1E. (B) The same but for the improved rates illustrated in the inset. (C) Dispersity corresponding to the data in (A) and (B). Blue circles are for the model curves with generic k_p, red circles are for the model improved curves, and black circles were obtained from the experiment data. (D) Experimental data (solid lines) and model curves (dashed lines) calculated with the generic k_p from Figure 7.2 for the initiator addition rate in Figure 7.1F. (E) The same as (C) but for the data in (D).

increasing rates accurately depicts the distribution shape but is less accurate in terms of overall fit. However, analogously to Figure 7.6, customized rates (Figure 7.8B) show improved fits and illustrate that even complex initiator addition rates can be predictably modeled with this theoretical strategy. Moreover, the calculated and experiment dispersity values (Figure 7.8C) were also improved with customized propagation rate constants. For the linearly decreasing initiator addition rates from Figure 7.1F the experimental MWDs were in good agreement with the precalculated MWDs, thus any improvement of the chain propagation rate for these two data sets was unnecessary. These sets of experiments demonstrate that MWDs can be predicted from a variety of previously unexplored initiator addition profiles and that the experimentally determined MWDs of the same rate profile match the predicted distribution functions with high fidelity.

7.7 Additional Modeling Considerations

In addition to varying the initiator addition rates and holding the initial monomer concentration constant, M_0, we examined our experimental system with a set of four polymerization experiments with “60 min” constant rate, Figure 7.1A, using different amounts of solvent resulting in a series of monomer dilutions, α:

$$\alpha = M_0/M_0^*, \tag{7.7}$$

where M_0^* is the new initial concentration of the monomer in the system. For each of the dilution datasets we performed least-square fit of the parameter κ, from Equation (7.5), while maintaining the propagation rate the same as in Figure 7.4 ($k_p(i)$ from Figure 7.2). The fitting of κ is illustrated in Figure 7.9, where the experimentally measured data curves are shown as solid lines and model fit as dashed lines. The inset of this figure suggests a strong correlation ($R^2 = 0.98$) between the fitted values of κ. The linear fit reveals that:

$$\kappa(\alpha) = -0.27 \log_2 \alpha + 0.91. \tag{7.8}$$

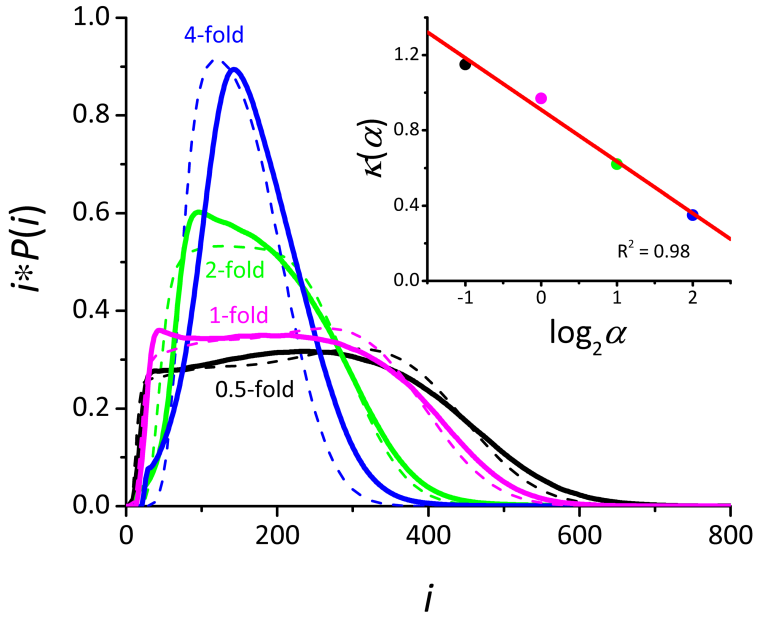

Figure 7.9. Experimental data (solid lines) and calculated curves, optimizing $\kappa(\alpha)$, (dashed lines) for the constant rate "60 min", Figure 7.1A (green line), used as a training set to determine dependence of the average *effective* propagation rate, shown in Figure 7.2, on the system dilution, α. The inset shows individual curves fits (solid dots) for 0.5, 1, 2 and 4-fold dilutions (left to right) color-coded to the distributions in this figure. The line in the inset is the linear fit of these four points.

We have also tested the sensitivity of our model predictions to the input parameters. As expected, the main controlling parameter, k_p, provides good linear control over the MWD shape. The small changes in MWD observed as k_0 and k_d are altered shows that these parameters are in the regime not limiting the system's dynamics. The calculations are shown in Figure 7.10, exemplified on the 60 min constant initiator addition rate, with $\kappa = 1$. The dotted line is experimental data, the black solid line is calculated with $1.0 * k_p$, $1.0 * k_0$ and $1.0 * k_d$. The blue lines show how the model's response is altered by varying the propagation rate from $0.9 * k_p - 1.1 * k_p$ (blue shaded area). The red and green shaded regions are for the parameters k_0 and k_d, respectively. These two parameters are already large enough not to limit the polymerization dynamics. Even significant decreases in these parameters (here taken as 20-fold) show little change in the overall fit.

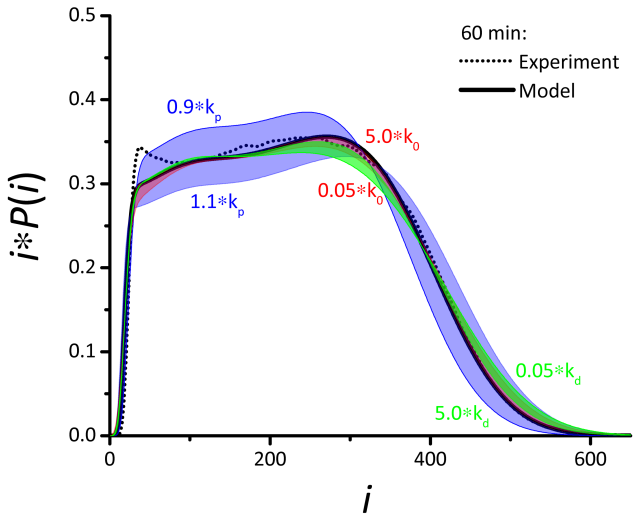

Figure 7.10. Sensitivity to the model parameters demonstrated by varying the propagation rate, initiation rate and dissociation rates from their optimized values, k_p, k_0 and k_d, respectively.

Theoretical modeling of the type presented in this work is beneficial for providing insight into the dynamics of the polymerization processes. To exemplify this we calculate the MWDs at the times when the monomer conversion is incomplete, see Figure 7.11, where we model the polymerization process with exponentially increasing rate of initiator addition within 80 min. The five traces shown in Figure 7.11A demonstrate the polymerization dynamics with the distributions shifting to the higher molecular weights as the chains grow. Figure 7.11B and 7.11C

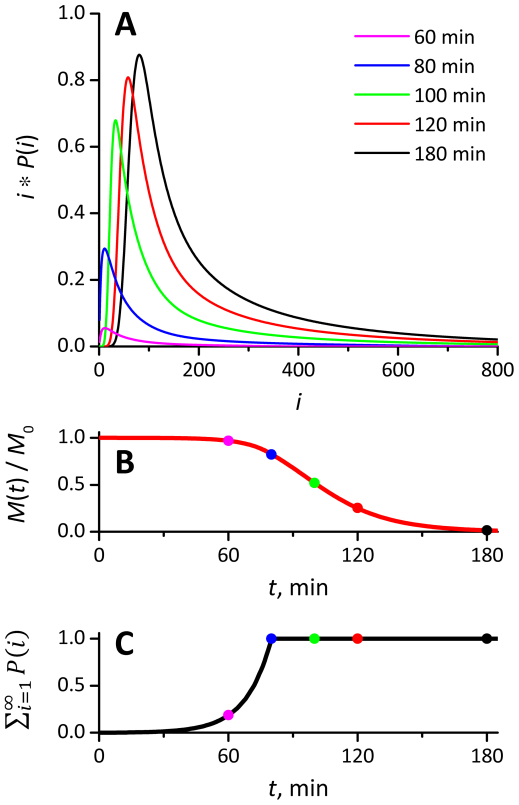

Figure 7.11. Detailed picture of the modeled polymerization process with exponentially increasing rate of initiator addition within 80 min. The chain propagation rate used for this Figure is that from Figure 7.2. (A) Snapshots of the distribution shown at different midway times indicated on the plot. (B) Fraction of the total amount of monomer left in the system as a function of time. (C) Fraction of the total number of polymer chains in the system as a function of time. The circles in panels (B) and (C) are color-coded to and indicate the times at which distributions in panel (A) were generated.

show how much monomer remains in the system and the number of polymer chains that have been initiated, respectively. The solid dots on panels (B) and (C) of Figure 7.11 are color-coded to the times of snapshots in panel (A). This type of analysis at different time points provides insight into the evolution of MWDs over time as more initiator is added to the polymerization reaction.

Another benefit of this model is the ability to simulate the MWDs for various new, yet unmeasured, initiator addition profiles. Figure 7.14 contains examples of the initiator addition rates, shown in the insets, which result in monomodal distributions. Figure 7.15, similarly to Figure 7.14, contains examples of the bimodal MWDs and their corresponding initiator addition profiles.

7.8 Conclusions

Control of polymer MWD shape through temporal control of polymer chain initiation is rapidly becoming a robust handle for tuning material nanostructure and physical properties. This work has been driven by a desire to predict an arbitrary MWD and formulate an initiator addition profile that would produce it. In order to fully employ the shape of polymer MWDs as a versatile strategy to control polymer function, a predictive model is essential. We have outlined two modeling approaches that can be applied to this endeavor, and show how to utilize the second approach, with an effective chain propagation rate parameter, as well as how to fit the experimental data. We clearly demonstrate that this model reproduces experimental MWDs with high fidelity and provides novel physical insight into the dynamics of the polymerization

process, such as simulating the MWDs for various new, yet unexplored, initiator addition profiles and calculating MWDs at times when monomer conversion is not complete. Interestingly, this model also describes the origin of increased rates of anionic polymerization for large polymer chains. We attribute this kinetic behavior to the complex relationship between propagation rate and the dynamics of heterogeneous mixtures of chain lengths, where longer chains have a lower affinity for association and thus propagate much faster. With the findings from this work, we anticipate that the use of polymer MWD shape to tailor material properties will proliferate, as initiation profiles for any arbitrary MWD can now be targeted through the use of this modeling approach.

7.9 References

(1) Lynd, N. A.; Meuler, A. J.; Hillmyer, M. A. Polydispersity and Block Copolymer Self-Assembly. *Prog. Polym. Sci.* **2008**, *33* (9), 875–893.

(2) Hustad, P. D.; Marchand, G. R.; Garcia-Meitin, E. I.; Roberts, P. L.; Weinhold, J. D. Photonic Polyethylene from Self-Assembled Mesophases of Polydisperse Olefin Block Copolymers. *Macromolecules* **2009**, *42* (11), 3788–3794.

(3) Grubbs, R. B.; Grubbs, R. H. 50th Anniversary Perspective: Living Polymerization—Emphasizing the Molecule in Macromolecules. *Macromolecules* **2017**, *50* (18), 6979–6997.

(4) Rubber Industry Sees Value in MWD. *Chem. Eng. News Arch.* **1965**, *43* (30), 40–41.

(5) Peplow, M. The Plastics Revolution: How Chemists Are Pushing Polymers to New Limits. *Nat. News* **2016**, *536* (7616), 266.

(6) Gentekos, D. T.; Dupuis, L. N.; Fors, B. P. Beyond Dispersity: Deterministic Control of Polymer Molecular Weight Distribution. *J. Am. Chem. Soc.* **2016**, *138* (6), 1848–1851.

(7) Kottisch, V.; Gentekos, D. T.; Fors, B. P. “Shaping” the Future of Molecular Weight Distributions in Anionic Polymerization. *ACS Macro Lett.* **2016**, *5* (7), 796–800.

(8) Nadgorny, M.; Gentekos, D. T.; Xiao, Z.; Singleton, S. P.; Fors, B. P.; Connal, L. A. Manipulation of Molecular Weight Distribution Shape as a

New Strategy to Control Processing Parameters. *Macromol. Rapid Commun.* **2017**, *38* (19), n/a-n/a.

(9) Sides, S. W.; Fredrickson, G. H. Continuous Polydispersity in a Self-Consistent Field Theory for Diblock Copolymers. *J. Chem. Phys.* **2004**, *121* (10), 4974–4986.

(10) Widin, J. M.; Schmitt, A. K.; Schmitt, A. L.; Im, K.; Mahanthappa, M. K. Unexpected Consequences of Block Polydispersity on the Self-Assembly of ABA Triblock Copolymers. *J. Am. Chem. Soc.* **2012**, *134* (8), 3834–3844.

(11) Lynd, N. A.; Hillmyer, M. A. Influence of Polydispersity on the Self-Assembly of Diblock Copolymers. *Macromolecules* **2005**, *38* (21), 8803–8810.

(12) Li, S.; Register, R. A.; Weinhold, J. D.; Landes, B. G. Melt and Solid-State Structures of Polydisperse Polyolefin Multiblock Copolymers. *Macromolecules* **2012**, *45* (14), 5773–5781.

(13) Cooke, D. M.; Shi, A.-C. Effects of Polydispersity on Phase Behavior of Diblock Copolymers. *Macromolecules* **2006**, *39* (19), 6661–6671.

(14) Oschmann, B.; Lawrence, J.; Schulze, M. W.; Ren, J. M.; Anastasaki, A.; Luo, Y.; Nothling, M. D.; Pester, C. W.; Delaney, K. T.; Connal, L. A.; et al. Effects of Tailored Dispersity on the Self-Assembly of Dimethylsiloxane–Methyl Methacrylate Block Co-Oligomers. *ACS Macro Lett.* **2017**, *6* (7), 668–673.

(15) Nichetti, D.; Manas-Zloczower, I. Influence of Molecular Parameters on Material Processability in Extrusion Processes. *Polym. Eng. Sci.* **1999**, *39* (5), 887–895.

(16) Listak, J.; Jakubowski, W.; Mueller, L.; Plichta, A.; Matyjaszewski, K.; Bockstaller, M. R. Effect of Symmetry of Molecular Weight Distribution in Block Copolymers on Formation of "Metastable" Morphologies. *Macromolecules* **2008**, *41* (15), 5919–5927.

(17) Meira, G. R.; Johnson, A. F. Molecular Weight Distribution Control in Continuous "Living" Polymerizations through Periodic Operation of the Monomer Feed. *Polym. Eng. Sci.* **1981**, *21* (7), 415–423.

(18) Alassia, L. M.; Couso, D. A.; Meira, G. R. Molecular Weight Distribution Control in a Semibatch Living-Anionic Polymerization. II. Experimental Study. *J. Appl. Polym. Sci.* **1988**, *36* (3), 481–494.

(19) Couso, D. A.; Alassia, L. M.; Meira, G. R. Molecular Weight Distribution Control in a Semibatch "Living" Anionic Polymerization. I. Theoretical Study. *J. Appl. Polym. Sci.* **1985**, *30* (8), 3249–3265.

(20) Laurence, R. L.; Vasudevan, G. Performance of a Polymerization Reactor in Periodic Operation. *Ind. Eng. Chem. Process Des. Dev.* **1968**, *7* (3), 427–433.

(21) Hungenberg, K.-D.; Knoll, K.; Wulkow, M. Absolute Propagation Rate Coefficients in Radical Polymerization from Gel Permeation Chromatography of Polymers Produced by Intermittent Initiation. *Macromol. Theory Simul.* **1997**, *6* (2), 393–426.

(22) Farkas, E.; Meszena, Z. G.; Johnson, A. F. Molecular Weight Distribution Design with Living Polymerization Reactions. *Ind. Eng. Chem. Res.* **2004**, *43* (23), 7356–7360.

(23) Gosden, R. G.; Meszena, Z. G.; Mohsin, M. A.; Auguste, S.; Johnson, A. F. Living Polymerisation Reactors. Part II. Theoretical and Experimental Tests on an Algorithm Which Predicts Mwds From CSTRs with Perturbed Feeds. *Polym. React. Eng.* **1997**, *5* (1–2), 45–81.

(24) Seno, K.-I.; Kanaoka, S.; Aoshima, S. Thermosensitive Diblock Copolymers with Designed Molecular Weight Distribution: Synthesis by Continuous Living Cationic Polymerization and Micellization Behavior. *J. Polym. Sci. Part Polym. Chem.* **2008**, *46* (6), 2212–2221.

(25) Gentekos, D. T.; Jia, J.; Tirado, E. S.; Barteau, K. P.; Smilgies, D.-M.; DiStasio, R. A.; Fors, B. P. Exploiting Molecular Weight Distribution Shape to Tune Domain Spacing in Block Copolymer Thin Films. *J. Am. Chem. Soc.* **2018**, *140* (13), 4639–4648.

(26) Li, H.; Collins, C. R.; Ribelli, T. G.; Matyjaszewski, K.; Gordon, G. J.; Kowalewski, T.; Yaron, D. J. Tuning the Molecular Weight Distribution from Atom Transfer Radical Polymerization Using Deep Reinforcement Learning. *Mol. Syst. Des. Eng.*, **2018**, 3, 496–508.

(27) Corrigan, N.; Manahan, R.; Lew, Z. T.; Yeow, J.; Xu, J.; Boyer, C. Copolymers with Controlled Molecular Weight Distributions and Compositional Gradients through Flow Polymerization. *Macromolecules*, **2018**, 51 (12), 4553–4563.

(28) Corrigan, N.; Almasri, A.; Taillades, W.; Xu, J.; Boyer, C. Controlling Molecular Weight Distributions through Photoinduced Flow Polymerization. *Macromolecules*, **2017**, 50 (21), 8438–8448.

(29) Sanchez, I. C. Irreversible Anionic Polymerization Kinetics Revisited. *Ind. Eng. Chem. Res.* **2010**, *49* (23), 11890–11895.

(30) Frontini, G. L.; Eliçabe, G. E.; Couso, D. A.; Meira, G. R. Optimal Periodic Control of a Continuous “Living” Anionic Polymerization. I. Theoretical Study. *J. Appl. Polym. Sci.* **1986**, *31* (4), 1019–1039.

(31) Frontini, G. L.; Eliçabe, G. E.; Meira, G. R. Optimal Periodic Control of a Continuous “Living” Anionic Polymerization II. New Theoretical Results. *J. Appl. Polym. Sci.* **1987**, *33* (6), 2165–2177.

(32) Costa, M. R. P. F. N.; Dias, R. C. S. An Improved General Kinetic Analysis of Non-Linear Irreversible Polymerisations. *Chem. Eng. Sci.* **2005**, *60* (2), 423–446.

(33) Quinebèche, S.; Navarro, C.; Gnanou, Y.; Fontanille, M. In Situ Mid-IR and UV–visible Spectroscopies Applied to the Determination of Kinetic Parameters in the Anionic Copolymerization of Styrene and Isoprene. *Polymer* **2009**, *50* (6), 1351–1357.

(34) Tsvetanov, K.; Mueller, A. H. E.; Schulz, G. V. Dependence of the Propagation Rate Constants on the Degree of Polymerization in the Initial Stage of the Anionic Polymerization of Methyl Methacrylate in Tetrahydrofuran. *Macromolecules* **1985**, *18* (5), 863–868.

(35) Morton, M.; Fetters, L. J.; Pett, R. A.; Meier, J. F. The Association Behavior of Polystyryllithium, Polyisoprenyllithium, and Polybutadienyllithium in Hydrocarbon Solvents. *Macromolecules* **1970**, 3, 327.

(36) Worsford, D. J.; Bywater, S. Degree of Association of Polystyryl-, Polyisoprenyl-, and Polybutadienyllithium in Hydrocarbon Solvents. *Macromolecules* **1972**, 5, 393.

(37) Wittig, V. G.; Meyer, F. J.; Lange, G. On the Behavior of Diphenyl Metals as Complexing Agents. *Ann.* **1951**, 571, 167.

(38) Morita, H.; Van Beylen, M. New Vistas on the Anionic Polymerization of Styrene in Non-Polar Solvents by Means of Density Functional Theory. *Polymers* **2016**, *8* (10), 371.

(39) Worsfold, D. J.; Bywater, S. Anionic Polymerization of Styrene. *Can. J. Chem.* **1960**, *38* (10), 1891–1900.

(40) Bywater, S.; Worsfold, D. J. Alkyllithium Anionic Polymerization Initiators in Hydrocarbon Solvents. *J. Organomet. Chem.* **1967**, *10* (1), 1–6.

(41) Lühmann, N.; Niu, A.; Allgaier, J.; Stellbrink, J.; Zorn, R.; Linnolahti, M.; Willbold, S.; Koenig, B. W.; Grillo, I.; Richter, D.; et al. The Initiation Mechanism of Butadiene Polymerization in Aliphatic Hydrocarbons: A Full Mechanistic Approach. *Macromolecules* **2016**, *49* (15), 5397–5406.

(42) Alger, Mark. Polymer Science Dictionary. New York: Elsevier Applied Science, 1989, 28.

(43) Fehlberg, E. Classical Fourth- and Lower Order Runge-Kutta Formulas with Stepsize Control and Their Application to Heat Transfer Problems. Computing 1970, *6* (1), 61–71.

(44) Shampine, L. F.; Watts, H. A.; Davenport, S. M. Solving Nonstiff Ordinary Differential Equations - The State of the Art. *SIAM Rev.* **1976**, *18* (Journal Article), 376–411.

(45) Lee, W.: Lee, H.; Cha, J.; Chang, T.; Hanley, K. J.; Lodge, T. P. Molecular Weight Distribution of Polystyrene Made by Anionic Polymerization **2000**, *33* (14), 376–411.

7.10 Appendix

Experimental Section and Data Processing

All reactions were performed in a Unilab MBraun Glovebox with a nitrogen atmosphere unless otherwise noted. To a freshly flame-dried 20 mL scintillation vial, equipped with a magnetic stir bar, was added styrene (0.8 mL) and cyclohexane (6.9 mL). A previously prepared stock solution of *s*-BuLi (320 μL, 0.16 M in cyclohexane) was then drawn into a plastic syringe and mounted onto a New Era NE-4000 Double Syringe Pump. Once the needle was submerged into the polymerization mixture, the addition profile was initiated causing the solution to slowly turn bright orange. Once the addition rate program was run to completion and full monomer conversion was reached, the reaction was quenched with a small amount of BHT, immediately turning the reaction from bright orange to colorless. The reaction mixture was then sampled for SEC analysis. It is important to note that for 80, 100, and 120 min exponentially ramped additions, an initiator stock solution of 0.053 M was prepared and 960 μL was added to the polymerization mixture (total amount of cyclohexane was also reduced to 6.3 mL).

Size Exclusion Chromatography (SEC)

Each polymer sample was monitored by SEC analysis, using a Tosoh EcoSEC HLC 8320GPC system with two SuperHM-M columns in series at a flow rate of 0.35 mL/min using THF as eluent. Number-averaged molar mass (M_n), weight-averaged molar mass (M_w), and dispersity ($Đ$) were calculated from

refractive index traces verse TSKgel polystyrene standards. Conversions were determined using a Varian 400 MHz NMR spectrometer in $CDCl_3$.

Data Processing

The data was recorded *via* SEC in the form shown in Figure 3A, where the refractive index response (proportional to concentration) is plotted as a function of the retention time for the case of the constant initiator addition during 60 min. The other initiator addition profiles will be discussed in detail in the Results and Discussion. In order to quantitatively compare this type of data to the modeling results, we performed the conversion steps exemplified in Figure 7.1. All the solid curves contain numerous points connected by straight lines and every hundredth data point is magnified as a solid blue dot.

We first convert the raw SEC retention time data into the logarithm MWD *via* the standard procedure of a calibration curve using polystyrene standards (Figure 7.12A-C). Next the molecular weight is converted to a linear scale to give weight fraction MWDs (Figure 7.12D-E) followed by transformation into the number fraction distribution (Figure 7.12F). The vertical axis, the refractive index detector response, is proportional to concentration and rewritten without any approximations using the following definition of the concentration of chains, N, of a given molecular weight, MW:

$$\frac{d\mathrm{wt}}{d\mathrm{MW}} = N(\mathrm{MW}) \ . \tag{7.9}$$

The data in Figure 3A, C and D are in arbitrary units and therefore needs to be normalized with a condition that all styrene monomer was converted to polymer chains,

$$P(k) = \frac{N(k)}{I_0} \frac{M_0}{\sum_{j=1}^{\infty} j \cdot N(j)}, \tag{7.10}$$

where $k = \mathrm{MW}/\mathrm{MW}_0$, $k \in \mathbb{R}$, with MW_0 being the molecular weight of one repeat unit in the chain, M_0 the total initial concentration of styrene, and I_0 the total concentration of the initiator added into the system. The normalized data (fraction of chains of length k) are shown in Figure 7.12F. The primary concern with this data is that k is not an integer. Since the degree of polymerization of the polystyrene chains must be an integer value, the data are discretized before comparing to modeling results.

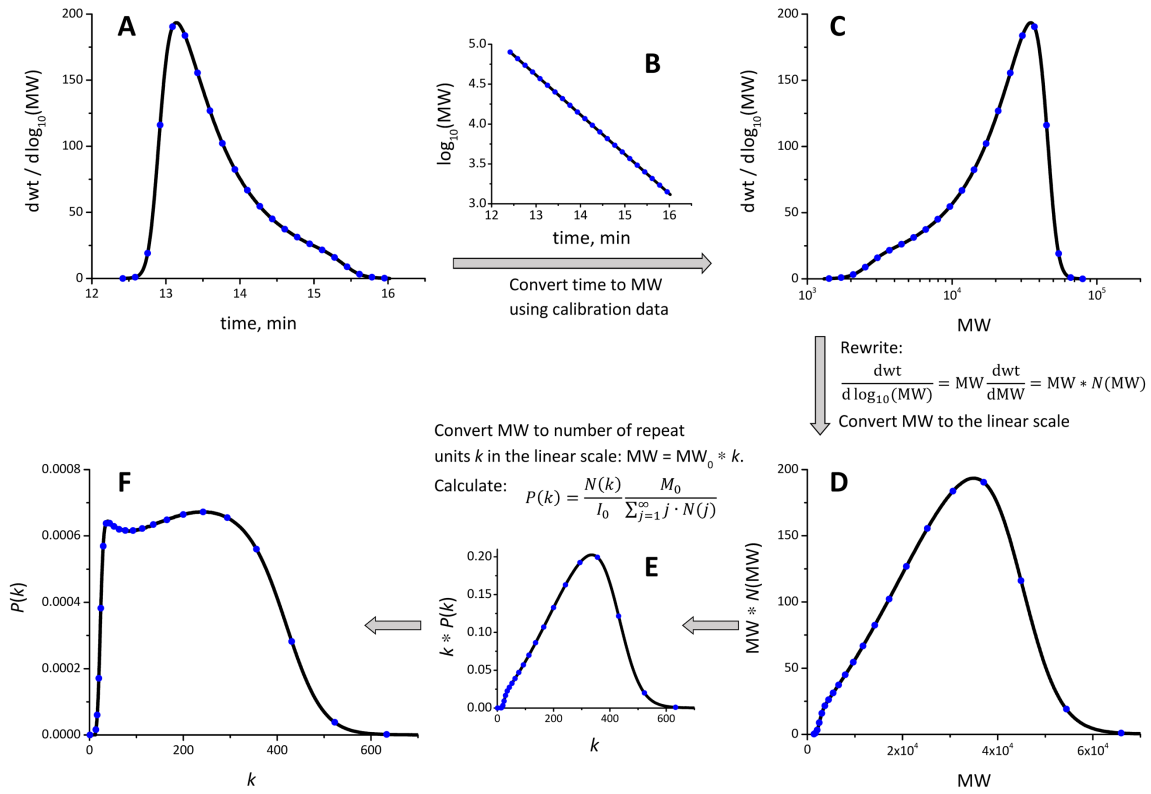

Figure 7.12. (A) Data recorded by the SEC instrument for the 60 min constant rate initiator addition profile. The solid curves contain numerous points connected by straight lines and every hundredth data point is magnified as a solid blue dot. (B) Calibration experiment with a known molecular weight distribution sample. (C), (D), (E) The experiment data, identical to panel (A), converted according to the procedures detailed in text.

To re-discretize the data from Figure 7.12F, it is convenient to prepare the cumulative chain fraction as a function of the chain length (Figure 7.13A):

$$\sum_{j=1}^{k_j \le i} P\left(k_j\right) , \tag{7.11}$$

where j is the index of the data points in Figure S1F. Next, preserving the cumulative chain fraction function, Equation (S3) determines the new

distribution of chain fractions as a function of integer values of chain length, $i \in \mathbb{N}$ (Figure 7.13B). The latter plot is converted into the weight fraction of chains (Figure 7.13C) for further comparison with the modeling results.

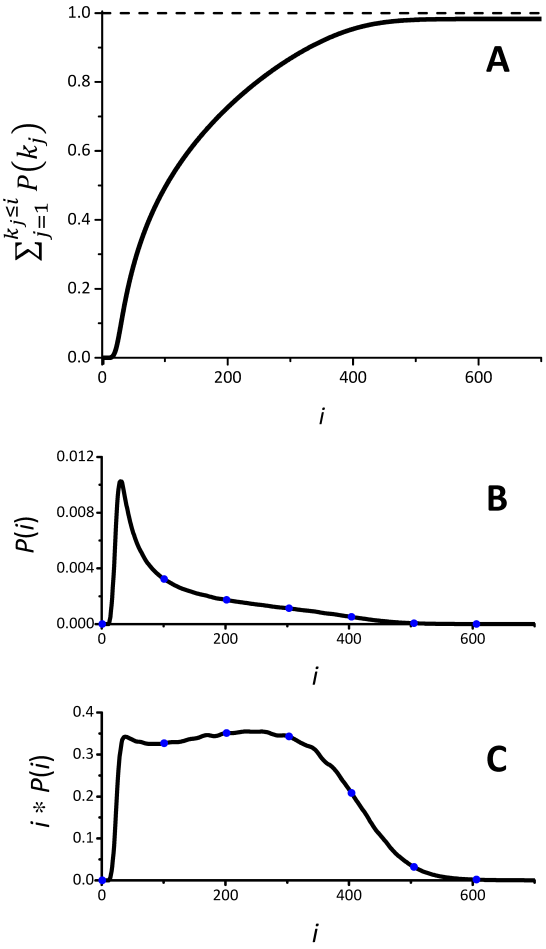

Figure 7.13. (A) Cumulative chain fraction as a function of the chain length. (B) distribution of chain fractions as a function of the chain length, $i \in \mathbb{N}$. (C) Chain fractions multiplied by the length of the chains in that fraction, see text for detail. Identically to Figure 7.3, the solid curves in (B) and (C) contain numerous points connected by straight lines and every hundredth data point is magnified as a solid blue dot.

Calibration Curve for the Transformation of Retention Time to Molar Mass

The calibration curve for size-exclusion chromatography (SEC) data was obtained using Tosoh TSKgel polystyrene (PS) standards. The relationship between the logarithm of molar mass and retention time is a third order polynomial shown in Equation 7.12:

$$\log MW = At^3 + Bt^2 + Ct + D \,, \tag{7.12}$$

where *MW* is the molar mass of the polymer chain, *t* is in minutes, $A = -0.0034$, $B = 0.1350$, $C = -2.2554$, and $D = 18.6905$.

Numerically Determined Effective Rate Constant from Figure 7.5

$$k_p(i) = 0.0806\left(108.6 - 107\sqrt{\frac{600}{i+600}} - e^{-0.0002(i-100)^2}\right)\left(9 + \frac{500^3}{i^3+500^3}\right) \tag{7.13}$$

Initiator Addition Rate Profiles

Initiator addition rates from Figure 1 have been used previously and are reported elsewhere.[1] The initiator addition rates from Figure 2 are reported in Tables 7.1 – 7.5.

Table 7.1. Figure 7.2A Black

Step Number	Rate (µL/h)	Volume (µL)
1	240.8	160.5
2	126.9	4.7
3	177.9	6.5
4	249.6	9.2
5	348.8	12.8
6	489.5	17.9
7	683.9	25.1
8	958.3	35.1
9	1342	49.2

Table 7.2. Figure 7.2A Red

Step Number	Rate (µL/h)	Volume (µL)
1	160.5	160.5
2	84.6	4.7
3	118.6	6.5
4	166.4	9.2
5	232.6	12.8
6	326.3	17.9
7	455.9	25.1
8	638.8	35.1
9	894.4	49.2

Table 7.3. Figure 7.2A Green

Step Number	Rate (µL/h)	Volume (µL)
1	120.4	160.5
2	63.4	4.7
3	88.9	6.5
4	124.8	9.2
5	174.4	12.8
6	244.7	17.9
7	341.9	25.1
8	479.1	35.1
9	670.8	49.2

Table 7.4. Figure 7.2B 30 min Linearly Decreasing Initiator Addition

Step Number	Rate (µL/h)	Volume (µL)
1	1247	31.2
2	1184	29.6
3	1120	28.0
4	1056	26.4
5	992.8	24.8
6	929.2	23.2
7	865.6	21.6
8	801.8	20.0
9	738.2	18.4
10	674.4	16.8
11	610.8	15.3
12	547.2	13.7
13	483.4	12.1
14	419.8	10.5
15	356	8.9
16	292.4	7.3
17	228.8	5.7
18	165.0	4.1
19	101.4	2.5
20	37.6	1.0

Table 7.5. Figure 7.2B 60 min Linearly Decreasing Initiator Addition

Step Number	Rate (µL/h)	Volume (µL)
1	623.8	31.2
2	592.0	29.6
3	560.1	28.0
4	528.3	26.4
5	496.4	24.8
6	464.6	23.2
7	432.8	21.6
8	400.9	20.0
9	369.1	18.4
10	337.2	16.8
11	305.4	15.3
12	273.6	13.7
13	241.7	12.1
14	209.9	10.5
15	178.0	8.9
16	146.2	7.3
17	114.4	5.7

18	82.5	4.1
19	50.7	2.5
20	18.8	1.0

Additional Modeling Results

Here we show that MWDs can be predicted from arbitrary initiator addition profiles, demonstrating the numerical modeling capability of this approach (Figure 7.14 and Figure 7.15). In these simulated reactions the initiator was added according to the profiles shown in the insets. These profiles are simulated as 50-step initiator addition rate profiles in a similar fashion the experiments described in the main text.

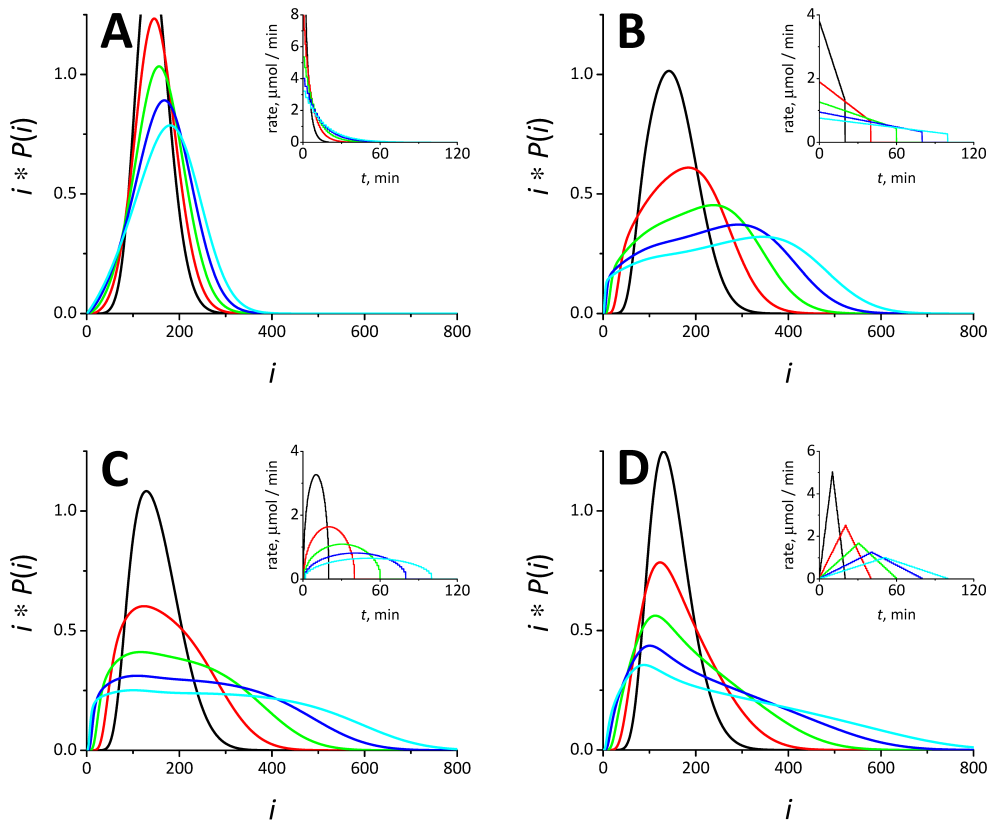

Figure 7.14. Sets of predicted, numerically calculated, distributions with the initiator addition rates shown in the insets (initiator addition rates not performed experimentally).

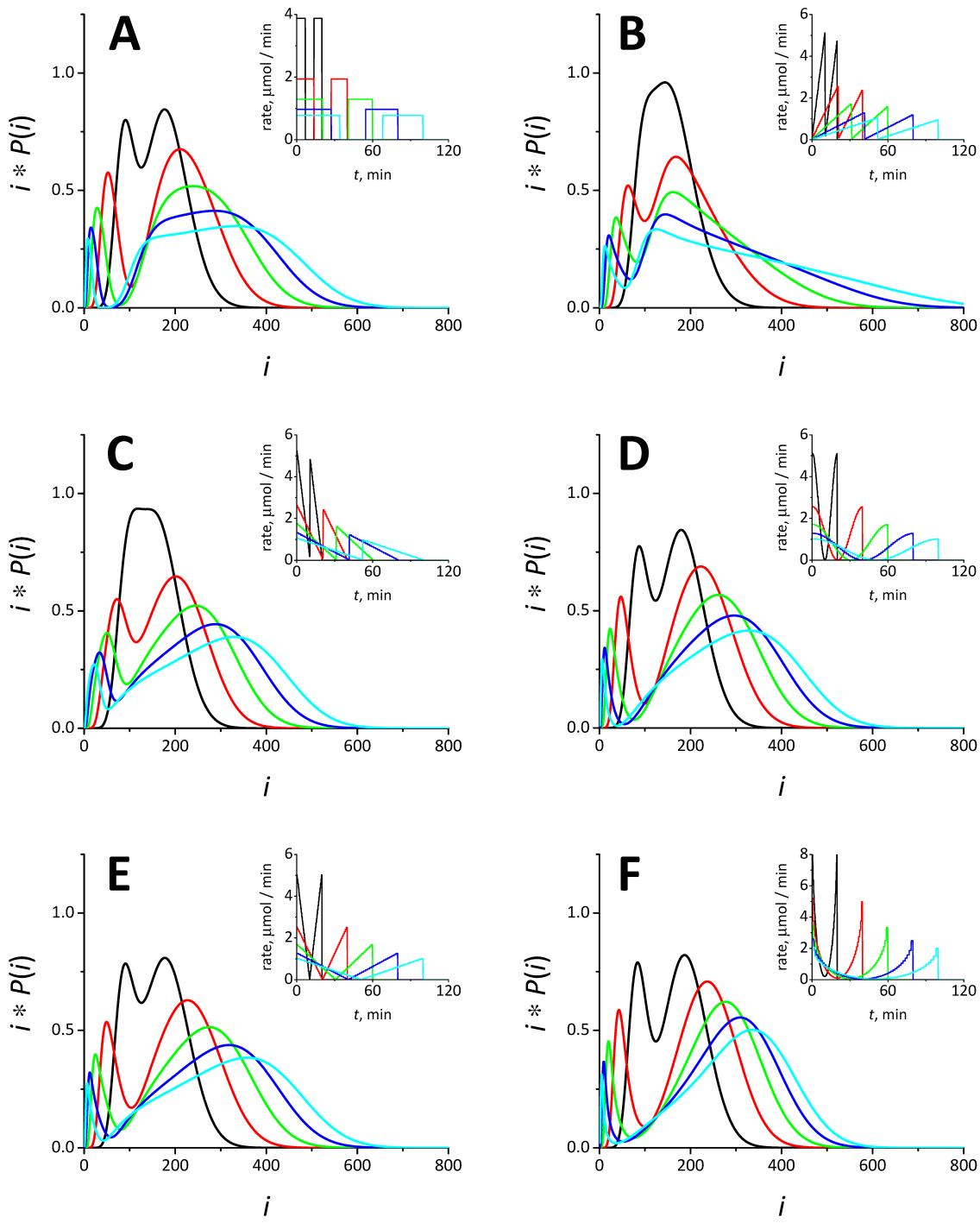

Figure 7.15. Numerical calculations to give bimodal distributions, with the initiator addition rates shown in the insets (the initiator addition rates not performed experimentally).

7.10 Appendix References

(1) Kottisch, V.; Gentekos, D. T.; Fors, B. P. *ACS Macro Lett*. **2016**, 5, 796.

(2) Worsfold, D. J.; Bywater, S. Anionic Polymerization of Styrene. *Can. J. Chem.* **1960**, 38, 1891.